INVESTIGATION OF MORTAR MIXTURES AFTER ADDITION OF SILICIC ACID ESTERS WITH REGARD TO ETTRINGITE AND THAUMASITE FORMATION

ALBERTO JOSÉ DUARTE SIMÃO

Dissertação submetida para satisfação parcial dos requisitos do grau de

MESTRE EM ENGENHARIA CIVIL — ESPECIALIZAÇÃO EM MATERIAIS E PROCESSOS DE CONSTRUÇÃO

Orientador: Prof. Dr.-Ing. Horst-Michael Ludwig

Orientador: Professor Doutor Arlindo Jorge Sá de Begonha

Mentor Científico: Dipl.-Ing Angela Eckart

SETEMBRO DE 2014

MESTRADO INTEGRADO EM ENGENHARIA CIVIL 2013/2014

DEPARTAMENTO DE ENGENHARIA CIVIL

Tel. +351-22-508 1901

Fax +351-22-508 1446

✉ miec@fe.up.pt

Editado por

FACULDADE DE ENGENHARIA DA UNIVERSIDADE DO PORTO

Rua Dr. Roberto Frias

4200-465 PORTO

Portugal

Tel. +351-22-508 1400

Fax +351-22-508 1440

✉ feup@fe.up.pt

http://www.fe.up.pt

To Angela Eckart,
Without whom this work would not be possible

Will it, and set to work briskly

Friedrich Schiller

ACKNOWLEDGMENTS

First of all, to Dipl.-Ing. Angela Eckart, the person who contributed the most to this work. For all the help, patience and teaching a thoughtful thank you. It was certainly a privilege to have worked by your side and to have learned with you.

To Prof. Dr. Ing. Horst-Michael Ludwig for the warm reception and for enable the desire to do this work in FA Finger-Institute to become a reality. This experience was an important milestone in my academic and personal life and allowed me to grow a lot as a person. I hope to have corresponded properly.

To Professor Dr. Arlindo Begonha, advisor of this work, for the joy and cheerfulness that he puts in everything he does, for the weight he had in my decision of choosing my field of expertise and for the availability and support, not only during this work but also throughout my academic career. I appreciate the trust and esteem that he always have put in me.

To the entire staff of FIB for made me feel at home during my stay in Germany. From the warm and friendly *"Guten Morgen"* to all the teaching and support provided during this work.

To all the friends that during my stay in Germany accompanied me in moments of leisure and relax, a big thank you. I will always remember the moments spent with nostalgia.

To Gonçalo Santos, my compatriot in Weimar, whom I have the pleasure of calling friend and, to whom I owe it all out of the thesis ambit. For his important role in the accomplishment of this work, a heartfelt thanks for all past times and for all the adventures in the discovery of Germany.

To my friends, André Gonçalves, Tiago Silva and Rui Ribeiro, who made me a visit while I was in Germany, and made me feel at home despite being 2400Km away.

To Diogo Jardim, my housemate for the past three years, for being like a brother to me, for all the moments, all the adventures and for his true friendship.

To all those who accompanied my during my academic career, particularly those who assiduously visited the affectionately called "Mouse House", who contributed to make all the experiences, in these past years, unforgettable.

Finally, to those whom I owe everything. To my father, Alberto, the best example I have in life and the person I most respect and will always respect. To my mother, Glória, engine of our home and family and the person who gave me more strength while performing this work, regardless of the distance imposed.

AGRADECIMENTOS

Em primeiro lugar, à Dipl.-Ing. Angela Eckart, a pessoa que mais contribuiu para a realização deste trabalho. Por toda a ajuda, paciência e ensinamentos um profundo obrigado. Foi, sem dúvida, um privilégio poder ter trabalhado a seu lado e ter aprendido consigo.

Ao Prof. Dr. Ing.Horst-Michael Ludwig pela forma calorosa como me recebeu e por ter permitido que o desejo de realizar este trabalho no F.A. Finger-Institut se tornasse realidade. Esta experiência representou um marco importante na minha vida académica e pessoal e permitiu-me crescer bastante enquanto pessoa. Só posso esperar ter correspondido devidamente.

Ao Professor Doutor Arlindo Begonha, orientador deste trabalho, pela alegria e boa disposição que o caracterizam, pelo peso que teve na escolha do meu ramo de especialização e pela disponibilidade e apoio, não só na realização deste trabalho mas também ao longo do meu percurso académico. Pelo seu "teria todo o gosto" aquando questionado se poderia ser o meu orientador de tese que muito me honrou. Agradeço a confiança depositada e a estima que sempre demonstrou por mim.

A todo o pessoal do FIB, por me terem feito sentir em casa durante a minha estadia, desde o caloroso e simpático *Guten Morgen* a todo o apoio e ensinamentos prestados durante a realização deste trabalho.

A todos os amigos que durante a minha estadia na Alemanha me acompanharam em momentos de lazer e descontração, um muito obrigado. Recordarei sempre os momentos passados com saudade.

Ao Gonçalo Santos, meu compatriota em Weimar, a quem tenho o prazer de chamar amigo e a quem devo tudo fora da tese, tendo sido extremamente importante durante a sua realização. Um profundo obrigado por todos os momentos passados e por todas as aventuras na descoberta da Alemanha.

Aos meus amigos André Gonçalves, Tiago Silva e Rui Ribeiro, pela visita que me fizeram enquanto me encontrava na Alemanha, fazendo-me sentir em casa mesmo a 2400 Km de distância.

Ao Diogo Jardim, *The Legend*, meu companheiro de casa durante os últimos 3 anos. Por ser como um irmão para mim, por todos os momentos, todas as peripécias e pela sua verdadeira amizade.

A todos aqueles que me acompanharam durante o meu percurso académico, em especial aos que assiduamente visitavam aquela que era carinhosamente apelidada por "casa do rato", que muito contribuiram para que as vivências ao longo destes anos sejam inesquecíveis.

Finalmente, àqueles a quem tudo devo. Ao meu pai Alberto, o maior exemplo que tenho na vida e a pessoa que mais respeito e respeitarei sempre. À minha mãe Glória, motor do nosso lar e família e a pessoa que mais força me deu durante a realização deste trabalho, independentemente da distância imposta.

ABSTRACT

Both ettringite and thaumasite were discovered long time ago but are still controversial subjects in the scientific community.

The aim of this work, which was proposed by the F.A Finger Institut, one of the most important research centers in what concerns these minerals, is to understand how the application of a stone/concrete strengthener – in this case KSE – with a silicic acid ester as active ingredient influences the formation of ettringite and thaumasite in mortars.

Without any previous investigations on this phenomenon, the objective of this thesis is to shed some light on the influence of KSE application in ettringite and thaumasite formation and to serve as a base to future works on this subject. In order to correspond to this objective, a large number of tests, specimens and products were selected (KSE).

The investigation on the mortar mixtures was based on the results of the following tests:

- Dynamic E-Modulus;
- Capillary absorption;
- Flexural strength;
- Compression strength;
- Porosimetry;
- KSE penetration;
- Expansion;
- Scanning electron microscopy (SEM);
- X-ray diffraction study (XRD).

The analysis of the results of the tests performed in specimens with and without KSE applied allowed some conclusion withdrawals.

KEYWORDS: Ettringite, Thaumasite, KSE, SEM, XRD

ZUSAMMENFASSUNG

Die Schadminerale Ettringit und Thaumasit sind bereits lange bekannt, werden aber in der wissenschaftlichen Gemeinschaft immer noch diskutiert.

Das Ziel dieser Arbeit, welche von der F.A. Finger-Institut, eines der wichtigsten Forschungszentren für Baustoffkunde, vorgeschlagen wurde, ist es, zu verstehen wie die Anwendung von Steinfestigern auf der Basis von Kieselsäureester (KSE) die Bildung von Ettringit und Thaumasit in Mörteln beeinflusst.

Da bisher noch keine Forschungen zu diesem Thema vorliegen, ist es das Ziel dieser Arbeit, erste Untersuchungen zum Einfluss der KSE-Anwendung in Mörteln auf die Ettringit und Thaumasitbildung durchzuführen, damit diese als Basis für zukünftige Arbeiten dienen können. Aus der diesem Grund wurde eine große Anzahl von Tests, Probekörpern und Produkten (KSE) ausgewählt.

Die Ergebnisse der Untersuchungen der Mörtelmischungen basieren auf folgenden Versuchen:

- Dynamische E-Modul;
- Kapillare Wasseraufnahme ;
- Biegefestigkeit;
- Druckfestigkeit;
- Quecksilberdruckporosimetrie;
- KSE-Eindringtiefe;
- Dehnung;
- Rasterelektronenmikroskopie (SEM);
- Röntgenbeugungsanalyse (XRD).

Die Auswertung durchgeführten Tests der Proben mit und ohne KSE lassen einige Rückschlüsse zu.

STICHWORTE: Ettringit, Thaumasit, Kieselsäureester, KSE, SEM, XRD

RESUMO

Quer a etringite quer a taumasite foram descobertas há muito tempo, no entanto, continuam a ser um assunto controverso na comunidade científica.

O objectivo deste trabalho, proposto pelo F.A. Finger Institut, um dos mais importantes centros de investigação em etringite e taumasite, é compreender de que forma a aplicação de um produto de reforço de pedra/betão – neste caso em concreto, KSE – cujo ingrediente activo é um éster de ácido de silício influencia a formação de etringite e taumasite em argamassas.

Tendo em conta que não existem investigações prévias acerca deste fenómeno, o objectivo deste trabalho é elucidar de que forma a aplicação de KSE pode condicionar a formação dos minerais supracitados e, também, servir de base a futuros trabalhos de investigação que possam vir a ser desenvolvidos neste âmbito. De maneira a conseguir corresponder a este objectivo, foi seleccionada uma grande variedade de testes, provetes e produtos (KSE).

A investigação, conduzida em diferentes misturas de argamassas, baseou-se nos resultados dos seguintes testes:

- Módulo de elasticidade dinâmica;
- Absorção por capilaridade;
- Resistência à flexão;
- Resistência à compressão;
- Porosimetria;
- Penetração dos KSE;
- Expansão;
- Microscopia electrónica de varrimento (MEV);
- Difracção dos Raios-X (DRX).

A análise cuidadosa dos resultados dos testes acima referidos, realizados em provetes sem e com a aplicação de KSE, permitiu que algumas ilações e conclusões pudessem ser tomadas.

PALAVRAS-CHAVE: Etringite, Taumasite, KSE, MEV, DRX

Index

FIGURES INDEX

TABLES INDEX

1 INTRODUCTION

1.1. CONSIDERATIONS

Throughout the world, the concern about the durability and sustainability of concrete has been increasing in the last decades. Even the biggest architectural works of mankind cannot resist against the ravages of Mother Nature and Man. Like the common living beings, concrete structures suffer deterioration over time during the aging phenomena. They cannot still be considered as eternal. Therefore, structures and materials started to have an associated lifetime.

As it can be easily understood by human condition, the desire for greatness and immortality lead to countless researches that were carried out with the purpose of expanding the lifetime of structures and materials. Different cement and concrete compositions and different additions were studied, tested and used in the construction of new structures. Although the study of better solutions for the durability of new structures can be really captivating, one of the biggest challenges of mankind has been to assure ways to preserve the heritage of our ancestors.

Aiming to respond to this challenge, a lot of techniques were debated and applied, as well as many products with different applications and objectives were created. That is how stone and concrete strengthener products first appear.

These types of products look forward to reinforce the matrix of the substrate and can be used in stones and cementitious materials. One example of these products is the KSE (from the German *Kieselsäureester* which in English stands for Silicic acid ester base) that can be used in stone materials, renders and joints in future, historical buildings and monuments. KSE reacts with water stored in the pore system or humidity. During this reaction amorphous hydrous silicon dioxide (SiO_2, "silica gel") is deposited as a binder. The mineral silica gel binder thus replaces the original binder lost through weathering.

Even though the application of these products has historically showed good results, specially in silicate rich rocks applied in historical buildings and monuments, the ways they affect the formation of phases in cement/concrete are not fully understand yet. This is a really important question to solve since expansion is usually associated to the new phases formation. This phenomenon can be either deleterious or beneficial and, consequently, must be studied in order to be better controlled.

Commonly, expansion in concrete/cement is related with the presence of magnesium oxide (MgO) and/or calcium oxide (CaO). However, it is not the percentage of these oxides, *per se*, that dictates the expansion, but the percentage of these oxides under crystalline form. The expansion reaction of the crystalline magnesium oxide (periclase) with water is not instantaneous and it could take several weeks, months or even years in order to form magnesium hydroxide without the previous dissolution.

The expansability due to hydration of periclase depends on the dimension of the crystals and their distribution. When crystals are smaller than 5 μm the cement is not expansive until percentages of MgO between 7 and 8%. The reaction can be prevented using pozzolan and granulated slag additions.

The expansion in concrete/cement can also be associated with the formation of ettringite and/or thaumasite.

This work was developed in Germany, a country with a long tradition and history in the study of sulfate attacks, in FIB of the Bauhaus-Universität Weimar, one of the leader institutes in the study of ettringite and thaumasite formation. The theme was proposed by Dipl.-Ing Angela Eckart and it concerns not only the crystallization of ettringite and thaumasite per se when sulfate attack occurs but also the study of the influence of the application of strengthening products in their formation in order to contribute to the better comprehension of cement hydration as well as to better preserve our architectonic heritage.

1.2. OBJECTIVES

The aim of this thesis is to evaluate in which ways the application of silicic acid esters (KSE) on mortars influences ettringite and thaumasite formation. To do so, not only different types of KSE were selected, but also different types of cements and also different types of applications.

Following the recommendations of the DIN EN 998-1 (2003) standard, flat prisms with CEM 42.5 N with two different water/cement ratios were produced. With the production of these specimens it is expected to compare between the properties of the specimens with and without KSE. The properties that were intended to be studied were:

- Dynamic E-Modulus;
- Capillary absorption;
- Flexural strength;
- Compression strength;
- Porosimetry;
- KSE penetration.

Although neither of these properties can, by itself, explain the influence of the application of KSE on mortars, the results obtained are important to perform a complete analysis of the problem and, can also be used to better understand the other analyses conducted in FIB. The application of KSE on the specimens was performed on the surface of the prisms.

In order to be able to understand the influence of the application of KSE in ettringite and thaumasite formation, specimens with KSE in the mixture were also studied. These specimens, unlike the specimens described before, were studied by Scanning electron microcopy (SEM) and X-Ray diffraction (XRD). Taking this in consideration, the specimens were produced in Le-Châtelier rings and, in addition to the KSE, it was also added gypsum to their composition. The addition of gypsum favors the formation of the crystals in study which can lead to better results. The Le-Châtelier ring allowed the determination of the expansion of the specimens.

1.3. STRUCTURE OF THE WORK

This work is divided in six chapters. In this chapter are presented the first considerations about the theme, the objectives and motivations to do it and, a small summary and structural scheme of its organization.

The second chapter contains the state of the art previous to the realization of this work. Since no previous works/studies were performed on the subject of this thesis, this chapter will only contain descriptions of the ettringite and thaumasite formation phenomena and information about the silicic acid esters applied in the studies.

In the third chapter, all the methodology inherent to the work performed such as the specimens selection casting and keeping and the description of all the test performed and the standards consulted and/or followed are referred.

The fourth chapter presents the results obtained in form of graphics, figures or tables, their discussion, analysis and correlations between the several tests carried out.

In the fifth chapter are presented the conclusions and the recommendations for future research.

In the Appendix are presented some results not shown in the previous chapters.

2
STATE OF THE ART

2.1. CONSIDERATIONS

The state of the art can be found in academic works and it has a crucial importance in the description of the development reached in the field in study (which can be translated by techniques, devices, procedures or methodology). There are no previous works performed that intended to understand and/or investigate the influence of silicic ester acids on the formation of ettringite and thaumasite.
One of the main goals of the state of the art is to provide a good evaluation of the contribution of the research work carried out in a certain field of knowledge.
Given this, a proper state of the art will be presented but instead of describing the development in the study of the influence of silicic acid esters in ettringite and thaumasite formation, the three main "keywords" – "ettringite formation", "thaumasite formation", "silicic acid esters", – will be described individually.

2.2. ETTRINGITE

2.2.1. HISTORY

Circa 1880, while studying the effect of sea water in hydrated cement, Candlot found the correlation between the amount of alumina (Al_2O_3) and calcium oxide (CaO) that led to expansion effects and cracking. Therefore, he predicted the existence of what came to be called Candlot's Salt, whose chemical formula was eventually determined correctly by Deval. This salt was, later on, named "Ettringite", the name for which is known today, due to the finding of the same mineral in Ettringen, Germany by Lehman in 1874 [1]. Figure 2.1 shows an ettringite crystal found in that area.

Fig. 2.1 – Ettringite crystals from the caspar quarry, Bellerberg Volcano, Ettringen, Germany. Picture by Stephan Wolfsried [2]

Only approximately one century after, in 1970, the first ettringite structural description model was proposed by Moore and Taylor [3][4].

After that, ettringite studies (which in this case are firmly related with sulfate attack studies and thaumasite studies) increase significantly in the mid 1990's when ettringite was associated with several cases of deterioration of concrete pavements and precast members which gained notoriety because of the uncertainty over the cause of their distress. [5]

Since the first model proposed by Moore and Taylor [3][4], ettringite structural description never ceased to improve until the more recent crystallographic works [6] [7]. The use of neutron [7] and high resolution [5] powder diffraction provided a full crystallographic description of ettringite, including a complete characterization of its hydrogen bonding network. The details of the structural description of ettringite were confirmed by Raman spectroscopic studies [8].

2.2.2. DESCRIPTION

Ettringite is the mineral name for calcium sulfoaluminate ($3CaO•Al_2O_3•3CaSO_4•32H_2O$) which rarely occurs in nature but is widely present in the mineralogy of hydrated cements, such as, in different types of Portland cement, in calcium aluminate cements in combination with calcium sulfates as well as in the calcium sulfoaluminate cement [9].

As it is known, calcium sulfate sources, such as gypsum, are intentionally added to Portland cement to regulate early hydration reactions to prevent flash setting, improve strength development, and reduce drying shrinkage. Gypsum and other sulfate compounds react with calcium aluminate in the cement to form ettringite within the first few hours after mixing with water. Ettringite is the first and the only hydrate formed during the hydration of tricalcium aluminate in the presence of gypsum. In cement chemistry, ettringite is commonly named Aft, similar to the AFm phases of the general formula $Ca_4(Al,Fe)_2(OH)_{12}•X_z•nH_2O$, where X is an anion [10]. The general definitions of these phases are somewhat technical, but for this description it will be taken in consideration, for example, that ettringite is an Aft phase because it contains three (t-tri) molecules of anhydrite ($3CaSO_4$). In contrast and also, for example, one of the most common AFm phases in hydrated cement is monosulfate, which is an AFm phase because it contains one (m-mono) molecule of anhydrite.

The formation of ettringite during the early hydration stage (also known as primary ettringite) is, therefore, important for controlling the rate of set of the highly reactive aluminate phases [11].

Nevertheless, its formation in mature cement stone can be destructive, such as the result of sulfate attack [12] or the formation of delayed ettringite (also known as secondary ettringite) [13].

This important mineral in cement chemistry is a necessary and beneficial component of Portland cement at early stages of hydration however, it may damage hardened concrete if formed in the cement stone after long times.

2.2.3. ETTRINGITE IN FRESH CONCRETE

The primary ettringite ($3CaO \bullet Al_2O_3 \bullet 3CaSO_4 \bullet 32H_2O$) formation from C_3A ($3CaO \bullet Al_2O_3$) and gypsum ($CaSO_4 \bullet 2H_2O$) in the presence of calcium hydroxide (($Ca(OH)_2$) starts right after the water (H_2O) addition to the mixture and can be translated by the following equation:

$$3CaO \bullet Al_2O_3 + 3(CaSO_4 \bullet 2H_2O) + 26H_2O \rightarrow 3CaO \bullet Al_2O_3 \bullet 3CaSO_4 \bullet 32H_2O \quad (1)$$

This reaction ends as soon as the sulfate concentration needed for the formation of ettringite decreases below the limit. Therefore, not all the C_3A is consumed in the reaction and then, it reacts with the already formed ettringite forming monosulfate and solid solutions between $C_3AC\bar{S}H_{12} - C_4AH_{13}$ which in aqueous solution again form ettringite and tetracalcium aluminate hydrate. This monosulfate is always formed since it is necessary 19% gypsum to transform 10% of C_3A fully into ettringite. The Portuguese and European standard, NP EN 197-1 (2001), establishes that the maximum sulfate content limit is 3.5 to 4%, depending on the type and strength class of the cement [14].

If the decomposition of the primary ettringite is not completed, then both ettringite and monosulfate occur in the normal hardened concrete. It is also important to refer that in the first hours of hydration, the shape and size of the ettringite and monosulfate crystals suffer changes, in dependence of the solution composition which influences the setting behavior [15].

Ettringite has the form of hexagonal-prismatic crystals, as it can be seen in Figure 2.2 and also in Figure 2.1.

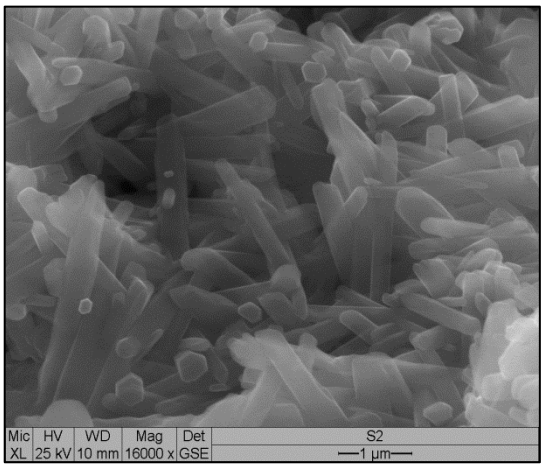

Fig. 2.2 – Ettringite crystal obtained by ESEM in an atmosphere of water vapor with no coating

According to the structural model proposed by Taylor [11], the crystals are based on columns of cations with the following composition:

$$\{Ca_3[Al(OH)_6] \bullet 12H_2O\}^{3+}$$

The $Al(OH)_6{}^{-3}$ octahedra bound with the CaO_8 polyhedra which mean that each aluminum ion in the crystal is connected to Ca^{2+} ions, with which they share OH^- ions. The intervening channels contain the SO_4^{2-} tetrahedra and the remaining H_2O molecules [13]. This can be better understood with the help of Figure 2.3.

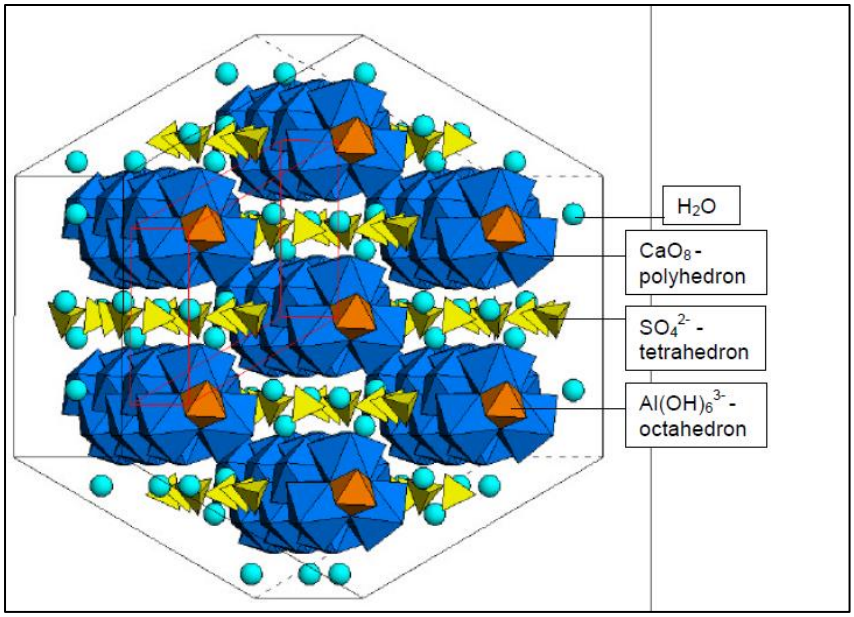

Fig. 2.3 – Structure model of ettringite according to J. Neubauer [14]

The H_2O molecules, as it can be seen in Figure 2.3, are very loose into the ettringite structure. This fact can help to understand the loss of water due to increased temperatures or during drying, which, therefore, explains the existence of ettringite crystals with different water contents.

2.2.4. Ettringite In Hardened Concrete

Stark and Bollman [14] refer that ettringite crystals can assume many different habits in concrete. The difference in the habits is not yet fully explained, although there are some hypotheses about this subject [15] [16] [17]. Accordingly to that, the factors that seem to influence ettringite shape are:

- The mixture composition and the pH value of the concrete pore solution;
- The formation mechanism.

Even though there were some agreement on the factors that influence the crystals habits, there were different approaches for the study of the correlation between that and the pH value of the reaction solution. For example, according to the works of Chartschenko *et al.* [17], long, fiber-shaped crystals were formed at pH values between 10 and 12 but, extremely microcrystalline ettringite was present at pH values above 13. Mehta [15] has a different approach and designated as Type I, the long, lath-like crystals (which could be 10 to 100 μm long and several μm thick), formed at low hydroxyl ion concentration, *i.e.* with low pH values. This Type I ettringite leads to high strengths but not to expansion effects, which lead to the characterization of Type I ettringite as not expansive. The acicular crystals (with 1 to 2 μm long and 0.1 to 0.2 μm thick or even smaller) that are formed during the hydration of Portland cements at high pH values were designated as Type II ettringite. This Type II ettringite, or microcrystalline ettringite, can cause expansion effects.

Given this, there is some disagreement in the scientific community in which conditions enable ettringite to be stable in hardened concrete. There were countless works that aimed to analyze ettringite stability in hardened concrete. The majority of them, as well as the already referred before, relates ettringite stability with pH of the pore solution. A summary of the conclusions of those works was elaborated by Stark and Bollmann [14] and can be found in Figure 2.4.

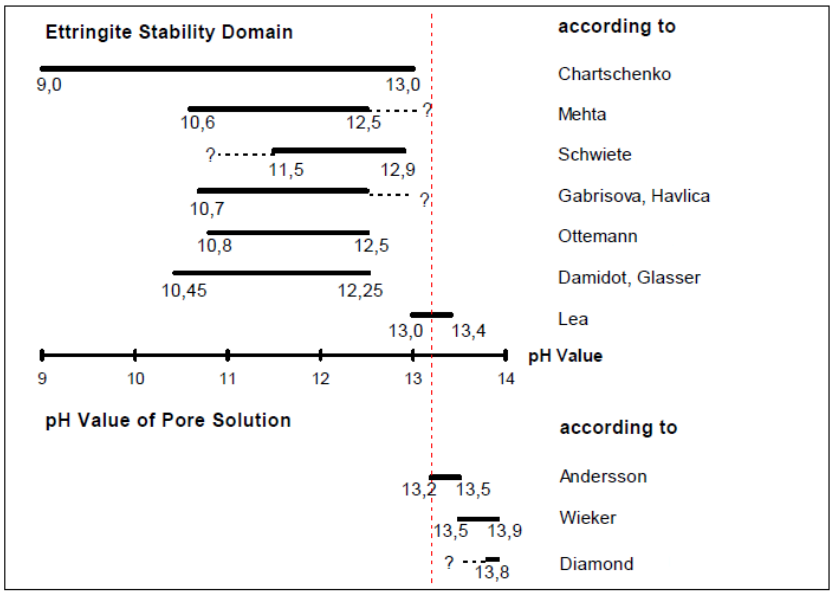

Fig. 2.4 – Relation between ettringite stability and pH value of pore solution. Adapted from [14]

As it can be understood by the figure above, different interpretations of the ettringite stability were presented. This fact can be explained taking in consideration that ettringite can be found in different ages in the hardened concrete, as well as in different environments. Therefore it is important to clarify which processes can lead to the accumulation of ettringite in hardened concrete.

These processes are, in accordance with Stark and Bollmann, the following [14]:

- Internal sulfate sources and late sulfate release;
  - After heat-treatment;
  - Due to freeze-thaw attack with and without de-icing salt;
  - Due to carbonation;
  - In the clinker components;
- Alternating moisture conditions;
- Marginal conditions which promote damage;
  - Pre-damage in the concrete;
  - Pore volume – the bigger the porosity the greater the expansion potential;
  - Cement and concrete composition;
- Re-crystallization;
  - In pores;
  - Phase transition zones;
  - And mature parts of the micro structure.

2.2.5. DAMAGE MECHANISMS AND CONCLUSIONS

Taking in consideration what was stated in 2.2.3 and 2.2.4 a question, which is still controversial, can be made:

Is ettringite the cause of cracks in concrete or does it only take place preferentially in cracks which already exist?

After analyzing the works carried out in this subject it possible to understand the following [14]:

- The primary ettringite formation during the initial hydration does not lead to damage since, this process occurs in the plastic matrix and, therefore, no stresses are produced;
- Microcrystalline ettringite formed primarily or secondarily (delayed) in the microstructure may cause damages in hardened concrete. These damages are the result of the development of an expansion pressure that exceeds the tensile strength of the microstructure;
- Ettringite formed in hardened concrete from less-sulfate containing compounds may, due to the crystals growth or due to the increase in volume, cause stresses which exceed the tensile strength of the structure and, therefore, damage the structure. For example, the transformation of monosulfate into ettringite causes a 2/3 times increase in volume;
- The recrystallization of ettringite in the hardened structure, due to moisture changes and accumulation of reactants, may also lead to structure damages because of the crystallization pressure and the increase in volume.

2.3. THAUMASITE

2.3.1. HISTORY

Until 1999, ettringite and gypsum were normally associated with sulfate attack [18]. After the results of the Thaumasite Expert Group [19], it became clear that a third sulfate material, thaumasite, could also be formed. Commonly, the sulfate solutions penetrate the concrete and react with the hydration products of the cement paste resulting in the formation of sulfate bearing phases like gypsum, ettringite or thaumasite causing deep modifications in the microstructure and strength of the original cement paste.

It was, afterward, discussed that thaumasite formation could be more aggressive than the ettringite formation whereas thaumasite was reported to be the cause of destruction in the majority of the concrete structures tainted by sulfate attack. The conventional form of sulfate attack, in which the reaction product ettringite (± gypsum) is formed, may have occurred early on in the deterioration process but it was not the persistent mechanism [20].

With this, the thaumasite formation became a subject of major interest in academic and field studies. It is important to refer the work of the Building Research Establishment [20], which, since the early 1990s has been carried out extensive research and, had concluded that, thaumasite formation has been the result of over 95% of the sulfate attack cases reported in the United Kingdom [20]. Furthermore, it is also important to refer the studies of E. Freyburg, *et al.*, that contain examples of sulfate attack with thaumasite formation in two completely different structures in Germany [21].

In addition to the above-mentioned, it is also important to state that through all Europe and mainly in Germany, since the end of the WWII, a lot of restoration works have been done in historic buildings. Ordinarily, these types of work are delicate and need skilled and experienced workers to be performed correctly, otherwise they could even, in the worst conditions, hasten the deterioration/degradation state

of the buildings. Thereby, there were also studies of the formation of ettringite and/or thaumasite in restoration mortars (injected in order to consolidate old stonework) and in lime mortars and plasters in masonry of historic buildings [22] [23] [24] [25] [26] [27].

It was also possible to determine the major risks of thaumasite formation [28], which are:

- Low temperatures;
- Sulphate attack from the environment;
- Presence of mobile water;
- Sources of calcium.

Nowadays, there is agreement that the addition of calcium carbonate facilitates the formation of thaumasite however, is not a pivotal prerequisite, inasmuch as the carbon dioxide can also be provided from the environment [18].

Even though all the studies and works conducted worldwide, the role of the cement type, the additives used as well as other chemical aspects on the formation of thaumasite are not yet clarified [29]. For example, there is still no agreement on the role of ground granulated blast furnace slag in the formation of thaumasite. In one study [29], it was concluded that blast furnace slag can instigate the formation of thaumasite, while slag cements accomplish better results than Portland cements in other studies[30] [31]. The results of the addition of coal combustion fly ash on the endurance against the formation of thaumasite are also controversial [20] [32] [33].

2.3.2. DESCRIPTION

Thaumasite is an uncommon mineral since it contains silicon in 6-coordination with hydroxyl. There are only very few minerals which contain silicon in 6-coordination with oxygen or hydroxyl and most of these are formed under pressure [34]. This is probably why this mineral was named, in 1878 by Nordenskjöld, from the Greek word *thaumazein* which means "to wonder at" or "to be surprised". Thaumasite contains $[Si(OH)_6]^{2-}$ groups which are very rare and are only also known to be present in the chromate analogue of thaumasite (chromatethaumasite) [35].

Thaumasite can be represented chemically as:

$$Ca_6[Si(OH)_6]_2(CO_3)_2(SO_4)_2 24H_2O$$

Or more simply as:

$$CaCO_3 \bullet CaSO_4 \bullet CaSiO_3 \bullet 15H_2O$$

And in pure state its chemical name is hexacalcium bis-hexahydroxosilicate dicarbonate disulfate tetracosahydrate. However, thaumasite is not a pure phase and contains a range of impurities in solid solution. This fact can help to understand how does thaumasite can be formed at atmospheric pressure although all other compounds with silicon in 6-coordination with oxygen are formed at high temperatures and pressures due to the strong polarisability of the Si^{4+} cation [36].

It is then important to discuss the formation processes of thaumasite.

2.3.3. FORMATION BY THE DIRECT ROUTE

Accordingly to the works developed by Bensted [34] [35] [36], thaumasite forms below 15º C (ideally between 0-5º C) by the reaction of sulfate with carbonate (either atmospheric CO_2 or CO_3^{2-} ion), silicate (including C-S-H) and excess water in the presence of calcium ions. The common reactants are normally gypsum, calcite ($CaCO_3$) and C-S-H ($Ca_3Si_2O_7 3H_2O$). Both the alite phase, C_3S, and the belite phase, C_2S, can provide the binder C-S-H that can react and form the non-binder thaumasite ($Ca_6[Si(OH)_6]_2(CO_3)_2(SO_4)_2 24H_2O$). These reactions can be consulted below:

$$Ca_3Si_2O_7 3H_2O + 2\{CaSO_4 2H_2O\} + 2CaCO_3 + 24H_2O \rightarrow Ca_6[Si(OH)_6]_2(CO_3)_2(SO_4)_2 24H_2O + Ca(OH)_2 \quad (2)$$

$$Ca_3Si_2O_7 3H_2O + 2\{CaSO_4 2H_2O\} + CaCO_3 + CO_2 + 23H_2O \rightarrow Ca_6[Si(OH)_6]_2(CO_3)_2(SO_4)_2 24H_2O \quad (3)$$

Normally, the calcium hydroxide ($Ca(OH)_2$) formed would not stay as such: it would most likely carbonate by reaction with atmospheric carbon dioxide or, with carbon dioxide dissolved in the water to become calcium carbonate, a potential or actual reactant for forming more thaumasite:

$$Ca(OH)_2 + CO_2 \rightarrow CaCO_3 + H_2O \quad (4)$$

The calcium hydroxide could as well “disappear” since it is a high lime reactant which can produce thaumasite in a more direct manner.

It is important to state that the reactions presented for the formation of thaumasite are very slow and normally took several months to obtain a significant yield [36] [37] [38].

2.3.4. FORMATION BY THE WOODFORDITE ROUTE

As well as the direct route previously described, the woodfordite route also takes place below 15ºC. This route to the formation of thaumasite is developed by the reaction between ettringite, silicate (particularly C-S-H) and carbonate (once again, either CO_3^{2-} ion or atmospheric CO_2) in the presence of excess water. Woodfordite is the name given to the solid solution whose end members are ettringite and thaumasite [34]. This reaction is, likewise the ones that take place in the direct route, very slow, but once thaumasite starts to form the rate of reaction increases significantly. Besides the alite and belite (which form C-S-H), also the aluminate, C_3A, and ferrite, C_4AF, and, of course, the gypsum, contribute to the formation of thaumasite by the woodfordite route. This reaction can be described as follows [34].

$$Ca_6\left[Al_xFe_{(1-x)}(OH)_6\right]_2(SO_4)_3 26H_2O + Ca_3Si_2O_7 3H_2O + 2CaCO_3 + 4H_2O \rightarrow Ca_6[Si(OH)_6]_2(CO_3)_2(SO_4)_2 24H_2O + CaSO_4 2H_2O + Al_{2x}(OH)_3 + Fe_{(2-2x)}(OH)_3 + 4Ca(OH)_2 \quad (5)$$

$$Ca_6\left[Al_xFe_{(1-x)}(OH)_6\right]_2(SO_4)_3 26H_2O + Ca_3Si_2O_7 3H_2O + CaCO_3 + CO_2 + 3H_2O \rightarrow Ca_6[Si(OH)_6]_2(CO_3)_2(SO_4)_2 24H_2O + CaSO_4 2H_2O + Al_{2x}(OH)_3 + Fe_{(2-2x)}(OH)_3 + 3Ca(OH)_2 \quad (6)$$

As well as described before and illustrated by equation number (4), commonly, the calcium hydroxide (portlandite) does not remain as an end-product, since it will readily react with carbon dioxide or CO_3^{2-} ion to form calcite and some water. The calcite produced can be available to serve as a reactant for the formation of more thaumasite. As well as in the direct route, it is also possible for portlandite to become directly involved as a high lime reactant in the formation of thaumasite via the woodfordite route.

The solid solution between ettringite and thaumasite is not continuous. A discontinuity in the solid solution (woodfordite) has been found in diffractograms and it is characterized by a gap between 11.11-11.17 $\dot{A}$ [34]. This discontinuity suggests that in practice, an unstable range of compositions might exist within the solid solution series [39].

2.4. SILICIC ACID ESTERS

The silicic acid esters are the active ingredient of the products that were used to perform this investigation work. Not much information can be found about it so only a small description about this chemical compound will be done.

The silicic acid ester which is also known as tetraethyl silicate, tetraethyl orthosilicate or simply as TEOS consists of four ethyl groups bounded to the SiO_4^{4-} ion and is represented by the following chemical formula and structure (Figure 2.5).

$$C_8H_{20}O_4Si$$

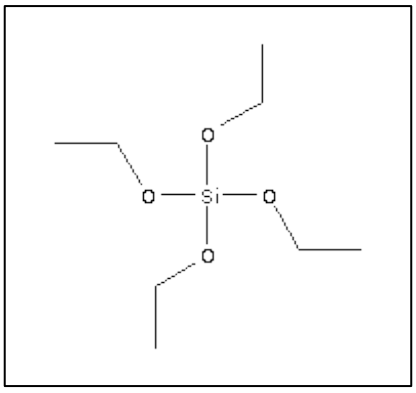

Fig. 2.5 – Chemical structure of TEOS. Adapted from [40]

Besides its usage in the KSE products it can also be used as crosslinking agent in silicone polymers, as a precursor to silicon dioxide in the semiconductor industry [41], for the synthesis of zeolites [42] and in the production of aerogel.

The tetraethyl orthosilicate has been studied and/or used in the consolidation of deteriorated granite stones affected by granular disintegration in several Portuguese monuments such as *Igreja São Pedro de Rates* [43], *Catedral* in Oporto [44], *Igreja Matriz* in Caminha [45] [46], *Igreja de Nossa Senhora da Lapa* [47] in Oporto and *Hospital da Santa Casa da Misericórdia de Viana do Castelo* [48].

3
METHODOLOGY

3.1. INTRODUCTION

In order to evaluate the effect of the application of KSE on mortars, a number of different methods has been considered, each of them measuring a different parameter that may, or may not, indicate the influence of this product regarding ettringite and thaumasite formation. On this study, it was decided to make destructive and non-destructive tests because, due to the impossibility to compare results with previous works, was important to do a great variety of tests in order to take the best conclusions possible about the KSE's application. Therefore, expansion measurements, mass loss/increase, strength loss/increase, elastic modulus variation and capillary network characterization were considered.

As it would be expectable, the use of different types of binders will offer different results in the end. As this work was performed in academic system, there was a time limit that precludes the study of all the possible binders so, it would be important to study, in the future, different binders in order to fully understand the effect of KSE's application on mortars/concrete. It is also important to refer that, not only different binders but also different water/cement ratios will lead to different results and, perhaps, different conclusions. Of course, to study all possible water/cement ratios would be utopian and, perhaps impossible, due to excess or lack of workability of the mortars, but it was decided to also study two different ratios during the realization of this work.

Concerning KSE's usage, the objective was to study as many as possible. Therefore all the KSEs in the lab's storage were considered. So, this work will contain results and conclusions of the application of KSE 100, KSE 300, KSE 510, KSE OH, all of them produced and distributed by Remmers, and KSE OH produced and distributed by Rajasil. The consideration of all of these KSEs is really important for the conclusions of the study because, all of them have different compositions, which can be of crucial importance to determine their effect regarding ettringite and thaumasite formation.

Although this work is mainly academic, the main aim and reason to perform this investigation is, of course, the "in situ" application of the product which can contribute to strengthen and protect the mortars where it is used. It is of the utmost interest to take lessons from this type of studies and apply them in "real life" problems in order to improve the knowledge and engineering practices on the field. This type of work contributes to the better understanding of new products and can lead to the loss of some obsolete engineering practices.

3.2. INITIAL CONSIDERATIONS

The scientific investigation work, as all the other types of investigation work, aims to fully understand the subject in study. Therefore, and on this concrete investigation, to fully understand the effect of KSE's application regarding ettringite and thaumasite formation it was important to study the KSE's effect on the surface and in the mixture.

With this desire, it was decided to produce flat prisms specimens with 40 mm x 40 mm x 160 mm with defined parts by mass of cement, sand and water/cement ratio. The first step was to study the flat prisms without the application of KSE: weight in dry state, calculation of density, determination of the dynamic elasticity module and compressive strength, characterization of the pore system and calculation of the water absorption coefficient. Then, the same tests were performed after the application of KSE on the surface of the flat prisms in order to compare the results.

To be able to study the effect in the mixture, it was settled that it was possible to perform soundness tests using the Le-Châtelier apparatus. The Le-Châtelier apparatus are moulds that consist of a 30 mm internal diameter, 30 mm high with two indicator stems which measure 165 mm from the points of the center line of the cylinder and O ring. With the Le-Châtelier apparatus, new specimens were produced and, gypsum and KSE were added to the mixture's composition. The soundness test, as all the tests conducted on the flat prisms, was performed in specimens with and without KSE.

The water/cement ratios in weight that were first decided to study were 0.5 and 0.7 but, during the production of the mortars, it was visible that 0.7 was not a viable ratio because the mortar produced did not have the needed workability. Therefore, it was then decided to try a mixture with 0.3 water/cement ratio but, this ratio also fail to acquire the desired workability. Given all this, the water/cement ratios that were studied were 0.5 and 0.4.

Points 3.4.1 and 3.4.2 deal only with the description of the flat prisms specimens. Points 3.4.3 and 3.4.4 deal with the Le-Châtelier apparatus samples.

3.3. SPECIMEN SELECTION

3.3.1. BINDER SELECTION

In the beginning of this work, one of the first, and perhaps one the most important steps was to choose the binder, among the large variety available that would best serve the purposes of this investigation.

This exercise had to be made in order to work with the binders that would offer interesting case studies. This means that the selection of the binder had to be made taking in consideration not only interesting comparisons between binders, but also good individual results per se that could broaden the range of conclusions. Therefore, the specimen selection lead to a challenge that was to define a standard binder for the flat prisms and a group of binders for the Le-Châtelier apparatus.

After doing a brief research in the laboratory storage, it was decided that the most representative binders for this work were:

- CEM I 42.5 (dw) (Where dw stands for "Dyckerhoff Weiss" that can be translated to Dyckerhoff white, being Dyckerhoff the name of the company of production) (Fig. 3.1);
- CEM I 42.5 R-HS/NA (Where HS stands for "Hoher Sulfatwiderstand" in German which can be translated as high sulfate resistance), or in European Standards referred to as SR. (Fig 3.2);
- CEM II/A-LL 42.5 N (Where LL stands for limestone, in this case 6 to 20% by mass) (Fig 3.3);
- CEM III/B N-LH/HS/NA (Where LH stands for low heat of hydration) (Fig. 3.4);

- CEM 42.5 N (Fig. 3.5);
- HSR Black label Tiefbohrzement (where tiefbohrzement can be translated as deep drilling cement and HSR stands for high sulfate resistance) (Fig 3.6).

Fig. 3.1 – CEM I 42.5 (dw)

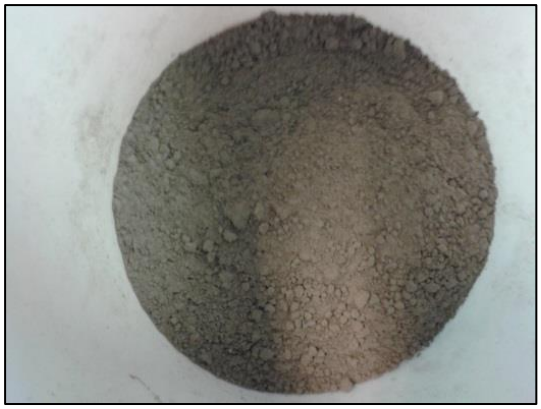

Fig. 3.2 – CEM I 42.5 R-HS/NA

Fig. 3.3 – CEM II/A-LL 42.5 N

Fig. 3.4 – CEM III/B N-LH/HS/NA

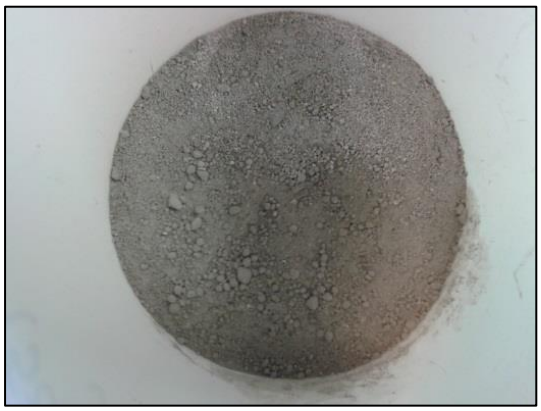

Fig. 3.5 – CEM 42.5 N

Fig. 3.6 – HSR black label Tiefbohrzement

With these different options in hand it was decided that the one that would be used for the flat prisms would be the cement 42.5 N. Even though the results with the other cements would be really interesting, the aim of the study of the flat prisms was to understand the effect of the application of KSE on the surface of the mortars so, and because it was impossible to make flat prisms for the six

cements in study, it was decided to use one of the most used cements "in situ" – or even the most used in some countries –, the cement 42.5 N.

Concerning the Le-Châtelier apparatus, all the cements will be used and comparisons will be made not only between results in different cements, but also, between the mixture composition with and without KSE.

It is expected to obtain interesting results among them all, since all the Portland Cements (Cement type I) have different Clinker percentages by mass, visual aspect, resistance to the penetration of external agents and strength gain ratio. Furthermore, the study also contains CEM II and CEM III, being the first one, accordingly to the definitions presented by NP EN 197-1 (2001), a Portland limestone cement, and the second one a blastfurnace cement which can relevantly contribute to enlarge the range of results. Finally, the study also counts with a Cement whose use is not so typical "in situ", since is a very expensive cement because of is really high performance – the HSR black label tiefbohrzement – that can also lead to results that, probably, would not be possible to obtain with the other cements.

From now on, in this work, the cements in study will be referred by acronym that is used to store them in the lab. So, all the cements acronym will start by the letter Z, which stands for "Zement" in German, and its number of storage:

- Z556 - CEM I 42.5 (dw);
- Z554 - CEM I 42.5 R-HS/NA;
- Z558 - CEM II/A-LL 42.5 N;
- Z557 - CEM III/B N-LH/HS/NA;
- Z559 - CEM 42.5 N;
- Z555 - HSR Black label Tiefbohrzement;

3.3.2. KSE SELECTION

Following the decision of choosing the most adequate binders to perform the work, it was also necessary to make a selection of which Silicic Esters – KSE – would be used.

The available Silicic Esters on the lab were:

- KSE 100 by Remmers;
- KSE 300 by Remmers;
- KSE 510 by Remmers;
- KSE OH by Remmers;
- KSE OH by Rajasil;

All the KSEs are described as stone strengtheners on a silicic acid ester base. And some of their shared properties are the non-yellowing, good penetration, high penetration depth and no hydrophobizing effect. The differences between all of them reside on the active ingredient content and in the gel deposit ratio. These values can be found in Table 3.1.

Table 3.1 – Description of the KSE used

	KSE 100	KSE 300	KSE 510	KSE OH	KSE OH Rajasil
Active Ingredient Content	20%	100%	100%	75%	75%
Gel deposit ratio	10%	30%	40%	30%	-

Regarding the KSE produced by Rajasil, it was impossible to know what its gel deposit ratio was because this company does not include that information on the product sheet.

As it can be seen on Table 3.1 the KSE 100 is really different, in composition, from the others and, of course, its usage is also different. While KSE 300, 510 and both OH are described as having a range of use for weathered, friable, medium-pored natural stone, particularly sandstone as well as cast stone, renders and mortar joints, the KSE 100 use is for especially fine-pored stone such as Baumberg sandstone. The low gel deposit rate prevents over-strengthening and it is described as a soft strengthener.

Due to the diversity of composition among the KSEs it was decided that all of them would be studied both in the flat prisms application and in the Le-Châtelier apparatus.

3.4. SPECIMEN CASTING AND KEPING

3.4.1. SPECIMEN CASTING: FLAT PRISMS

All specimens were produced according to DIN EN 998-1 (2003).

As said before, it was decided to produce specimens with different water/cement ratio and, after some attempts to make specimens with water/cement ratio in weight (W/C) of 0.7 and, afterwards 0.3, that reveled themselves pointless because of the lack of workability of the mortars. Mortars with 0.5 and 0.4 water/cement ratios were produced. The constituents considering each binder are:

- 0.5 W/C ratio mortar:
    - 450g of cement;
    - 1350 ± 5g of normalized sand;
    - 225g of water;

- 0.4 W/C ratio mortar:
    - 450g of cement;
    - 1350 ± 5g of normalized sand;
    - 180g of water;

With all the mortar constituents prepared and weighted correctly within the tolerance limits, the mixing process can begin.

All the mortars were prepared according to NP EN 196-1 (2006) and, there were produced 36 specimens with 0.5 W/C ratio, 35 with 0.4 W/C ratio and also, 3 specimens with 0.3 ratio (this 3 were produced while the investigation, about which W/C ratio that would be chosen to work with, was ongoing). Figures 3.7, 3.8, 3.9 and 3.10 could help to understand the production of the specimens.

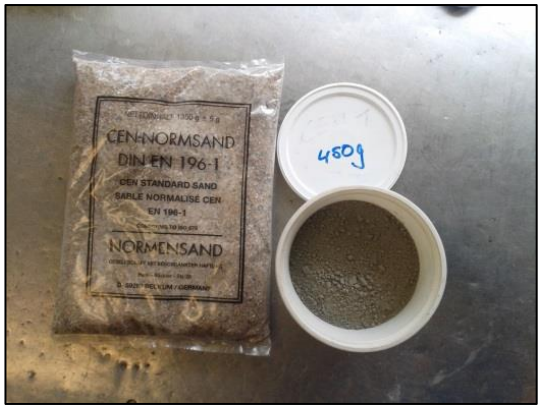

Fig. 3.7 – Cement and Normalized Sand

Fig. 3.8 – Mixer used in the production

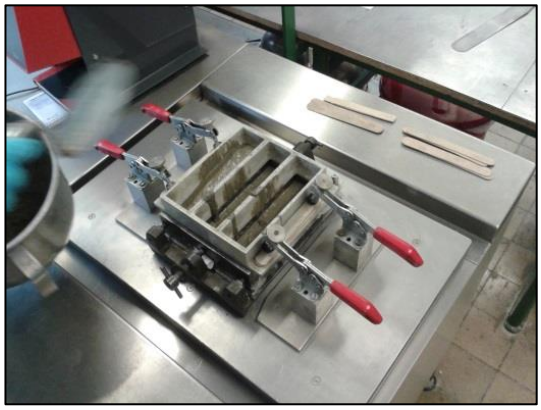

Fig. 3.9 – Vibrating table and molds

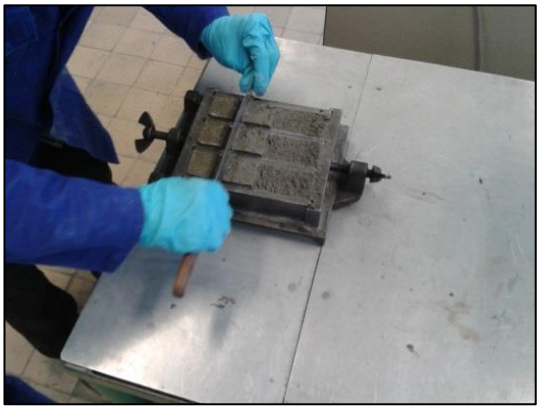

Fig. 3.10 – Flat Prims in the molds

3.4.2. SPECIMEN STORAGE: FLAT PRISMS

When the casting process is over, all the specimens must go through a curing stage to achieve required strength and follow what is required in the Portuguese and European Standard NP EN 196-1 (2006).

This same standard requires that, during the next 24h after the molding process is finished, the molds are placed inside a humidity cabinet, with moist air reaching all faces of the mold and no molds being placed over each other.

Always according to NP EN 196-1 (2006) immediately after de-molding (Fig 3.11), each batch of prisms was immersed in water and stored in a controlled environment room for 28 days. This room has a constant temperature of 20º C and a constant relative humidity of 50%. The purpose of this procedure is to keep the hydration processes happening for that period, in perfect conditions in order to have the specimens properly cured for the beginning of the tests.

All prisms were stored in white rectangular boxes, with 200 x 400 mm^2 dimensions. Inside them, supports were placed in order to maintain prisms separate from each other and the box itself.

When the date was due, all specimens were removed from their boxes, weighted and then stored in shelving in the lab as illustrated on Figure 3.12.

Fig. 3.11 – Flat Prims after being de-molded

Fig. 3.12– 28 days old flat prisms

3.4.3. SPECIMEN CASTING: LE-CHÂTELIER RINGS

As stated before, the expansion test that will be performed via the Le-Châtelier apparatus, took a really important role in this work. This subject should have been treated and described as a test, it was decided that due to its importance to the work, the Le-Châtelier cement cylinders, would also be treated as specimens.

The same water/cement ratios of the flat prisms were intended to be adopted but, it was impossible, due to the use of different cements and, consequently, different compositions and hydration heat, to be able to produce specimens with 0.4 water/cement ratio. As said before, this is an investigation work, and many decisions idealized theoretically are not possible to realize practically. Therefore, all the Le-Châtelier specimens were produced with 0.5 water/cement ratio, independently, of the cement type used. The constituents of the specimens are the following:

- Specimens without KSE
  - 50g of cement;
  - 33g of gypsum;
  - 25g of water.

- Specimens with KSE
  - 50g of cement;
  - 33g of gypsum;
  - 25g of water;
  - 2g of KSE.

With these constituents were produced two rings for the same combination of cement or cement plus KSE in order to always have an available comparison and a backup sample if some error occurs and a sample have to be discarded. Due to the lack of Le-Châtelier apparatus in the laboratory, and, of course, the time deadline, only 3 KSE, (KSE 100, KSE 300, KSE OH from Remmers) could have been study which performs a total of 48 rings or, 24 pairs of rings.

Gypsum was added to the mixture in order to favor the process of ettringite and thaumasite formation since, after finalizing the expansion test provided by the Le-Châtelier apparatus, the specimens will be

analyzed with the Scanning Electron Microscopy and with X-ray diffraction. (This will be described and discussed later on the development of this work).

All the specimens produced for the Le-Châtelier apparatus can be observerd in the appendix A5.

3.4.4. SPECIMEN STORAGE: LE-CHÂTELIER RINGS

After 24h, the cement setting is complete and the process of casting reaches its end therefore, all the specimens must go through a curing stage to achieve required strength.

The specimens were also stored in white rectangular boxes, with 200 x 400 mm^2 dimensions with water with approximately 8mm high. Inside them, supports were placed in order to maintain the rings separate from each other and the water in the box's bottom and to keep the sufficient space in order to the two indicator stems of each ring could move without hitting any kind of obstacle.

The boxes were then stored in a special room that has a constant relative humidity of 50% and a constant temperature of 20º C. This conditions are, as said before, the most suitable to favor the happening of the hydration processes during the period.

Is also important to refer, in which concerns the specimen storage that during the curing stage, measurements of the distance between the two indicator stems were realized, which means that during that time they were taken away for the storage and the boxes. These measurements aim to determine the soundness of the cement and will be discussed and analyzed in 3.12.

3.5. APPLICATION OF KSE ON FLAT PRISMS

3.5.1. INITIAL CONSIDERATIONS

It is important to include this point in the work before starting to describe the methodology inherent to the tests performed because, all the tests that will be described in the next points of this chapter were performed first in the samples prior to the application of the KSE, and after, in samples were KSE was applied (usually, also plus a control sample without KSE).

It is also important to refer that, there is no standards or guidelines for the application of the products in study. Given this, the method that will be describe for the application may not be the most accurate one and, in further investigations it can be improved or rethought. Even though, no problems were detected.

3.5.2. APPLICATION OF KSE ON FLAT PRISMS

Before starting to apply the KSEs on the flat prisms, the prism were weighted and their mass determined. After that, and as stated before on point 3.3.2, five KSEs were studied per each one of the water/cement ratios. It was decided that five specimens for each one of the KSEs would be enough to perform all the tests planed, and so, 25 specimens per water/cement ratio were separated and organized in groups of five specimens.

Afterwards, the KSE was applied on the prisms. The application method was the same to all the prims and consists of the following:

One of the prims' faces (other than the one of the molding direction) was carefully sanded with sanding paper. After, using a paint brush that was impregnated with KSE (previously taken for the

recipient using a pipette), the prisms were brushed, always in the same direction, approximately 3 times (depending on the person that was brushing the prisms) until the visual sensation that the prisms' surface was wet. Then, approximately 10 minutes after the first application, (10 minutes was the theoretical estimated time for the KSE to penetrate the prism but, during the practical application was visually obvious that some of the KSE took more time than others to be absorbed. For example, the KSE 510 besides having a really stronger smell than the others, took at least 25 minutes to penetrate the prisms) this procedure was once again done. After the second application was done and after waiting the necessary time to the surface to appear dry (as said before, approximately 10 minutes, but varying for specimen to specimen and, of course, for KSE to KSE), a third and last time procedure was done. After this, the specimens were stored at standard temperature and standard relative humidity, and were allowed to dry at rest during 28 days.

3.6. DYNAMIC E-MODULUS TEST

3.6.1. MEASUREMENT FREQUENCY

The measurements of this test, as well as all the other conducted in this work, were first done in the specimens without the application of the KSE and, later, they were, once again, done to achieve the results after the application of the KSE. The first measurement was after 28 days and was performed in 6 specimens (3 with W/C ratio of 0.4 and 3 with 0.5). The second one was performed at 91 days (or 28 days after the application of a layer of KSE on one of the prisms' surface) and, this time, 30 specimens were measured. The 30 specimens can be divided in groups of 3 specimens for each of the 5 KSE in study per the two water/cement ratios in study.

3.6.2. PRIOR MEASUREMENTS TO THE TEST

Before starting the dynamic E-Modulus test, some measurements have to be done. The samples were measured 3 times in each direction using a digital caliper rule and the average length, thickness and height were determined. Also, the samples were weighed and, therefore their mass was also determined. With these values the bulk density of the samples was calculated by:

$$\rho = \frac{m}{V} \tag{7}$$

Where,

- ρ is the bulk density of the prism, in g/cm^3;
- V is the volume of the prism, in cm^3;
- m is the mass of the prism, in g.

3.6.3. TEST DESCRIPTION

The dynamic E-Modulus determination for the flat prisms was made using the method described in the NP EN 14146 (2006) standard, the continuous excitation method. Even though, this standard is for natural rocks and not for mortars/concrete, its application is possible because the principle is the same. It's also important to refer that, this standard is only referenced here as a theoretical and guideline

support because the procedure described was not fully followed during the realization of the tests. The specimens were measured at the dates established before.

The dynamic Elastic Modulus is obtained in this test by measuring the resonant frequency of each prism. This is done using a proper apparatus for this purpose, a resometer. The resometer is composed by an emitter, a receiver and a support for the prism, all of these in an external vibration free system. The data values can then be read in dials that show the applied frequency at the time and the correspondent amplitude from it. The emitter is then positioned in different positions in the prims in order to obtain the longitudinal, torsional and flexural frequencies. The final value, and the value of interest in this test, is to obtain the frequency to which the amplitude measured is higher, as it befits the notion of resonant frequency.

The value of the Dynamic Elastic Modulus is expressed in the standard NP EN 14146 (2006) by the equation:

$$E_d = 4 \times 10^{-6} \times l^2 \times F^2 \times \rho \quad (8)$$

Where,

- E_d is the dynamic E-modulus value, in MPa;
- l is the length of the prism, in millimetres;
- F is the measured frequency for the maximum amplitude, in Hertz;
- ρ is the bulk density of the prism, in kg/m^3

The apparatus used to perform the dynamic E-Modulus test is presented in Figures 3.13 and 3.14.

Fig. 3.13 – Dynamic E-Modulus test

Fig. 3.14 – Frequency measurement equipment

3.7. CAPILLARY RISE TEST

3.7.1. MEASUREMENT FREQUENCY

All the measurements performed during this test were done according to the DIN EN 1015-18 (2003). The specimens were measured before they were putted in water, and after that were measured after 5, 10, 20, 30, 60, 360 and 1440 minutes. Also, and like, the dynamic E-Modulus test, the measurements were performed at 28 days in samples with no KSE application and at 91 days (or 28 days after the KSE application). In the first measurement, the capillary coefficient, C, was calculated for 4

specimens (two with 0.4 W/C ratio and two with 0.5 ratio) and, on the second measurement the capillary coefficient was calculated for 24 specimens, two per each of the five KSEs in study plus two specimens without KSE applied, for the two water/cement ratios in study.

3.7.2. Specimens Preparation

Before starting to perform the capillary rise test, all the samples needed to be prepared for the test. Following the guidelines contained in the DIN EN 1015-18 (2003), all the samples endure some procedures in order to attain the best results in the capillary rise test.

First, a face of each of the flat prisms specimens involved in the test was selected and was sanded using adequate sanding paper. This face will be the one that will be in direct contact with the water and will be the vehicle for the water rise by capillarity. The opposite face to the one selected was left untouched. The rest of the faces of the prisms needed to be sealed and, with this purpose, liquid paraffin wax previously heated until the melting point (between 47º C and 64ºC) was used. Pure paraffin wax is an excellent electrical insulator, with an electrical resistivity of between 10^{13} and 10^{17} ohm meter (Ω.m). The paraffin wax was applied in the surfaces until a layer of paraffin was formed and fully involve the face leaving no parts without wax.

3.7.3. Capillary Rise Test Description

The capillary rise test for the determination of the capillary coefficient of the flat prisms was made using the guidelines and procedures described in the DIN EN 1015-18 (2003) standard.

The coefficient of capillary absorption is determined using the prescribed prismatic mortars specimens at standard atmospheric pressure conditions. After the specimens dry to constant weight, a surface of the test sample is immersed in water, for a specified period (described in 3.6.1), at 5 to 10 mm. Subsequently, the mass increase is determined. After that, it is possible to determine the water absorption coefficient using an expression adapted from the standard:

$$\mathrm{C} = \frac{0.001}{(0.04 \times 0.16)} \times (M_3 - M_o) \quad (9)$$

Where,

- C is the water absorption coefficient, in Kg/m^2;
- M_3 is the mass of the specimens after 24h in water, in g;
- M_0 is the mass of the dried specimens mass before immersed in water, in g.

The following picture (Fig 3.15), withdrawal from the DIN EN 1015-18 (2003) standard, helps to better understand the test.

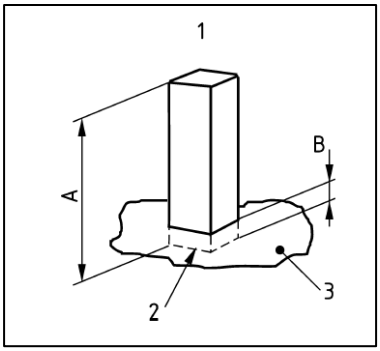

Fig. 3.15 – Capillary rise test Explanation in the DIN EN 1015-18 (2003) Standard

Where,

- 1 refers to the prism;
- 2 is the immersed face of the specimen;
- 3 is the water used to perform the test;
- B is the water height: between 5 and 10 mm;
- A is the prism length.

Once again, the standard helps to understand the test, but not all the requirements were fully followed. The prisms were place horizontally, which means that the surface that was in contact to the water was a rectangular one (instead of the square one in the picture) with dimensions of, approximately, 160 x 40 mm.

Also, when the KSE was applied in one surface of the prisms, when the test was performed again, that surface was selected as the opposite of the one that would be in direct contact with water, and, of course, all the others were sealed with the paraffin wax, as described before.

3.8. 3-POINT BENDING TEST

3.8.1. MEASUREMENT FREQUENCY

As well as the previous test, the 3-point bending test was conducted first on specimens without the application of KSE and second on specimens with KSE applied. The first test was performed in three samples per water/cement ratio, at the age (of the specimens) of 56 days. The second measurement was done at 93 days (It was idealized to be performed at 91 days, but the date coincided with a weekend and, therefore, the laboratory work was not possible) and, 36 specimens were studied. This value corresponds to 3 specimens for each of the five KSE in study plus 3 specimens for control (without KSE) per each of the water/cement ratios.

3.8.2. CONSIDERATIONS

Normally, the 3-point bending test, also known as, simply, flexural test, is more used in plastic and metallic materials and aims to provide values for the elasticity modulus in bending, flexural stress, flexural strain and flexural stress-strain response of the material in study. In this work, the test was carried out until the specimens fracture and the stress that leads to that fracture was determined. This fracture occurs along the outermost sample edge, which is under a tensile load.

The 3-point bending test, was followed by the compression test (which will be described in 3.9), therefore, it also worked as a specimen preparation for that test.

It is also important to refer that, standards like ISO 12135 (2002), ASTM E1290 (2008), ASTM D790 (2010), ISO 12737 (2010) and ISO 178 (2010) were important guidelines for the test but, as it was expected since they provide guidelines for different materials from the ones in study, were not fully followed.

The equipment used to carry out the test has a capacity of 10 kN.

3.8.3. 3-Point Bending Test Description

The 3-point bending test, as well as the 4-point bending test, characterizes the behavior of a slender structural element subjected to an external load applied perpendicularly to a longitudinal axis of the element, as demonstrated in Figures 3.16 and 3.17.

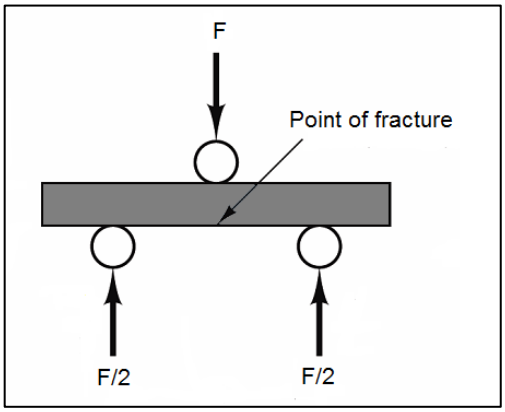

Fig. 3.16 – 3-point bending test

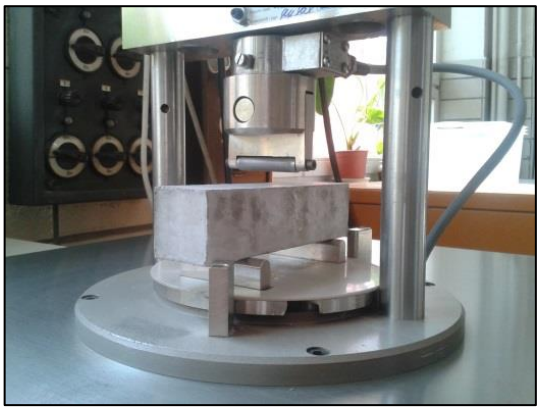

Fig. 3.17 – 3-point bending test

After the specimens are placed in the position shown above, the load is applied with and increase ratio of 50 ± 10 N/s until the fracture of the specimen. Later on, the flexural strength or modulus of rupture (σ_{bz}) is determined using the equation for rectangular cross sections:

$$\sigma_{bz} = \frac{3FL}{2bd^2} \quad (10)$$

Where,

- F is the Load at the rupture, in N;
- L is the support span, in mm;
- b is the width of the cross section, in mm;
- d is the height of the cross section, in mm.

As stated before, more properties can be calculated by the use of the 3-point bending test but, their determination will not be described, since the only measurement done by the means of the 3-point bending test was the flexural strength/modulus of rupture.

3.9. COMPRESSION TEST

3.9.1. MEASUREMENT FREQUENCY

The compression test and the 3-point bending test should have been, perhaps, described together since in this work development they were made sequentially and the specimens used in the compression test were the ones provided by the 3-point bending test.

Comprehensibly, after endure the 3-point bending test, the specimens were broke in two approximately by the middle, which results of specimens with approximately 80 mm x 40 mm x 40 mm that were used in the compression test.

Naturally, the measurement frequency or in this case the measurement days, were the same for both the 3-point bending test and the compression test. Therefore, the first test was conducted at 56 days and the second one at 93 days (these days represent the age of the specimens). As is understandable, the number of compression tests doubled the number of 3-point bending test, but, unfortunately not all the test produced good results due to not acceptable ruptures.

3.9.2. CONSIDERATIONS

As the specimens used in this test were the ones that result for the 3-point bending test, their dimensions were not accordingly with the NP EN 12390-1 (2003) standard but, taking in consideration the annex B of the same standard, the specimens were tested.

The NP EN 12390-3 (2003) standard was used as a guideline to the tests conducted. It is important to refer some procedures that are crucial for the test to occur without any trouble. All the specimens' surfaces were cleaned and the specimens were always placed in the machine in a position that enables the load to be applied perpendicularly to the molding direction. This is important because if the compression test machine notices the irregularities in the surface (that may or may not be associated to the molding direction) it will automatically stop and the test will be, probably, discarded. With this in mind, the test machine was also cleaned after every test.

3.9.3. DESCRIPTION

The principle of this test is simple to understand. Specimens are tested until the rupture in a compression test machine. Then, the maximum load supported by the specimen is registered and the resistance to compression is calculated.

The equipment used to perform this test has a capacity of 300 kN and the compression load speed applied was, according to the standard, 2400 N/s.

It is important to dissociate the rupture types that can be accepted and the ones that cannot. Figures 3.18 and 3.19 will help to understand the differences.

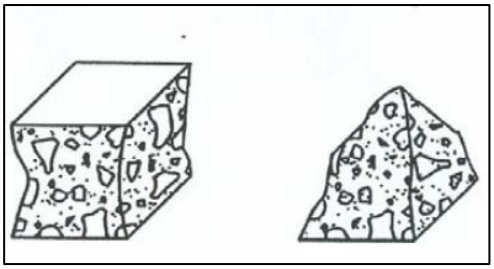

Fig. 3.18 – Accepted types of ruptures

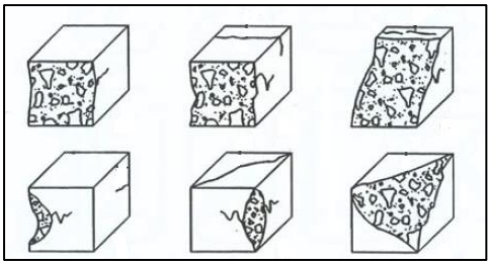

Fig. 3.19 – Non accepted types of rupture

After perform the tests and dissociate the ones that can be accepted from the ones that cannot, it's time to calculate the compression resistance, σ_d, of the specimens by the equation:

$$\sigma_d = \frac{F}{A_c} \tag{11}$$

Where,

- σ_d is the compression strength/resistance, in MPa;
- F is rupture load, in N;
- A_c is the cross section area, equal to 1600 mm^2.

Figures 3.20 and 3.21 show the specimens prior to the test and after the test (with an acceptable type of rupture), as well as the test machine used.

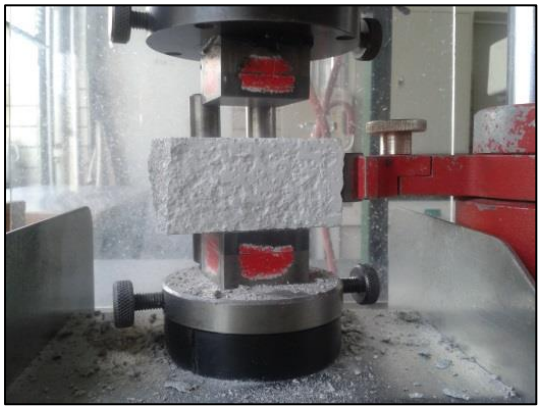

Fig. 3.20 – Specimen prior to the test

Fig. 3.21 – Acceptable rupture after the test

3.10. MERCURY POROSIMETRY TEST

3.10.1. CONSIDERATIONS

The Mercury porosimetry is an extremely important characterization process for porous materials. Since many specimens' porous network was intended to be studied, the mercury porosimetry test was select whereas a complete analysis can be done in approximately half an hour. This test provides a large variety of important information, which cannot be determined by the use of any other porosity

characterization technique, such as, the pore size distribution, the total pore volume or porosity, the skeletal and apparent density, and the specific surface area of a sample. Although all this information could be determined with this method, it is commonly used for only determine the pore size distribution and the percent porosity of the sample.

The most known limitation of this test resides on the fact that this method measures the largest entrance towards the pore however it does not measure the actual inner size of a pore. Comprehensibly, the test also fails to closed pores, since the mercury has no way of entering that pore.

Also, it is important to refer that the assumption of a cylindrical pore geometry by the means of the Young-Laplace equation (Commonly known as Washburn equation [49]) shown below can also lead to major differences between the actual pore network and the analysis.

$$\Delta P = \frac{2\gamma \cos\theta}{r_{pore}} \tag{12}$$

Where,

- ΔP is the pressure difference across the curved mercury interface;
- γ is the surface tension of mercury;
- r_{pore} is the pore radius;
- θ is the contact angle between the solid and mercury.

These differences can be explained because the real pore shape can be, indeed, quite distinct from the one assumed.

3.10.2. Sample Preparation

The samples selected to this test were, once again, prepared from the flat prisms specimens. From the surface where the KSE was previously applied (as described in point 3.5), samples with approximately 5 mm of maximum dimension were cut off like it is exemplified in Figure 3.22. Figure 3.23 shows the samples with approximately 5 mm of maximum dimension that were after tested by the mercury porosimetry technique.

Fig. 3.22 – Samples preparation

Fig. 3.23 – Mercury porosimetry test samples

One of the most important concepts to keep in mind during the samples preparation is their weight. As it is easily understandable, porous materials are prone to absorb water or other types of fluids/chemicals. Therefore, the samples were dried, during one day, at 35º C.

For this test only 12 samples were tested: 6 per water/cement ratio being 5 with the different KSE applied and one without KSE for control.

3.10.3. TEST DESCRIPTION

Mercury does not wet the majority of the substances and will not penetrate pores by capillary action. Therefore it must be forced into the pores by the application of external pressure. Comprehensibly, the required pressure is inversely proportional to the size of the pores, as only slight pressure is required for mercury to penetrate into large macropores, whereas much greater pressures are needed to force mercury into small pores (or micropores). Logically, the pressure required to penetrate the porous is strictly controlled during the progressive intrusion of mercury into the sample's porous. Then, from the pressure versus intrusion data, the instrument generates volume and size distributions using the Washburn equation as described in point 3.10.1 and the volume of pores in the corresponding size class is known.

The volume of mercury that intrudes the pores is measured using a mercury penetrometer (an electrical capacitance dilatometer), which can detect changes in mercury volume under 0.1μL.

The penetrometer is formed by an insulator (glass) and filled with a conductor (mercury). Also, the steam of the penetrometer is a capillary that acts like a reservoir for the analytical volume of mercury. This steam is plated with metal (also a conductor) which is separated from the other conductor (mercury) by the insulator (glass) forming, therefore, a coaxial capacitor. As the applied pressure pushes mercury into the sample, mercury inside the steam decreases as well as its capacitance. Therefore, the decrease of capacitance is proportional to the volume of mercury leaving the capillary with each change in pressure. The following Figure 3.24 adapted from Micromeritics Instrument Corporation will help to better characterize the mercury penetrometer.

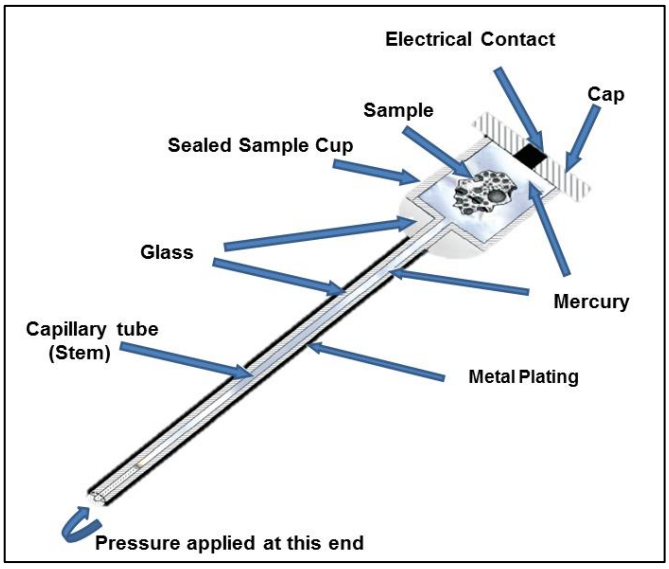

Fig. 3.24 – Cross section view of a mercury penetrometer adapted from [50]

3.10.4. SUMMARY REPORT AND KEY SPECIFICATIONS OF THE TEST

Tables 3.2, 3.3 and 3.4 show the parameters concerning the penetrometer ((07) 5 Bulb, 0.392 Stem, Solid), mercury and low pressure, respectively. Table 3.5 contains a summary of the intrusion data. Also it is important to refer that no blank corrections were performed from 0 to 206,0MPa.

Table 3.2 – Penetrometer parameters

Pen. Constant	10,898 μL/pF
Stem Volume	0,392 mL
Pen. Volume	5,921 mL
Pen. Weight	69,110 g
Max. Head Pressure	0,0307 MPa
Assembly Weight	129,191 g

Table 3.3 – Mercury parameters

Adv. Contact Angle	141,300º
High Surface Tension	485,000 dyn/cm
Rec. Contact Angle	141,300º
Density	13,539 g/mL

Table 3.4 – Low pressure parameters

Evacuation Pressure	50 µmHg
Evacuation Time	5 mins
Mercury Filling Pressure	0,0034 MPa
Equilibration Time	10 s

3.11. KSE PENETRATION DEPTH

3.11.1. CONSIDERATIONS

It was important for the study to measure the KSE penetration depth into the specimens. This test although simple offered a lot of difficulties because, there is no standard indicator (like, for example, phenolphthalein indicator to measure the carbonation depth) to measure the KSE penetration. Given this, the indicator had to be synthetized in the lab. A lot of indicators were done and tested in disposable samples in order to understand if their behavior was the most suitable to the work in progress. After many tests were conducted, the indicator was found. This was obtain because the KSE solutions contain Tin (Sn) at very low concentrations as catalyst. Tin is a malleable, ductile and highly crystalline silver-white metal. It is known that Dithizone (also known as Diphenylthiocarbazone), a sulfur-containing organic compound that is traduced by the molecular formula of $C_{13}H_{12}N_4S$ and whose IUPAC name is (1E)-3-anilino-1-phenylimino-thiourea, forms complexes with heavy metal ions, which are insoluble in water but soluble in solutions of carbon tetrachloride. The dithizone solutions have a characteristic color that, in this case is red (or approximately red), and is marked in Figure 3.25 as X.

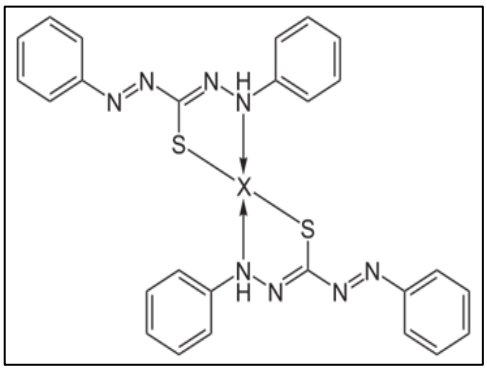

Fig. 3.25 – Dithizone indicator with marked color X

3.11.2. MEASUREMENT FREQUENCY

This test was performed between the 3-point bending test (3.8) and the compression test (3.9). All the specimens that were broke by the 3-point bending test were sprayed with the dithizone indicator before they were subjected to the compression test. Comprehensibly, and accordingly to points 3.8.1 and 3.9.1, only the samples that had been previously prepared with KSE were subjected to the KSE penetration depth test. Given this, the measurements were done at 93 days and 60 specimens were studied, 30 per each of the water/cement ratios with 6 specimens per KSE.

3.11.3. TEST DESCRIPTION

After the specimens endure the 3-point bending test, they were sprayed with the dithizone indicator and the depth of penetration was determined using an digital caliper, measured in the cross section obtained by the fracture induced by the 3-point bending test from the surface where KSE was previously applied until the end of the red coloration, was determined using an digital caliper. Later on the development of this work, when the results and their inherit discussion were presented, it will be understandable that the digital caliper become obsolete to the measurements and was not used to perform them. However, since this was the procedure that was previously idealized to perform this test, it's important to describe it in this way.

3.12. EXPANSION TEST

3.12.1. CONSIDERATIONS

To perform the expansion test, the Le-Châtelier apparatus was used. The samples were previously prepared as described in points 3.4.3 and 3.4.4.

It is important to explain, before the description of the test, the decision of adding calcium sulfate (gypsum) in the specimens' mixture. In the hydration of Portland cements, C_3A and gypsum form ettringite. During the ettringite formation, the amounts of ettringite and gypsum are inversely proportional. Therefore, the continued ettringite formation consumes the gypsum and an ettringite network thus replaced the solid network of gypsum. Comprehensibly, when all the gypsum, and thus the sulfate, is consumed, the amount of ettringite reaches its maximum level. [51]

If the system contains insufficient amounts of sulfate in comparison to the equivalent amounts of calcium and aluminium to form ettringite, the remaining C_3A reacts with water and forms monosulfate (sulfate- AFm) by consumption of the ettringite. [52]

Gypsum addition aimed to favor the specimens' ettringite and thaumasite formation and, consequently, the specimens' expansion. This decision also took in consideration that the specimens would also be used in the SEM and XRD analyses (described in 3.13 and 3.14, respectively).

3.12.2. MEASUREMENT FREQUENCY

Twenty four hours after the specimens casting, the expansion between the two indicator stems was measured. This procedure was also performed after 3, 4, 7 and 28 days for all the specimens. Measurements at 11 and 17 days were also performed but the first one was only performed on the specimens without KSE applied an on the specimens with KSE 300 and KSE OH and, the second one was only carried out on the specimens with KSE 100. It is also important to refer that a last measurement was done in all the specimens, before they were demolded and broken in order to prepare samples for the Scanning Electron Microscopy and the X-Ray powder diffraction, at 35 days.

3.12.3. TEST DESCRIPTION

The test was easily performed using a ruler and measuring the difference, in millimeters, between the two indicator stems at the days referred in point 3.12.2.

3.13. SCANNING ELECTRON MICROSCOPY TEST

3.13.1. INITIAL CONSIDERATIONS

The application of the Scanning Electron Microscopy (SEM) in petrographic analysis of cementitious materials and concrete microstructure [53], [54], [55] is becoming increasingly common nowadays. This increase in usage can be explained taking in consideration that SEM provides better detailed images of the microstructure than the stereo and optical microscopy, previously used in this type of analyses.

The main advantages of this test are the high-contrast images of the microstructure, the high spatial resolution of the images, and the ability to perform simultaneous imaging and chemical analysis.

The procedure principle of the test is that SEM scans a focused beam of electrons across the specimen and measures any signal resulting from the interaction between the electron beam and the specimen. There are three types of imaging modes that can be used in the SEM:

- Secondary electrons;
- Backscattered electrons;
- X-Ray.

Only the first type of imaging modes, Secondary electron, will be described because it was the only one adopted in this work. Nevertheless, the other imaging type modes could also provide important results in further investigations conducted in this subject.

3.13.2. SECONDARY ELECTRON IMAGING

Secondary electrons (SE) are low-energy electrons produced as a result of an inelastic collision between a primary electron beam with an electron of an atom within the specimen. [56] The incident beam causes electron to be emitted from the sample due to elastic and inelastic scattering events within the sample's surface and near-surface material (Figure 3.26 illustrates in a simple way, this process). This beam can eject high-energy electrons or low-energy electrons.

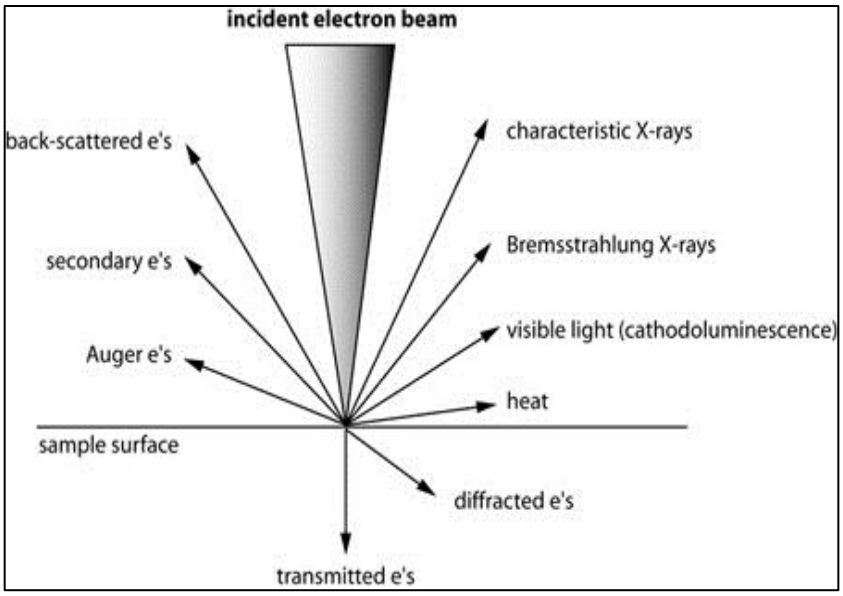

Fig. 3.26 – Interaction of electron beams with matter. Adapted from [57]

When an electron beam collides with a sample, electron scattering and photon and X-ray production develops in a volume (known as the electron interaction volume and represented in Figure 3.27) that depends on several factors. These factors include:

- The beam's energy (accelerating potential) increases the interaction volume however decreases the elastic scattering;
- The interaction volume decreases as a function of the mean atomic weight;
- Samples inclined relative to the electron beam develop smaller and more asymmetric interaction volumes.

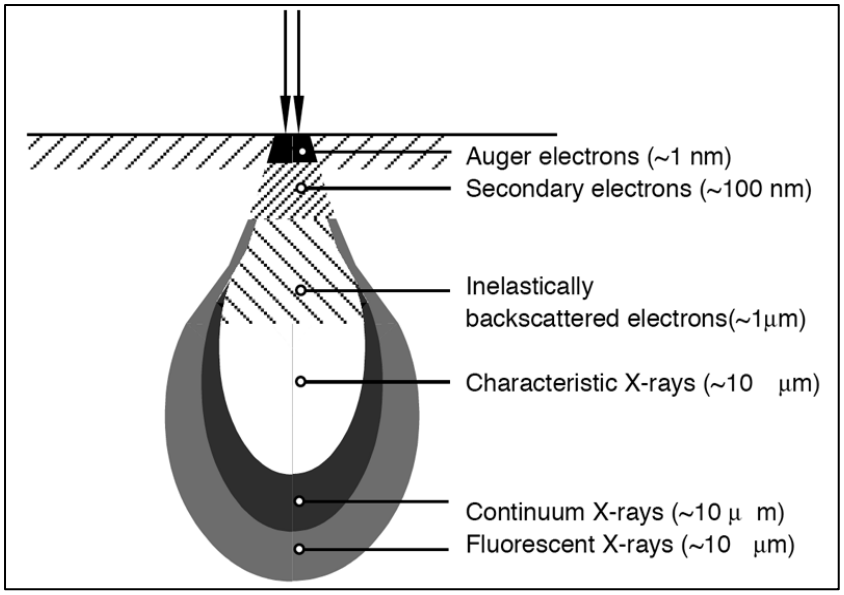

Fig. 3.27 – Interaction volumes is the depth range probed by the various types of scattered electrons and x-rays, where imaging resolution is dependent on the volume generated by the emission type. [58]

Besides being formed by the ejection of loosely bound electrons from the sample, the secondary electrons can also be formed by collisions with the nucleus, where substantial energy loss occurs. Commonly, secondary electrons energy is 50 electronvolt or less. Due to this low energy, the secondary electrons are readily absorbed and only those produced near the surface escape and produce detailed images of the surface topography. The apparent shadowing in images is a result of the absorption of the SEs by intermediary parts of the specimen.

In order to create an SEM image, the emitted electrons, for each position in the scanned area, are detected by an electron detector. The intensity of the emitted electron signal is displayed as brightness on a cathode ray tube (CRT). With the synchronization of the CRT scan and the incident electron beam scan, the CRT displays the morphology of the sample surface area scanned by the beam.

Secondary electrons imaging is therefore particularly useful in the examination of early-age paste microstructure, high magnification imaging, examination of secondary crystal growth and fragments of material that may be plucked from a larger specimen, and examination of aggregate texture.

3.13.3. Sample Selection

The samples used in the Scanning Electron Microscopy were selected among the Le-Châtelier rings described in point 3.4.3. First, and since the aim of this test is to understand the changes in the phases inducted by the application of KSE, a control sample was select. The control sample select was taken from the ring with CEM 42,5 N that had the biggest expansion at 28 days. The expansion at 28 days was an indicator for the samples selection because, it is expected that in the samples with bigger expansion, thaumasite and ettringite could be found easily among the phases. Then, among the specimens that had KSE in the mixture composition, were selected 6 rings that had the biggest expansion. The selection of 6 rings was decided because there was no time to perform a SEM analysis in all of the 36 rings with KSE in the mixture; also, it was only intended to perform the analysis in 5 rings (the ones with the biggest expansion) but, when the sample's selection occurred, a specimen that did not correspond to the ones with biggest expansion was taken for the analysis by mistake. This

mistake is not serious and could even be called as a fortunate mistake because it allowed to another KSE (OH) to be analyzed in the SEM, since all the 5 samples that had the biggest expansions had KSE 100 in the mixture.

According to the description above, the samples studied by SEM were:

- Z554;
- Z559 ;
- Z555 + KSE OH;
- Z556 + KSE 100;
- Z554 + KSE 100;
- Z558 + KSE 100;
- Z557 + KSE 100.

The samples expansion can be consulted in point 4.9 and in appendix A5.

3.13.4. SAMPLE PREPARATION

As said in previous point, the samples selected from the SEM test were taken from the Le-Châtelier rings. For this purpose, the rings were demolded and broken into 5 or 6 pieces, as it can be seen in Figure 3.28, and stored in a box for 14 days at a 20ºC temperature and 50% of relative humidity.

After the storage time, and before the test was performed, the specimens were, once again, cut and a small sample, as it can be seen in Figure 3.29, was collected and analyzed.

Fig. 3.28 – Samples before being cut to SEM test

Fig. 3.29 – Samples used in the SEM test.

Normally, when sample preparation for the SEM test is discussed, types of coatings are analyzed and described. The explanation of samples coating lies on the fact that nonconductive samples tend to charge when scanned by the electron beam and, especially in secondary electrons imaging mode, this causes scanning faults and other image errors. Therefore, the samples are usually coated with an electrically conducting material, commonly gold or gold-palladium but platinum osmium, iridium, tungsten, chromium and graphite can also be used.

Fortunately, the laboratory was equipped not only with SEM but also with ESEM (Environment Scanning Electron Microscopy) which allows the user to perform the analysis without having to do the coating and destroying the usefulness of the samples. The ESEM machine has a mode, the “wet”

mode, which enables the analysis on nonconductive samples. It is possible to image the sample, modify the sample, and image the sample again, *ad infinitum*, which cannot be done in coated samples. Basically, this can be achieved by introducing water vapor on the specimen chamber which neutralizes the charge induced by the beam. This process can be better understood with the help of Figures 3.30, 3.31, 3.32., and 3.33. Figures 3.34 and 3.35, which illustrate the equipment used and its key specifications were also added to this work and contribute to the best understanding of the methodology inherent to the test.

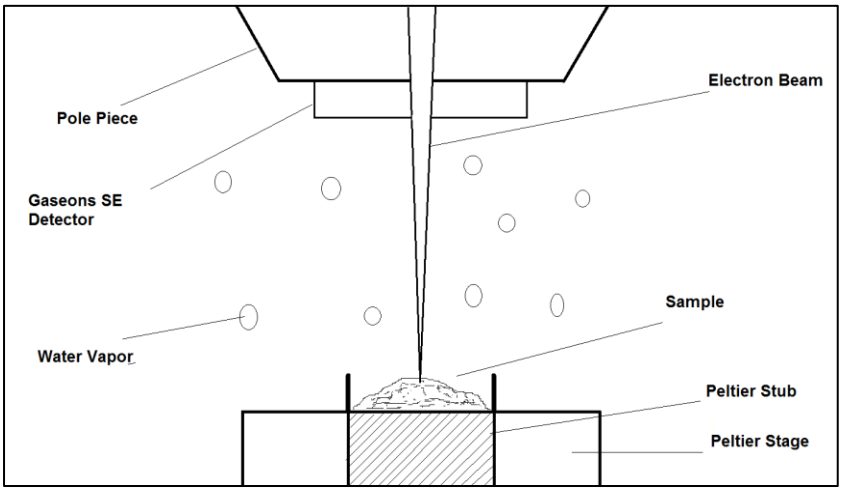

Fig. 3.30 – Description of an ESEM chamber

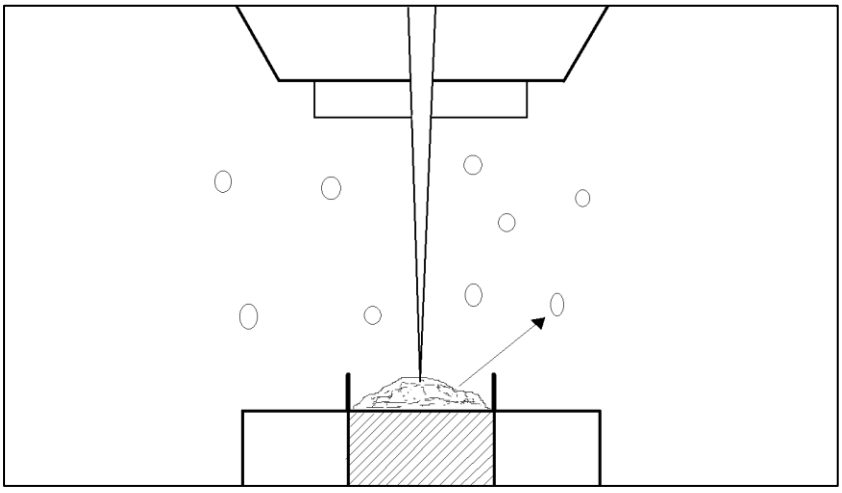

Fig. 3.31 – Secondary electrons ejected from the sample surface strike the water vapor molecules

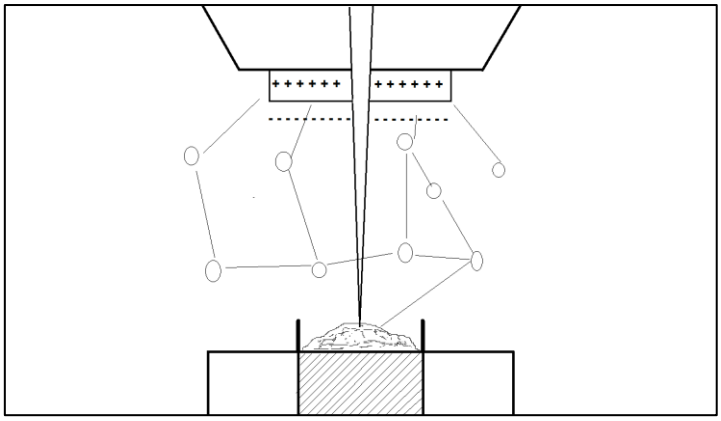

Fig. 3.32 – The water vapor molecules produced SE that then strike other water vapor molecules, creating a chain of electrons attracted to the Gaseous SE detector with positive charge

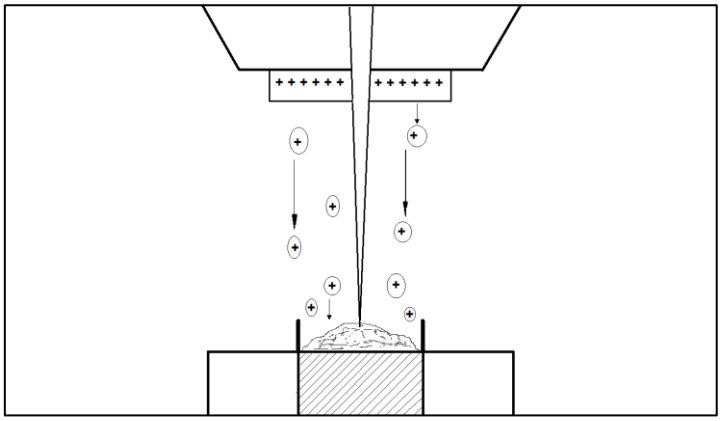

Fig. 3.33 – The positively charged water vapor ions (because of having lost a SE) are now forced towards the sample which is negatively charged, neutralizing the samples charge

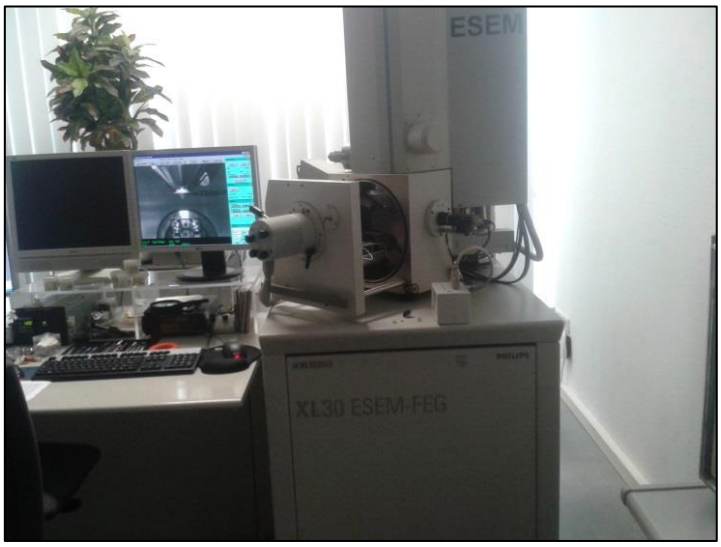

Fig. 3.34 – XL30 ESEM-FEG equipment used in the SEM test

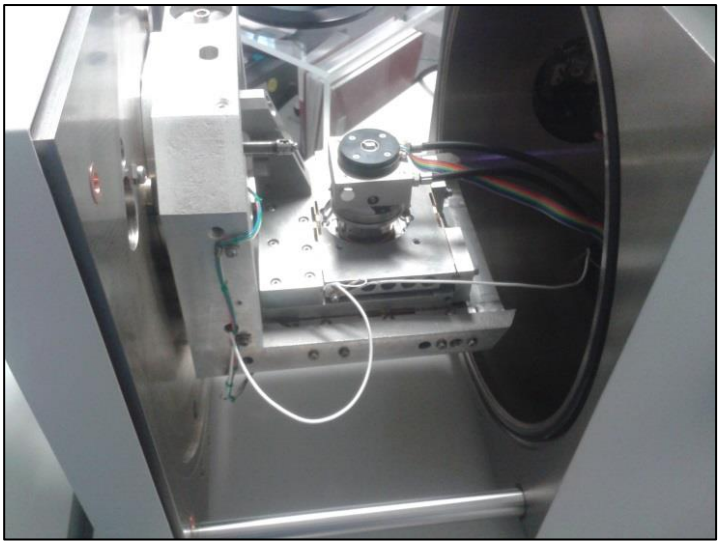

Fig. 3.35 – ESEM chamber with a sample

3.13.5. KEY SPECIFICATIONS OF THE EQUIPMENT

The key specifications of the equipment used to carry out the ESEM study were transcribed from the equipment's technical sheet and can be consulted below:

- SEM
  - Schottky FEG
- Detectors
  - SE and BSE
- Resolution
  - 2nm at 30KV
  - 5nm at 1KV
  - Long WD imaging capabilities
- Software
  - Windows NT OS
  - FEI MCNT UI
- Stage
  - 4-axis motorized eucentric
  - Manual tilt
  - 50x50 mm full travel
  - -15 to 75 degree manual tilt
  - Can easily fit 4-6" wafer in chamber (8" possible)
- Vacuum
  - Turbo pump with dual mechanical RP
  - Low vacuum capable – ESEM mode
- Analytical
  - EDS and EBSD capable
  - Probers, EBIC, cryo-stage and other options available

3.14. X-RAY DIFFRACTION STUDY

3.14.1. INITIAL CONSIDERATIONS

The X-Ray Diffraction (XRD) usage in material investigations has become increasingly common and its innumerous applications has been tested in a large variety of investigation fields. In cement, it is commonly used to identify and to quantify the different crystalline phases. This became possible when Hugo Rietveld [59] invented a method that enabled and easier quantification of the crystalline phases. The Rietveld Method contribute largely to the optimization and efficiency of the test since the older methods used to quantify each of the crystalline phases present in the samples required an extraordinary amount of time.

As well as the SEM test, the XRD working principle is to focus a beam into a sample of interest, and, by the study of its resulting diffracted beam, retrieve the sample's information. As the test's name suggests, the beam used it's an X-Ray beam.

An XRD machine is essentially composed of 3 main important components: a sample stage holder capable of rotation by means of a goniometer, an X-Ray beam emitter and a receiver, these two components can be moved as can be seen in Figure 3.36.

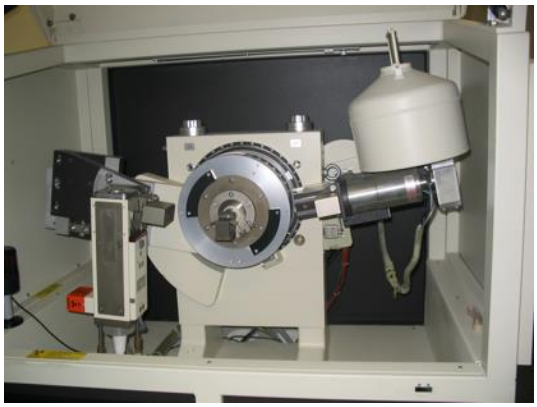

Fig. 3.36 – XRD equipment. From left to right: emitter, sample holder, receiver

3.14.2. CRYSTALLOGRAPHY OF THE SAMPLE

An XRD measurement can only be applied to crystalline materials. Only these enable the X-Ray beam diffraction and consequently, the sample study. If any non-crystalline (or amorphous) matter is present in the sample, it will be simply undetected and not taken into consideration to neither phase detection nor quantification. Given this, the crystallography of the sample assumes a crucial role in the XRD study.

In order to be crystalline, materials have to own two very important properties: first it has to be solid and, more importantly, it must have a long range order. When attractive forces become strong enough that the particles cannot easily move away from one another, matter becomes solid. Solids are characterized by having both shape and volume. Although particles in a solid can be randomly distributed, an ordered and repetitive pattern is more common, as it corresponds to a lower energy state. It is important to state that not all solids are crystalline or ordered. For example, glasses have both shape and volume, but they also have a high degree of disorder, and therefore, are classified as amorphous solids. This means that any crystal, to be defined as such, needs to have a certain periodic,

defined and uninterrupted repetition of their atoms or molecules in space. This repetition is not always uninterrupted since defect and impurities might occur.

Theoretically, periodic crystals are infinite, and this constitutes an important assumption in how XRD works. However, their periodicity extends from about 10^3 to 10^{20} atomic or molecular dimensions and, of course any crystal must end at some point. [60]

So, crystals are organized in a given order and in a given dimension. This can be in three, two or even one directions. Regardless of the case, it is assumed, as stated before, that the crystal has perfect periodicity and that this periodicity is repeated by unit cells and lattices. Unit cells are single molecules that will be repeated along the lattice. Therefore, a unit cell represents the molecular structure that will be repeated along the crystal, and the lattice represents the planes where the repetition will occur, as can be seen in Figure 3.37.

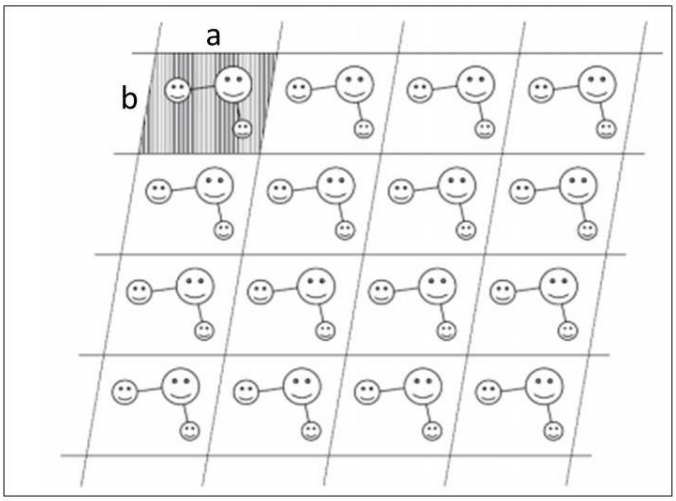

Fig. 3.37 – Illustration of a two-dimensional lattice with one unit cell hatched vertically [60]

The repetition development is determined by the organization of the unit cell. Each unit cell, in order to be studied three dimensionally, must be described using three noncoplanar vectors, commonly named a, b, and c, which will form a three dimensional space of that unit cell. As an example, in the figure above, the lattice is created by the repetition of the two vectors represented, a and b in all the unit cells. This takes into consideration that the origin point can be anywhere, the lattice is infinite and the vectors can have positive or negative values. [60]

However, the definition of these three parameters is not enough to fully characterize the unit cell. After the intensity of the vectors is defined, their direction must be defined as well. This is achieved by using three other parameters that represent angles between each vector. Therefore, α, β and γ which are the angles formed between b and c, a and c and a and b, respectively, are also defined and, along with a, b and c which are the "sides" of each unit cell, the definition is complete. Commonly, the unit cell parameters are measured in Ångström, Å (1 Å=10^{-10} m), and the angles in degrees (º). [60]

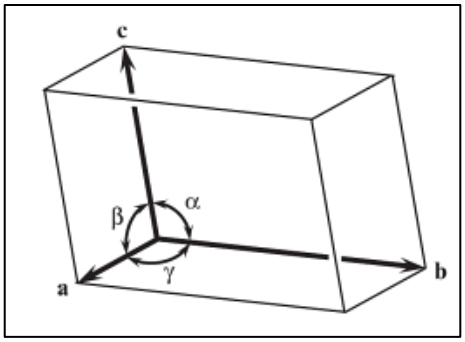

Fig. 3.38 – Unit Cell in three dimensions. [60]

3.14.3. DIFFRACTION AND DIFFRACTOGRAM COLLECTION

As stated previously in point 3.14.1, the XRD procedure consist of sending an X-Ray beam towards the crystals present in the sample and measure their respective diffraction patterns.

When the beam travels through the sample, considering, as an example, only one crystal, there are three major occurrences [60] that are important to refer in the diffraction process:

- Coherent scattering, which is the production of a beam with the same wavelength (photon energy), as the incident beam;
- Incoherent scattering, where the wavelength of the beam changes due to energy loss by the photons when electron collisions occur;
- Absorption of the X-Rays, as some photons are dispersed in random directions and other lose electrons.

Only the coherent scattering will be further discussed and analyzed, since the influence of the last two occurrences can be neglected and therefore, not taken into consideration for diffraction studies.

When coherent scattering happens, the scattering occurs in every direction around the affected unit cells. Taking in consideration the physical properties of the lattice and its randomness and theoretical infinity and also that coherent scattering generates beams with the same wavelength from all electrons and in all directions, what will happen is a cancelling of the diffracted beams in all direction, but one. This direction is what defines the whole process of X-Ray diffraction. [60]

Also, being the sample in study only one crystal, among each lattice, several beams with different maximum intensities, associated to the concentration of beams at that given point, are produced. More importantly, these beams are “seen” at certain specific angles of diffraction.

These diffraction angles are explained by Braggs’ Law [61] whose principle is illustrated in Figure 3.39 and given by equation 7.

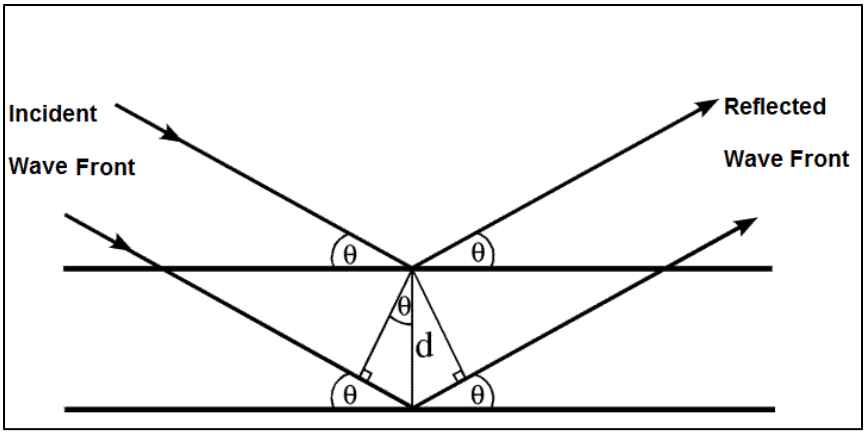

Fig. 3.39 – Braggs' Law principle

$$n\lambda = 2d \sin\theta \tag{13}$$

Where,

- n is an integer;
- λ is the wavelength;
- d is the spacing between planes in the lattice;
- θ is the angle between the incident beam and the planes.

As it can be easily understandable in the figure above, "$2d \sin\theta$" represents the extra path that the beam below must make in comparison to the upper beam. When this path is equal to an integer multiple of the wavelength (taken as 1 in all calculations), satisfying Braggs' Law, a constructive interference is obtained and the Braggs' peaks are formed (in the final diffractogram), representing the intensity of the constructed diffracted beam. [61]

Then the XRD equipment varies both the incident beam angle θ (emitter position) and the resulting diffractioned beam angle $2\,\theta$ (receiver position). This variation assures that each crystal present in the sample will "send" intensity peaks to the receiver at certain $2\,\theta$ values, which are clearly defined for each crystal in existence. The relative peak intensity can be different for the same mineral, which can be interpreted as different physical states (for example, different pressures in the formation of the crystal). Given this, the final result obtained is a diffractogram, or commonly, pattern which relates the $2\,\theta$ variation and the intensity count, as exemplified on Figure 3.40 for a large number of crystals.

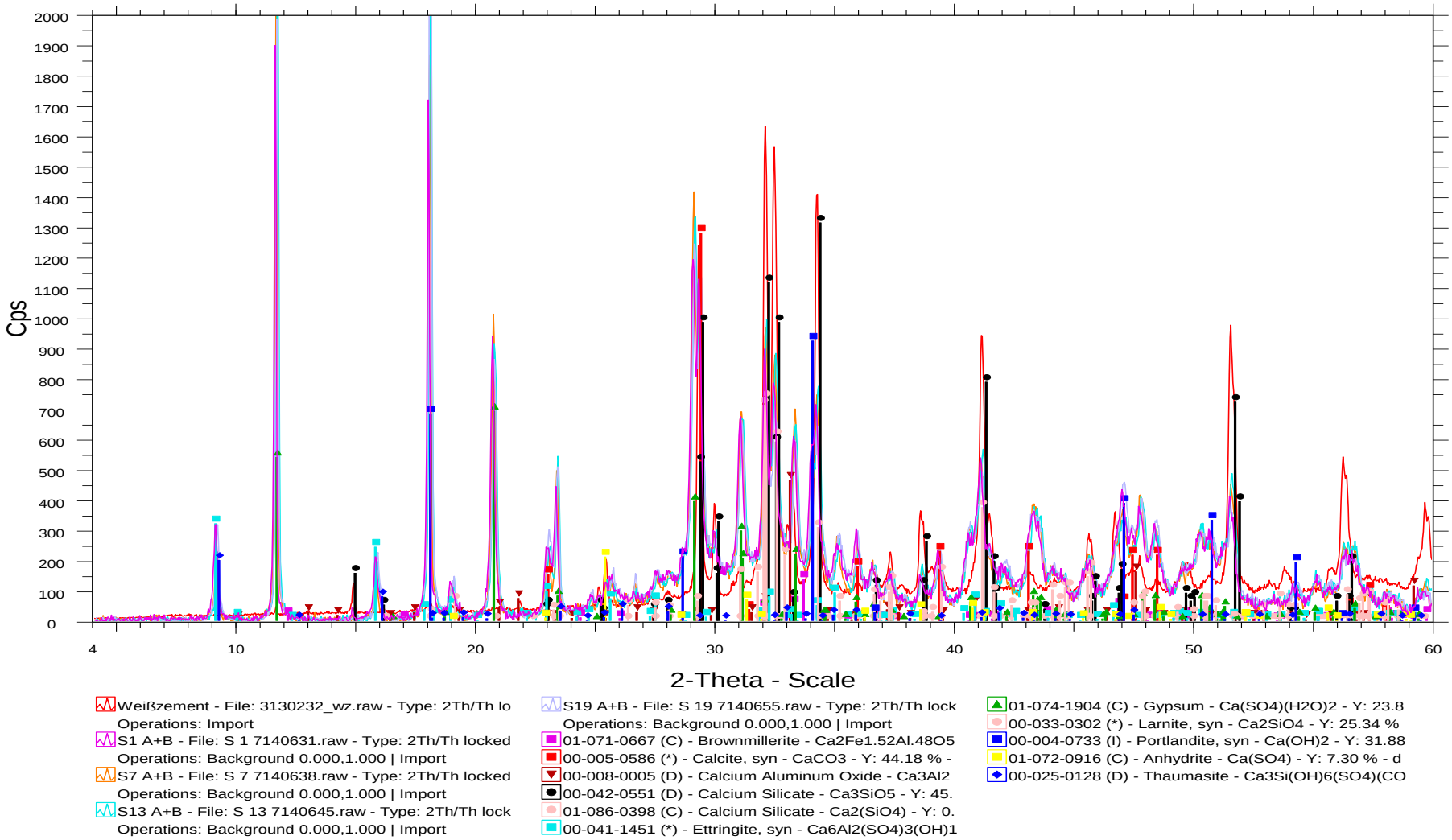

Fig. 3.40 – Diffractogram of the different crystalline composition of the samples with Z556, Z556 + KSE 300, Z556 + KSE OH and Z556 + KSE 100

To run the obtained pattern, EVA (version 12) by Bruker AXS software was used and, finally, with existing databases - in this case, Powder Diffration Files, PDF-2 (NIST) and ICSD database (FIZ Karlsruhe) - it was possible to identify the existing phases in the sample by comparison with previous results. This process is usually referred to as Qualitative Analysis, and its difficulty varies with the existing database, the complexity of the analyzed diffractogram and mostly with the user's experience in analyzing it.

3.14.4. RIETVELD ANALYSIS

Following the qualitative analysis a quantitative analysis needs to be performed in order to obtain the relative concentration of each phase observed. This step acquires crucial importance regarding objectives completion, data gathering and result analysis. One of the many quantitative analysis, and the one used in this study, is the Rietveld analysis. This analysis, along with the other types of quantitative analysis, has a high difficulty level and requires very much fine tuning and requirements to be respected to obtain satisfying results [61].

The principle of this method is to assume that the 2θ peaks retrieved from the qualitative analysis belong to only one unit cell of each phase. Then, applying a Scale Factor to each phase, the values of the unit cells are normalized and fitted in the diffractogram [61]. This procedure of quantitative phase analysis based on the values of scale factors determined by Rietveld refinement was introduced by Howard and Hill [62]. The Rietveld method was applied successfully in the microstructure characterization and in the verification of qualitative phase composition of multiphase materials [63]-[69].

The Scale Factor values represent the number of unit cells present in the sample or, in other words, how much of a phase exists in it. By the means of these factors, and with the phase identification previously performed, it is possible to infer the relative weight fractions of phases in a multiphase material, as described by Hill and Howard [62] using the following formula:

$$W_p = \frac{S_p(Z.M.V)}{\sum_{i=1}^{n} S_i\ (Z.M.V)} \times 100\% \quad (13)$$

Where,

- W_p is the relative weight fraction of phase p in the mixture of n phases;
- S_p is the Rietveld scale factor of phase p;
- Z is the number of formula units per unit cell;
- M is the mass of formula unit (in atomic mass units);
- V is the unit cell volume (in $\dot{A}^3$).

All these values are known from the databases referred before, being the only exception the scale factor that must be calculated from the Rietveld analysis.

This method was applied to all the samples described in 3.4.3 in order to identify and quantify the existing phases and to better understand how the application of the KSE influences them, especially, and accordingly to the title of this work, ettringite and thaumasite.

In this process, TOPAS-Academic (Version 4.2) was used.

3.14.5. SAMPLE PREPARATION

The samples used in the X-Ray Diffraction analysis were obtained from the Le-Châtelier rings. After the specimens were demolded and broke for the SEM test (as it can be seen in Figure 3.28), a small sample was taken and grinded in order to be used for the XRD test. For the grinding were used a pestle and a mortar and it was possible to produce the powder that was used in the XRD test. Figure 3.41 shows the mortar and pestle used, as well as the powder produced.

Fig. 3.41 – Sample's grinding for the XRD

3.14.6. SUMMARY OF THE TEST AND KEY SPECIFICATIONS OF THE EQUIPMENT

The X-Ray diffraction analyses were carried out on powder samples obtained from the mortar and pestle and, afterwards, grinded during 2 minutes in the ball mill (McCrone, Korundmahlsatz).

To determine the X-Ray amorphous components of the 24 samples analyzed, 20% (percentage in mass) of ZnO was added. The samples were then, mixed approximately during 15 seconds.

The measurements were performed using a Siemens D5000 diffractometer with the following measurement parameters:

Table 3.5 – Siemens D5000 specifications

Generator Voltage	40 kV
Tube Current	40 mA
Anode Material	Cu
Deflectors	Variable, Automatically
Detector Bruker	SolX, energy disp. Semiconductor detector
Angular Range	6º-70º - 2 θ
Step width	0,03º
Counting Time	5s/step

4
RESULT PRESENTATION

4.1. CONSIDERATIONS

This chapter contains the results obtained from the tests described in Chapter 3. The analysis of the results is first individual, *i.e.*, for each one of the test and then, in point 4.12, possible correlations between the test results are also analyzed.

It is important to refer that, even though the KSE application on flat prisms is not a test but, instead, a procedure, this chapter will also contain results of this application (described in 3.5) because it can also be important for the discussion of the results and conclusions of this work.

For a better understanding, the results will be presented in the same order as the tests were described in the previous chapter.

Although the results presented in this chapter correspond to the tests already described in the previous chapter, a small description of the graphics and/or figures will be done in order to enable the best understanding of the variables studied to the reader.

4.2. KSE APPLICATION ON FLAT PRISMS

All the graphics have as vertical axis the value of the mass of KSE applied, in grams. In the horizontal axis, with the exception of Figures 4.6, 4.12 and 4.13, are referred the samples names, with only the purpose to differentiate them in the lab. In blue are presented results concerning the W/C ratio of 0.5 and in red the W/C ratio of 0.4. Figures 4.6 and 4.12 show the comparison between the average values of each one of the KSE applied per W/C ratio of 0.5 and 0.4, respectively. Concerning Figure 4.13, it compares the average values in grams of each one of the KSEs per W/C ratio.

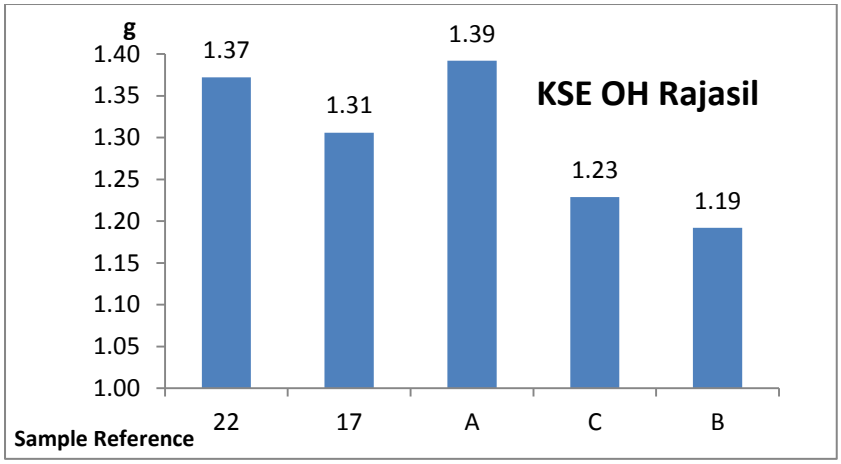

Fig. 4.1 – Application of KSE OH from Rajasil in specimens with W/C of 0.5

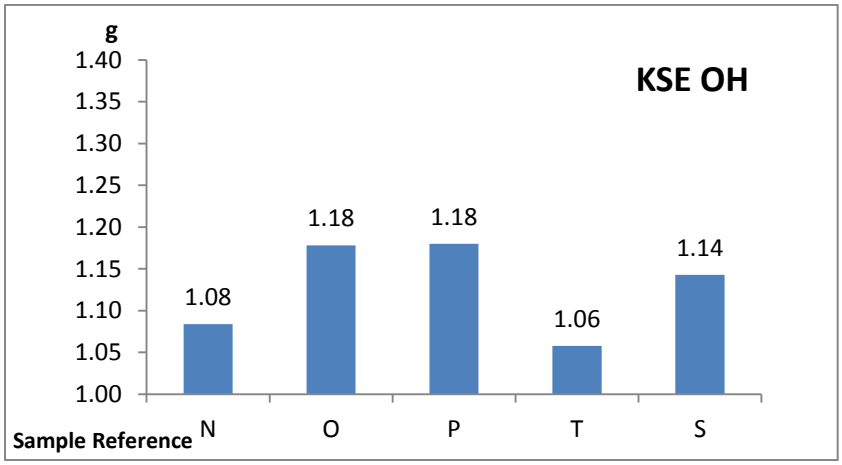

Fig. 4.2 – Application of KSE OH from Remmers in specimens with W/C of 0.5

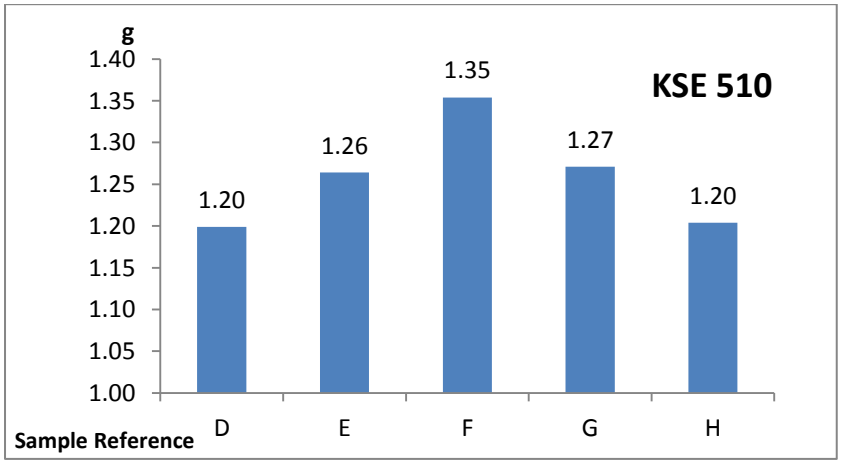

Fig. 4.3 – Application of KSE 510 from Remmers in specimens with W/C of 0.5

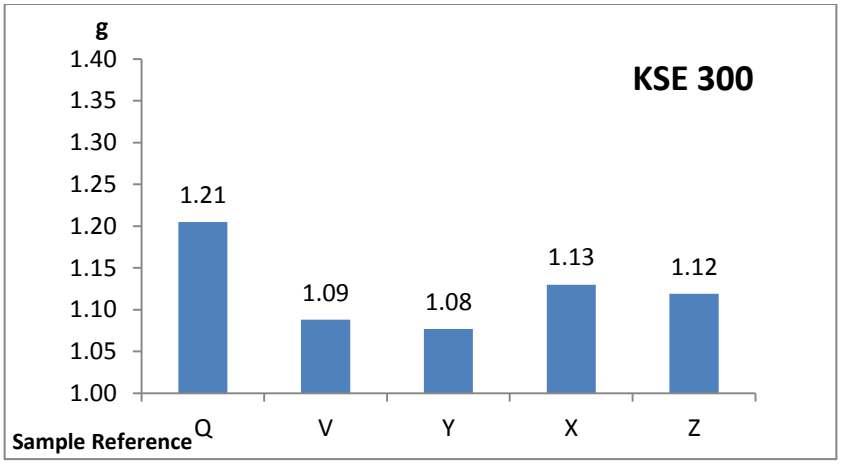

Fig. 4.4 – Application of KSE 300 from Remmers in specimens with W/C of 0.5

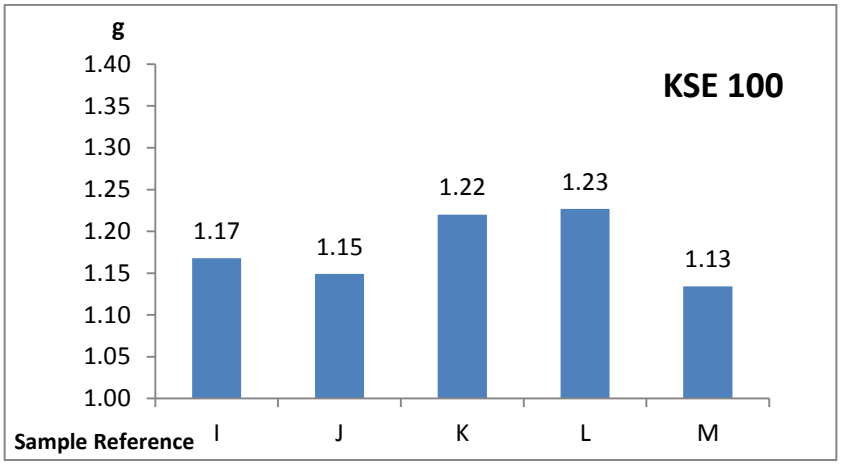

Fig. 4.5 – Application of KSE 100 from Remmers in specimens with W/C of 0.5

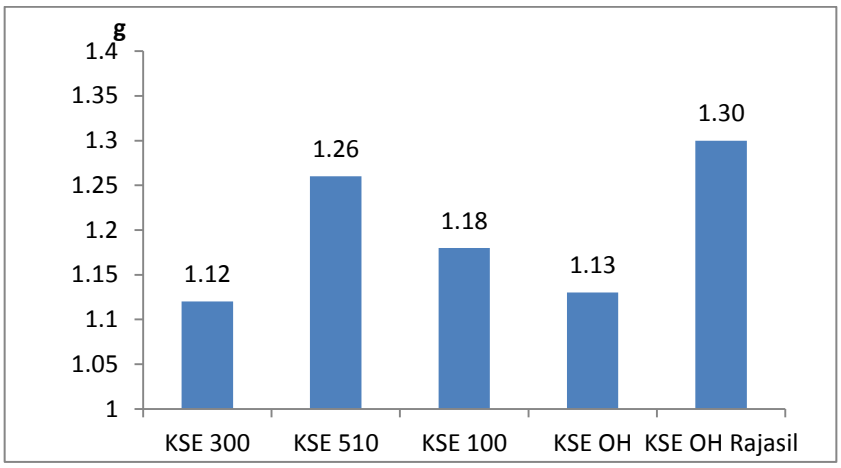

Fig. 4.6 – Average value, in grams, of each one the KSEs applied on the specimens with 0.5 W/C ratio

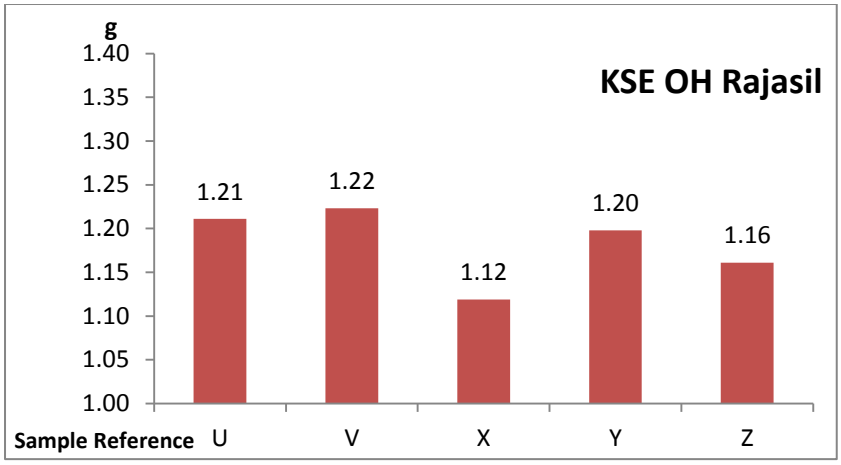

Fig. 4.7 – Application of KSE OH from Rajasil in specimens with W/C of 0.4

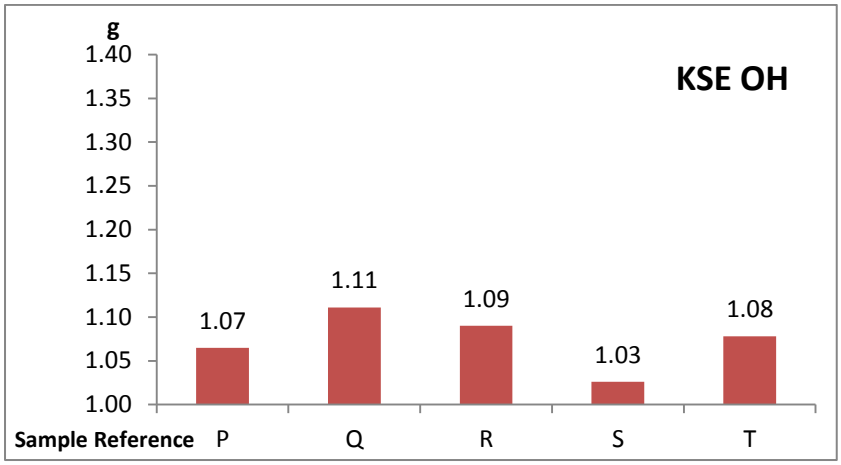

Fig. 4.8 – Application of KSE OH from Remmers in specimens with W/C of 0.4

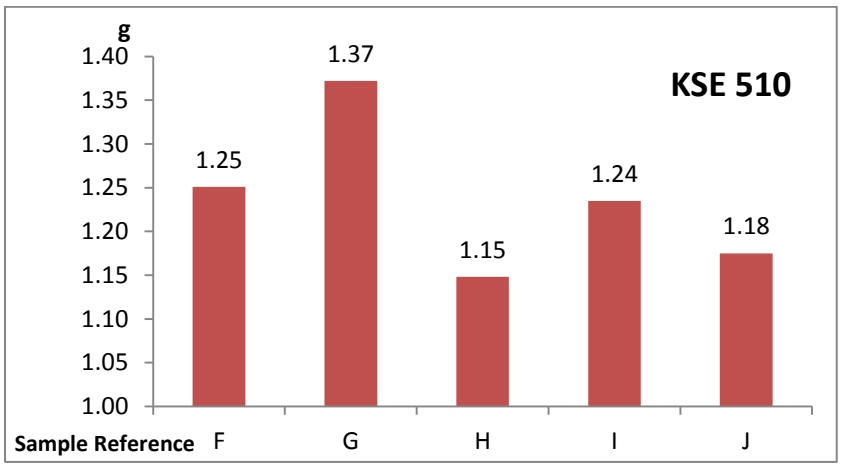

Fig. 4.9 – Application of KSE 510 from Remmers in specimens with W/C of 0.4

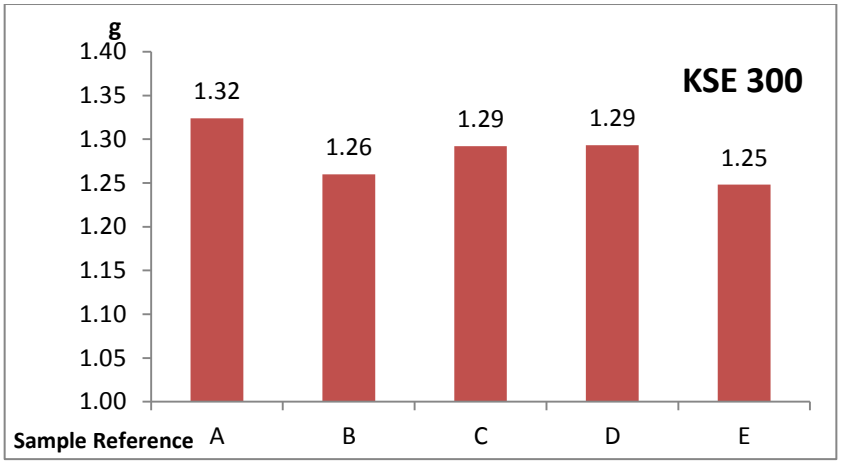

Fig. 4.10 – Application of KSE 300 from Remmers in specimens with W/C of 0.4

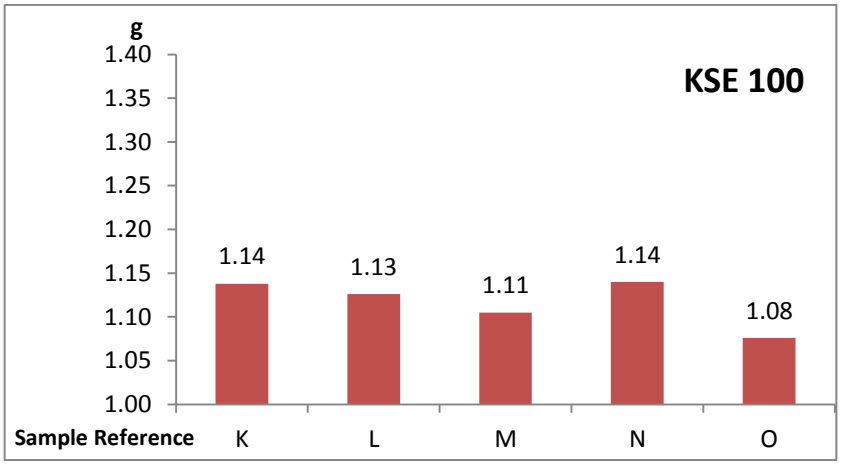

Fig. 4.11 – Application of KSE 100 from Remmers in specimens with W/C of 0.4

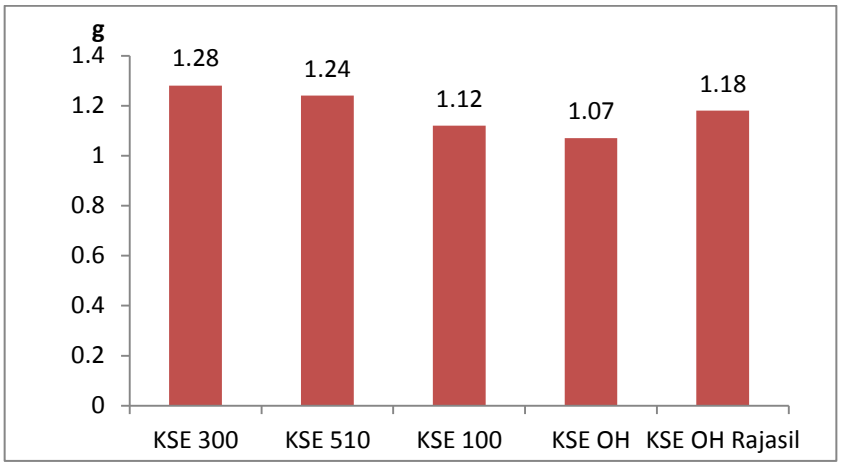

Fig. 4.12 – Average value, in grams, of each one the KSEs applied on the specimens with 0.4 W/C ratio

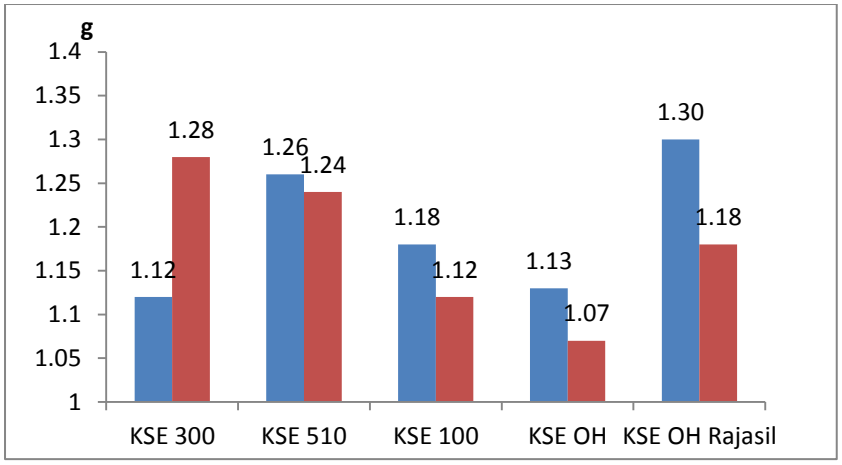

Fig. 4.13 – Comparison between the average values, in grams, of each one the KSEs per W/C ratio.

As it was described in 3.5.2 the application of the KSE in the prisms was made using a paint brush, therefore, to apply a precise and unique value in each one of the samples was impossible. Thus, the main objective was to keep the values per series *i.e.*, for each one of the five groups of KSE specimens, as close as possible. Considering the ten series (five with 0.4 W/C and five with 0.5 W/C) each composed of five specimens, after the interpretation of the figures above, it is possible to identify that the biggest discrepancy between the five specimens of each series is of 0.20 grams between specimens "A" and "B" from the KSE OH Rajasil series with 0.5 W/C ratio (Figure 4.1). It is also important to refer that the biggest difference between the average values of each one of the 0.5 W/C ratio and 0.4 W/C ratio, per KSE is of 0.16 grams, for the KSE 300, as it is illustrated in Figure 4.13.

It was important to underline and identify the biggest differences in the values of KSE applied because they could be translated by different results in the subsequent tests. All the results are presented in Appendix A1.

4.3. DYNAMIC E-MODULUS TEST

This point contains the results of the Dynamic E-modulus test. The first two graphics presented are the dynamic E-modulus, in MPa, in function of the bulk density, in g/cm^3, of the 3 specimens per W/C ratio (Figures 4.14 and 4.15). The last two graphics show the average E-modulus, in MPa, of 3 samples per each one of the KSEs applied (Figures 4.16 and 4.17).

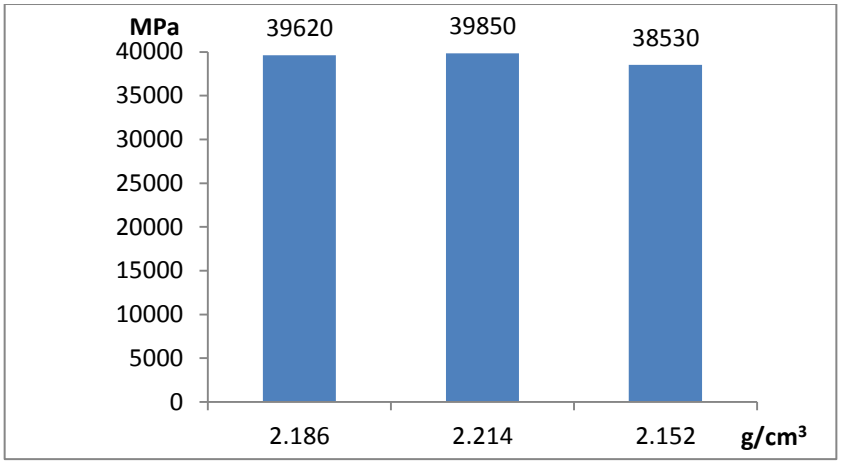

Fig. 4.14 – E-Modulus and correspondent density of samples with W/C ratio of 0.5 at 28 days.

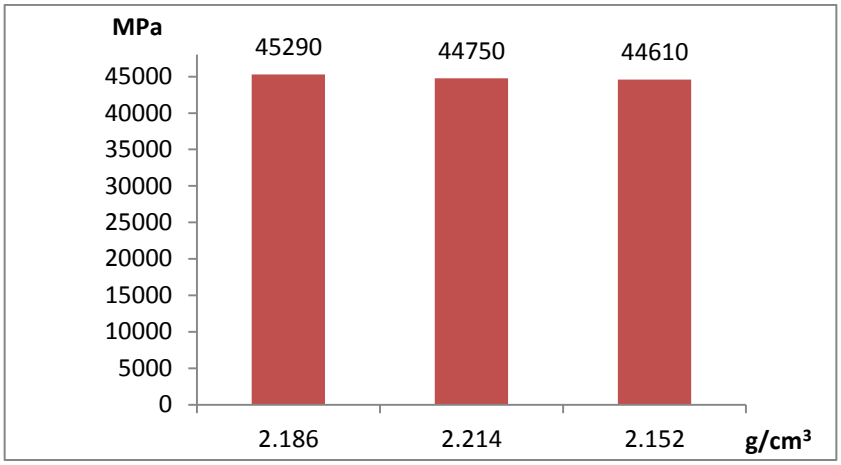

Fig. 4.15 – E-Modulus and correspondent density of samples with W/C ratio of 0.4 at 28 days.

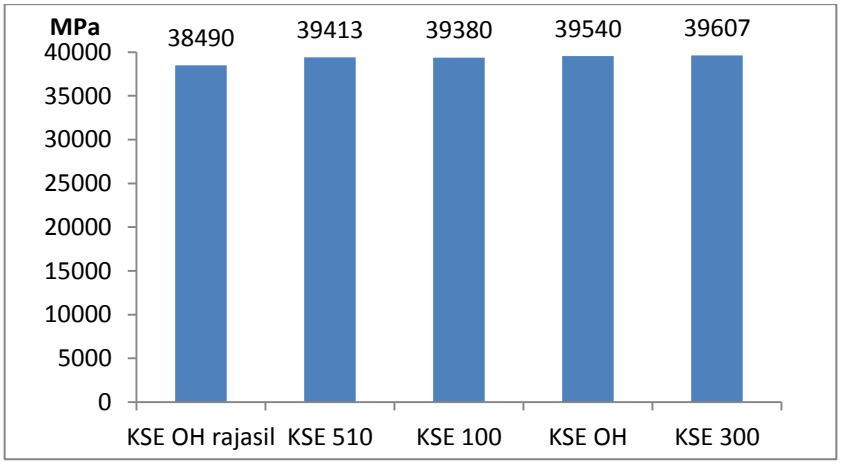

Fig. 4.16 – Average E-Modulus of the 3 specimens studied for each of the KSEs with 0.5 W/C ratio at 93 days.

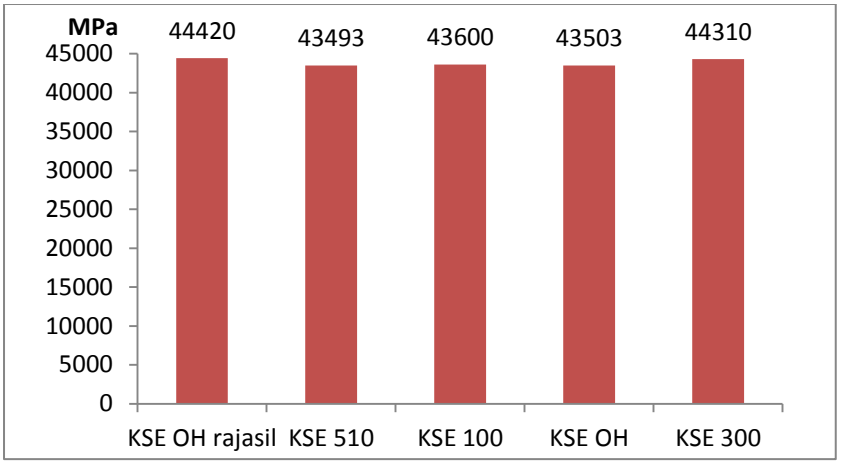

Fig. 4.17 – Average E-Modulus of the 3 specimens studied for each of the KSEs with 0.4 W/C ratio at 93 days.

After the analysis of the four figures above there are two major conclusions that can be unmistakably withdraw:

- The Dynamic E-Modulus assumes higher values in the specimens with 0.4 water/cement ratio (red bares – 44610 to 45290 MPa, with an average of 44883 ± 293 MPa) than in the specimens with 0.5 water/cement ratio (blue bars – 38530 to 39850 MPa , with an average of 39333 ± 576 MPa);
- There are no major differences between the values of the Dynamic E-Modulus of the specimens at 28 days without the application of KSE and at 93 days with the application of KSE. In fact, the average value of the specimens with 0.4 W/C ratio at 93 days is 43865 ± 411 MPa and the average values of the specimens with 0.5 W/C at 93 days is 39286 ± 406 MPa.

The higher values in the specimens with 0.4 W/C ratio are easily explained by the ratio itself. As it is known, the lower this ratio is, the higher is the durability and resistance of the mortar. Thus, the higher frequencies measured in the specimens with 0.4 W/C ratio lead to higher Dynamic E-Modulus in accordance with equation 7 in 3.6.3.

The results regarding each one of the specimens are shown in Appendix A2.

4.4. CAPILLARY RISE TEST

Figures 4.18, 4.20 and 4.21 show the results of the calculation of the water absorption coefficient C in Kg/m^2 from Equation (8). As well as in previous results in this chapter, the blue bars correspond to 0.5 W/C ratios and the red ones to 0.4. Figures 4.19, 4.22 and 4.23 demonstrate the mass increasing over square root of time ($min^{0.5}$) due to water absorption. In these three figures, the coefficient of water absorption by capillarity A was obtained by linear regression. Figures 4.18 and 4.19 show the results obtained from specimens 1, 2, 3 and 4 (reference names).

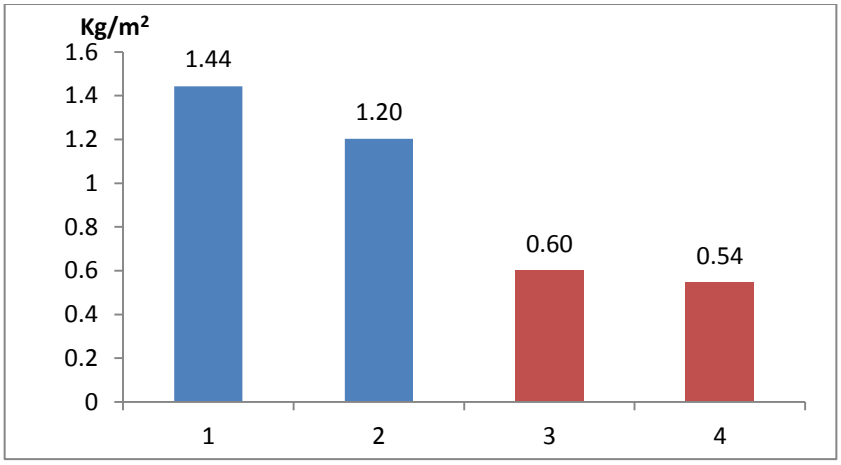

Fig. 4.18 – Water absorption coefficient C for two specimens per each of the W/C ratios at 28 days.

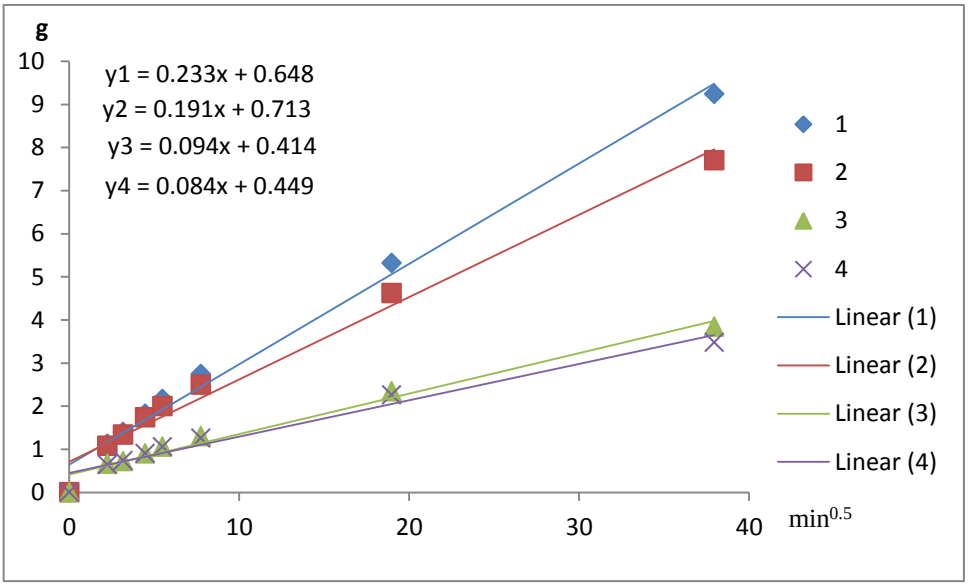

Fig. 4.19 – Mass increasing ratio and values of the water absorption coefficient of capillarity A during the measurements performed at 28 days

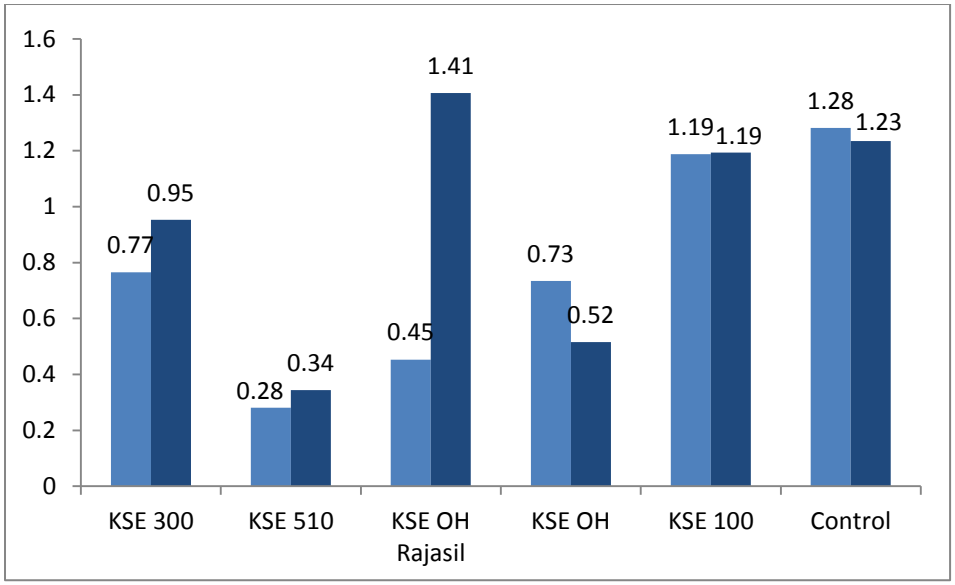

Fig. 4.20 – Water absorption coefficient C for two specimens for each of the KSEs with W/C of 0.5 at 93 days

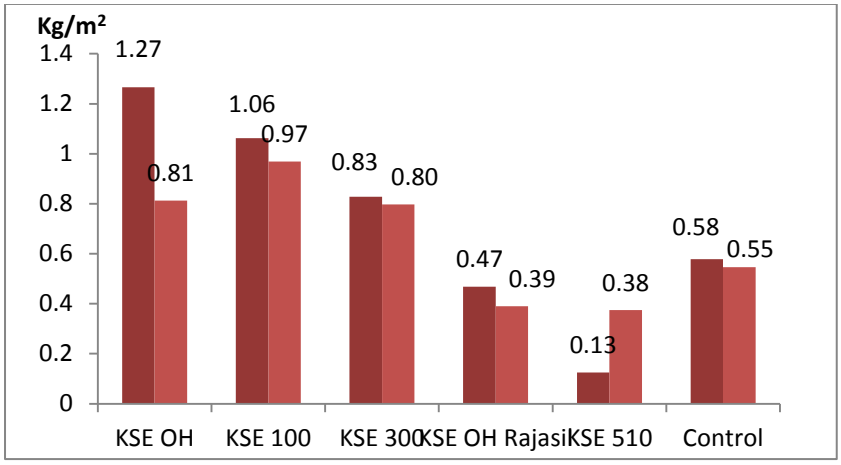

Fig. 4.21 – Water absorption coefficient C for two specimens for each of the KSEs with W/C of 0.4 at 93 days.

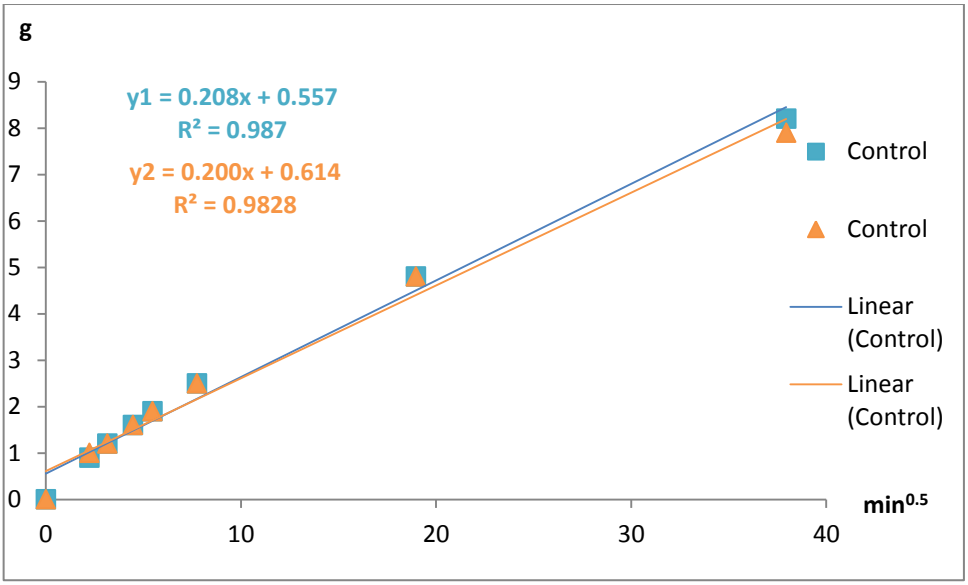

Fig. 4.22 – Mass increasing and water absorption coefficient of capillarity A in the control specimens with 0.5 W/C ratio at 93 days

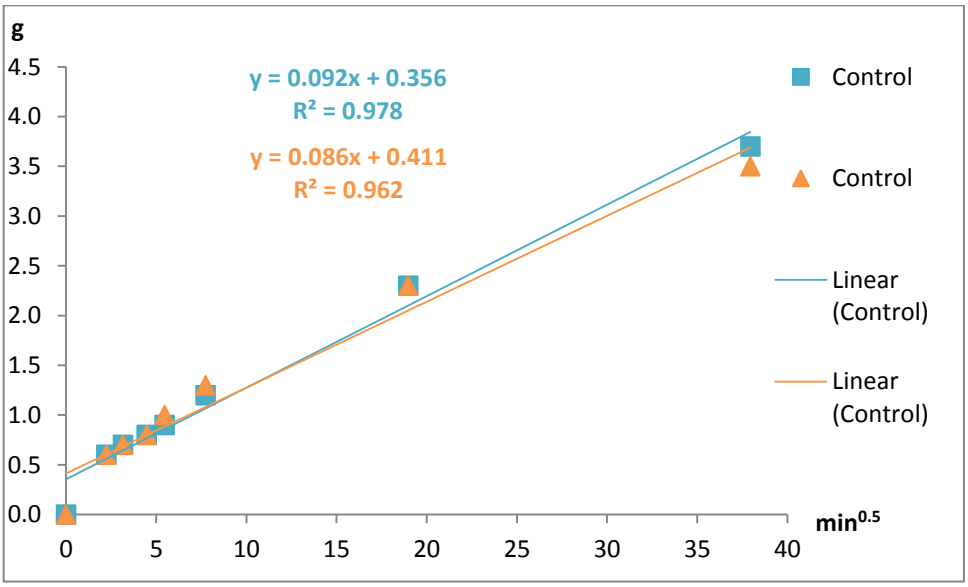

Fig. 4.23 - Mass increasing and water absorption coefficient of capillarity A in the control specimens with 0.4 W/C ratio at 93 days

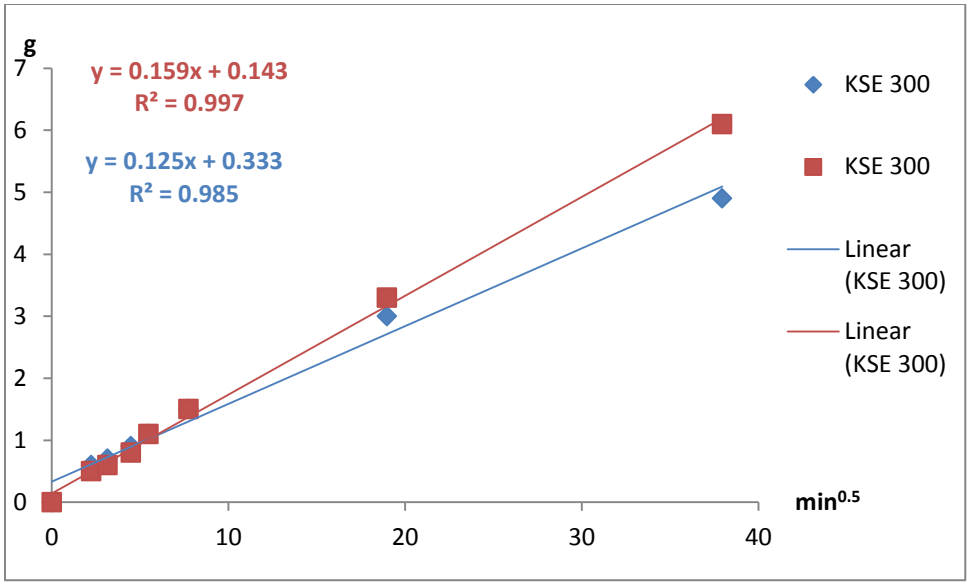

Fig. 4.24 - Mass increasing and water absorption coefficient of capillarity A in the KSE 300 specimens with 0.5 W/C ratio at 93 days.

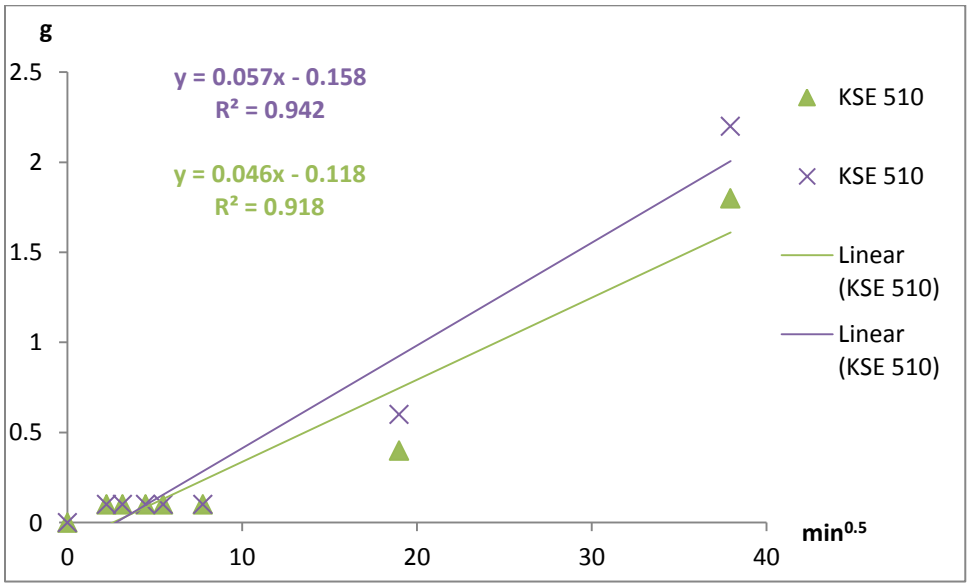

Fig. 4.25 - Mass increasing and water absorption coefficient of capillarity A in the KSE 510 specimens with 0.5 W/C ratio at 93 days

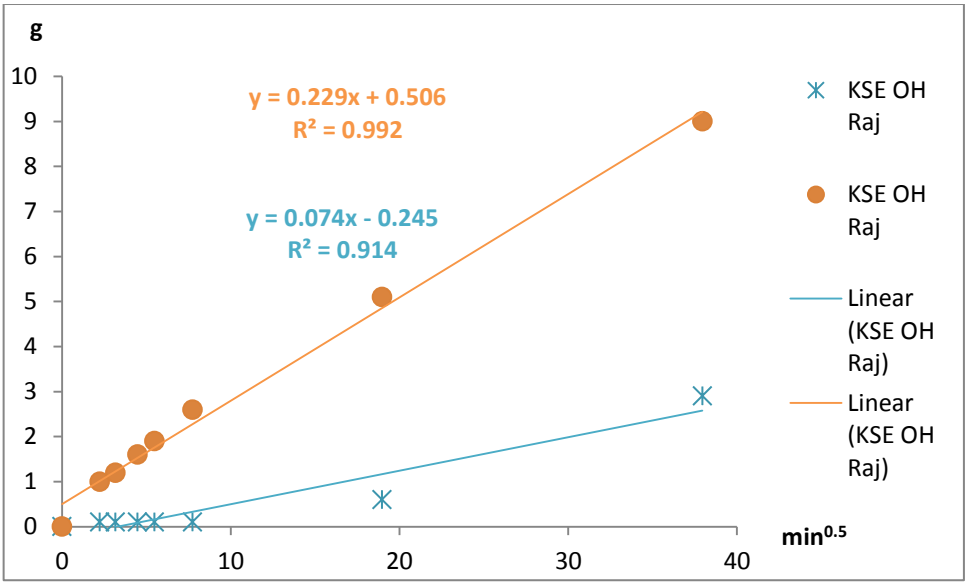

Fig. 4.26 - Mass increasing and water absorption coefficient of capillarity A in the KSE OH from Rajasil specimens with 0.5 W/C ratio at 93 days

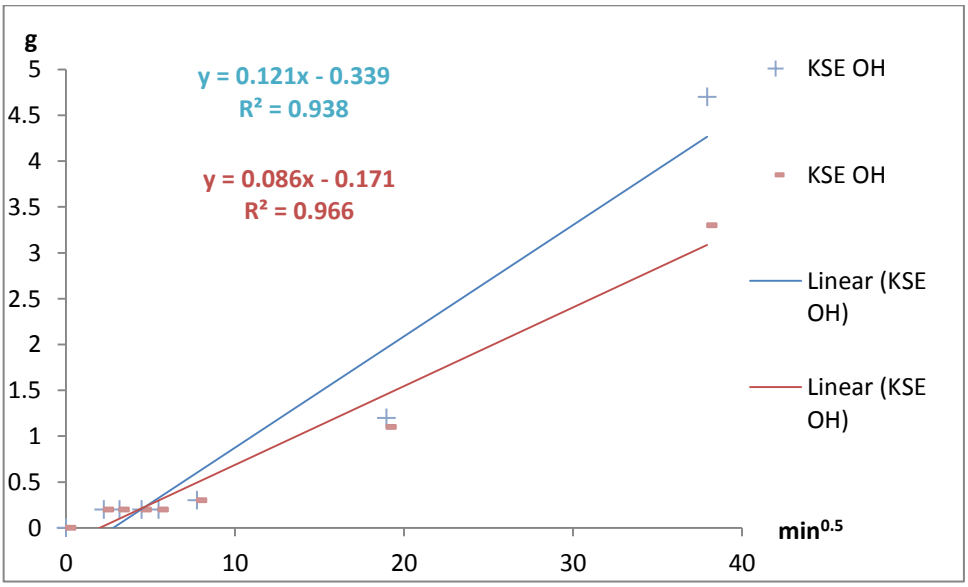

Fig. 4.27 - Mass increasing and water absorption coefficient of capillarity A in the KSE OH specimens with 0.5 W/C ratio at 93 days

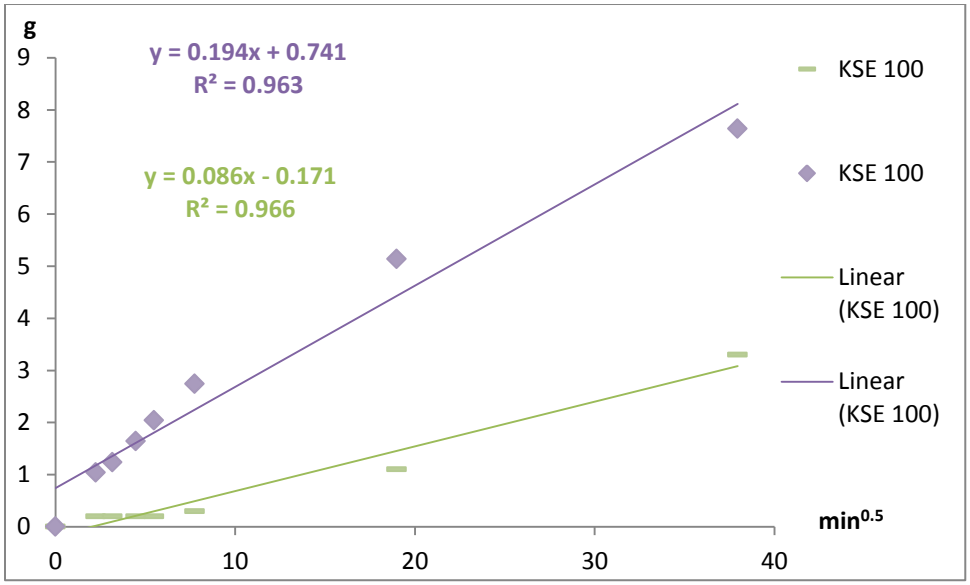

Fig. 4.28 - Mass increasing and water absorption coefficient of capillarity A in the KSE 100 specimens with 0.5 W/C ratio at 93 days

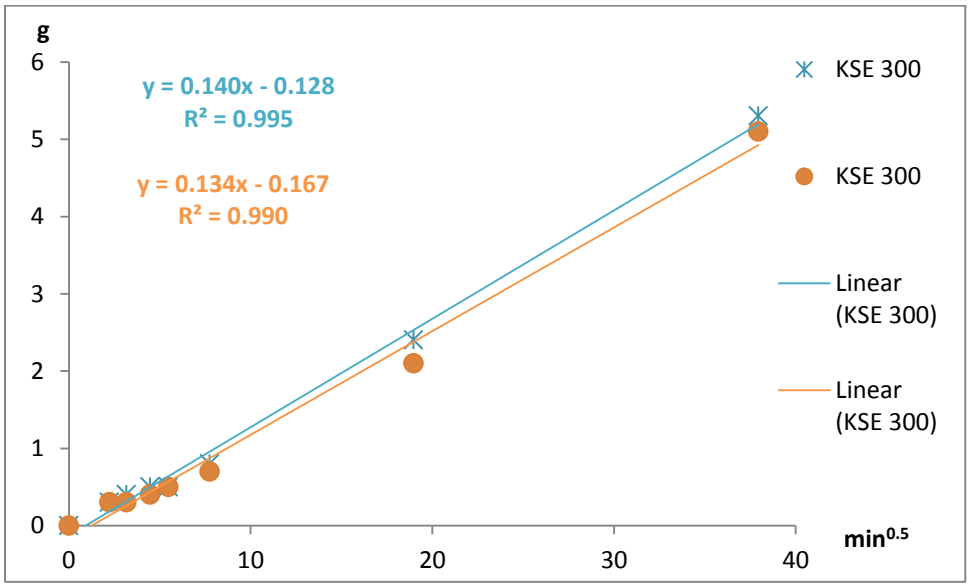

Fig. 4.29 - Mass increasing and water absorption coefficient of capillarity A in the KSE 300 specimens with 0.4 W/C ratio at 93 days

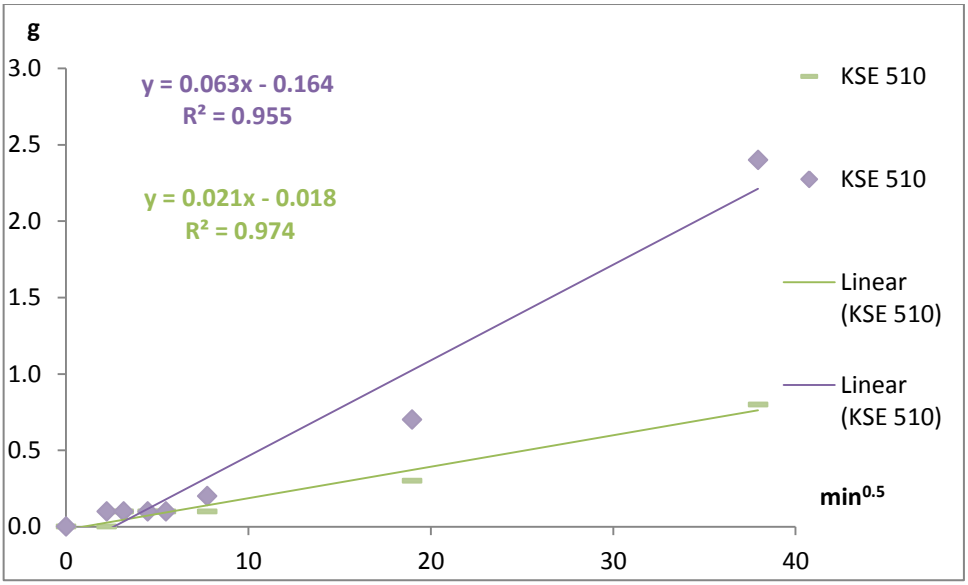

Fig. 4.30 - Mass increasing and water absorption coefficient of capillarity A in the KSE 510 specimens with 0.4 W/C ratio at 93 days

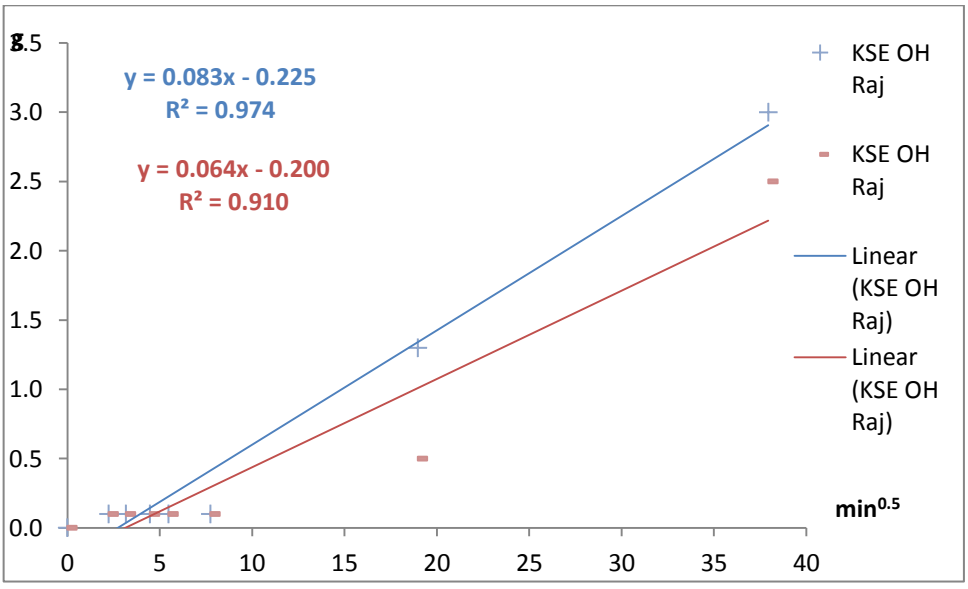

Fig. 4.31 - Mass increasing and water absorption coefficient of capillarity A in the KSE OH from Rajasil specimens with 0.4 W/C ratio at 93 days

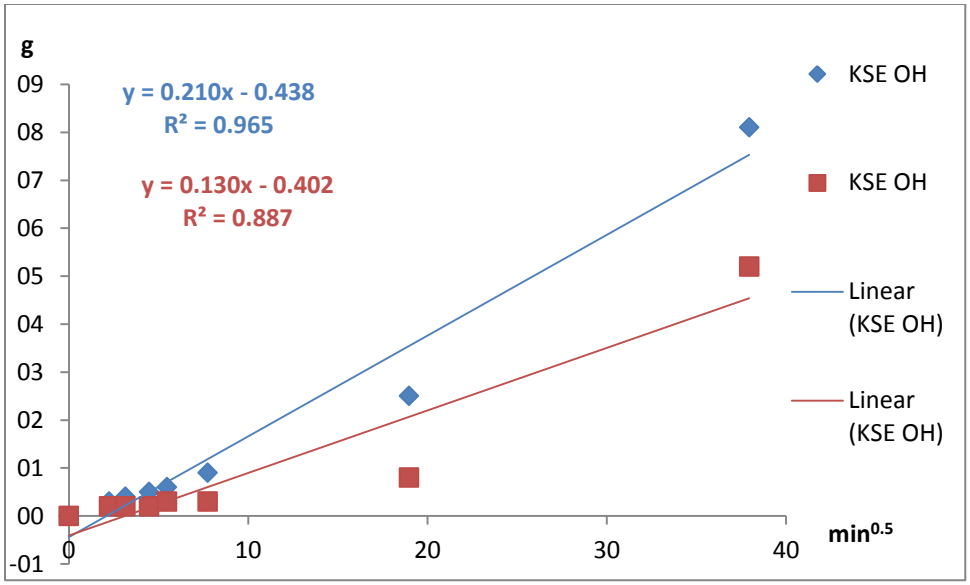

Fig. 4.32 - Mass increasing and water absorption coefficient of capillarity A in the KSE OH specimens with 0.4 W/C ratio at 93 days

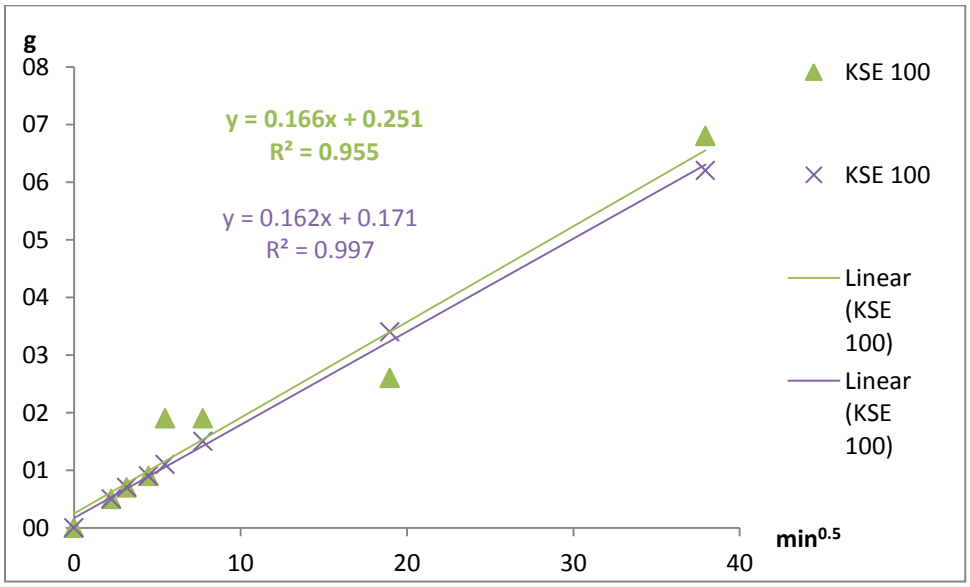

Fig. 4.33 - Mass increasing and water absorption coefficient of capillarity A in the KSE 100 specimens with 0.4 W/C ratio at 93 days

Taking in consideration the results presented in Figures 4.20 to 4.21 there is something that can be distinguished at first sight: the application of KSE influences the water absorption coefficient, C, and therefore, the ratio of mass increasing of water during the measurements.

The first thing to notice is that the control values of the specimens at 28 days (Figures 4.18 and 4.19) is in the same range of the ones tested at 93 days (Figures 4.20, 4.21, 4.22 and 4.23). For instance if the average values of the water absorption coefficient of the specimens at 28 and 93 days is compared the same magnitude of results are obtained. The average value of the control specimens with W/C

ratio of 0.5 at 28 days is 1.32 Kg/m^2 and the specimens with W/C of 0.4 is 0.57 Kg/m^2 while at 93 days the values are 1.26 Kg/m^2, and 0.57 Kg/m^2, respectively.

The results concerning the application of KSE, in order to make a better interpretation of the results showed in the graphics two table were created. Table 4.2 contains the average values of the water absorption coefficient C calculated by the Equation (8) described in 3.7.3 while Table 4.3 contains the values of the coefficient of water absorption by capillarity A determined from the linear regression ($y = mx + b$) adopted to better suit the scatter values of each specimen (A=m).

Table 4.1 – Average of the water absorption coefficient C at 93 days

C	control	300	510	OH Raj	OH	100
	[Kg/m^2]					
0.4	0.58	0.83	0.38	0.47	1.27	1.06
	0.55	0.80	0.13	0.39	0.81	0.97
0.5	1.23	0.95	0.34	1.41	0.73	1.19
	1.28	0.77	0.28	0.45	0.52	1.19

Table 4.2 – Coefficient of water absorption by capillarity A at 93 days

A	control	300	510	OH RAJ	OH	100
	[g.min$^{-0.5}$]					
0.4	0.0919	0.1403	0.0626	0.0825	0.2100	0.1661
	0.0863	0.1342	0.0206	0.0637	0.1302	0.1616
0.5	0.2080	0.1594	0.0571	0.2294	0.1214	0.1943
	0.1999	0.1254	0.0455	0.0744	0.0858	0.0858

The analisis of the values of Tables 4.2 and 4.3 show that the application of KSE lead to a decrease in the values of the water absorption coefficients C and A in all the specimens with 0.5 W/C except one of the results of KSE OH from Rajasil. This result is exceptionally high and contrasts with the other one with 0.5 W/C ratio and with the two results with 0.4 W/C where the KSE OH from Rajasil was applied. Eventually, the exceptionally high result obtained with 0.5 W/C ratio could be explained by an ineffective sealing with the paraffin wax.

Concerning the specimens with 0.4 W/C ratio, the conclusions are difficult to be withdrawn. The comparison between the C and A values of the specimens with KSE applied and those of the control specimens shows that the behavior of this two coefficients is the same. Either both coefficients increase or both coefficients decrease. Indeed, the application of KSE 510 and KSE OH from Rajasil result in the decrease of C and A values while the application of KSE 300, OH and 100 increased those values.

The correlation between the results of the capillary rise, mercury porosimetry and KSE penetration depth tests will be discussed in 4.12.2.

4.5. 3-POINT BENDING TEST

The results of the flexural strength of the mortars are presented in Figures 4.34 to 4.36. The red bars of the graphics correspond to W/C ratios of 0.4 and the blue ones to W/C ratios of 0.5.

Figure 4.34 shows the results obtained at 56 days in three specimens with W/C ratios of 0.4 and 0.5 before the application of KSE.

Figures 4.35 and 4.36 present results of the flexural strength at 93 days in specimens with each of the KSE applied plus three specimens without KSE (control) with W/C ratio of 0.5 (Figure 4.35) and with a W/C ratio of 0.4 (Figure 4.36).

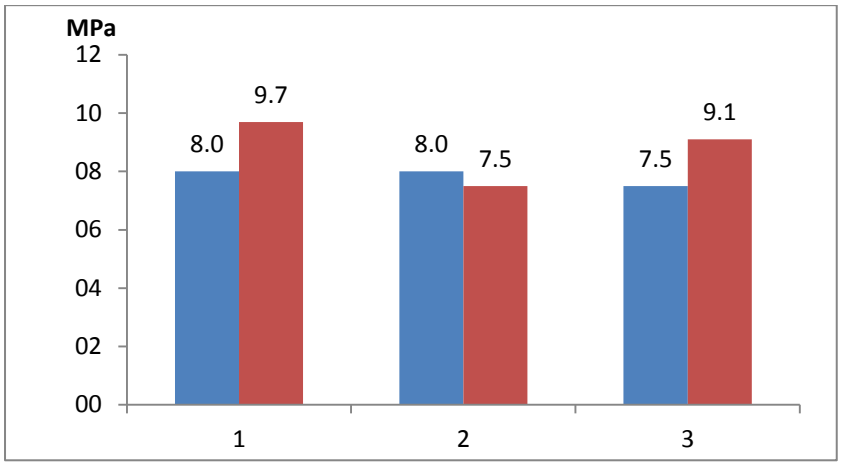

Fig. 4.34 – Flexural strength of 3 specimens per water/cement ratio at 56 days

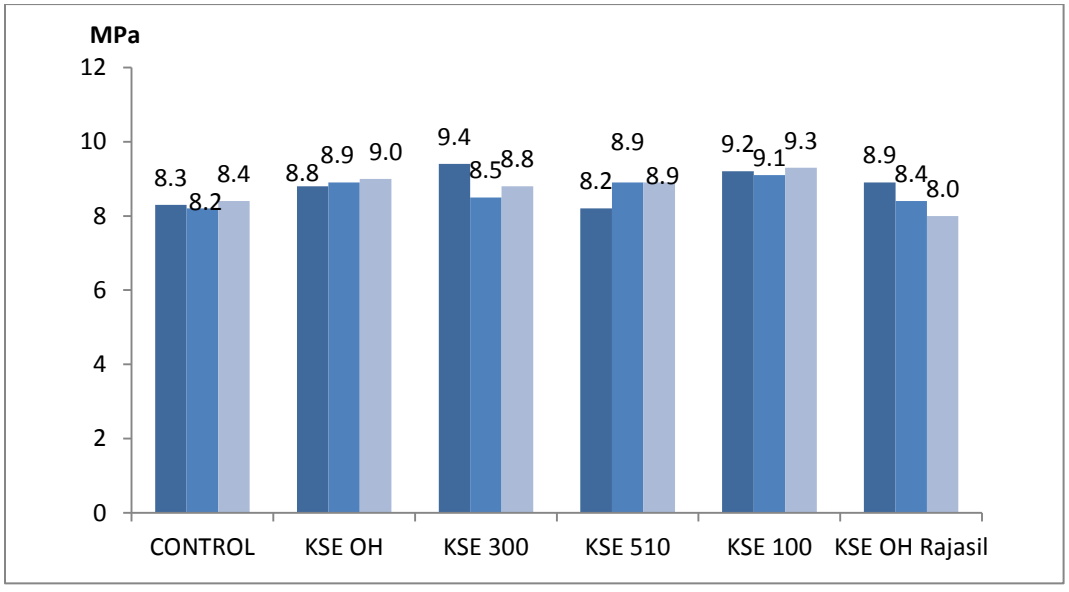

Fig. 4.35 – Flexural strength of 3 specimens per each of the KSE applied plus 3 specimens without KSE applied with a W/C ratio of 0.5 at 93 days

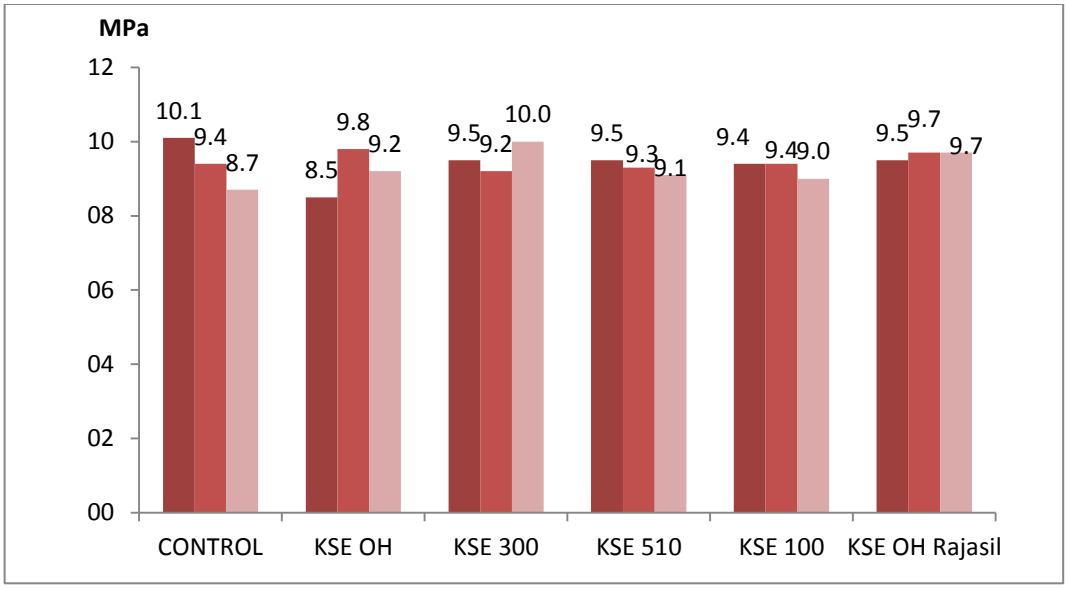

Fig. 4.36 – Flexural strength of 3 specimens per each of the KSE applied plus 3 specimens without KSE applied with a W/C ratio of 0.4 at 93 days

As expected, the decrease in W/C ratio leads to an increase in the flexural strength between the specimens with 0.5 and the specimens with 0.4 ratios.

In what concerns the values for the specimens with KSE applied, the application of KSE it is not translated by significant alterations in the flexural strength of the specimens. As it can be seen in Figures 4.35 and 4.36 all the specimens are in the same range of values as the ones used for control. Even though there was a slightly increase in the values of the specimens with W/C ratio of 0.5.

All the results can be consulted in Appendix A4.

4.6. COMPRESSION TEST

Figures 4.37 to 4.40 present the results of the compression test. The red and blue bars still represent the values of the specimens with 0.4 and 0.5 W/C ratios, respectively.

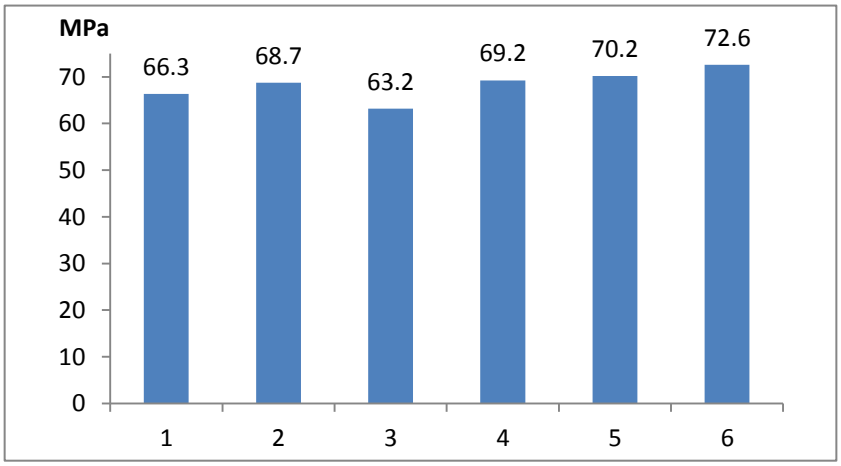

Fig. 4.37 – Compression strength of 6 control specimens (without any KSE) with W/C ratio of 0.5 at 56 days

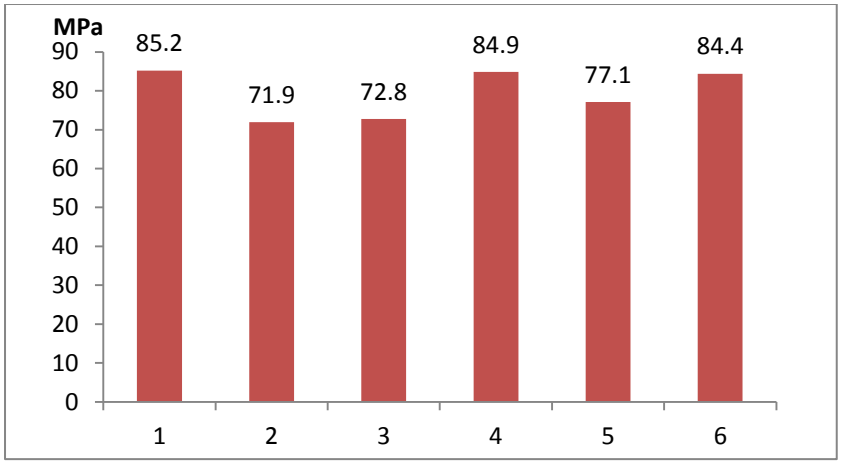

Fig. 4.38 – Compression strength of 6 control specimens (without any KSE) with W/C ratio of 0.4 at 56 days

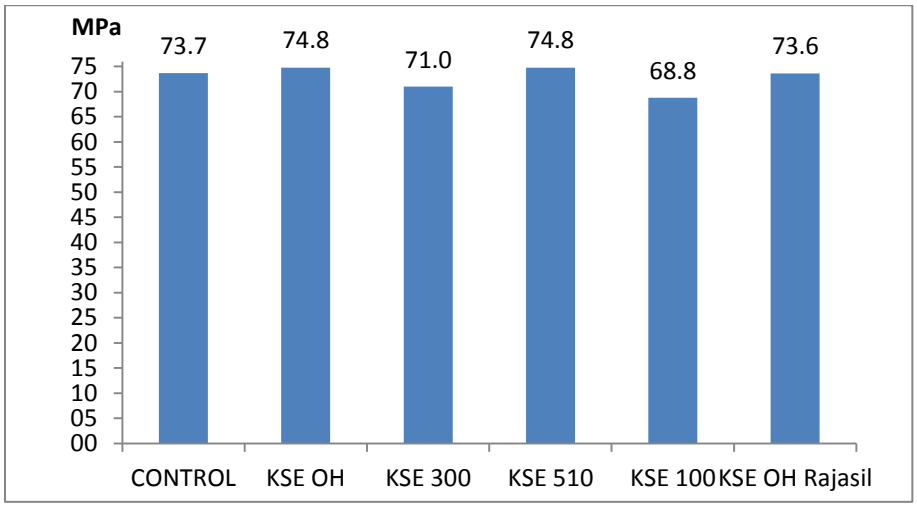

Fig. 4.39 – Average value of the compression strength of 6 specimens per each of the KSE with W/C ratio of 0.5 at 93 days

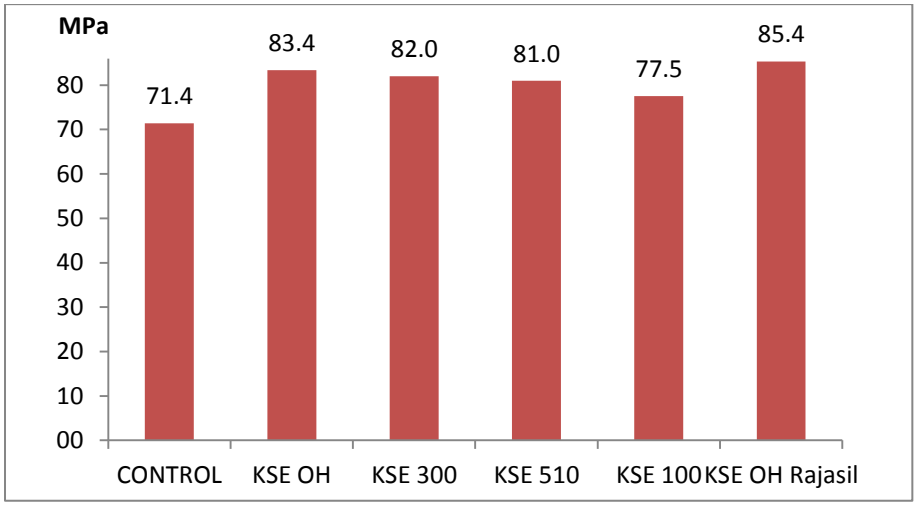

Fig. 4.40 – Average value of the compression strength of 6 specimens per each of the KSE with W/C ratio of 0.4 at 93 days

As explained in 3.9, the specimens that were used to perform the compression test were the same used in the 3-point bending test. Taking in consideration the results of the Dynamic E-Modulus test, it was expected that the KSE application would not cause major differences in the magnitude of the values obtained in this test.

If only Figures 4.40 would be taken in consideration in this discussion, maybe, the main conclusions would be that KSE does affect the compressive strength of the specimens. For example, there is a difference between the average values of the control specimens and the KSE OH from Rajasil specimens of 14 MPa, which could be considered an important difference. Although, some other aspects should be taken in consideration:

- The Figures 4.39 and 4.40 only express average values, which can be misleading to the analysis, since, for example, in the calculation of the average values of the KSE OH from Rajasil, two results were not considered since they didn't had the appropriate type of rupture (as illustrated in Figures 3.18 and 3.19), which contributed to a higher average value;
- Figures 4.37 and 4.38 show that the range of the values for specimens in the same conditions can be also significant. For example, in Figure 4.38 the major difference (between specimen "1" and "2") assumes the valor of 13.3 MPa, which is close to the one obtained between control and KSE OH from Rajasil in the specimens with 0.4 W/C ratio (Figure 4.40).

Taking this in consideration, the application of KSE does not seem to influence significantly the compression strength of the mortars in study.

All the test results can be found in the Appendix A4.

4.7. MERCURY POROSIMETRY TEST

The mercury porosimetry test results are represented by six graphics per W/C ratio (Figures 4.41 to 4.46 for an W/C ratio of 0.4 and Figures 4.47 to 4.52 with and W/C ratio of 0.5). These graphics contained the relation between the pore diameter (in μm), in horizontal axis, and the pore volume (in ml/g), in vertical axis. The intrusion data summary is showned in tabled 4.3 and 4.3 for W/C ratio of 0.4 and 0.5, respectively.

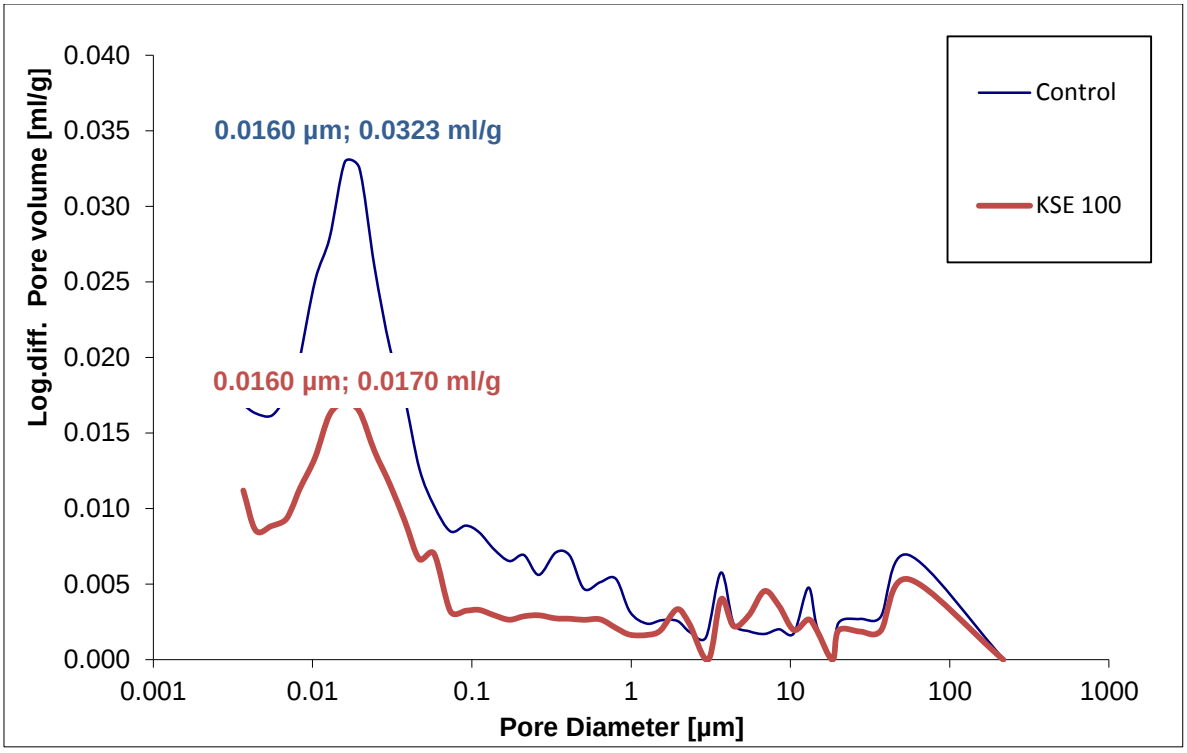

Fig. 4.41 – Porosimetry test results of the control and KSE 100 specimens with 0.4 W/C ratio

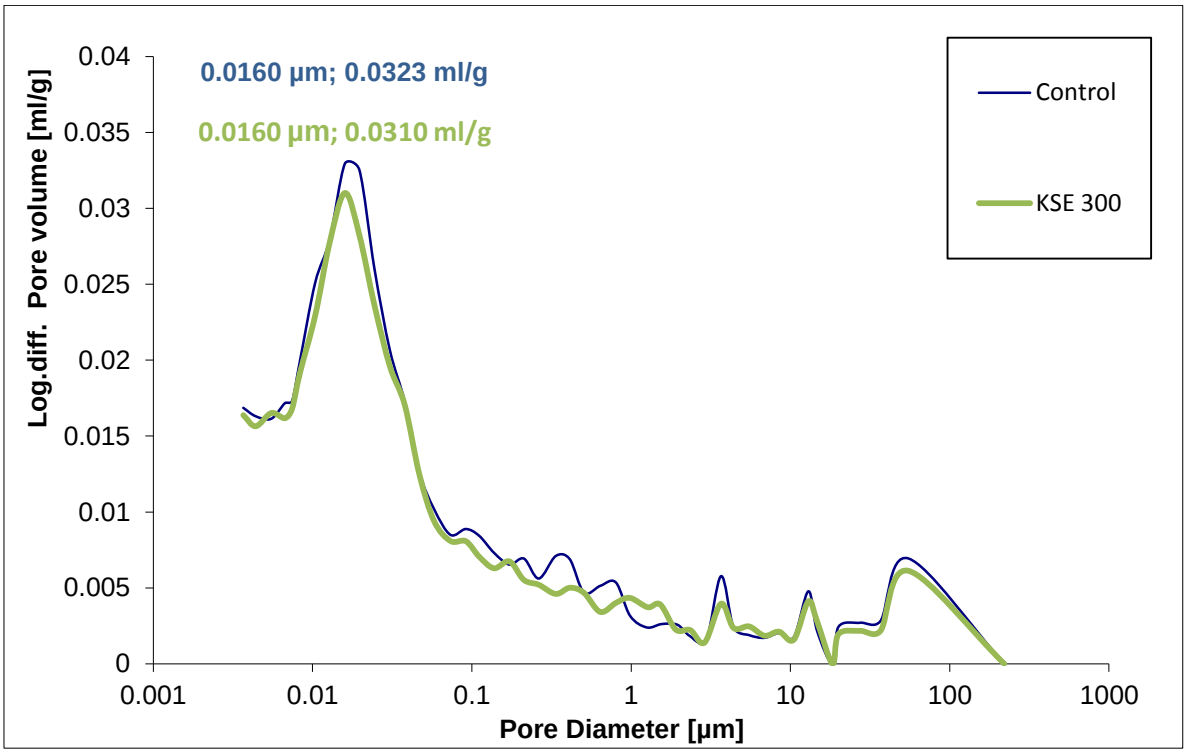

Fig. 4.42 - Porosimetry test results of the control and KSE 300 specimens with 0.4 W/C ratio

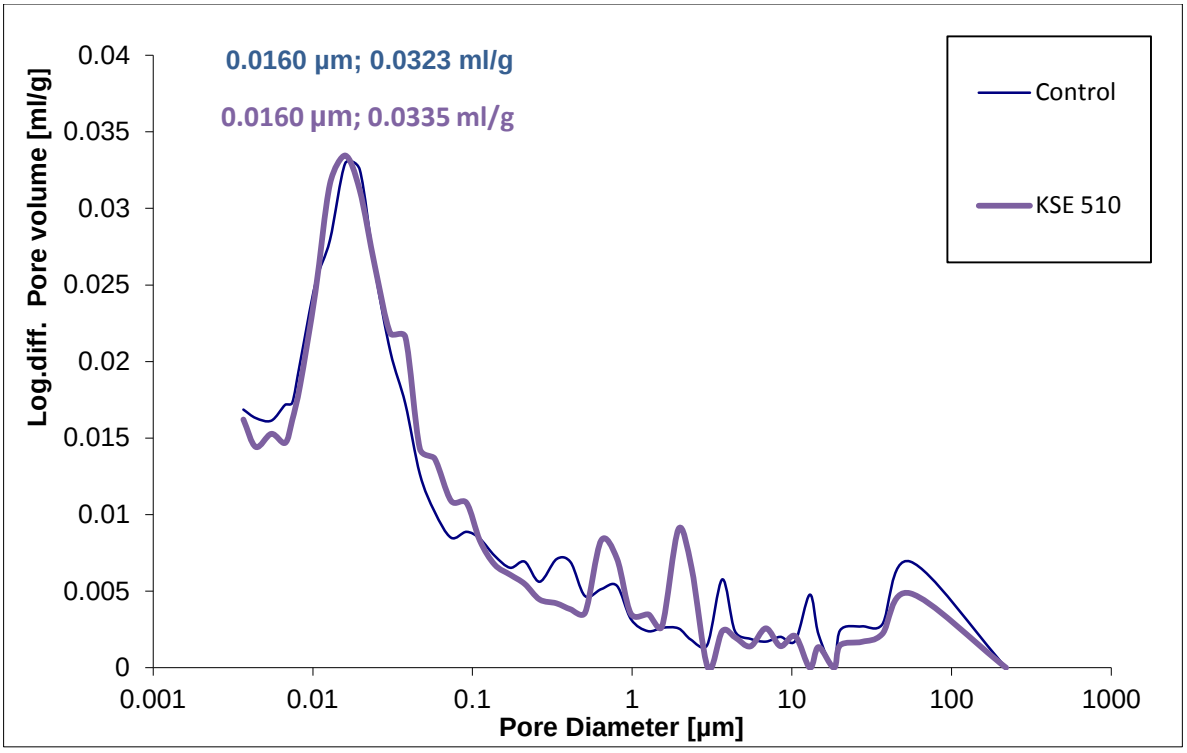

Fig. 4.43 - Porosimetry test results of the control and KSE 510 specimens with 0.4 W/C ratio

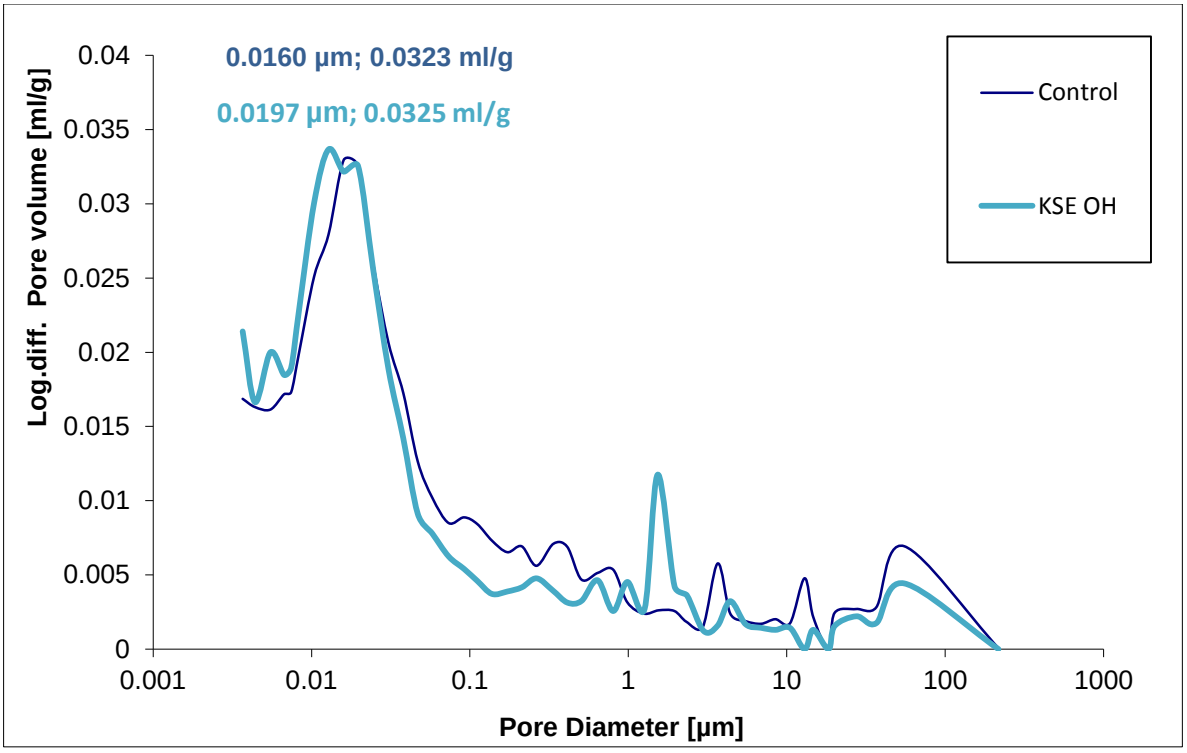

Fig. 4.44 - Porosimetry test results of the control and KSE OH specimens with 0.4 W/C ratio

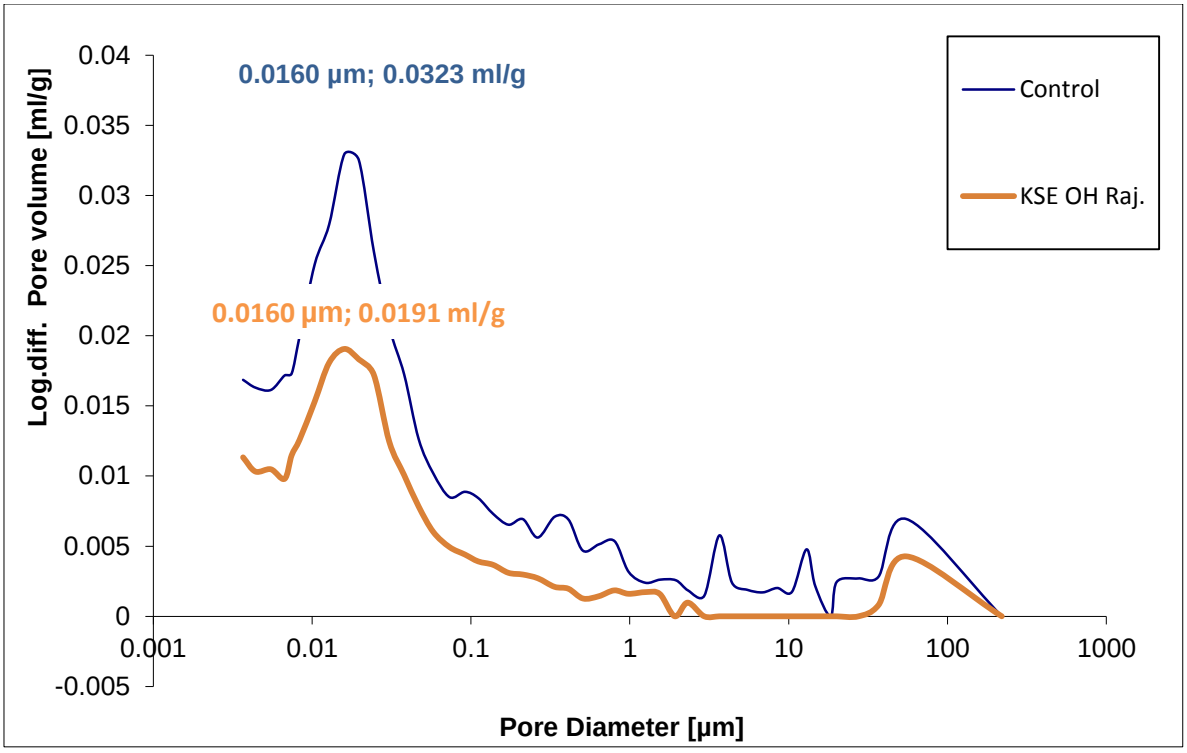

Fig. 4.45 - Porosimetry test results of the control and KSE OH from Rajasil specimens with 0.4 W/C ratio

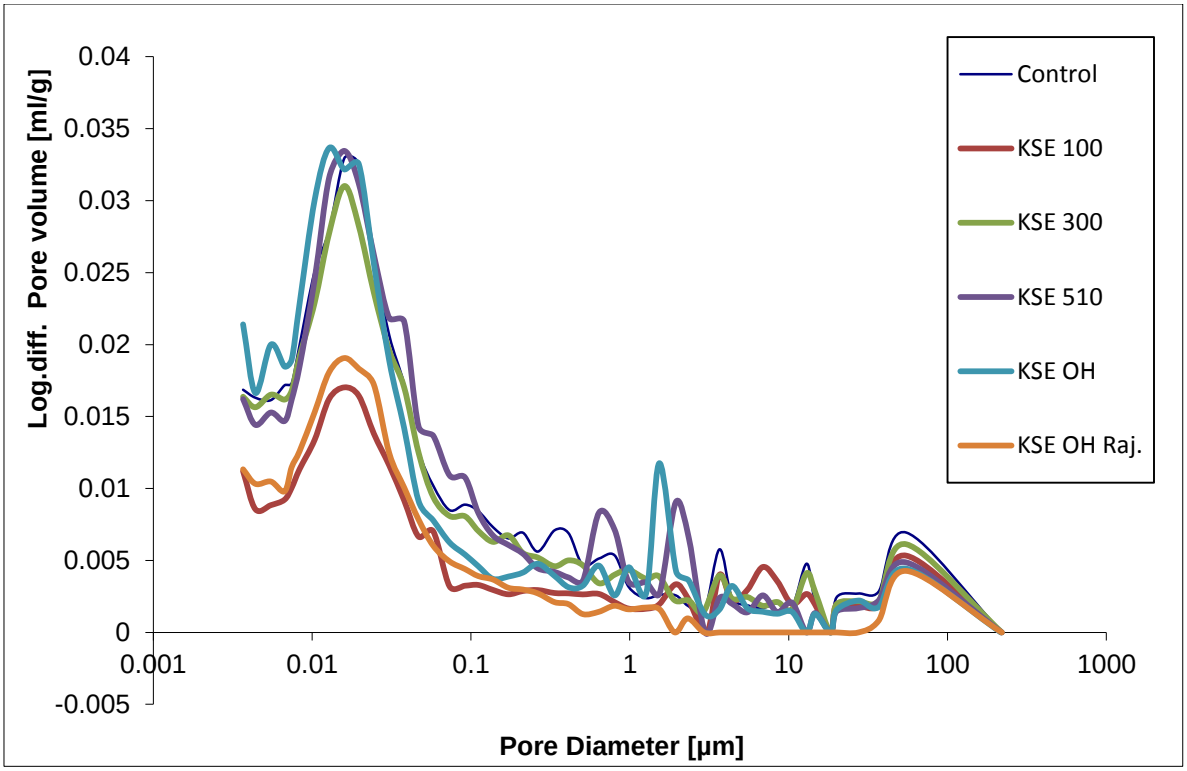

Fig. 4.46 - Pore diameter and volume of the samples with 0.4 W/C ratio

Table 4.3 – Summary of the tests performed in the specimens with 0.4 W/C ratio

0.4 W/C	Control	KSE 100	KSE 300	KSE 510	KSE OH	KSE OH Raj
Total Intrusion Volume (mL/g)	0.0433	0.0254	0.0402	0.0427	0.0403	0.0241
Median Pore Radius (Volume) (µm)	0.0314	0.0376	0.0305	0.0316	0.0231	0.0259
Median Pore Radius (Area) (µm)	0.0087	0.0083	0.0084	0.0092	0.0082	0.0083
Average Pore Radius (2V/A) (µm)	0.0192	0.0202	0.0187	0.0195	0.0162	0.0171
Porosity (%)	10.1061	5.7236	8.9281	10.7589	8.9461	5.3759
Radius of the most important family of pores (μm)	0.016	0.016	0.016	0.016	0.020	0.016

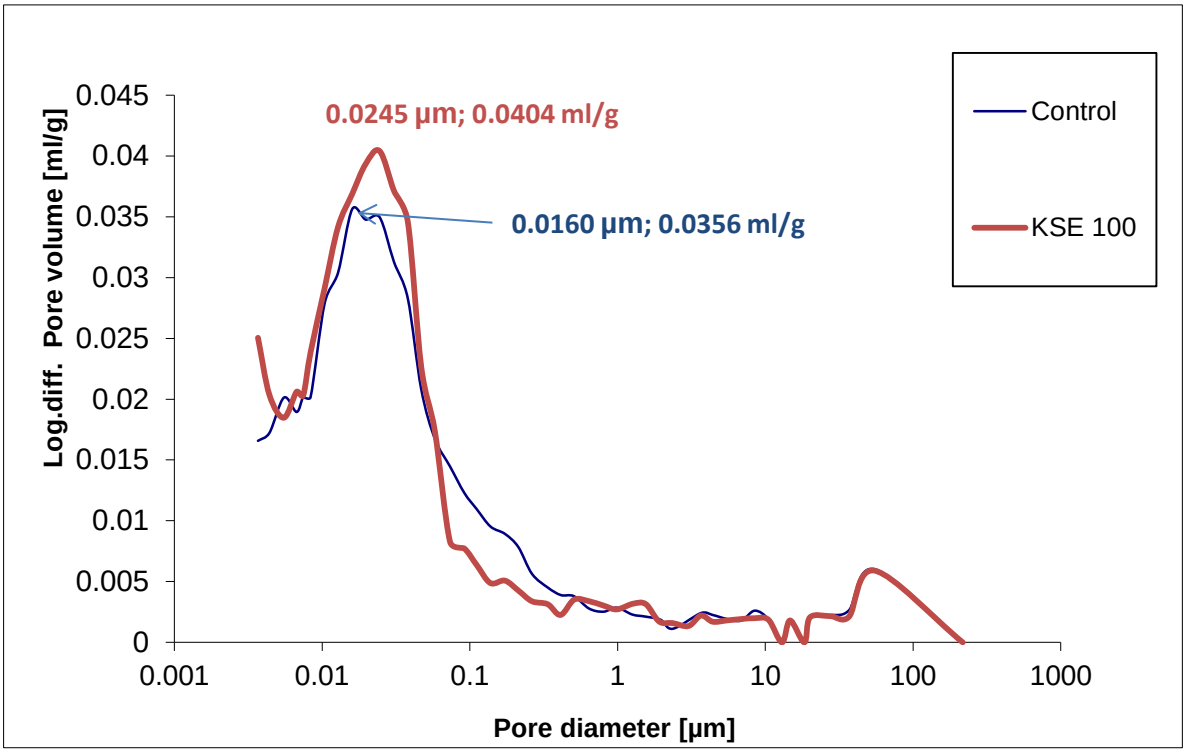

Fig. 4.47 - Porosimetry test results of the control and KSE 100 specimens with 0.5 W/C ratio

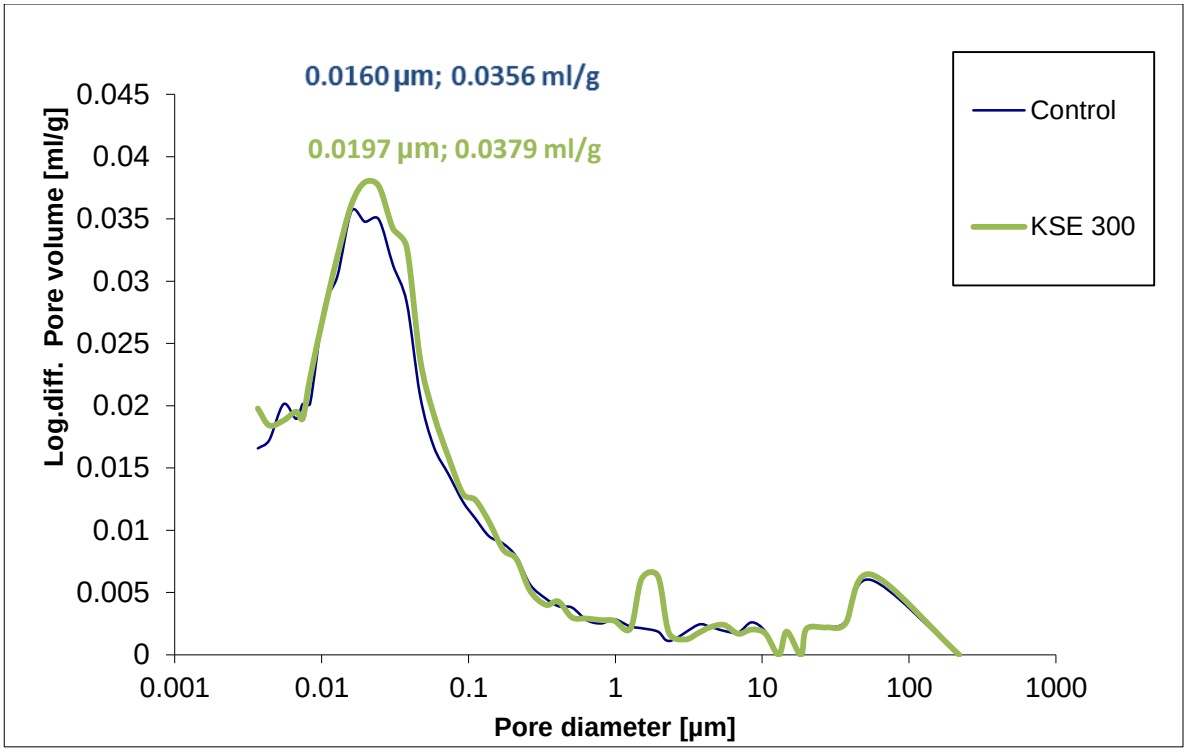

Fig. 4.48 - Porosimetry test results of the control and KSE 300 specimens with 0.5 W/C ratio

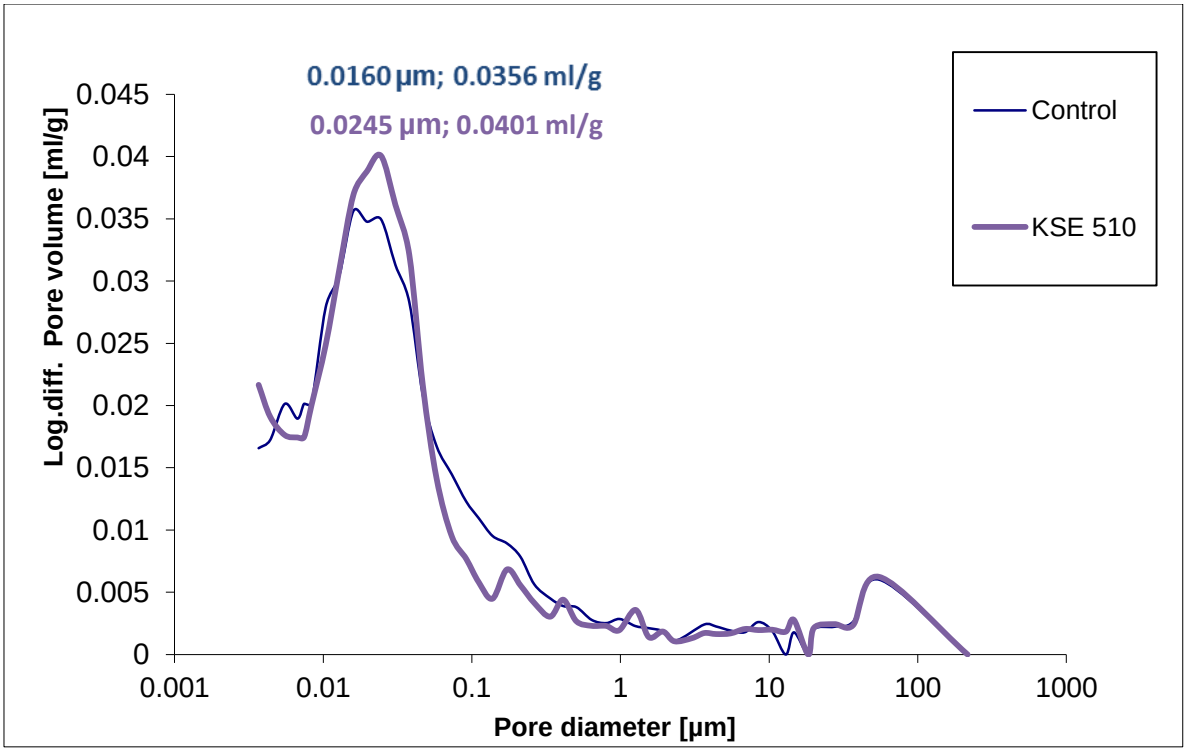

Fig. 4.49 - Porosimetry test results of the control and KSE 510 specimens with 0.5 W/C ratio

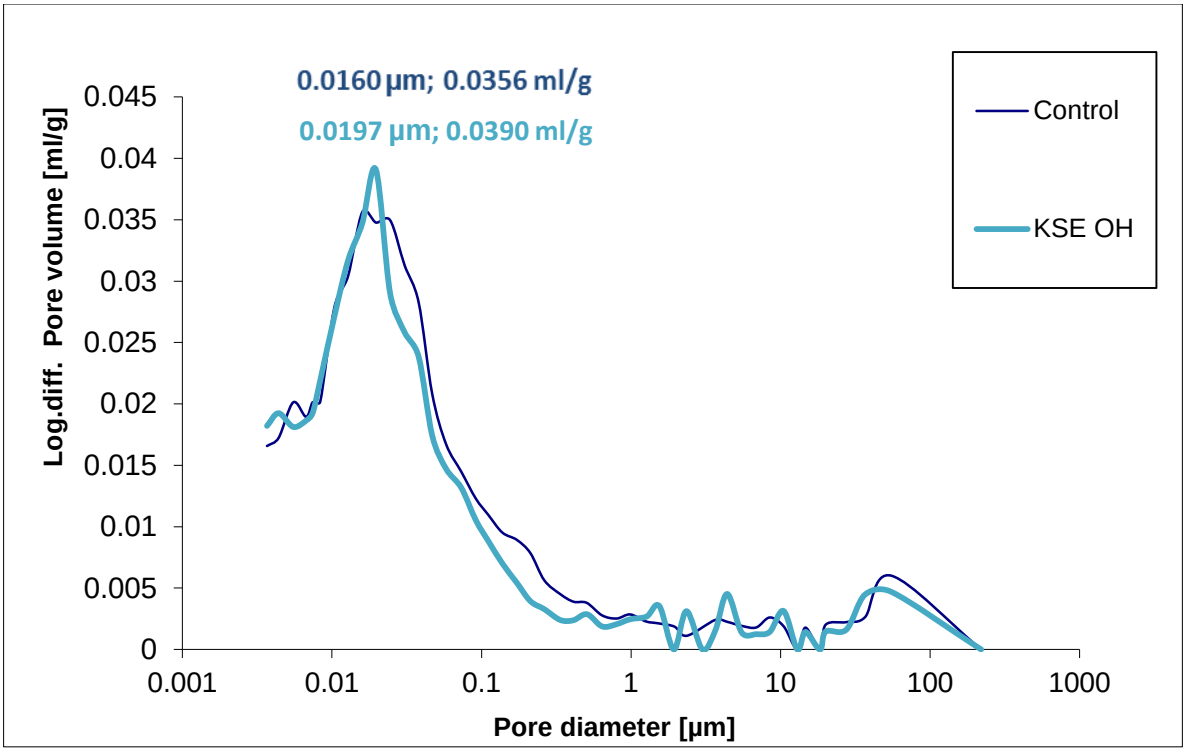

Fig. 4.50 - Porosimetry test results of the control and KSE OH specimens with 0.5 W/C ratio

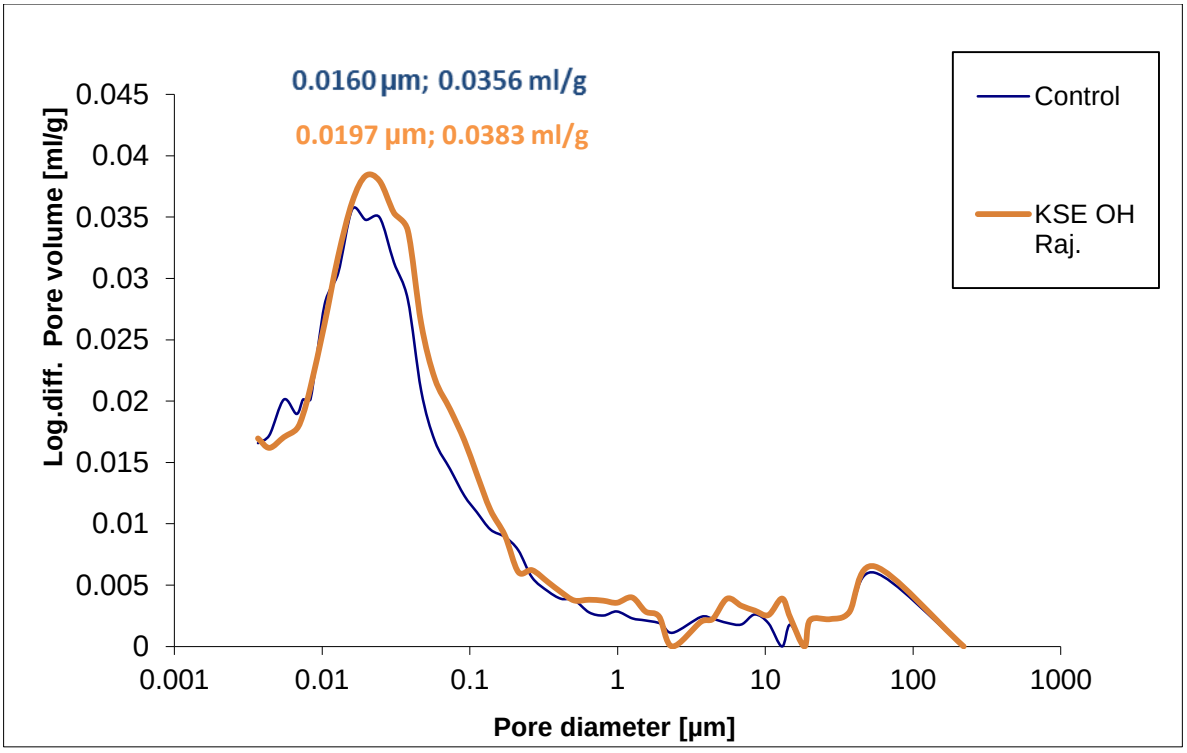

Fig. 4.51 - Porosimetry test results of the control and KSE OH from Rajasil specimens with 0.5 W/C ratio

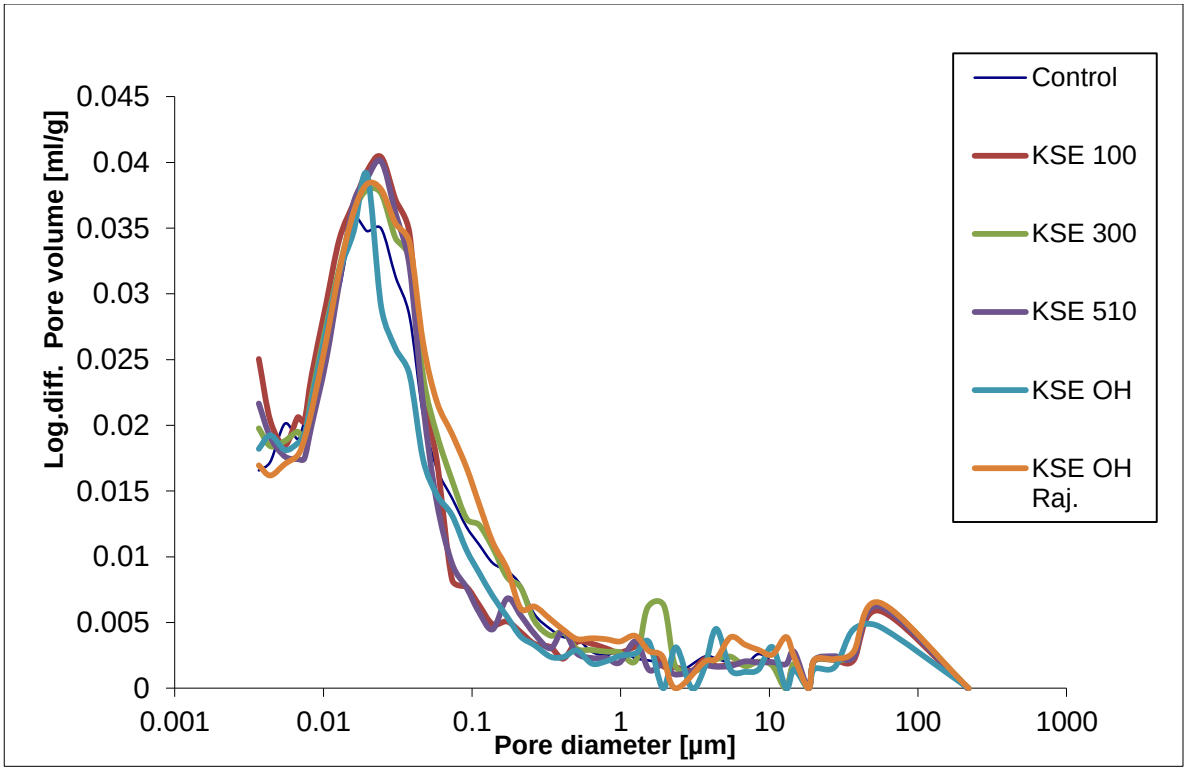

Fig. 4.52 - Pore diameter and volume of the samples with 0.5 W/C ratio

Table 4.4 – Summary of the tests performed in the specimens with 0.5 W/C ratio.

0.5 W/C	Control	KSE 100	KSE 300	KSE 510	KSE OH	KSE OH Raj
Total Intrusion Volume (mL/g)	0.0484	0.0494	0.0520	0.0472	0.0444	0.0532
Median Pore Radius (Volume) (µm)	0.0313	0.0274	0.0327	0.0286	0.0266	0.0359
Median Pore Radius (Area) (µm)	0.0090	0.0086	0.0091	0.0088	0.0087	0.0098
Average Pore Radius (2V/A) (µm)	0.0191	0.0172	0.0194	0.0180	0.0175	0.0209
Porosity (%)	10.3966	10.6299	11.1838	10.3287	9.5091	11.5767
Radius of the most important family of pores (μm)	0.016	0.025	0.020	0.025	0.020	0.20

Considering Tables 4.3 and 4.4 and Figures 4.41 to 4.52, the results of total intrusion volume (ml/g), median pore radius (volume – μm), median pore radius (area- μm), average pore radius (2V/A – μm) and radius of the most important family of pores (μm) are in the same order of magnitude.

Indeed, the total intrusion volume (ml/g) of the control specimen with 0.4 W/C ratio is 0.043 ml/g and the values of the specimens with different KSE applied are comprehended between 0.024 and 0.043 ml/g. The total intrusion volume (ml/g) of the control specimen with 0.5 W/C ratio is 0.048 ml/g and the values of the specimens with different KSE applied are comprehended between 0.044 and 0.053 ml/g.

The median pore radius (volume – μm) of the control specimen with 0.4 W/C ratio is 0.031μm and the values of the specimens with different KSE applied are comprehended between 0.023 and 0.038 μm. The median pore radius (volume – μm) of the control specimen with 0.5 W/C ratio is 0.031 μm

and the values of the specimens with different KSE applied are comprehended between 0.027 and 0.036 μm.

The median pore radius (area- μm), of the control specimen with 0.4 W/C ratio is 0.0087μm and the values of the specimens with different KSE applied are comprehended between 0.0082 and 0.0092 μm. The median pore radius (area – μm) of the control specimen with 0.5 W/C ratio is 0.0090 μm and the values of the specimens with different KSE applied are comprehended between 0.0086 and 0.0098 μm.

The average pore radius (2V/A – μm), of the control specimen with 0.4 W/C ratio is 0.019μm and the values of the specimens with different KSE applied are comprehended between 0.016 and 0.020 μm. The average pore radius (2V/A – μm), of the control specimen with 0.5 W/C ratio is 0.019 μm and the values of the specimens with different KSE applied are comprehended between 0.017 and 0.021μm.

The radius of the most important family of pores (μm), of the control specimen with 0.4 W/C ratio is 0.016μm and the values of the specimens with different KSE applied are comprehended between 0.016 and 0.020 μm. The radius of the most important family of pores (μm), of the control specimen with 0.5 W/C ratio is 0.016 μm and the values of the specimens with different KSE applied are comprehended between 0.020 and 0.025μm.

The porosity values (%) of the specimens with 0.5 W/C ratio are in the same order of magnitude. The control specimen has a porosity of 10.4 % and those with different KSE applied are between 9.5 and 11.6 %.

On the opposite, there are major differencies between the specimens with 0.4 W/C ratio. The control specimen has a porosity of 10.11% and those where KSE 300, KSE 510 and KSE OH has been applied are between 8.93 and 10.76%. In specimens where KSE 100 and KSE OH from Rajasil has been applied, porosity is about one half of that of the control specimen, ranging between 5.38 and 5.72%.

It can be concluded that the application of similar quantities of the different KSE did not change the dimensions of the pores or they became slightly bigger.

The application of the different KSE strengthning products did not affect the compression strength. There is no significant results between the control specimens and those with different KSE applied. However, the porosity was reduced to half of the control specimen in those two where KSE 100 and KSE OH were applied which is contrary to the results of the compression test that did not show significant differences. A major reduction of the porosity of the specimens should be translated by a significant increase of the compressive strength and a high decrease in the total intrusion volume of mercury.

4.8. KSE PENETRATION DEPTH TEST

The KSE penetration depth results are illustrated in Figures 4.53 to 4.56. In these figures, it is possible to notice the action of the indicator in the specimens which is translated by a color change. Although only four figures are showed, they illustrate the results of all the specimens, since the same result was obtained in all the tests.

Fig. 4.53 – KSE penetration depth test

Fig. 4.54 – KSE penetration depth test

Fig. 4.55 – Comparison between the coloration samples with and without KSE applied.

Fig. 4.56 – Comparison between the coloration of samples with and without KSE applied

The results of this test far exceeded the ones that were expected. Taking in consideration that the KSE was applied in one face, it was expectable that the penetration developed from that face until some millimeters deep, establishing (with the help of the indicator used) a line/border in the cross section.

This would, therefore, enable to measure the penetration depth with a caliper.

This line/border was not formed and, instead, all the cross section assumed a red tone, meaning that the penetration was 40mm (Figures 4.54 and 4.55). This happened for all the specimens.

After performing the tests, the veracity of the indicator was putted in doubt:

Should all the samples be red?

Maybe the indicator was badly chosen and it is not truly indicate the presence of KSE.

The better way to erase these doubts was to apply the same indicator in specimens without KSE and see if the specimens also acquire a red tone. Those specimens did not change their color to red. This comparison illustrated in Figures 4.56 and 4.57 proves that KSE penetrated, indeed, in all the cross section of the specimens.

4.9. EXPANSION TEST

Before going forward in the results of the expansion test, it is important to remember some information that was present in point 3.3.1 and 3.3.2.

First the description of the cements:

- CEM I 42.5 (dw) (Where dw stands for "Dyckerhoff Weiss" that can be translated to Dyckerhoff white, being Dyckerhoff the name of the company of production);
- CEM I 42.5 R-HS/NA (Where HS stands for "Hoher Sulfatwiderstand" in German which can be translated as high sulfate resistance), or in European Standards referred to as SR;
- CEM II/A-LL 42.5 N (Where LL stands for limestone, in this case 6 to 20% by mass);
- CEM III/B N-LH/HS/NA (Where LH stands for low heat of hydration);
- CEM 42.5 N ;
- HSR Black label Tiefbohrzement (where tiefbohrzement can be translated as deep drilling cement and HSR stands for high sulfate resistance);

Then, all the acronyms correspondence:

- Z556 - CEM I 42.5 (dw);
- Z554 - CEM I 42.5 R-HS/NA;
- Z558 - CEM II/A-LL 42.5 N;
- Z557 - CEM III/B N-LH/HS/NA;
- Z559 - CEM 42.5 N;
- Z555 - HSR Black label Tiefbohrzement;

And finally, the KSE description (Table 4.5):

Table 4.5 – Description of the KSE used

	KSE 100	KSE 300	KSE 510	KSE OH	KSE OH Rajasil
Active Ingredient Content	20%	100%	100%	75%	75%
Gel deposit ratio	10%	30%	40%	30%	-

The difference, in millimeters, between the expansion of the specimens observed at 24 hours and at 28 days are showned in Figures 4.57 to 4.62. On these graphics, the color of the bars is not important or representative. All the specimens had a W/C ratio of 0.5. The detailed expansion (values and images)

of each one of the specimens in all the measure frequencies (24 hours, 3, 4, 7, 11, 17, 28 and 35 days) referred in point 3.12.2 can be consulted in Appendix A5.

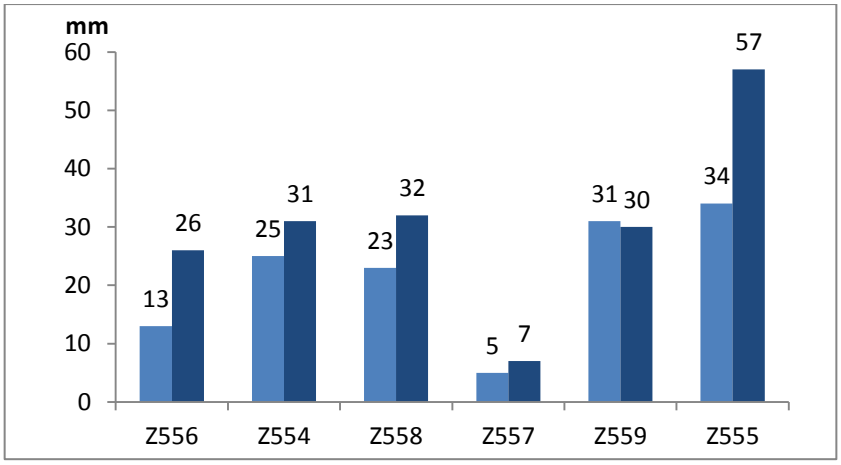

Fig. 4.57 – Results of the difference, in mm, between the expansion at 24 hours and the expansion at 28 days measured in two rings per type of cement Z554 to Z559

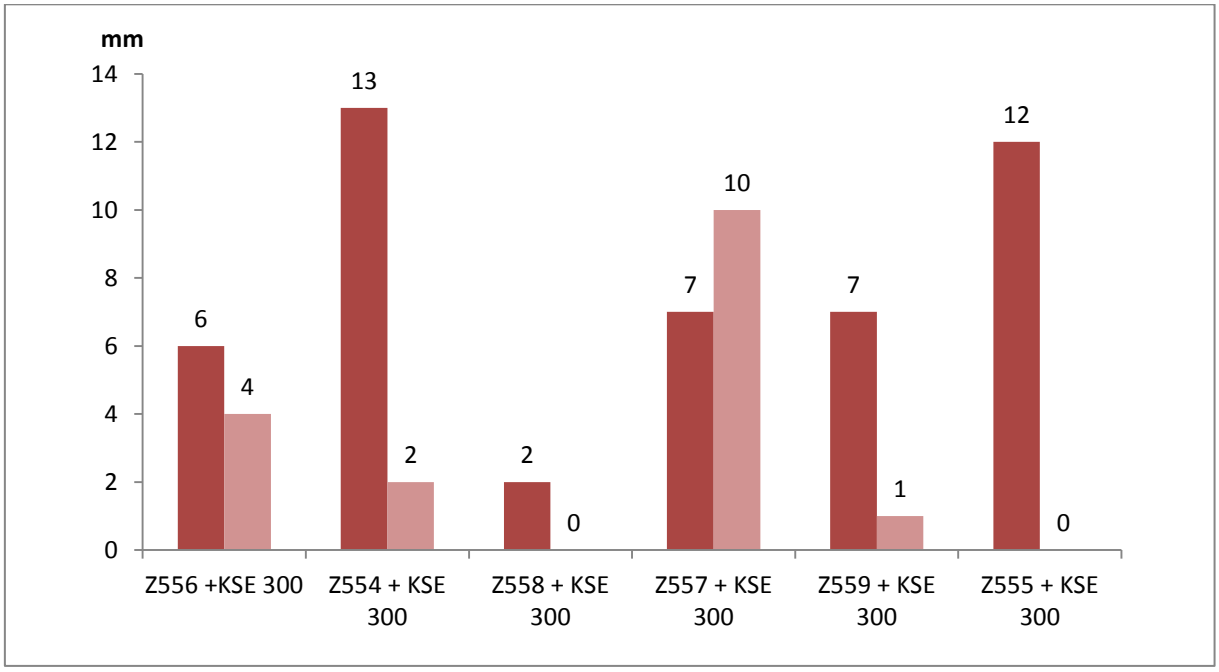

Fig. 4.58 Results of the difference, in mm, between the expansion at 24 hours and the expansion at 28 days measured in two rings per type of cement plus KSE 300.

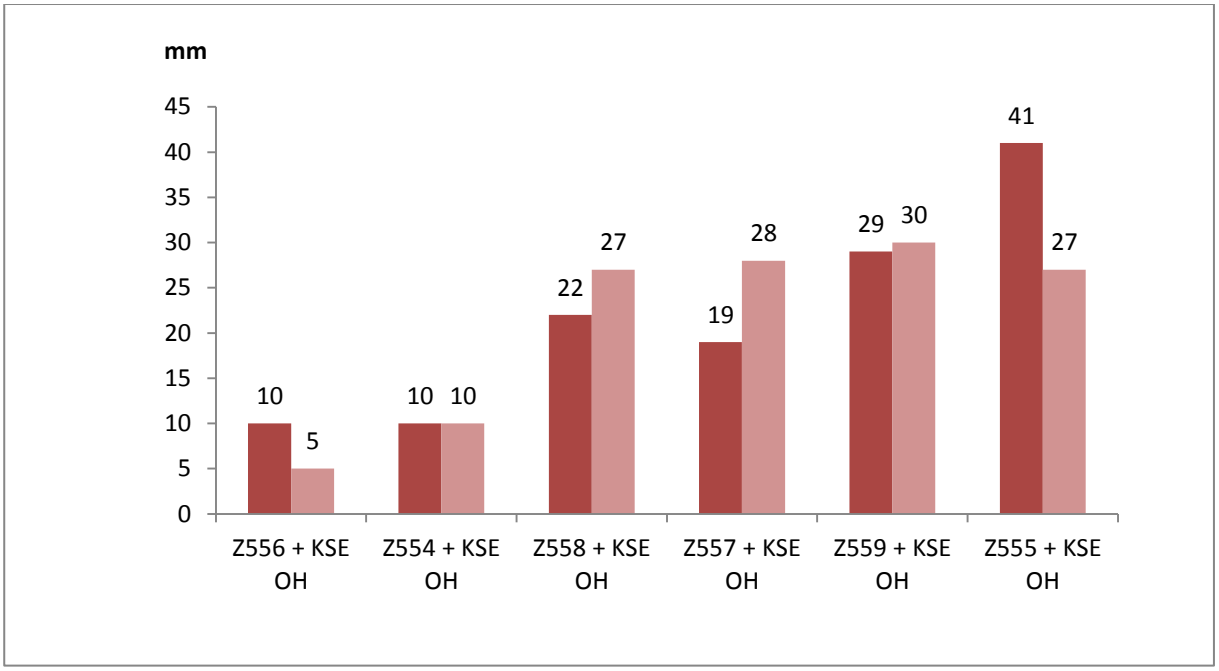

Fig. 4.59 Results of the difference, in mm, between the expansion at 24 hours and the expansion at 28h measured in two rings per type of cement plus KSE OH.

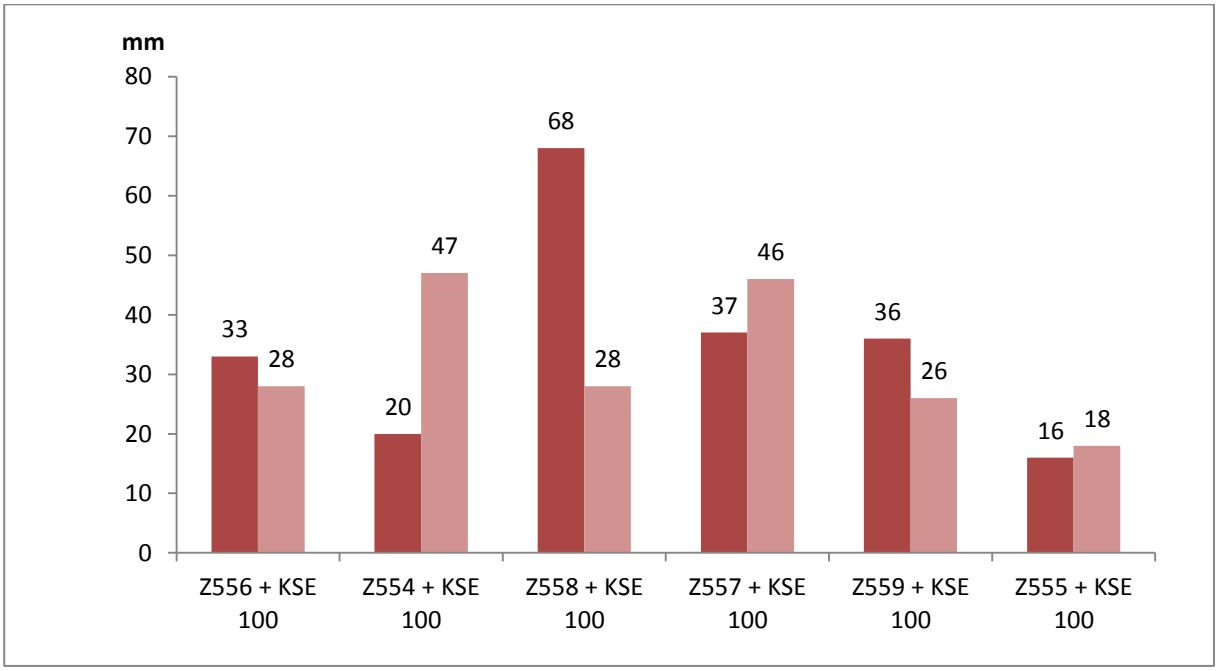

Fig. 4.60 – Results of the difference, in mm, between the expansion at 24 hours and the expansion at 28h measured in two rings per type of cement plus KSE 100.

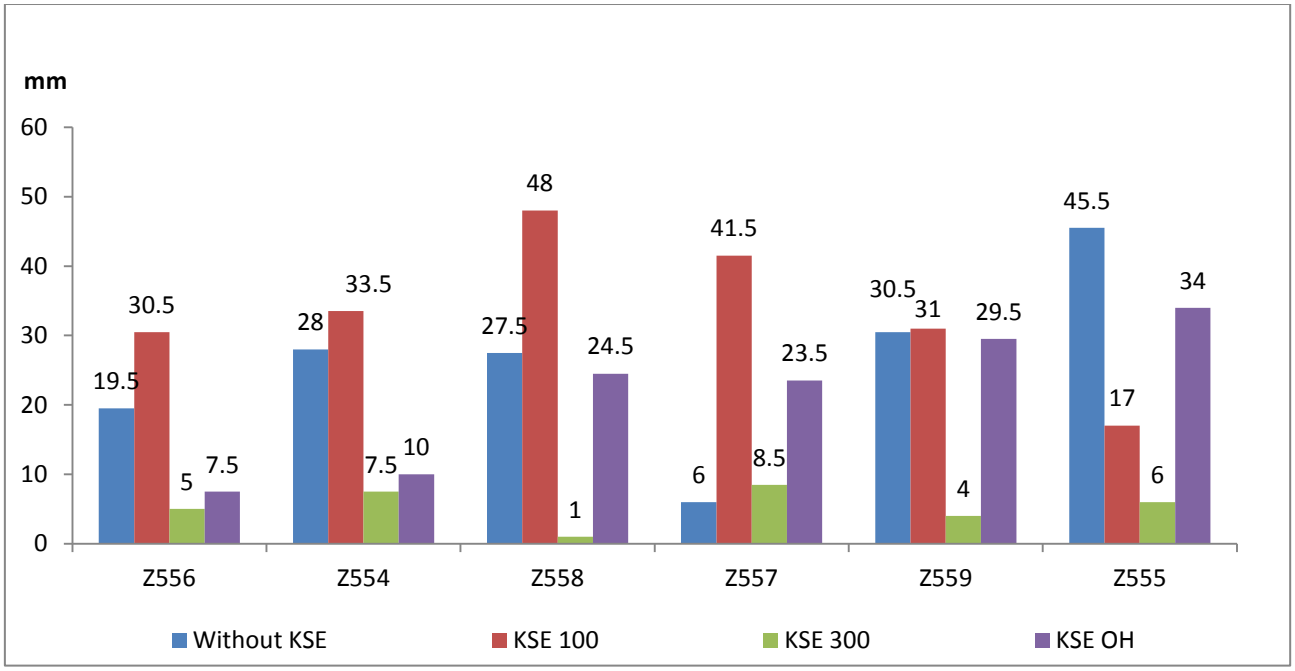

Fig. 4.61– Average expansion value, at 28 days, of two rings per all combinations of cement or cement + KSE.

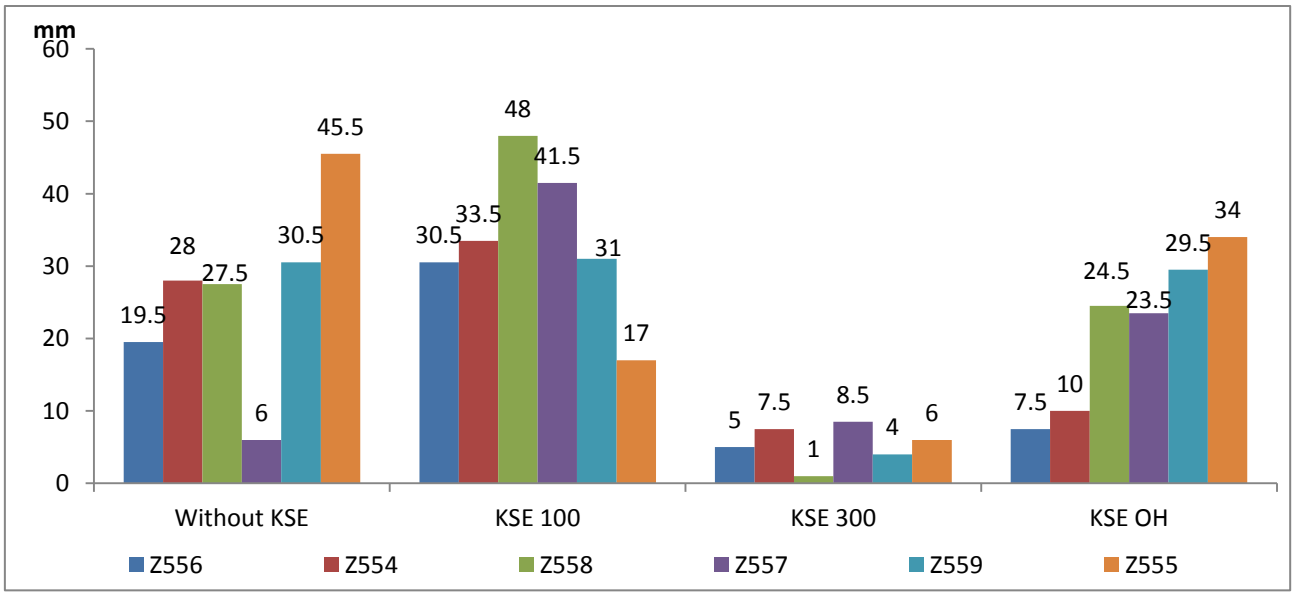

Fig. 4.62 - Average expansion value, at 28 days, of two rings per all combinations of cement or cement + KSE.

There are several aspects that can be understood by the analysis of Figures 4.57 to 4.62.

- The first one to be notice is that the application of KSE increased the expansion values in all the specimens of Z557;
- In the cements Z555 and Z559, the application of KSE decreased the expansion values with the exception of the KSE 100 with a slightly increase of 0.5 mm;
- KSE 300 and KSE OH decreased the expansion in all the cement types besides Z557;

- The KSE with lower values of expansion was the KSE 300;
- KSE 100 increases the expansion in all cement types besides, the previously referred, Z555.

With the first aspects referred in this discussion and with the information that was "recalled" from Chapter 3, it is possible to take conclusions about the results of this study.

There are two probable explanations for increased expansion verified in the Z557:

- The blast furnace slag;
- The Low heat of hydration.

These are the only characteristics than cannot be found in any other of the specimens in study, and, therefore may be the ones responsible for the increase in the expansion values in comparison with the control samples. It is though not possible to know if only one of them is causing the expansion or if the expansion is caused by both of these characteristics. Test with cements with only one of these two characteristics should be carried out in order to have some results allowing any conclusions.

If the cements do not have neither of these properties, the higher the active ingredient content, tetraethyl ortholisicate, the lower the expansion values. The lowest expansion values correspond to KSE 300 which contains 100% of the active ingredient. The lower this ingredient content is, more random are the expansion values. For example, KSE 100 which has 20% of active ingredient either increases or decreases the expansion.

4.10. SCANNING ELECTRON MICROSCOPY ANALYSIS

The results of the SEM test are the images obtained. Only some of the images with 1000x and 16000x zoom are presented. Figures 4.63 to 4.68 show the images with 1000x zoom. Figures 4.70 to 4.75 show the images with 16000 zoom. The rest of them can be consulted in Appendix A6.

In the figures with 1000x it is mainly possible to identify the CSH gel and some pores.

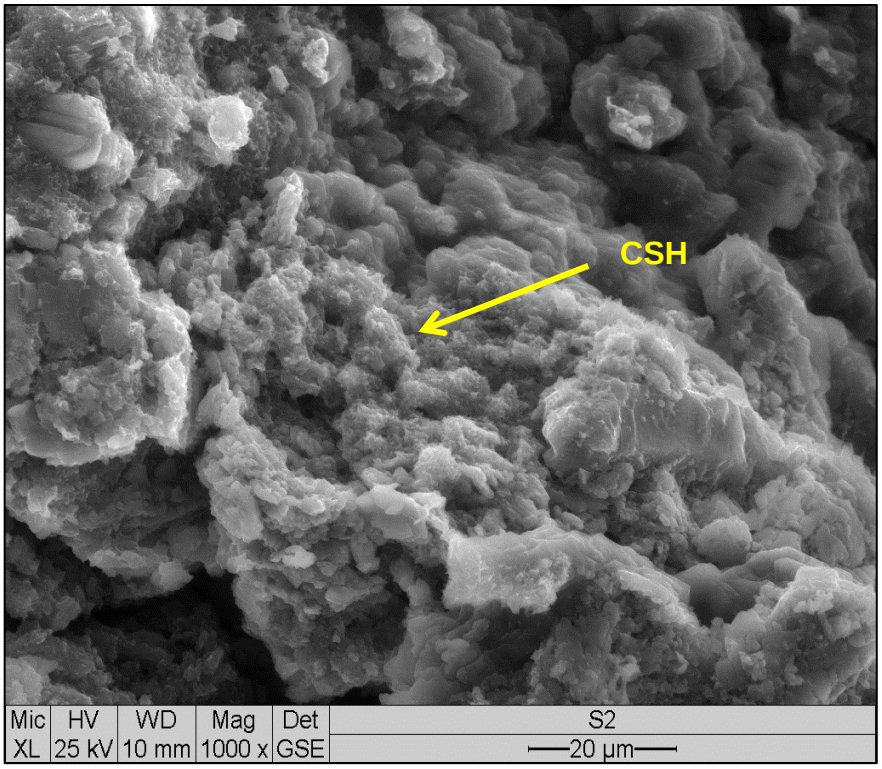

Fig. 4.63 – SEM image of a sample with Z556 mixture

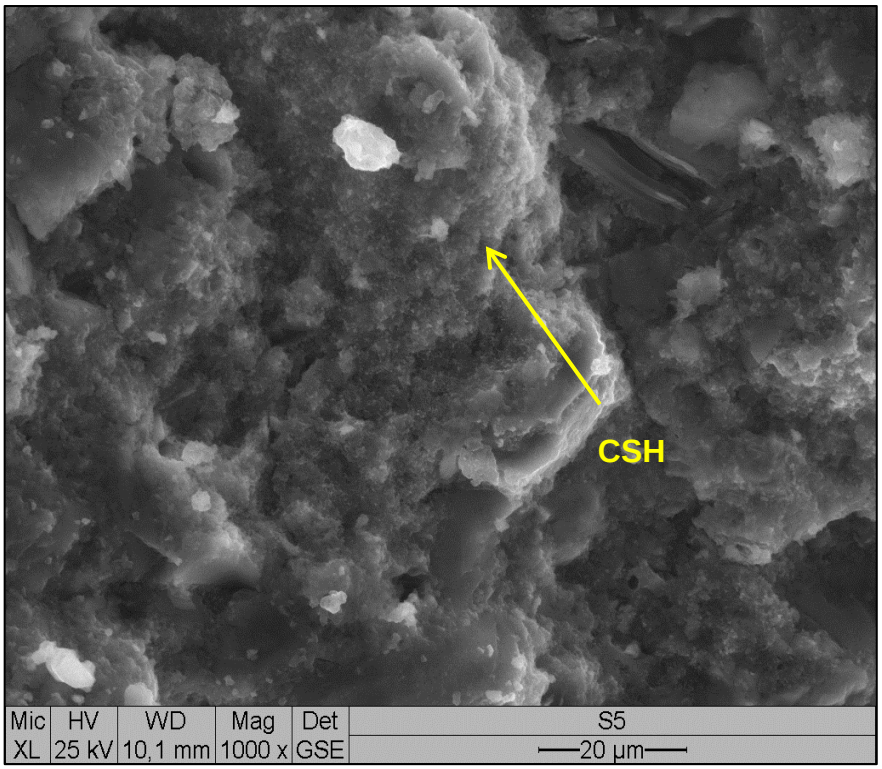

Fig. 4.64 – SEM image of a sample with Z559 mixture

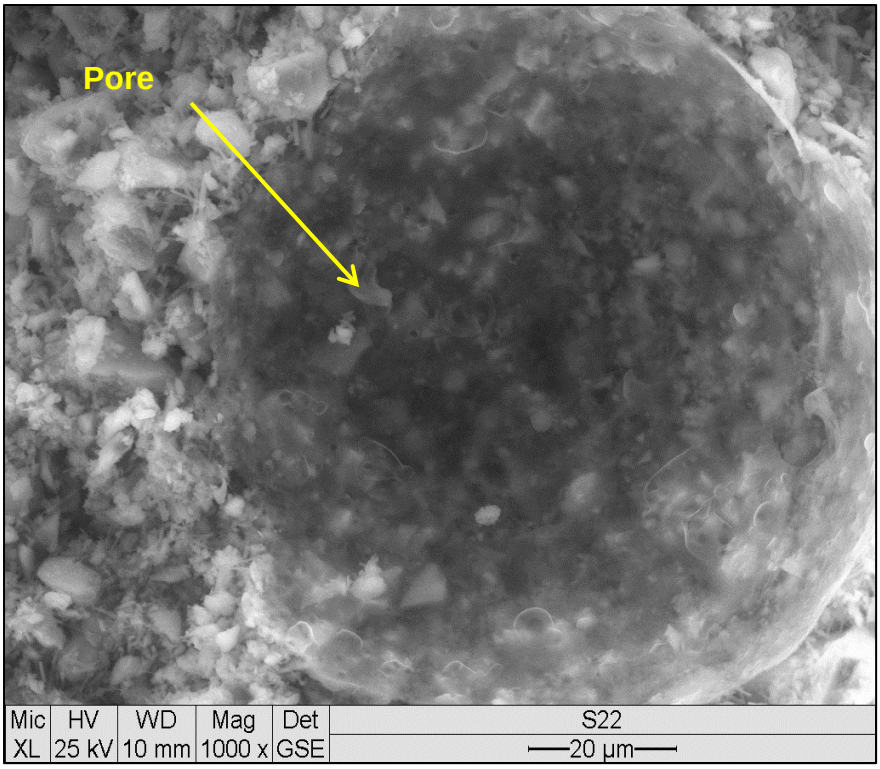

Fig. 4.65 – SEM image of a sample with Z555 + KSE OH mixture

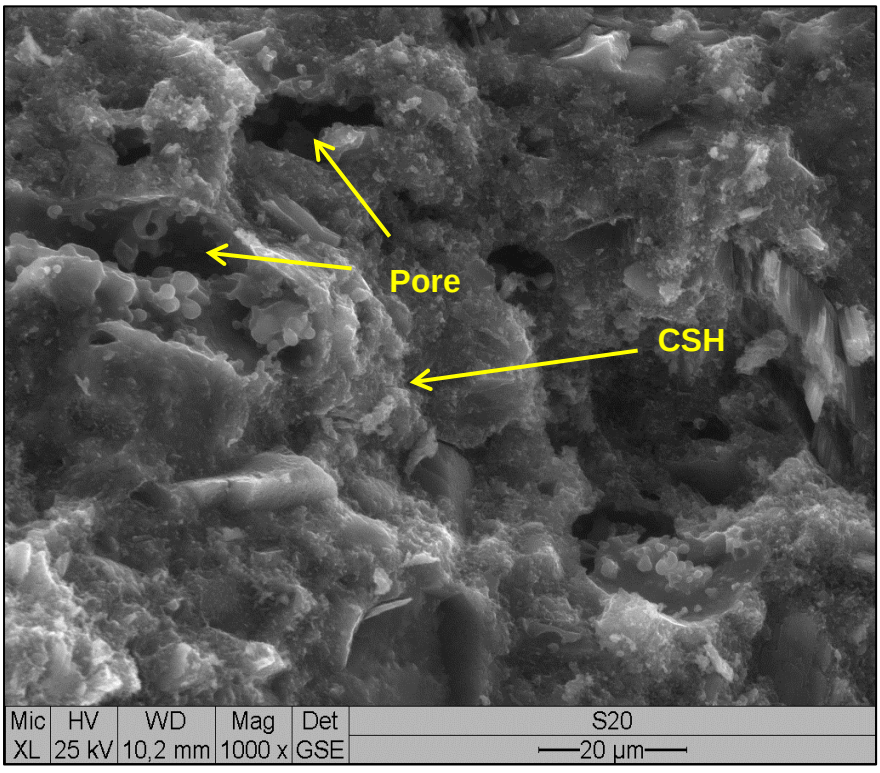

Fig. 4.66 – SEM image of a sample with Z554 + KSE 100 mixture

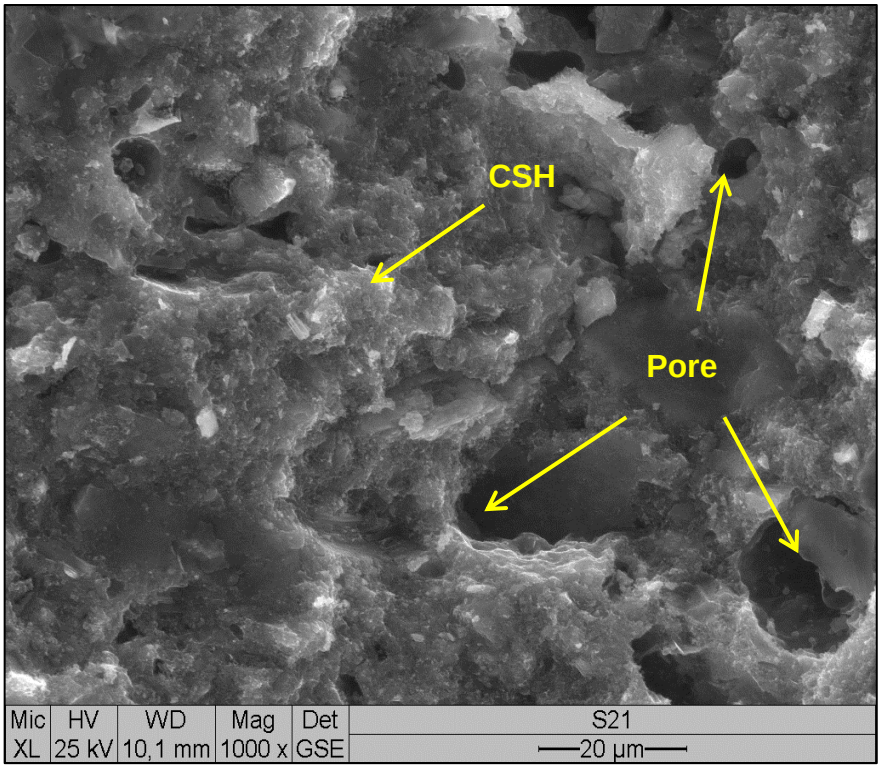

Fig. 4.67 – SEM image of a sample with Z558 + KSE 100 mixture

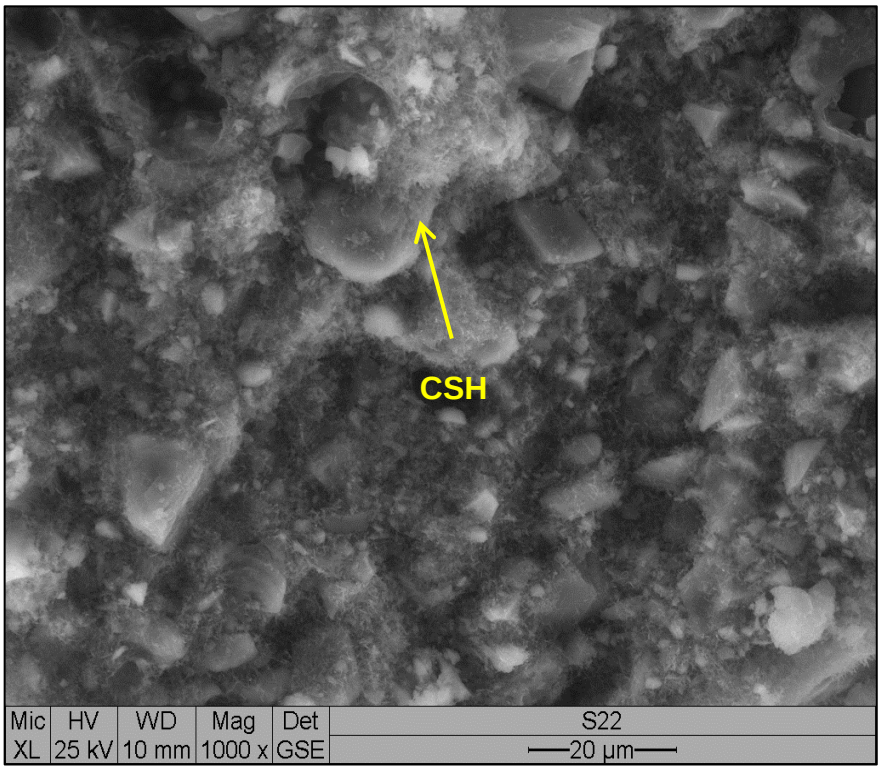

Fig. 4.68 – SEM image of a sample with Z557 + KSE 100 mixture

In the next group of figures it is possible to observe the formation of ettringite. Figures 4.69 and 4.70 show the formation of ettringite in two samples without the application of KSE. With the observation

of these figures it is possible to notice that the crystals are arranged very close to each other and that the expected hexagonal cross section of the crystals is almost perfect.

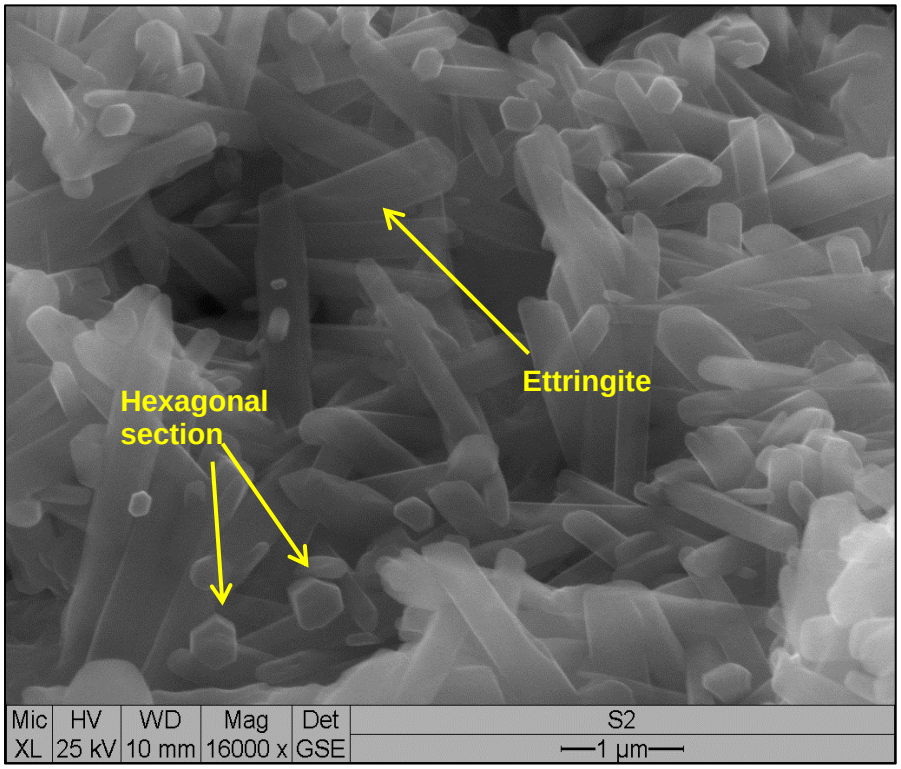

Fig. 4.69 – SEM image of a sample with Z556

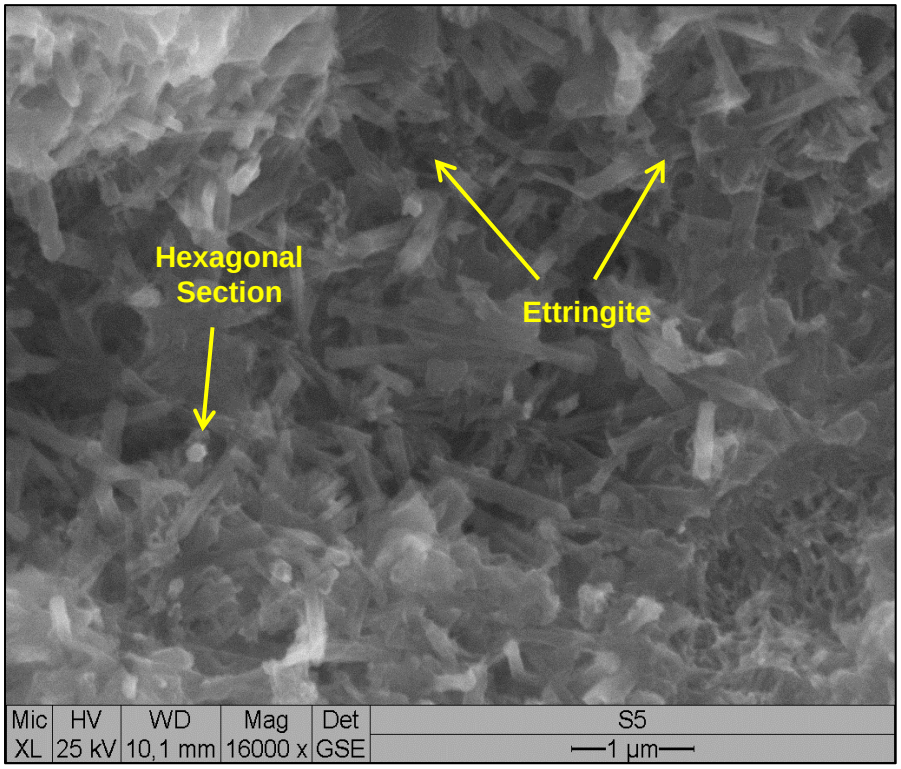

Fig. 4.70 – SEM image of a sample with Z559 mixture

Figures 4.71 to 4.74 correspond to SEM images of the specimens with the application of KSE. It is possible to notice that the crystals acquire a more acicular habit and the crystals are thinner than the ones presented in Figures 4.69 and 4.70. Moreover, it is also possible to see that the section of the crystals is not as hexagonal as before and some of them even acquire a slightly round shape. Besides, the crystals are not arranged as close to each other as before and, therefore, there is more space between them.

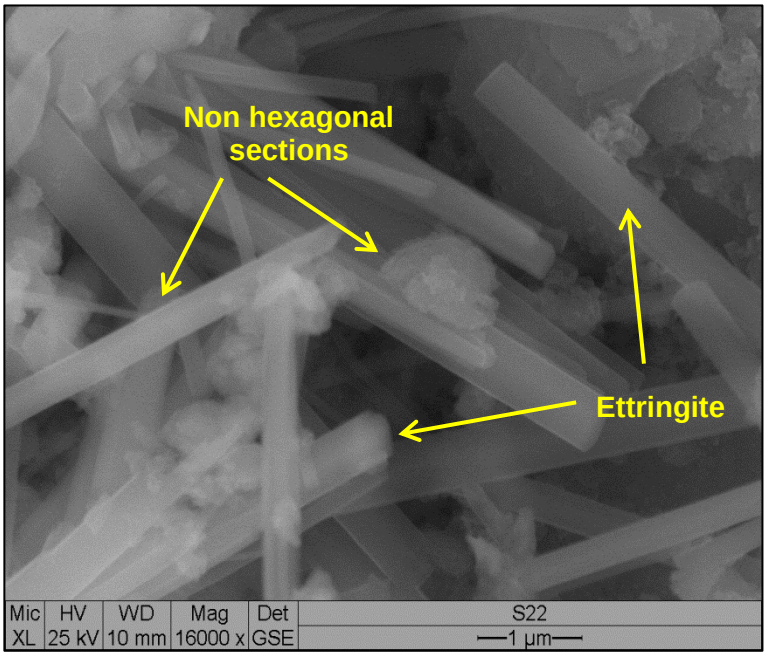

Fig. 4.71 – SEM image of a sample with Z555 + KSE OH mixture

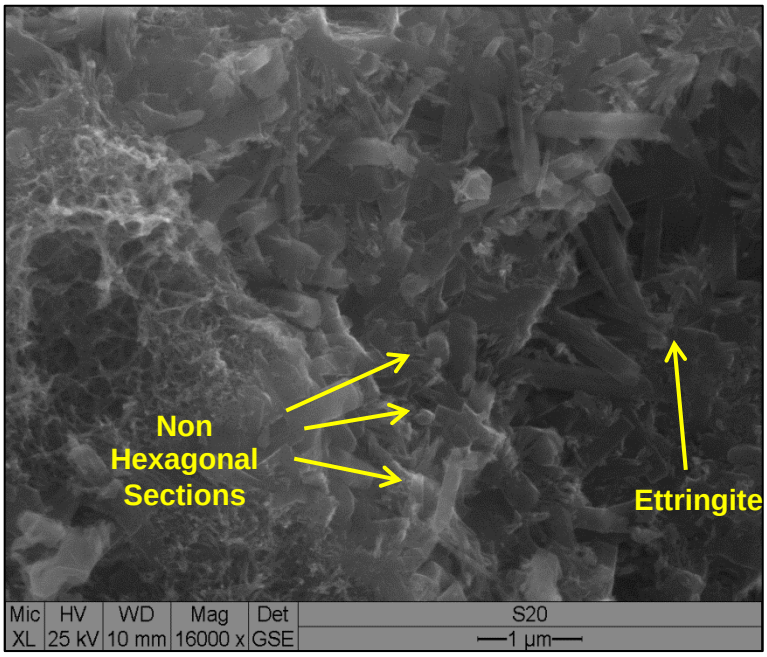

Fig. 4.72 – SEM image of a sample with Z554 + KSE 100 mixture

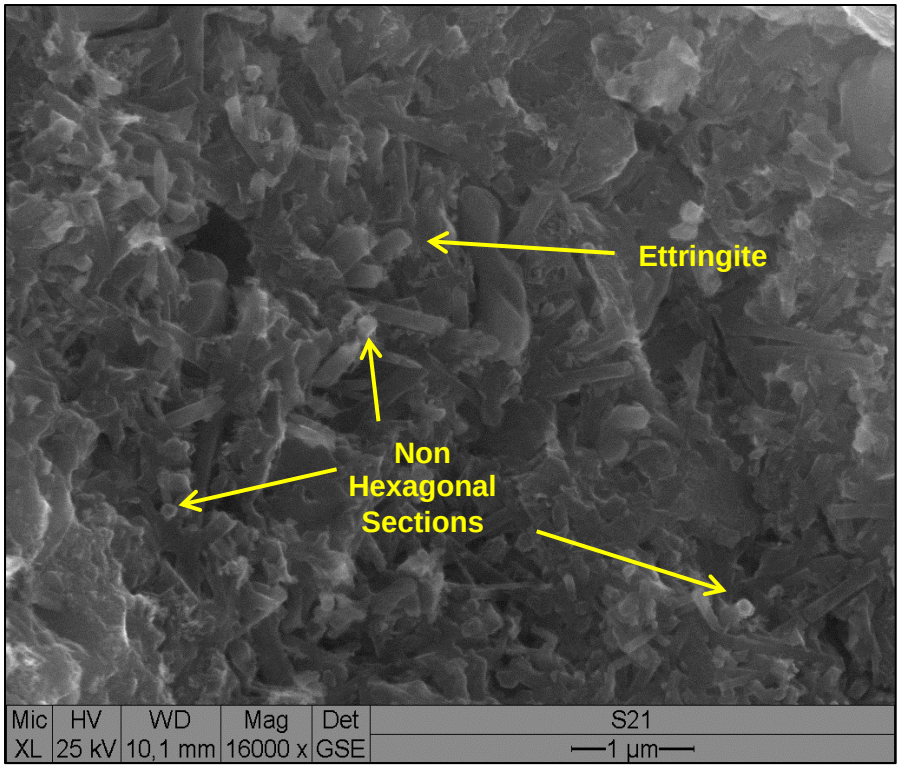

Fig. 4.73 – SEM image of a sample with Z558 + KSE 100 mixture

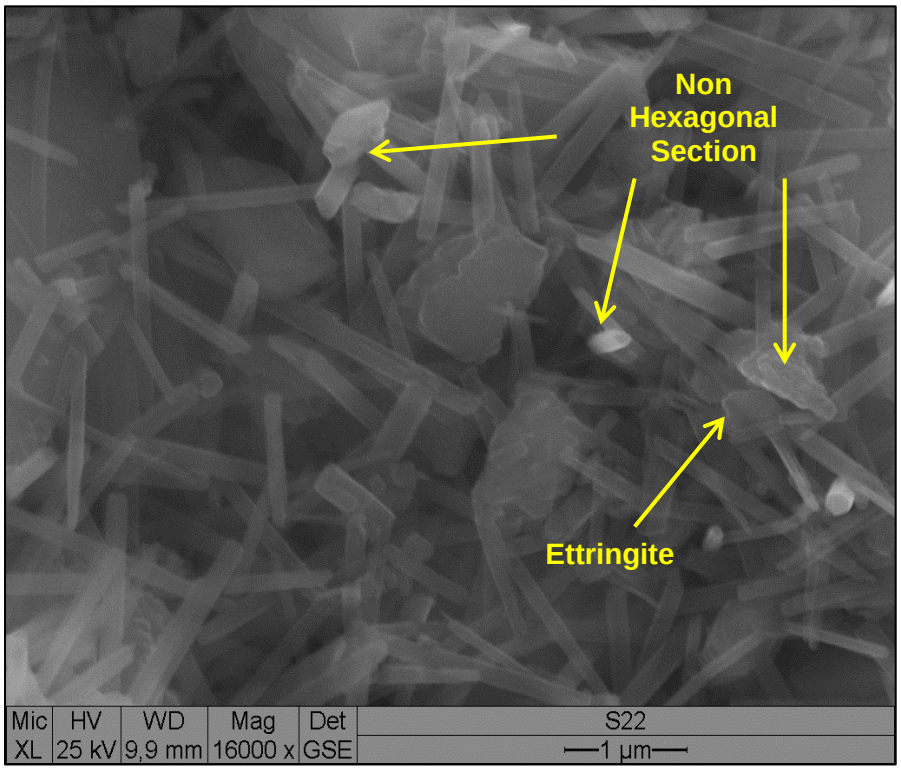

Fig. 4.74 – SEM image of a sample with Z557 + KSE 100 mixture

4.11. X-RAY POWDER DIFFRACTION STUDY

The Rietveld quantitative analysis are really complex and time consuming (it takes at least 8 weeks to do it properly) and, due to the time limit imposed to the realization of this work, it was only possible to perform the Rietveld analysis in two of the cement types (Z556 and Z554).

However it was possible to do a semi-quantitative analysis that included all the specimens that enabled conclusions to be withdrawal.

The six diffractograms (one for each cement type and containing the four case studies for each one of them, *i.e.* only cement, cement plus KSE 300, OH and 100) that lead to the semi-quantitative analysis are presented in Figures 4.75 to 4.80 and Tables 4.6 to 4.11. Figures 4.81 to 4.84 show the results of the Rietveld analysis performed.

The results of the semi-quantitative analysis will be present by the means of "+", with the following correspondence:

"+++++" – highest concentration;

"+" – very low concentration;

"(+)" – near the detection limit.

From the semi-quantitative analysis expressed in Tables 4.6 to 4.11. it is possible to understand that the application of KSE did not lead to significant differences on the phases. If only the semi-quantitative analysis would be taken in consideration, for the two phases that are the aim of this thesis, ettringite and thaumasite, one major conclusion could be withdrawn:

The application of KSE slightly decreases or maintains the percentage of ettringite and thaumasite formed in the specimens in study.

The results of the Rietveld analysis are represented in percentage. The percentage values of ettringite and thaumasite are always shown above the bars.

Although this conclusion seems undeniable looking at the results of the semi quantitative analysis, the Rietveld analysis performed in the specimens with cement 42,5 dw and 42,5 R HS/NA (Z556 and Z554 respectively) reveals a different result. The application of KSE 100 did not maintain the percentage of the crystals but, instead, increased ettringite percentage in both cement mixtures and thaumasite in the Z556 as illustrated in Table 4.12.

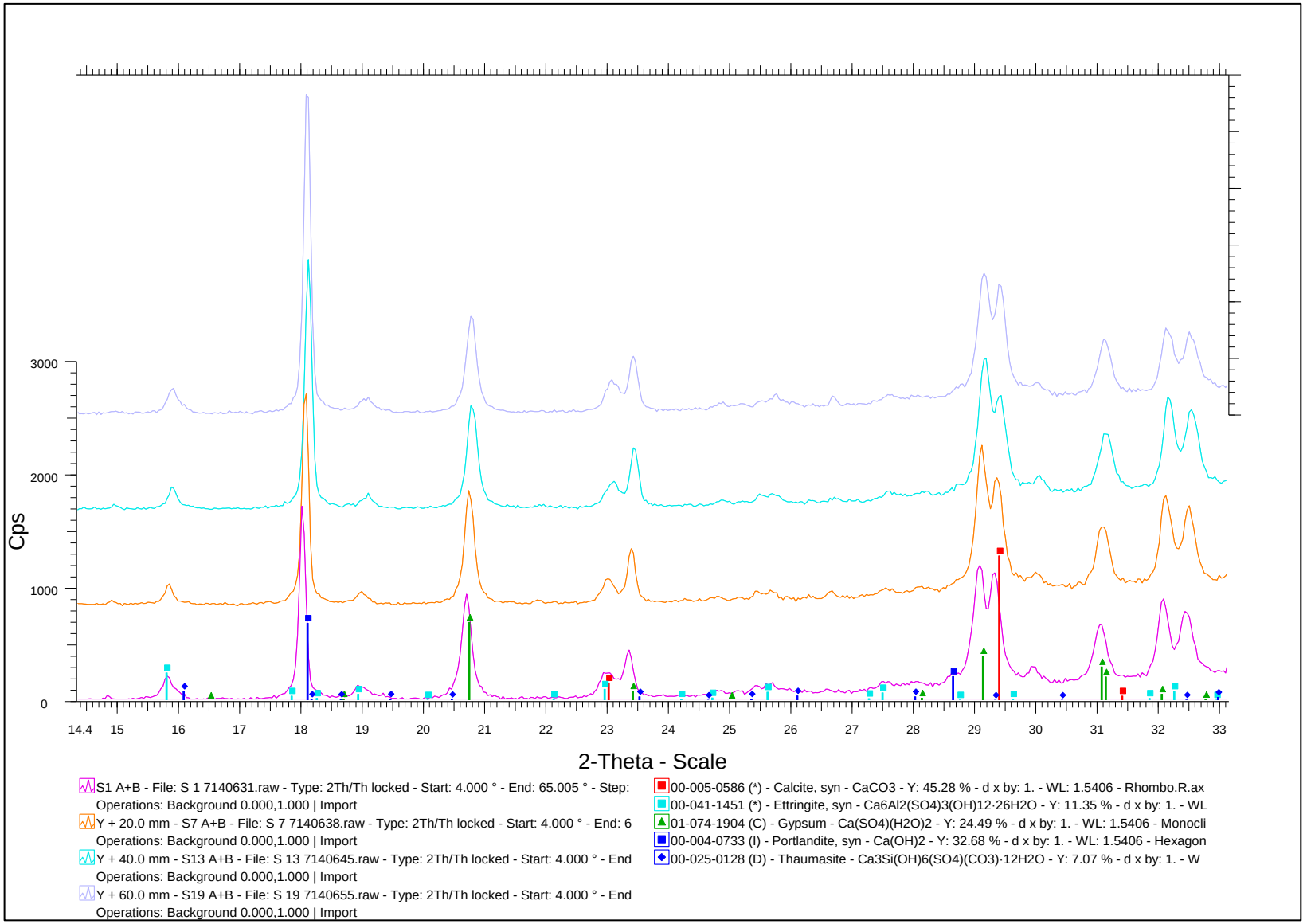

Fig. 4.75 - Diffractograms of the four specimens performed with cement Z556 and its hydration products.

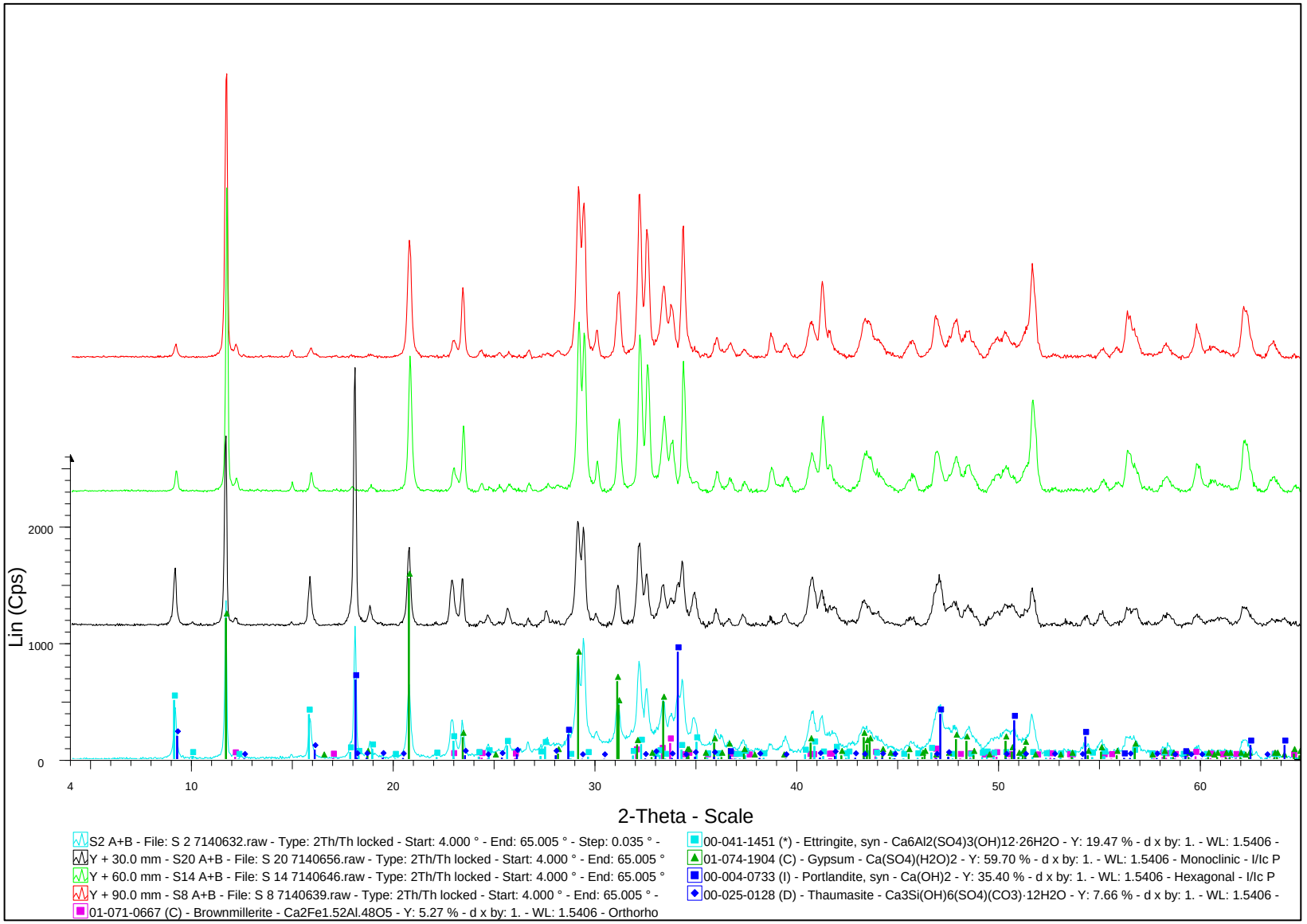

Fig. 4.76 - Diffractograms of the four specimens performed with cement Z554 and its hydration products.

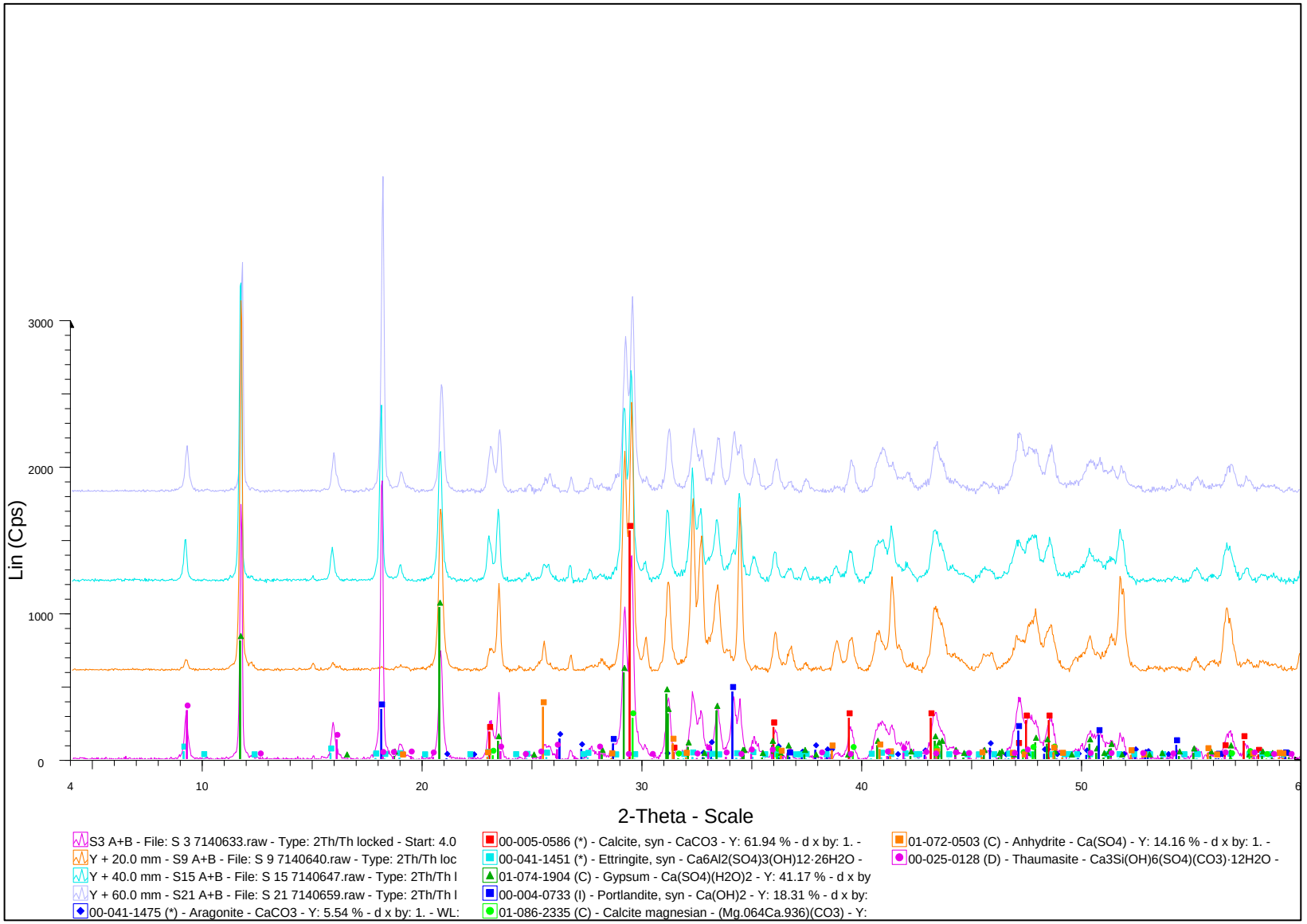

Fig. 4.77 - Diffractograms of the four specimens performed with cement Z558 and its hydration products.

Fig. 4.78 - Diffractograms of the four specimens performed with cement Z557 and its hydration products

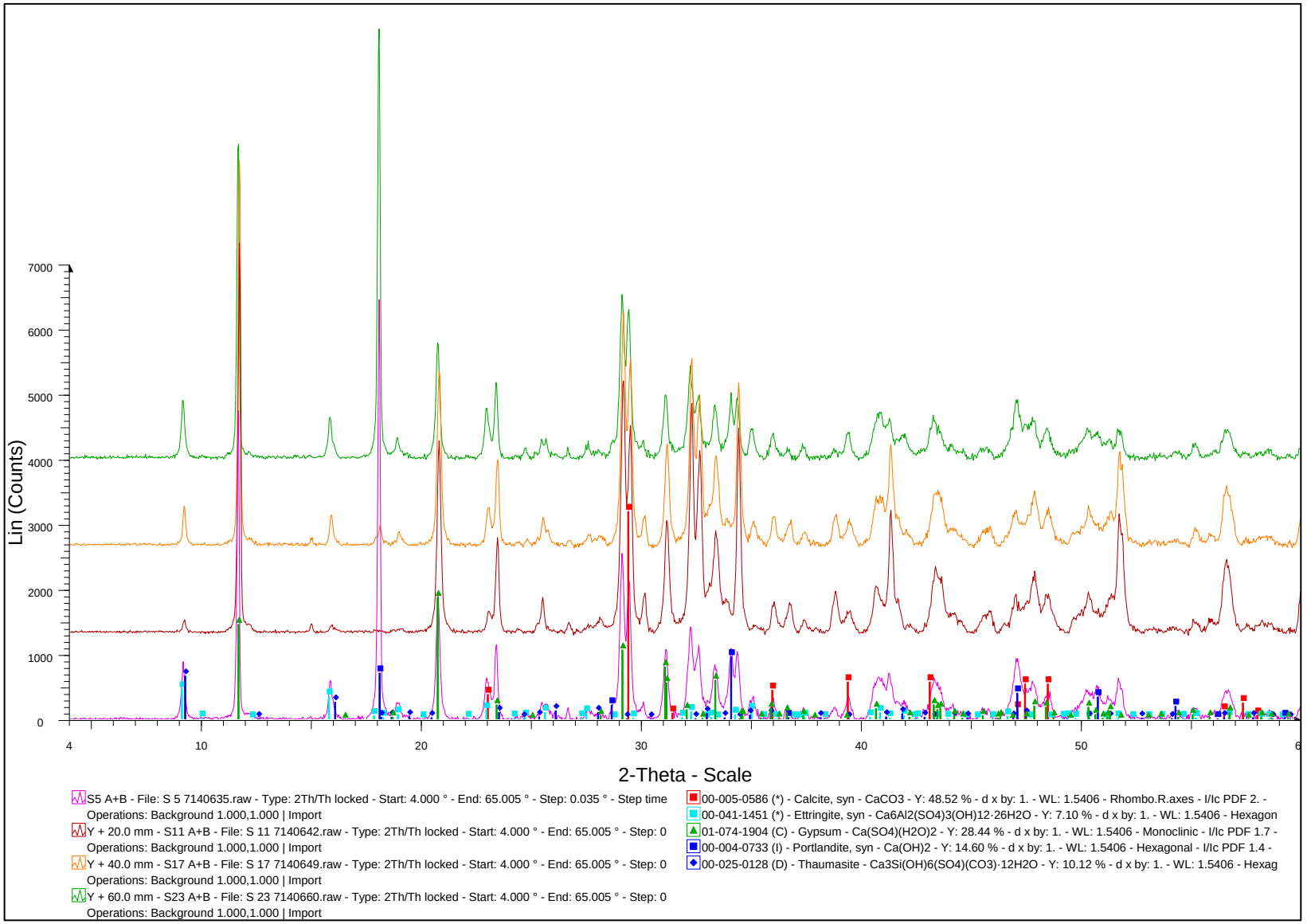

Fig. 4.79 - Diffractograms of the four specimens performed with cement Z559 and its hydration products

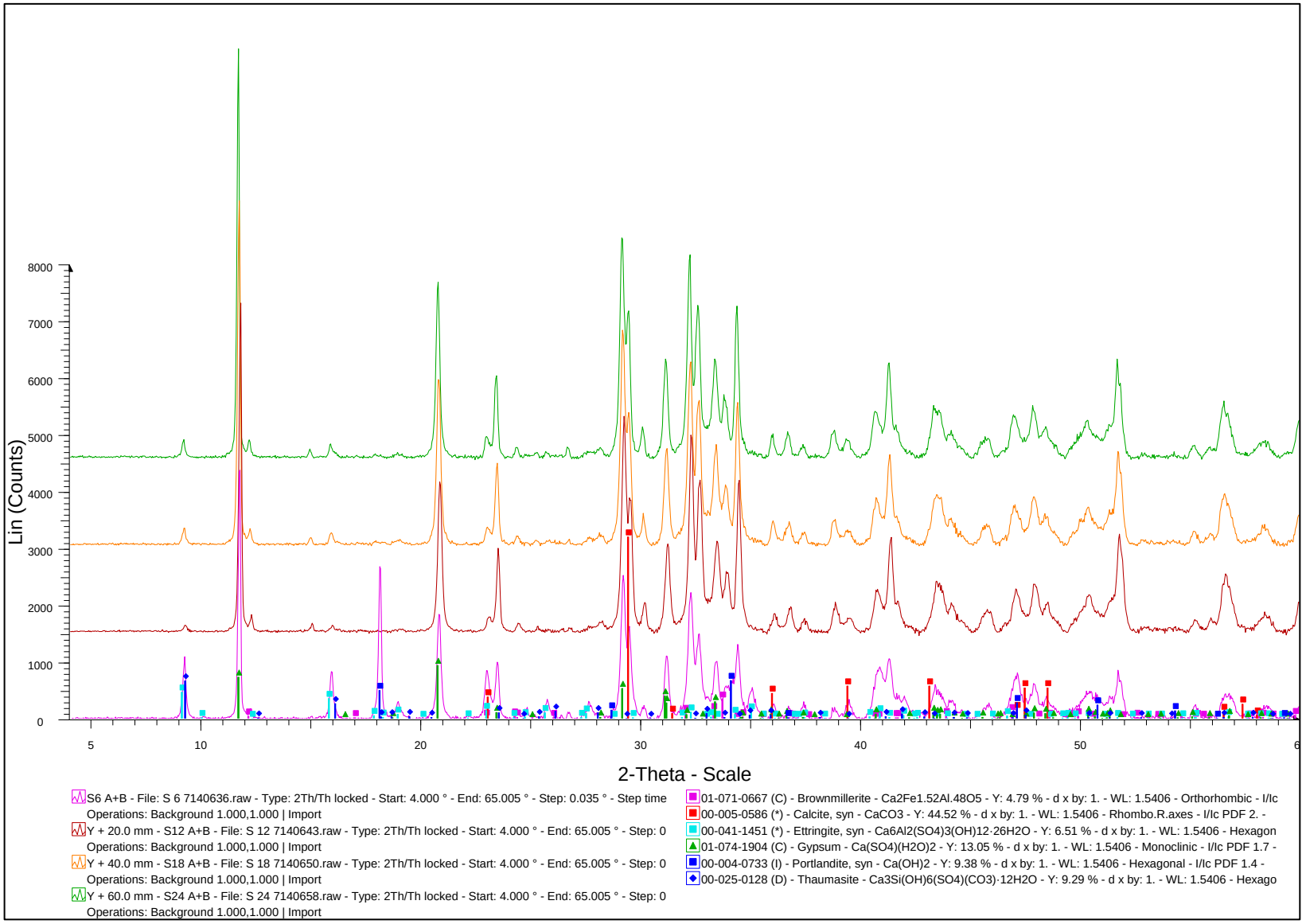

Fig. 4.80 – Diffractograms of the four specimens performed with cement Z555 and its hydration products.

Table 4.6 – Semi-quantification of the mineral phases constituents of the samples of cement 556 with and without KSE

	Z556	Z556 + KSE 300	Z556 + KSE OH Raj	Z556 + KSE 100
Gypsum	+++++	+++++	+++++	+++++
Ettringite	++	++	++	++
Thaumasite	(+)	(+)	(+)	(+)
Portlandite	+++++	+++++	+++++	+++++
Calcite	+++	+++	+++	+++

Table 4.7 - Semi-quantification of the mineral phases constituents of the samples of cement 554 with and without KSE

	Z554	Z554 + KSE 300	Z554 + KSE OH Raj	Z554 + KSE 100
Gypsum	+++	+++++	+++++	+++
Ettringite	++	+	+	++
Thaumasite	(+)	-	-	-
Portlandite	++	-	-	++++
Calcite	-	-	(+)	-

Table 4.8 - Semi-quantification of the mineral phases constituents of the samples of cement 558 with and without KSE

	Z558	Z558+ KSE 300	Z558+ KSE OH Raj	Z558+ KSE 100
Gypsum	++++	++++	+++++	+++++
Ettringite	++	+	++	++
Thaumasite	+	(+)	+	+
Portlandite	++++	(+)	+++	++++
Calcite	++++	++++	++++	++++

Table 4.9 - Semi-quantification of the mineral phases constituents of the samples of cement 557 with and without KSE

	Z557	Z557 + KSE 300	Z557 + KSE OH Raj	Z557 + KSE 100
Gypsum	+++++	+++++	+++++	+++++
Ettringite	(+)	(+)	(+)	(+)

Thaumasite	+	-	(+)	+
Portlandite	-	-	-	-
Calcite	(+)	(+)	(+)	(+)

Table 4.10 - Semi-quantification of the mineral phases constituents of the samples of cement 559 with and without KSE

	Z559	Z559 + KSE 300	Z559 + KSE OH Raj	Z559 + KSE 100
Gypsum	++++	+++++	+++++	++++
Ettringite	++	(+)	++	++
Thaumasite	(+)	(+)	(+)	(+)
Portlandite	+++++	-	(+)	+++++
Calcite	++	++	++	++

Table 4.11 - Semi-quantification of the mineral phases constituents of the samples of cement 555 with and without KSE

	Z555	Z555 + KSE 300	Z555 + KSE OH Raj	Z555 + KSE 100
Gypsum	++++	+++++	+++++	+++++
Ettringite	++	(+)	+	+
Thaumasite	+	+	+	+
Portlandite	++	-	-	-
Calcite	++	+	+	+

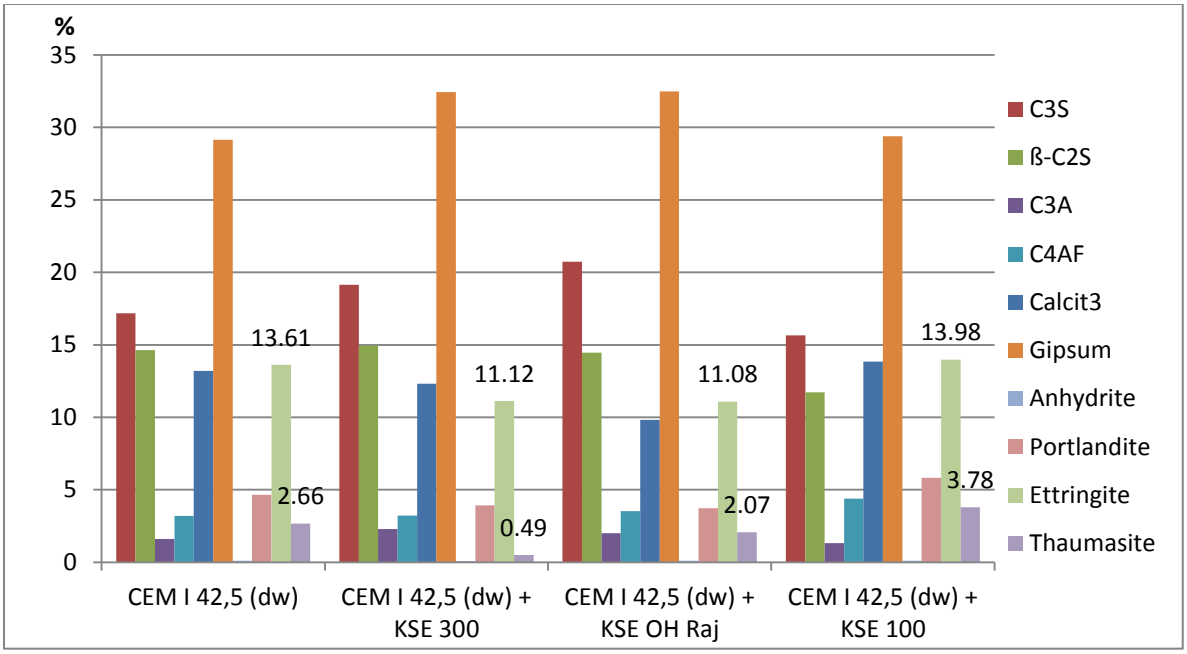

Fig. 4.81 – Phases present, in percentage, in the studied samples with Z556 and Z556 plus KSE. Results obtained by the Rietveld analysis

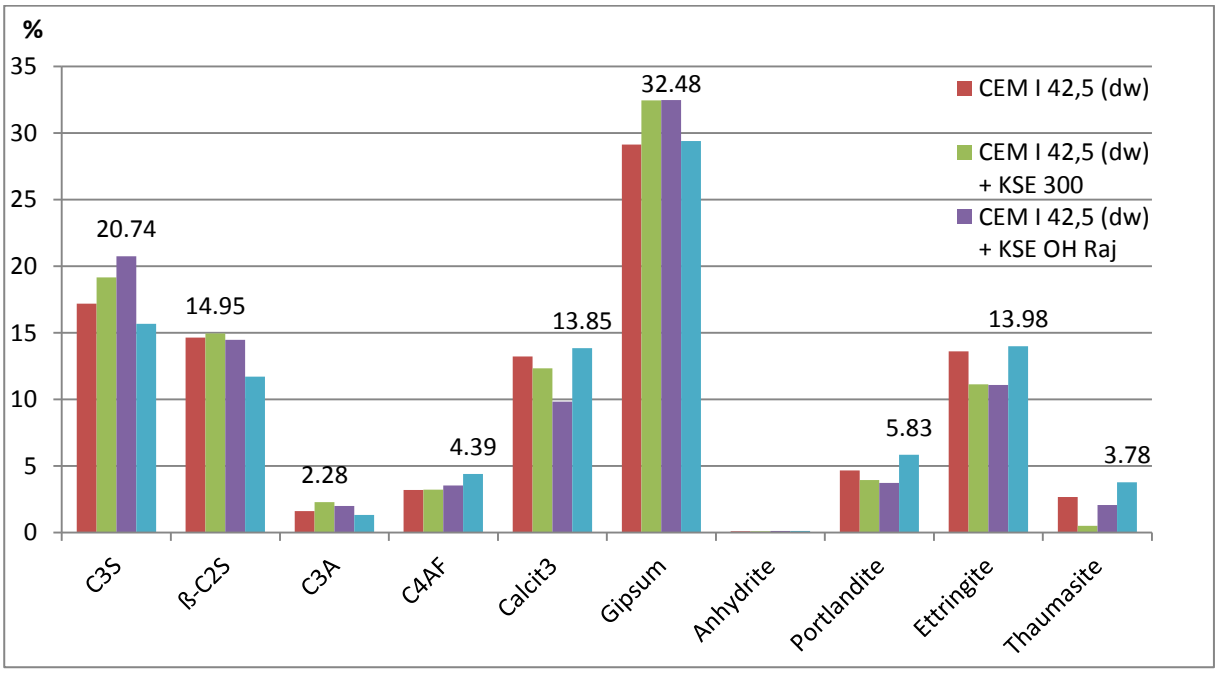

Fig. 4.82 – Comparison between the phases present in Z556 and Z556 plus KSE. Results obtained by the Rietveld analysis

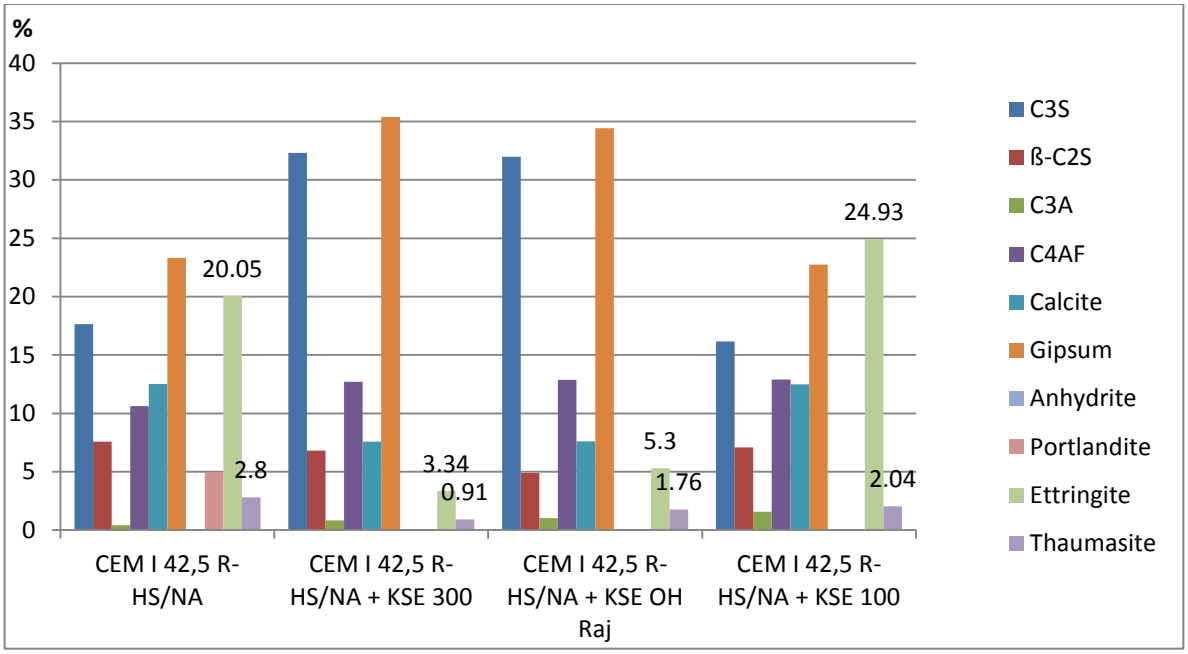

Fig. 4.83 - Phases present, in percentage, in the studied samples with Z554 or Z554 plus KSE. Results obtained by the Rietveld analysis

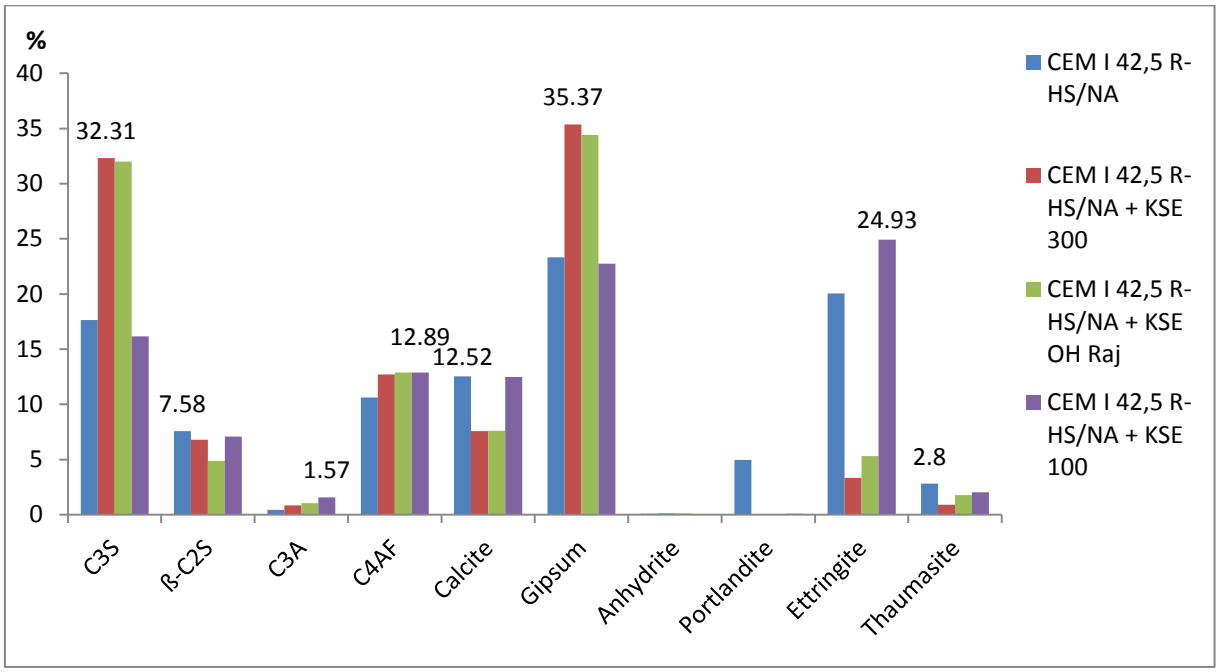

Fig. 4.84 – Comparison between the phases present in Z554 and Z554 plus KSE. Results obtained by the Rietveld analysis

Table 4.12 - Differences between the control and the KSE specimens

		Control [%]	KSE 300 [%]	KSE 0H [%]	KSE 100 [%]
Etringite	Z556	13.61	-2.49	-2.53	0.37
	Z554	20.05	-16.71	-14.75	4.88
Thaumasite	Z556	2.66	-2.17	-0.59	1.12
	Z554	2.8	-1.89	-1.04	-0.76

This table contains the differences between the control specimens and the specimens with KSE calculated from the percentages obtained by the Rietveld analysis.

Although the increase observed is so small that cannot even be detected with the semi-quantitative analysis, in cement Z554 there was an increase of 4.88% in ettringite percentage and in cement Z556 there was an increase of 0.37% in ettringite and 1.12% in thaumasite. The Rietveld analysis shows that maybe more small increases can be "hidden" in the semi-quantitative analysis. It is important to underline that these increases only happened in the specimens that were tested with KSE 100 which only has 20% of active ingredient in the composition. Both applications of KSE 300 and OH decreased the percentage of ettringite and thaumasite in the mixtures. For example, the results of the Rietveld analysis show that in the mixture with Z554, KSE 300 lead to a decrease of 16.71% in ettringite and the application of KSE OH to a decrease of 14,75%.

Table 4.12 shows that, normally (with only one exception) KSE 300 leads to the most significant decreases in percentage of crystals, followed by KSE OH, which can be related with their percentage of active ingredient (100 and 75% respectively).

The application of KSE 100 can be translated by small increases or decreases in ettringite and thaumasite percentages.

Table 4.13 contains the percentage difference of ettringite and thaumasite between the KSE specimens and the control specimen.

Table 4.13 – Percentage variation of ettringite and thaumasite between the control and the KSE specimens

		Control [100%]	KSE 300 [%]	KSE OH [%]	KSE 100 [%]
Etringite	Z556	13.61	-18.30	-18.59	2.72
	Z554	20.05	-83.34	-73.57	24.34
Thaumasite	Z556	2.66	-81.58	-22.18	42.11
	Z554	2.8	-67.50	-37.14	-27.14

Tables 4.13 evidences the magnitude of the differences in both ettringite and thaumasite percentages induced by the use of KSE. Both KSE 300 and KSE OH lead to high decreases in ettringite and thaumasite.

This table also shows that the application of KSE 100 lead to increases in ettringite and different behavior in thaumasite (increase of 42.11% in Z556 and a decrease of 27.14% in Z554).

In conclusion, it is possible to state that the influence of KSE in ettringite and thaumasite formation is related with the percentage of active ingredient, tetraethyl orthosilicate. The higher this percentage is, the more significant are the decreases in ettringite and thaumasite.

4.12. CORRELATION BETWEEN THE RESULTS

Taking in consideration the results presented before and the analysis already made, it easily understandable that there are tests that can be complemented by the results of other tests. To better underline this relation, it is possible to organize the test in the following way:

- Compression, Flexural, and Dynamic E-modulus tests;
- Capillary rise, Mercury porosimetry and KSE Penetration depth tests;
- Expansion, Scanning electron microscopy and X-Ray powder diffraction tests.

4.12.1. COMPRESSION, FLEXURAL AND DYNAMIC E-MODULUS TESTS

Taking in consideration what is stated in 4.3, 4.5 and 4.6, KSE application on the mortars was not translated by significant alterations in their resistance properties, since the results of the tests performed in specimens with KSE are in the same range as the ones carried out in the control specimens.

The obtaining of similar results in these three tests is an indicator that in the tests preparation and execution were not committed mistakes and that the application of KSE does not influences, significantly the resistance to compression and flexion and the Dynamic E-Modulus of the specimens.

4.12.2. CAPILLARY RISE, MERCURY POROSIMETRY AND KSE PENETRATION DEPTH

All the KSE applied penetrated all the cross section of all the specimens. The KSE strengthning products seem to have not decreased the size of the pores, neither in the specimens with 0.5 W/C ratio nor in the specimens with 0.4 W/C ratio, as shown in the mercury porosimetry tests. Mercury porosity is similar in the control and in the KSE specimens with 0.5 W/C ratio but there are two major differences between the mercury porosity of the control specimens and thoses of the KSE 100 and OH from Rajasil with W/C ratio of 0.4. In the specimens where these two products were applied, it would be expected that the C and A values would decrease. This only happened in the specimens where KSE OH from Rajasil was applied. KSE 100 has a paradoxal behavior concerning the mercury porosimetry and the capillary rise tests.

4.12.3. EXPANSION, SCANNING ELECTRON MICROSCOPY AND X-RAY POWDER DIFFRACTION TESTS

The correlations between these three tests help to clarify some of the results obtained. For instance, some of the results that were intriguing in the expansion test correspond to the specimens with KSE 100. These specimens had, in the different types of cement, different results, *i.e.*, in the cements CEM I 42.5 (dw) (Z556), CEM I 42.5 R-HS/NA (Z554), CEM II/A-LL 42.5N (Z558) and CEM III/B N-LH/HS/NA (Z557) there was an increase in the expansion, while, in the cements HSR black label tiefbohrzement (Z555) and CEM 42.5 N (Z559) there was a decrease.

Taking into account the results of the expansion and XRD, it is possible to relate the expansion values with the formation of ettringite and thaumasite obtained in the XRD.

The results of the Rietveld analysis show that in the cements Z556 and Z554, the percentage of ettringite in the specimens with KSE 100 increased when compared with the control specimens. Besides this, the expansion test results and the semi-quantitative values obtained by XRD in Z555 where the different KSE where applied are in accordance, since the expansion decrease as well as the semi quantitative values of ettringite and thaumasite. Therefore, taking in attention the expansion values in the Z558 specimens (increase) and in the Z559 specimens (decrease) it is possible to predict that, in the Z558 specimen there was a slight increase in the percentage in ettringite and thaumasite, and, in the Z559 there was a slight decrease in the percentages of the same minerals percent, although the semi quantitative analysis did not notice these differences.

The same reasoning can be adopted to the analysis of KSE 300 and KSE OH since their expansion values were lower than the control values for all the cement types besides Z557. It is expected that the results expressed in the semi quantitative analysis equal to the control ones are actually lower than them.

Finally, only the results of cement Z557 (CEM III/B N-LH/HS/NA) needed to be explained. When comparing the results of the expansion test with the results of the XRD analysis, it seems contradictory, taking in consideration the results of the other cements, that all the KSE applied lead to an increase of the expansion and that ettringite values are near the detection limit. As stated in 4.9, this happened, probably because of the composition of the cement. Taking this in consideration, the cement classification shows that cement Z557 is composed by 66-80% of ground granulate blast furnace (ggbs) and 20-34% of clinker. This ggbs has in its composition CaO (30-50%), SiO_2 (28-38%), Al_2O_3 (8-24%), and MgO (1-18%). These oxides, especially the calcium oxide and the magnesium oxide are really expansive and, perhaps, are responsible to the expansion values obtained. The low values of ettringite and thaumasite formed, are probably, the result of the small percentage of clinker in the mixture.

5
CLOSURE

5.1. CONCLUSIONS

The main objective of this thesis is illustrated on its title:

Investigation of mortar mixtures after addition of silicic acid esters with regard to ettringite and thaumasite formation.

Taking this in consideration, the main purpose of this thesis was fulfilled. The higher the percentage of silicic acid ester, the active ingredient of KSE, the lower the quantity of ettringite and thaumasite phases in the hydration products of the mortars. Therefore, the investigation conclusion was that silicic acid esters decrease the formation of both ettringite and thaumasite.

It was also possible to notice that in the specimens where KSE was applied both the habit and the cross section of the ettringite crystals formed suffer alterations.

However, the realization of this work enabled the understanding of other aspects of the application of silicic acid esters in mortars besides the main one (the influence on ettringite and thaumasite formation). For instance, it was also possible to conclude that:

Silicic acid esters do not affect, significantly, the resistance properties of the mortars. Compression and Flexural strength as well as the Dynamic E-Modulus of the specimens do not suffer significant alterations with and without the esters.

All the KSE strengthning products applied penetrated all the cross section of all the specimens. The KSE seem to have not reduced the size of the pores in the specimens with 0.5 W/C ratio and 0.4 W/C ratio, as shown in the mercury porosimetry tests. Mercury porosity is identical in the control and in the KSE specimens with 0.5 W/C ratio but there are two major differences between the mercury porosity of the control specimens and thoses of the KSE 100 and OH from Rajasil with W/C ratio of 0.4. In the specimens where these two products were applied, it would be expected that the coefficients of capillarity C and A values would decrease. This only happened in the specimens where KSE OH from Rajasil was applied. KSE 100 has a paradoxal behavior concerning the mercury porosimetry and the capillary rise tests.

5.2. RECOMMENDATIONS FOR FUTURE RESEARCH

As stated in the first two chapters of this thesis, no previous research was carried out on this subject and, therefore one of the author's objectives was to provide a work that future studies could rely on.

There are some recommendations that might help the realization of future works.

First of all, it could be interesting to perform the same tests in specimens that suffer internal sulfate attack or external sulfate attack. As it is known, these kind of attacks favor the formation of both thaumasite and ettringite. Since the thaumasite formed in the specimens analyzed in this work was, significantly small or even near the detection limit, it could, perhaps, be important to carry out the tests in specimens with higher percentages of thaumasite in the hydration phases, in order to better understand the influence of the application of silicic acid esters in the formation of this mineral.

Tests on other cements CEM III could be performed in order to truly understand/confirm if the expansions obtained are due to the formation of the calcium and magnesium oxides and if KSE acts like a catalyzer of the expansion and why in this type of cements.

Finally, to fully carry out a Rietveld analysis in all cement and KSE combinations to verify the assumptions made in this thesis taking in account the correlations between XRD and expansion tests.

BIBLIOGRAPHIC REFERENCES

[1] Araújo, D. D. "Sulfate Attack on Cementitious Materials", Civil Engeneering, Faculdade de Engenharia da Universidade do Porto, 2013.

[2] http://www.mindat.org/photo-74372.html, 25/04/2014

[3] Moore, A.E. Taylor, H.F.W. *Nature* 218 (1968) 1048.

[4] Moore, A.E. Taylor, H.F.W. *Acta Crystallographic*. B26 (1970) 386.

[5] http://www.cement.org/docs/default-source/fc_concrete_technology/is417-ettringite-formation-and-the-performance-of-concrete.pdf?sfvrsn=2, 23/04/2014

[6] Goetz-Neunhoeffer, F. Neubauer, J. *Powder Diffraction* 21 (1) (2006) 4.

[7] Hartman, M.R. Berliner, R. *Cement Concrete Resistance* 36 (2006) 364.

[8] Renaudin, G. Segni, R. Mentel, D. Nedelec, J.-M. Leroux, F. Taviot-Gueho, C. J. *Advanced*

Concrete Technology 5 (2007) 299

[9] Renaudin, G. Filinchuk, Y. Neubauer, J. Goetz-Neunhoeffer, F. *A comparative structural study of wet and dried ettringite* in Cement and Concrete Research 40 (2010) 370-375

[10] Hartman, M.R. Berliner R., *Solid State Chemistry* 178 (2005) 3256.

[11] Taylor, H.F.W. *Cement Chemistry*, 2nd ed., Thomas Telford, London, 1997.

[12] Santhanam, M. Cohen, M.D. Olek, J. Cem. Concr. Res. 31 (2001) 845.

[13] Taylor, H.F.W. Famy, C. Scrivener, K.L. Cem. Concr. Res. 31 (2001) 683.

[14] Stark, J. Bollmann, K. *Delayed Ettringite Formation in Concrete*, Bauhaus-University Weimar.

[15] Mehta, P.K.: Mechanism of Sulfate Attack on Portland Cement Concrete - Another Look.

Cement and Concrete Research 13 (1983), pp. 401-406

[16] Gabrisova, A., Havalica, J., Sahu, S.: Stability of Calciumsulfoaluminate Hydrates in

Water Solution with Various pH Values. CCR 21 (1991) 6, pp. 1023-1027.

[17] Chartschenko, I., Volke, K., Stark, J.: Untersuchungen über den Einfluß des pH-Wertes

auf die Ettringitbildung. Wissenschaftliche Zeitschrift der Hochschule für Architektur und Bauwesen Weimar 39 (1993) 3, pp. 171-176.

[18] Bellman, F. on the formation of thaumasite CaSiO3.CaSO4.CaCO3.15H2O: Part III. In Advances in Cement Research, 2007, 19, No. 4, October, 139–146 doi: 10.1680/adcr.2007.19.4.139

[19] Department for the Environment, Transport and Regions. The Thaumasite Form of Sulfate Attack: Risks, Diagnosis, Remedial Works and Guidance on New Construction. DETR, London, 1999, Report of the Thaumasite Expert Group

[20] Crammond N. J. *The thaumasite form of sulfate attack in the UK*. in Proceedings of the First International Conference on Thaumasite in Cementitious Materials, 19–21 June 2002, Garston, UK, paper 17.

[21] Freyburg, E. Berninger, A.M. *Field experiences in concrete deterioration by thaumasite formation: possibilities and problems in thaumasite analysis*. Cement & Concrete Composites 25 (2003) 1105–1110

[22] Collepardi, M., *Thaumasite formation and deterioration of historical buildings*, Cem. Conc. Comp. 21 (1999) 147e154.

[23] Begonha, A. *Meteorização do Granito e Deterioração da Pedra em Monumentos e Edifícios da Cidade do Porto*, Feup Edições 2001, 445.

[24] Van Hees, R.P.J. Wijffels, T.J. Van der Klugt, L.J.A.R. *thaumasite swelling in historic mortars: field observations and laboratory research*. In Cement and Concrete Composites, Volume 25, Issue 8, December 2003, Pages 1165-1171.

[25] Teles, M. Begonha, A., Fernandes, I. In Revista Internacional Construlink – Estruturas e Construção, Estudo Petrográfico de Betões e Argamassas nº5 Fev 2004 Vol.2 4-20.

[26] Tesch, V. Middendorf, B. *occurrence of thaumasite in gypsum lime mortars for restoration*. In Cement and Concrete Research, Volume 36, Issue 8, August 2006 Pages 1516-1522.

[27] Ciliberto, E. Ioppolo, S. Manuella, F. *Ettringite and thaumasite: A chemical route for their removal from cementious artefacts* Journal of Cultural Heritage 9 (2008) 30-37.

[28] Proceedings of the First International Conference on Thaumasite in Cementitious Materials, 19–21 June 2002, Garston, UK.

[29] Nobst, P. Stark, J. *investigations on the influence of cement type on thaumasite formation*. In Cement & Concrete Composites 25 (2003) 899–906.

[30] Brown P. W., Hooton R. D. and Clark B. A. *The co-existence of thaumasite and ettringite in concrete exposed to magnesium sulfate at room temperature and the influence of blastfurnace slag substitution on sulfate resistance*. In Proceedings of the First International Conference on Thaumasite in Cementitious Materials, 19–21 June 2002, Garston, UK, paper 59.

[31] Higgins D. D. and Crammond N. J. *Resistance of concrete containing ggbs to the thaumasite form of sulfate attack*. In Proceedings of the First International Conference on Thaumasite in Cementitious Materials, 19–21 June 2002, Garston, UK, paper 53.

[32] Mulenga D. M., Stark J. and Nobst P. *thaumasite formation in concrete and mortars containing fly ash*. In Cement and Concrete Composites, 2003, 25, No. 8, 907–912.

[33] Tsivilis S., Kakali G., Skaropoulou A., Sharp J. H. and Swamy R. N. *Use of mineral admixtures to prevent thaumasite formation in limestone filler cement mortar*. In Proceedings of the First International Conference on Thaumasite in Cementitious Materials, 19–21 June 2002, Garston, UK, paper 64.

[34] Bensted, J. *Thaumasite direct, woodfordite and other possible formation routes* in Cement & Concrete Composites 25 (2003) 873–877

[35] Bensted J, Varma SP. *Studies of thaumasite*—Part 2. Silicates Ind 1974;39(1):11–9.

[36] Bensted J. *Mechanism of thaumasite sulfate attack in cements, mortars and concretes* 2000;53(12):704–9.

[37] Bensted J. *Scientific background to thaumasite formation in concrete*. World Cem Res 1998;29 (11):102–5.

[38] Bensted J. *Thaumasite—background and nature in deterioration of cements, mortars and concretes*. Cem Concr Comp 1999; 21:117–21.

[39] Barnett SJ, Adam CD, Jackson ARW. *Solid solutions between ettringite, Ca6Al2(SO4)3(OH)12 Æ 26H2O, and thaumasite, Ca3-SiSO4CO3(OH)6 Æ 12H2O*. J Mater Sci 2000;35:4109–14.

[40] http://webbook.nist.gov/cgi/cbook.cgi?ID=C78104&Mask=80 6/6/2014

[41] Bulla, D.A.P; Morimoto, N.I (1998). "*Deposition of thick TEOS PECVD silicon oxide layers for integrated optical waveguide applications*".Thin Solid Films 334: 60. doi:10.1016/S0040-6090(98)01117-1

[42] Kulprathipanja, Santi (2010) *Zeolites in Industrial Separation and Catalysis*, Wiley-VCH Verlag GmbH & Co. KGaA, ISBN 3527629572.

[43] Begonha. A, *Estudo da Aplicação de Consolidantes em Pedras da Igreja de São Pedro de Rates*. Report DEGENN-FEUP-Estudo dos materiais pétreos e argamassas. FEUP, Porto, 2003. 66.

[44] Ferreira, J. F. O. *Caracterização da acção da água em edifícios de petra*. MSc Thesis Escola de Engenharia Universidade do Minho – Guimarães, 2004 177.

[45] Fojo, A. C. O. T. *Estudo da aplicação de consolidantes e hidrófugos em pedras graniticas da Igreja Matriz de Caminha*. MSc Thesis FEUP. Porto 2006 446.

[46] Begonha A. Fojo, A. *Application and Efficiency of water repllents and consolidating products in two two-mica granites used in the Matriz de Caminha Church*. Procedings 11th International Congress on Deterioration and Conservation of stone. Toruń 2008 Vol. II 785-793

[47] Begonha, A. Patologia da Pedra. Casos de Obra. Primeiras Jornadas de Materiais na construção, secção de materiais de construção FEUP. Álvaro Cunha, Afonso Serra Neves, Ana Maria Sarmento, Ana Maria Proença Editores. Porto 2011 83-113

[48] Silva, A. Estudo Diagnóstico, cartografia e proposta de tratamento das deteriorações do ranito do Hospital de Santa Casa da Misericórdia de Viana do Castelo Msc Thesis, Especialização Materiais e Processos de Construção, Porto 2012, 326.

[49] Washburn E. W., The Dynamics of capillary flow in the Physical Review, 17, 273-283 (1921)

[50 http://www.micromeritics.com/Repository/Files/Mercury_Porosimetry_Theory_poster.pdf 5/6/2014

[51] Evju C., Hansen S. *Expansive properties of ettringite in a mixture of calcium aluminate cement*, Portland cement and β-calcium sulfate hemihydrate. In Cement and Concrete Research Volume 31, Issue 2, February 2001, Pages 257–261

[52] Taylor, H.F.W. *Cement Chemistry* Academic Press, London (1990)

[53] Bentz D P and Stutzman P E 1994 SEM analysis and computer modelling of hydration of Portland cement particles Petrography of Cementitious Materials, ASTM STP 1215 ed S M Dehayes and D Stark (Philadelphia, PA: American Society for Testing and Materials)

[54] Stutzman P.E. *Applications of scanning electron microscopy in cement and concrete petrography* (1993)

[55] Stutzman P.E. *Serial sectioning of hardened cement paste for scanning electron microscopy* (1990)

[56] E. Schreiber and H.-J. Fitting, J. Electron Spec. and Rel. Phen., *Secondary Electron Emission and Self-consistent Charge Transport and Storage in Bulk Insulators: Application to Alumina* 124, 25 (2002)

[57] Properties of Electrons, their Interactions with Matter and Applications in Electron Microscopy by Frank Krumeich Laboratory of Inorganic Chemistry, ETH Zurich, HCI-H111, CH-8093 Zurich

[58] Werner, W.. *Interaction of electron beams with matter*. 2012

[59] Rietveld, H. M. 1969. "*A Profile Refinement Method for Nuclear and Magnetic Structures*." J. Appl. Cryst. (2):65-71.

[60] Pecharsky, V. K. and P. Y. Zavalij. 2009. *Fundamentals of Powder Diffraction*, 2nd Edition. 2nd Edition ed.: Springer Science+Business Media, LLC.

[61] Bragg, W. H. 1969. "The Intensity Reflection of X-Rays by Crystals." Acta Cryst. no. A25:3-11. doi: 10.1107/S0567739469000039

[62] Hill, R.J. Howard, C.J. *Quantitative phase analysis from neutron powder diffraction data using the Rietveld method*, Journal of Applied Crystallography 20 (1987) 467-474.

[63] Bish, D.L. Howard, S.A. *Quantitative phase analysis using the Rietveld method*, Journal of Applied Crystallography 21 (1988) 86-91.

[64] O'Connor, B.H. Raven, M.D. *Applications of the Rietveld refinement procedure in assaying powdered mixtures*, Powder Diffraction,3 (1988) 2-6.

[65] Bish, D.L. Post, J.E. *Quantitative mineralogical analysis using the Rietveld full-pattern fitting method*, American Mineralogist 78 (1993) 932-940

[66] Pająk, L. Formanek, B. Dercz, G. *Rietveld analysis of intermetallic phases from Ni-Al system*, *Proceedings of the 11th Scientific International Conference* "Achievements in Mechanical and Materials Engineering" AMME'2002, GliwiceíZakopane, 2002, 405-408.

[67] Dercz, G. Formanek, B. Prusik, K. Pająk, L. *Microstructure of Ni(Cr)-TiC-Cr3C2-Cr7C3 composite powder*, Journal of Materials Processing Technology 162-163 (2005) 15-19.

[68] Dercz, G. Formanek, B. Prusik, K. Pająk, L. *Microstructure of Ni(Cr)-TiC-Cr3C2-Cr7C3 composite powder*, Proceedings of the 13th Scientific International Conference "Achievements in Mechanical and Materials Engineering" AMME'2005, GliwiceíZakopane, 2005, 99-102.

[69]Dercz, G. Prusik, K. Pająk, L. *Structure investigations of commercial zirconia ceramic powder*, Journal of Achievements in Materials and Manufacturing Engineering 18 (2006) 259-262.

Standards

NP EN 197-1 (2001)

DIN EN 998-1 (2003)

EN NP 196-1 (2006)

NP EN 14146 (2006)

DIN EN 1015-18 (2003)

ISO 12135 (2002)

ISO 12737 (2010)

ASTM D790 (2010)

ASTM E1290 (2008)

NP EN 12390-1 (2003)

NP EN 12390-3 (2003)

APPENDIX

A1.

Table A.1 – Application of KSE on the mortars with W/C ratio of 0.4

0.4	sample name	Mass	1st layer of KSE	2nd layerof KSE	3rd layer of KSE
			[g]	[g]	[g]
KSE 300	A	581.630	0.701	0.414	0.209
	B	580.360	0.707	0.398	0.155
	C	576.545	0.692	0.414	0.186
	D	572.275	0.761	0.383	0.149
	E	583.140	0.705	0.382	0.161
KSE510	F	580.395	0.773	0.321	0.157
	G	592.190	0.795	0.381	0.196
	H	574.925	0.708	0.31	0.13
	I	577.050	0.776	0.33	0.129
	J	573.090	0.701	0.276	0.198
KSE 100	K	583.680	0.691	0.32	0.127
	L	581.680	0.685	0.315	0.126
	M	566.965	0.643	0.337	0.125
	N	570.565	0.664	0.353	0.123
	O	582.640	0.642	0.299	0.135
KSE OH	P	577.345	0.652	0.278	0.135
	Q	573.050	0.685	0.277	0.149
	R	581.385	0.67	0.27	0.15
	S	567.270	0.624	0.256	0.146
	T	572.275	0.655	0.294	0.129
KSE OH Raj	U	582.850	0.79	0.263	0.158
	V	584.780	0.77	0.267	0.186
	X	581.575	0.703	0.245	0.171
	Y	582.365	0.767	0.278	0.153
	Z	580.680	0.746	0.252	0.163

Table A.2 - Application of KSE on the mortars with W/C ratio of 0.5

0.5	sample name	mass	1st layer of KSE	2nd layer of KSE	3rd layer of KSE
		[g]	[g]	[g]	[g]
KSE OH Raj	22	555.065	0.777	0.42	0.175
	17	577.245	0.739	0.386	0.181
	A	569.945	0.666	0.35	0.376
	C	563.805	0.924	0.201	0.104
	B	559.935	0.705	0.369	0.118
KSE 510	D	563.740	0.631	0.378	0.19
	E	564.955	0.66	0.376	0.228
	F	564.410	0.693	0.395	0.266
	G	567.745	0.679	0.344	0.248
	H	571.920	0.672	0.332	0.2
KSE 100	I	562.205	0.669	0.331	0.168
	J	560.205	0.674	0.327	0.148
	K	586.025	0.688	0.387	0.145
	L	563.425	0.648	0.411	0.168
	M	562.680	0.636	0.369	0.129
KSE OH	N	580.390	0.622	0.3	0.162
	O	578.875	0.64	0.331	0.207
	P	559.455	0.689	0.298	0.193
	T	589.390	0.619	0.279	0.16
	S	558.645	0.611	0.33	0.202
KSE 300	Q	577.250	0.661	0.334	0.21
	V	578.460	0.683	0.273	0.132
	Y	579.370	0.629	0.294	0.154
	X	579.500	0.673	0.284	0.173
	Z	573.645	0.656	0.304	0.159

A2.

Table A.3 – Dynamic E-modulus test results

Sample	Lenght	Thickness	Height	Mass	Density	Flexural frq.	Torsion frq.	Longitudinal frq.	E-Modul
	l [mm]	b [mm]	h [mm]	m [g]	ρ [g/cm³]	f_b [kHz]	f_t [kHz]	f_l [kHz]	E_L [N/mm²]
23	160.0	39.2	40.3	552.5	2.186	5.784	7.865	13.29	39620
24	159.3	39.0	40.0	550.3	2.214	5.768	7.855	13.30	39850
25	159.6	40.1	40.1	552.2	2.152	5.758	7.799	13.24	38530
60	160.2	40.1	39.9	574.9	2.243	6.062	8.325	14.09	45290
61	160.2	40.2	40.0	572.8	2.224	6.079	8.264	13.99	44750
62	159.3	40.8	40.1	576.6	2.212	6.148	8.392	14.08	44610

Table A.4 – Dynamic E-modulus results for all the specimens tested

Sampe-	Sample	Mass	Lenght	Thickness	Height	Density	Flexural frq.	Torsion freq	Longitudinal freq.	E-Modul
Description		**m [g]**	**l [mm]**	**b [mm]**	**h [mm]**	**ρ [g/cm³]**	**f_b [kHz]**	**f_t [kHz]**	**f_l [kHz]**	**E_L [N/mm²]**
W/C 0,5 + KSE OH Raj	A	569.0	159.78	39.90	40.39	2.210	-	-	-	0.000
	B	558.8	159.00	39.91	40.28	2.186	5.822	7.970	13.27	38980
	C	562.7	161.30	40.04	40.15	2.170	5.599	7.688	12.96	38000
W/C 0,5 + KSE 510	F	563.4	160.34	40.53	40.02	2.166	5.631	7.770	13.04	37990
	G	566.8	160.77	40.50	39.95	2.179	5.640	7.753	13.16	39070
	H	571.0	160.78	39.85	40.12	2.221	5.791	7.959	13.38	41180
W/C 0,5 + KSE 100	K	584.4	159.88	40.69	40.03	2.244	5.756	7.932	13.34	40940
	L	561.9	159.63	40.81	40.20	2.146	5.731	7.954	13.37	39170
	M	561.2	159.87	41.00	40.01	2.140	5.674	7.863	13.17	38030
W/C 0,5 + KSE OH	P	558.3	159.24	40.40	40.09	2.165	5.736	7.827	13.17	38140
	S	588.1	160.23	41.65	40.03	2.201	5.784	7.910	13.32	40160
	T	557.5	160.29	40.14	40.25	2.153	5.800	8.074	13.49	40320
W/C 0,5 + KSE 300	X	578.3	159.62	41.00	40.25	2.195	5.743	7.924	13.43	40400
	Y	578.1	159.55	41.26	40.21	2.184	5.751	7.891	13.25	39100
	Z	572.4	159.00	40.79	40.09	2.201	5.758	7.904	13.28	39320
W/C 0,4 + KSE OH Raj	X	580.9	159.40	40.51	40.14	2.241	6.072	8.290	13.93	44340
	Y	581.7	159.42	40.51	40.72	2.212	6.171	8.403	14.01	44240
	Z	579.9	160.13	40.70	40.11	2.218	6.106	8.356	14.00	44680
W/C 0,4 + KSE 510	H	574.4	160.85	40.15	40.28	2.208	6.038	8.264	13.77	43340
	I	576.7	160.33	40.34	40.41	2.207	6.021	8.238	13.82	43460
	J	572.6	160.04	39.84	40.69	2.207	6.055	8.238	13.88	43680
W/C 0,4 + KSE 100	M	565.9	160.24	39.51	40.05	2.232	5.838	8.168	13.81	43760
	N	569.4	160.19	40.36	40.56	2.171	6.077	8.296	13.91	43120
	O	581.5	160.27	40.71	40.49	2.201	6.055	8.289	13.92	43920

Table A.4 – Dynamic E-modulus results for all the specimens tested

Sampe-	Sample	Mass	Lenght	Thickness	Height	Density	Flexural frq.	Torsion freq	Longitudinal freq.	E-Modul
Description		**m [g]**	**l [mm]**	**b [mm]**	**h [mm]**	**ρ [g/cm³]**	**f_b [kHz]**	**f_t [kHz]**	**f_l [kHz]**	**E_L [N/mm²]**
W/C 0,4 + KSE OH	R	580.6	160.21	40.77	40.60	2.189	6.113	8.326	13.87	43280
	S	566.4	160.10	40.21	39.98	2.201	6.081	8.263	13.95	43990
	T	571.5	160.52	40.23	40.38	2.192	6.034	8.199	13.82	43240
W/C 0,4 + KSE 300	C	575.8	160.40	40.18	40.44	2.209	6.021	8.283	13.96	44430
	D	571.5	159.71	40.44	40.23	2.199	5.978	8.252	13.85	43200
	E	582.4	159.71	40.34	40.33	2.241	6.094	8.383	14.05	45300

A3.

Table A.5 – Measurements of the capillary rise test and correspondent water absorption coefficients

W/C	Age	sample name	0	5	10	20	30	1	6	24	C
	[days]		[min]	[min]	[min]	[min]	[min]	[h]	[h]	[h]	[Kg/m2]
0.5	28	1	584.02	585.14	585.42	585.84	586.18	586.76	589.34	593.26	5.775
0.5	28	21	573.82	574.9	575.16	575.56	575.82	576.32	578.44	581.52	4.8125
0.4	28	44	584.14	584.8	584.86	585.04	585.2	585.44	586.48	587.98	2.4
0.4	28	50	588.62	589.26	589.36	589.52	589.68	589.88	590.88	592.1	2.175

Table A.6 - Measurements of the capillary rise test and correspondent water absorption coefficients with W/C ratio of 0.5

0.5	Sample name	0	5	10	20	30	1	6	24	C
		[mim]	[mim]	[mim]	[mim]	[mim]	[h]	[h]	[h]	[Kg/m2]
300	q	576.3	576.9	577.0	577.2	577.4	577.8	579.3	581.2	3.0625
	v	577.4	577.9	578.0	578.2	578.5	578.9	580.7	583.5	3.8125
510	D	563.2	563.3	563.3	563.3	563.3	563.3	563.6	565.0	1.125
	E	564.4	564.5	564.5	564.5	564.5	564.5	565.0	566.6	1.375
OH Raj	22	552.3	552.4	552.4	552.4	552.4	552.4	552.9	555.2	1.8125
	17	576.5	577.5	577.7	578.1	578.4	579.1	581.6	585.5	5.625
OH	O	577.9	578.1	578.1	578.1	578.1	578.2	579.1	582.6	2.9375
	N	579.5	579.7	579.7	579.7	579.7	579.8	580.6	582.8	2.0625
100	J	558.9	559.9	560.2	560.6	561.0	561.7	564.1	566.5	4.75
	I	560.9	561.9	562.1	562.5	562.9	563.6	566.0	568.5	4.775
Control	1	585.7	586.6	586.9	587.3	587.6	588.2	590.5	593.9	5.125
	21	574.7	575.7	575.9	576.3	576.6	577.2	579.5	582.6	4.9375

Table A.7 - Measurements of the capillary rise test and correspondent water absorption coefficients with W/C ratio of 0.4

0.4	Sample name	0	5	10	20	30	1	6	24	C
		[mm]	[mm]	[mm]	[mm]	[mm]	[h]	[h]	[h]	[Kg/m2]
OH	P	576.8	577.1	577.2	577.3	577.4	577.7	579.3	584.9	5.0625
	Q	572.5	572.7	572.7	572.7	572.8	572.8	573.3	577.7	3.25
100	K	582.9	583.4	583.6	583.8	584.8	584.8	586.5	589.7	4.25
	L	581.2	581.7	581.9	582.1	582.3	582.7	584.6	587.4	3.875
300	A	581.1	581.4	581.5	581.6	581.6	581.9	583.5	586.4	3.3125
	B	579.8	580.1	580.1	580.2	580.3	580.5	581.9	584.9	3.1875
OH Raj	U	582.4	582.5	582.5	582.5	582.5	582.5	583.7	585.4	1.875
	V	584.3	584.4	584.4	584.4	584.4	584.4	584.8	586.8	1.5625
510	G	592.3	592.3	592.4	592.4	592.4	592.4	592.6	593.1	0.5
	F	580.3	580.4	580.4	580.4	580.4	580.5	581.0	582.7	1.5
Control	44	584.5	585.1	585.2	585.3	585.4	585.7	586.8	588.2	2.3125
	50	588.7	589.3	589.4	589.5	589.7	590.0	591.0	592.2	2.1875

A4.

Table A.8 – Flexural and compression tests of 3 control specimens

Nr 0.4W/C	Test	ID	L [mm]	A [mm2]	Fm kN	Nr	σbz N/mm2	σD N/mm2
1	3-point- bending test	1	100	1600	4.2	1	9.7	
2	3-point- bending test	2	100	1600	3.2	2	7.5	
3	3-point- bending test	3	100	1600	3.9	3	9.1	
4	compression test	1		1600	136.3	4		85.2
5	compression test	1		1600	115	5		71.9
6	compression test	2		1600	116.5	6		72.8
7	compression test	2		1600	135.8	7		84.9
8	compression test	3		1600	123.3	8		77.1
9	compression test	3		1600	135.1	9		84.4

TableA.9 - Flexural and compression tests of 3 control specimens

Nr 0.5 W/C	Test	ID	L [mm]	A [mm2]	Fm kN	Nr	σbz N/mm2	σD N/mm2
1	3-point- bending test	1	100	1600	3.4	1	8.0	
2	3-point- bending test	2	100	1600	3.4	2	8.0	
3	3-point- bending test	3	100	1600	3.2	3	7.5	
4	compression test	1		1600	106	4		66.3
5	compression test	1		1600	109.9	5		68.7
6	compression test	2		1600	101.2	6		63.2
7	compression test	2		1600	110.7	7		69.2
8	compression test	3		1600	112.3	8		70.2
9	compression test	3		1600	116.1	9		72.6

Table A.10 - Flexural and compression tests of 3 specimens with KSE OH and a W/C ratio of 0.4

KSE OH	W/C	ID	l	A	Fm	σbz	σD
	-	-	[mm]	[mm2]	[kN]	[N/mm2]	[N/mm2]
3 point bending test	0.4	R	100	1600	3.6	8.5	
3 point bending test	0.4	S	100	1600	4.2	9.8	
3 point bending test	0.4	T	100	1600	3.9	9.2	
compression test	0.4	R1		1600	134.2		83.9
compression test	0.4	R2		1600	131.8		82.3
compression test	0.4	S1		1600	137.9		86.2
compression test	0.4	S2		1600	111.0		-
compression test	0.4	T1		1600	76.6		-
compression test	0.4	T2		1600	132.2		82.5

Table A.11 - Flexural and compression tests of 3 specimens with KSE 300 and a W/C ratio of 0.4

KSE 300	W/C	ID	l	A	Fm	σbz	σD
	-	-	[mm]	[mm2]	[kN]	[N/mm2]	[N/mm2]
3 point bending test	0.4	C	100	1600	4	9.5	
3 point bending test	0.4	D	100	1600	3.9	9.2	
3 point bending test	0.4	E	100	1600	4.3	10	
compression test	0.4	C1		1600	136.9		85.6
compression test	0.4	C2		1600	138.2		86.4
compression test	0.4	D1		1600	124.3		77.7
compression test	0.4	D2		1600	125.4		78.3
compression test	0.4	E1		1600	157.6		-
compression test	0.4	E2		1600	108.4		-

Table A.12 - Flexural and compression tests of 3 specimens with KSE 510 and a W/C ratio of 0.4

KSE 510	W/C	ID	l	A	Fm	σbz	σD
	-	-	[mm]	[mm2]	[kN]	[N/mm2]	[N/mm2]
3 point bending test	0.4	H	100	1600	4.1	9.5	
3 point bending test	0.4	I	100	1600	4.0	9.3	
3 point bending test	0.4	J	100	1600	3.9	9.1	
compression test	0.4	H1		1600	139.7		87.3
compression test	0.4	H2		1600	131.0		81.9
compression test	0.4	I1		1600	132.8		83.0
compression test	0.4	I2		1600	127.1		79.5
compression test	0.4	J1		1600	117.6		73.5
compression test	0.4	J2		1600	129.3		80.8

Table A.13 - Flexural and compression tests of 3 specimens with KSE 100 and a W/C ratio of 0.4

KSE 100	W/C	ID	l	A	Fm	σbz	σD
	-	-	[mm]	[mm2]	[kN]	[N/mm2]	[N/mm2]
3 point bending test	0.4		100	1600	4.0	9.4	
3 point bending test	0.4		100	1600	4.0	9.4	
3 point bending test	0.4		100	1600	3.8	9.0	
compression test	0.4			1600	132.6		82.9
compression test	0.4			1600	115.0		71.9
compression test	0.4			1600	117.7		73.6
compression test	0.4			1600	137.4		-
compression test	0.4			1600	121.5		76.0
compression test	0.4			1600	135.7		-

Table A.14 - Flexural and compression tests of 3 specimens with KSE OH from Rajasil and a W/C ratio of 0.4

KSE OH Raj	W/C	ID	l	A	Fm	σbz	σD
	-	-	[mm]	[mm2]	[kN]	[N/mm2]	[N/mm2]
3 point bending test	0.4		100	1600	4	9.5	
3 point bending test	0.4		100	1600	4.1	9.7	
3 point bending test	0.4		100	1600	4.1	9.7	
compression test	0.4			1600	139.1		86.9
compression test	0.4			1600	140.1		87.5
compression test	0.4			1600	139.6		87.3
compression test	0.4			1600	117.2		-
compression test	0.4			1600	127.6		79.7
compression test	0.4			1600	120.4		-

Table A.15 - Flexural and compression tests of 3 control specimens with a W/C ratio of 0.4

CONTROL	W/C	ID	l	A	Fm	σbz	σD
	-	-	[mm]	[mm2]	[kN]	[N/mm2]	[N/mm2]
3 point bending test	0.4		100	1600	4.3	10.1	
3 point bending test	0.4		100	1600	4.0	9.4	
3 point bending test	0.4		100	1600	3.7	8.7	
compression test	0.4			1600	124.0		77.5
compression test	0.4			1600	125.4		78.3
compression test	0.4			1600	112.0		70.0
compression test	0.4			1600	115.0		71.9
compression test	0.4			1600	99.6		62.3
compression test	0.4			1600	109.8		68.6

Table A.16 - Flexural and compression tests of 3 specimens with KSE OH and a W/C ratio of 0.5

KSE OH	W/C	ID	l	A	Fm	σbz	σD
	-	-	[mm]	[mm2]	[kN]	[N/mm2]	[N/mm2]
3 point bending test	0.5	P	100	1600	3.8	8.8	
3 point bending test	0.5	S	100	1600	3.8	8.9	
3 point bending test	0.5	T	100	1600	3.8	9	
compression test	0.5	P1		1600	113.8		71.1
compression test	0.5	P2		1600	119.1		74.5
compression test	0.5	S1		1600	116.7		72.9
compression test	0.5	S2		1600	124.3		77.7
compression test	0.5	T1		1600	120.7		75.4
compression test	0.5	T2		1600	123.0		76.9

Table A.17 - Flexural and compression tests of 3 specimens with KSE 300 and a W/C ratio of 0.5

KSE 300	W/C	ID	l	A	Fm	σbz	σD
	-	-	[mm]	[mm2]	[kN]	[N/mm2]	[N/mm2]
3 point bending test	0.5	X	100	1600	4.0	9.4	
3 point bending test	0.5	Y	100	1600	3.6	8.5	
3 point bending test	0.5	Z	100	1600	3.8	8.8	
compression test	0.5	X1		1600	111.9		70.0
compression test	0.5	X2		1600	112.7		70.4
compression test	0.5	Y1		1600	109.8		68.6
compression test	0.5	Y2		1600	113.2		70.8
compression test	0.5	Z1		1600	117.3		73.3
compression test	0.5	Z2		1600	116.1		72.6

Table A.18 - Flexural and compression tests of 3 specimens with KSE 510 and a W/C ratio of 0.5

KSE 510	W/C	ID	l	A	Fm	σbz	σD
	-	-	[mm]	[mm2]	[kN]	[N/mm2]	[N/mm2]
3 point bending test	0.5	F	100	1600	3.5	8.2	
3 point bending test	0.5	G	100	1600	3.8	8.9	
3 point bending test	0.5	H	100	1600	3.8	8.9	
compression test	0.5	F1		1600	113.4		70.9
compression test	0.5	F2		1600	116.1		72.6
compression test	0.5	G1		1600	118.9		74.3
compression test	0.5	G2		1600	115.7		72.3
compression test	0.5	HH1		1600	127.9		79.9
compression test	0.5	H2		1600	126.3		79.0

Table A.19 - Flexural and compression tests of 3 specimens with KSE 100 and a W/C ratio of 0.5

KSE 100	W/C	ID	l	A	Fm	σbz	σD
	-	-	[mm]	[mm2]	[kN]	[N/mm2]	[N/mm2]
3 point bending test	0.5	K	100	1600	3.9	9.2	
3 point bending test	0.5	L	100	1600	3.9	9.1	
3 point bending test	0.5	M	100	1600	4.0	9.3	
compression test	0.5	K1		1600	102.5		64.1
compression test	0.5	K2		1600	108.4		67.7
compression test	0.5	L1		1600	77		0
compression test	0.5	L2		1600	115.7		72.3
compression test	0.5	M1		1600	115.7		72.3
compression test	0.5	M2		1600	108.1		67.6

Table A.20 - Flexural and compression tests of 3 specimens with KSE OH from Rajasil and a W/C ratio of 0.5

KSE OH Raj	W/C	ID	l	A	Fm	σbz	σD
	-	-	[mm]	[mm2]	[kN]	[N/mm2]	[N/mm2]
3 point bending test	0.5	A	100	1600	3.8	8.9	
3 point bending test	0.5	B	100	1600	3.6	8.4	
3 point bending test	0.5	C	100	1600	3.4	8.0	
compression test	0.5	A1		1600	112.1		70.1
compression test	0.5	A2		1600	113.2		70.4
compression test	0.5	B1		1600	116.7		72.9
compression test	0.5	B2		1600	123.0		76.9
compression test	0.5	C1		1600	115.7		72.3
compression test	0.5	C2		1600	126.3		79.0

Table A.21 - Flexural and compression tests of 3 control specimens with W/C ratio of 0.5

Control	W/C	ID	l	A	Fm	σbz	σD
	-	-	[mm]	[mm2]	[kN]	[N/mm2]	[N/mm2]
3 point bending test	0.5	1	100	1600	3.5	8.3	
3 point bending test	0.5	2	100	1600	3.5	8.2	
3 point bending test	0.5	3	100	1600	3.6	8.4	
compression test	0.5	1		1600	116.2		72.6
compression test	0.5	1		1600	117.0		73.1
compression test	0.5	2		1600	121.0		75.6
compression test	0.5	2		1600	125.2		78.2
compression test	0.5	3		1600	115.6		72.2
compression test	0.5	3		1600	112.5		70.3

A5.

Table A.22 – Results of the measurements of the specimens expansion

Nr	Cem, ref.	Ring, ref	Expansion							
			24h	3days	4days	7days	11days	17days	28days	35days
			[mm]	[mm]	[mm]	[mm]	[mm]		[mm]	[mm]
1	Z556	7.1	20	20	20	23	26		33	33
		257	25	33	35	41	44		51	53
2	Z554	230	20	22	24	30	35		45	46
		355	21	27	29	35	41		52	52
3	Z558	31	15	15	18	20	30		38	39
		163	10	14	17	23	32		42	43
4	Z557	181	33	33	33	34	35		38	40
		9	25	26	26	27	27		32	35
5	Z559	105	22	29	30	33	39		53	55
		73	3	5	5	11	16		33	34
6	Z555	214	6	12	15	21	23		40	40
		17	11	16	21	33	44		68	72
7	Z556 + KSE 300	15.1	18	21	21	22	23		24	24
		241	10	11	12	12	13		14	14
8	Z554 + KSE 300	34	8	8	9	10	10		21	23
		X	8	8	8	9	9		10	10
9	Z558 + KSE 300	13.1	19	19	19	19	20		21	21
		179	18	18	18	18	18		18	19
10	Z557 + KSE 300	12.1	18	18	19	22	22		25	25
		4	18	18	19	19	19		28	28
11	Z559 + KSE 300	188	12	12	12	14	15		19	20
		18.1	15	15	15	16	16		16	16

Table A.22 – Results of the measurements of the specimens expansion

Nr	Cem, ref.	Ring, ref	Expansion							
			24h	3days	4days	7days	11days	17days	28days	35days
			[mm]	[mm]	[mm]	[mm]	[mm]		[mm]	[mm]
12	Z555 + KSE 300	12.1	2	2	3	4	4		14	14
		131	13	13	13	13	13		13	14
13	Z556 + KSE OH	110	8	9	10	12	14		18	18
		10.2	33	34	34	36	38		38	46
14	Z554 + KSE OH	330	8	8	8	9	11		18	20
		5	11	11	11	13	15		21	22
15	Z558 + KSE OH	56	30	31	31	34	37		52	53
		358	17	17	18	21	25		44	44
16	Z557 + KSE OH	6.1	16	16	16	20	23		35	36
		4.1	26	27	27	31	34		54	54
17	Z559 + KSE OH	269	21	22	24	26	38		50	51
		220	14	14	14	21	29		44	47
18	Z555 + KSE OH	18.2	4	4	4	6	11		28	28
		92	13	14	15	17	24		40	41
19	Z556 + KSE 100	32	16	19		30		46	49	59
		59	12	12		21		36	40	42
20	Z554 + KSE 100	554/1	29	29		30		46	49	49
		291	27	28		47		69	74	75

Table A.22 – Results of the measurements of the specimens expansion

Nr	Cem, ref.	Ring, ref	Expansion							
			24h	3days	4days	7days	11days	17days	28days	35days
			[mm]	[mm]	[mm]	[mm]	[mm]		[mm]	[mm]
21	Z558 + KSE 100	101	6	7		42		65	74	76
		102	14	18		27		41	42	42
22	Z557 + KSE 100	20	28	28		40		53	65	67
		21	34	34		44		68	80	83
23	Z559 + KSE 100	51	4	6		24		37	40	41
		52	11	11		18		35	37	37
24	Z555 + KSE 100	71	4	4		5		18	20	22
		72	4	4		5		18	22	22

Fig. A.1 – Expansion of control specimens of Z556, Z554, Z558 and Z557

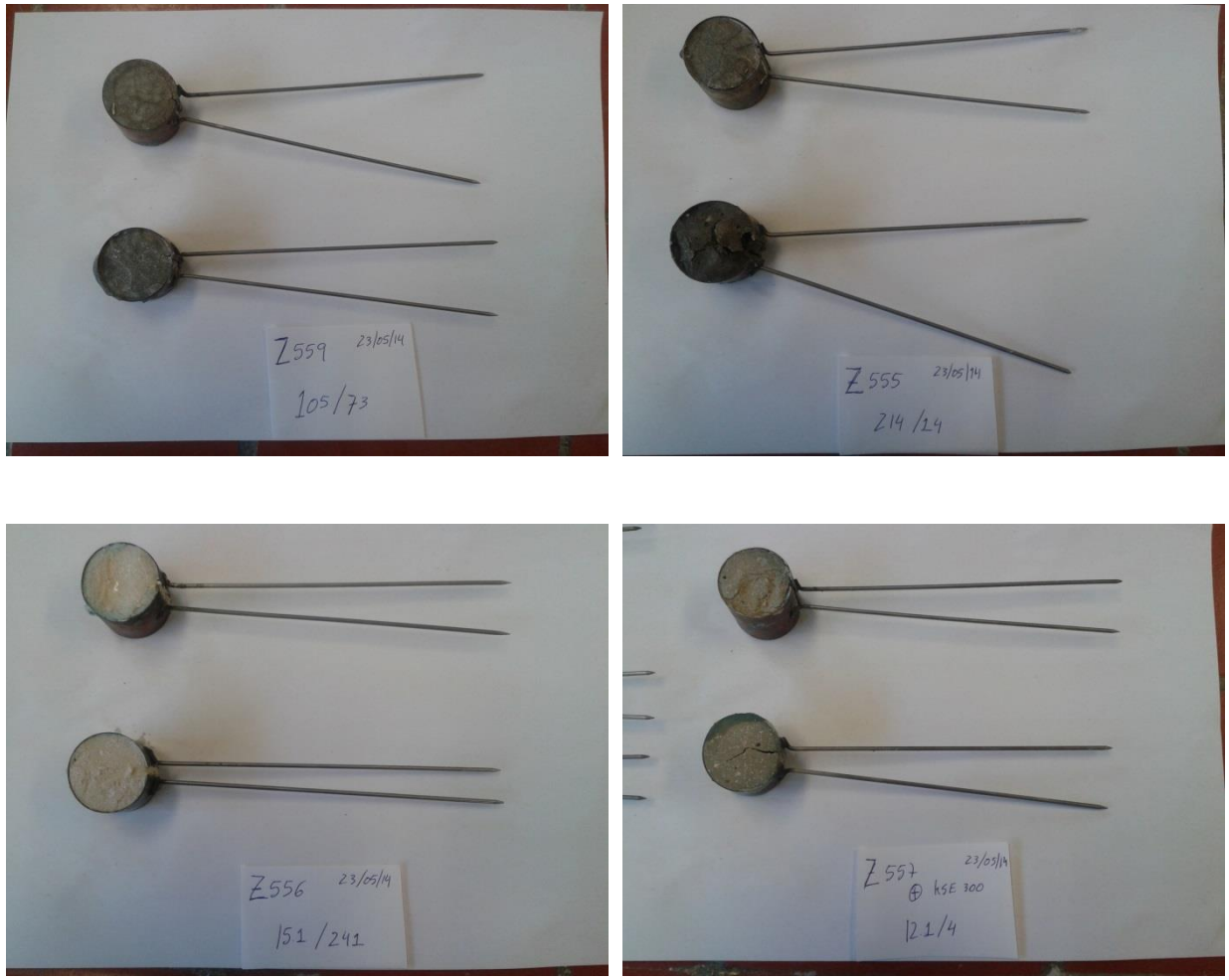

Fig. A.2 – Expansion of control specimens of Z559 and Z555, and of Z556 and Z557 with KSE 300

Fig. A.3 – Expansion of specimens of Z554 and Z558, and of Z559 and Z555 with KSE 300

Fig. A.4 – Expansion of specimens of Z556 and Z554, and of Z558 and Z557 with KSE OH

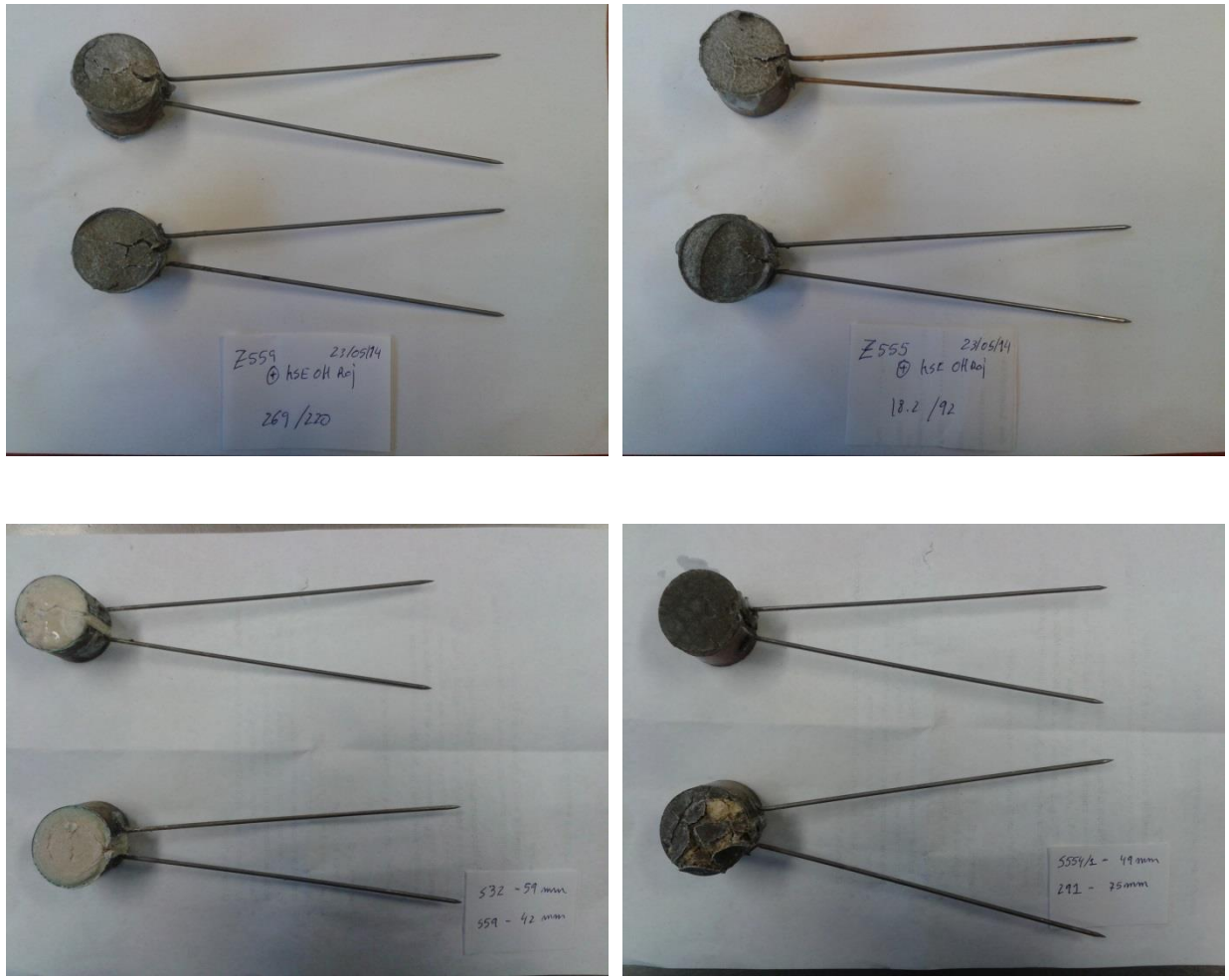

Fig. A.5 – Expansion of specimens of Z559 and Z555 with KSE OH and, and of Z556 and Z554 with KSE 100

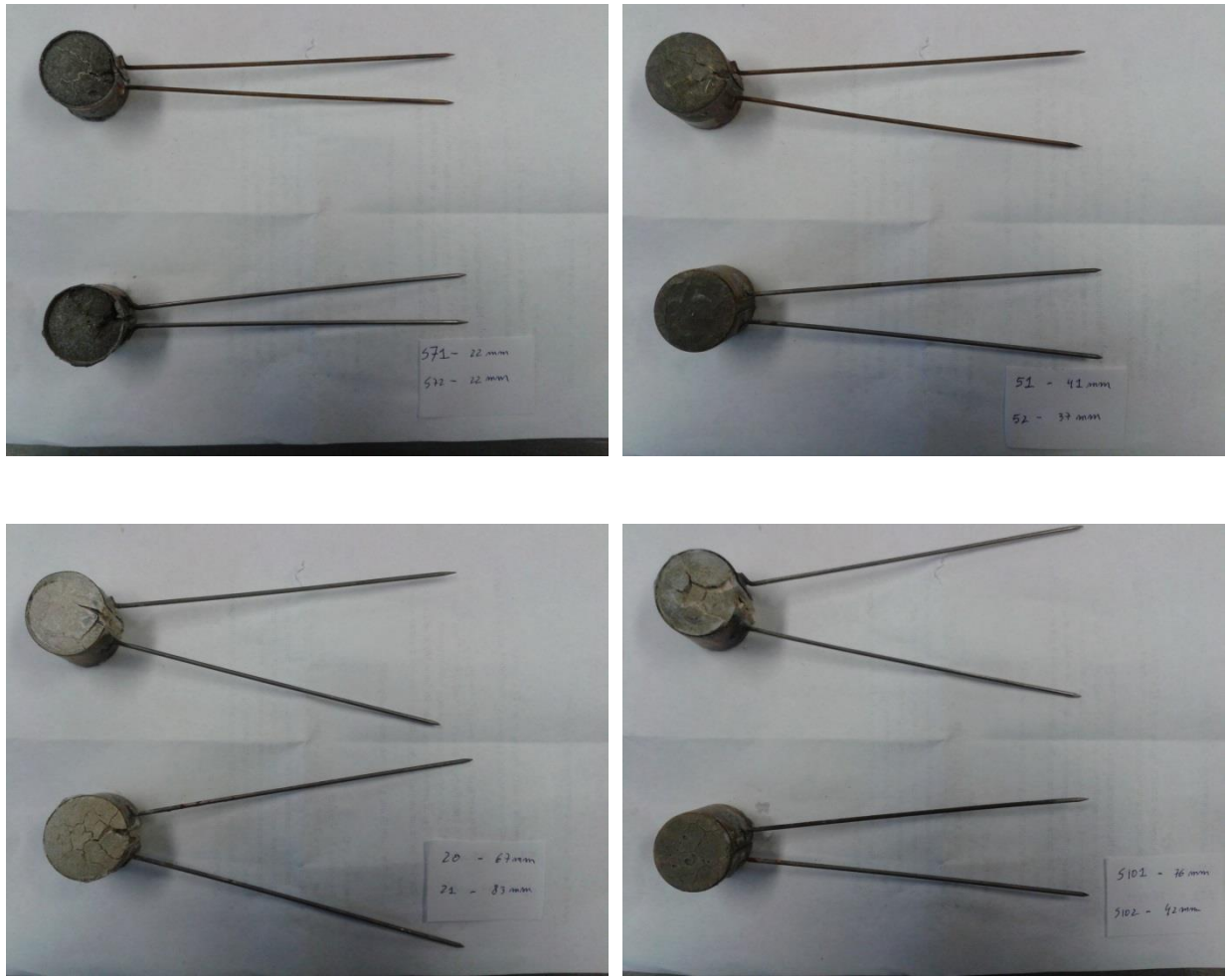

Fig. A.6 – Expansion of specimens of Z555, Z559, Z557 and Z558 with KSE 100

A6.

A6 contains all the ESEM figures of the specimens studied. The reference in the pictures has the following correspondence to the specimens:

"S2" – Z556

"S5" – Z559

"S22" – Z555 + KSE OH

"32" – Z556 + KSE 100

"S20" – Z554 + KSE 100

"S21" – Z558 + KSE 100

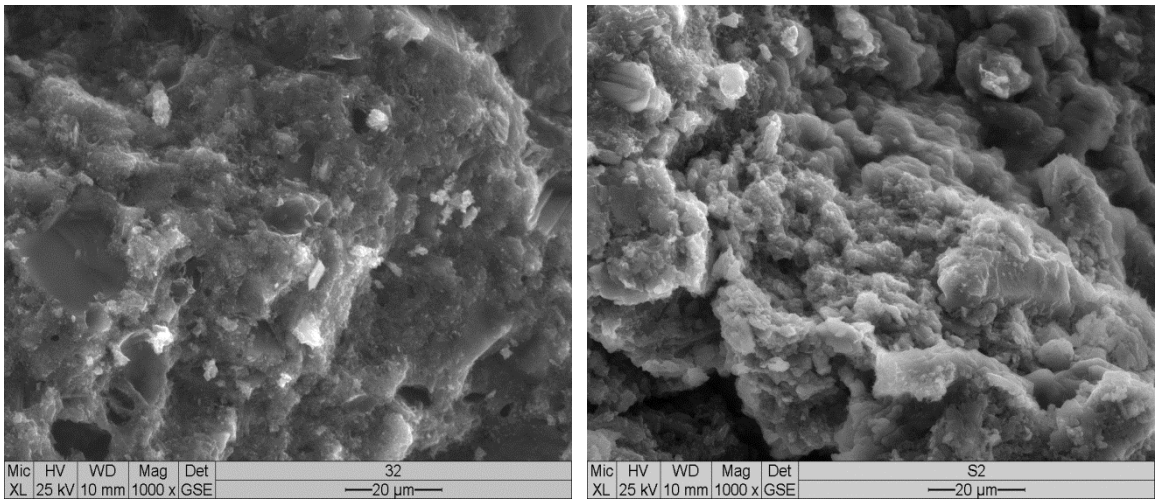

Fig. A.7 – ESEM pictures of specimens with Z556 + KSE 100 and Z556

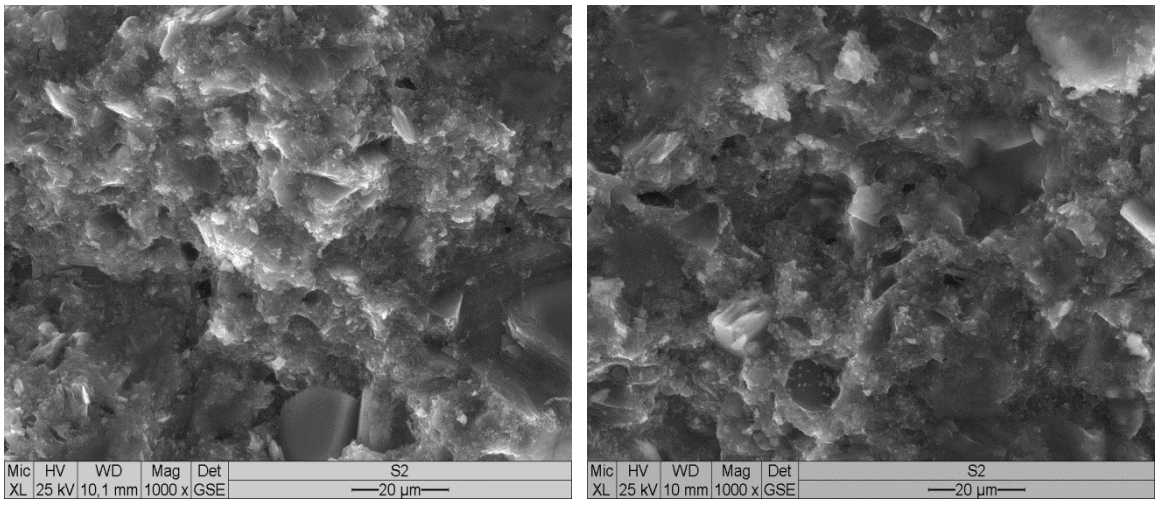

Fig. A.8 – ESEM pictures of the specimens with Z556

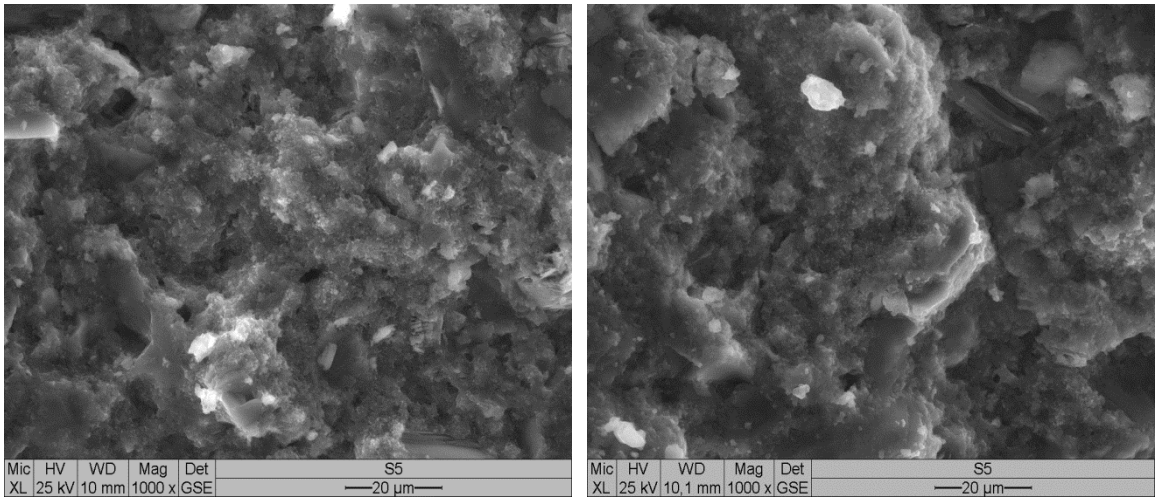

Fig. A.9 – ESEM pictures of the specimens with Z559

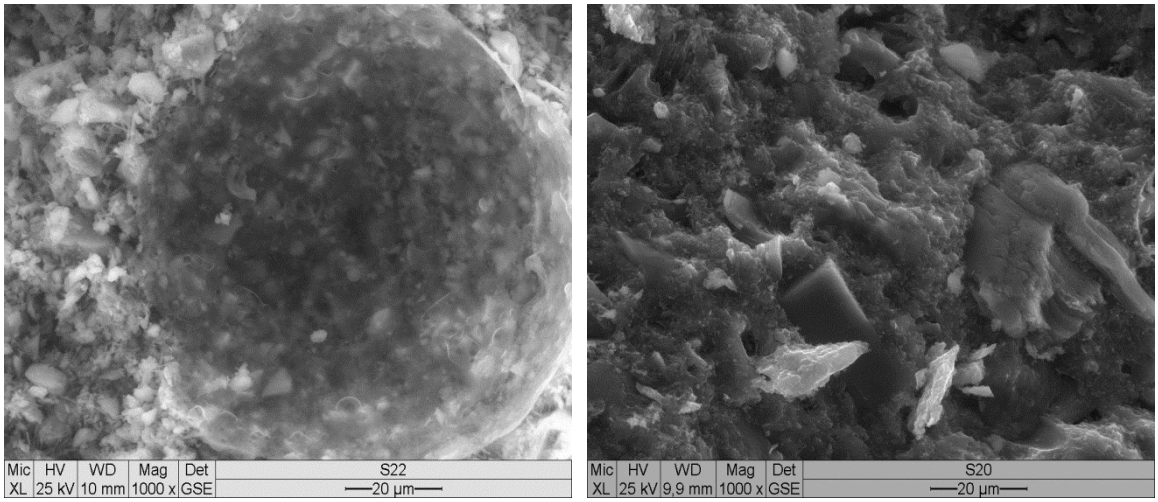

Fig. A.10 – ESEM pictures of the specimens with Z555 + KSE OH and Z554 + KSE 100

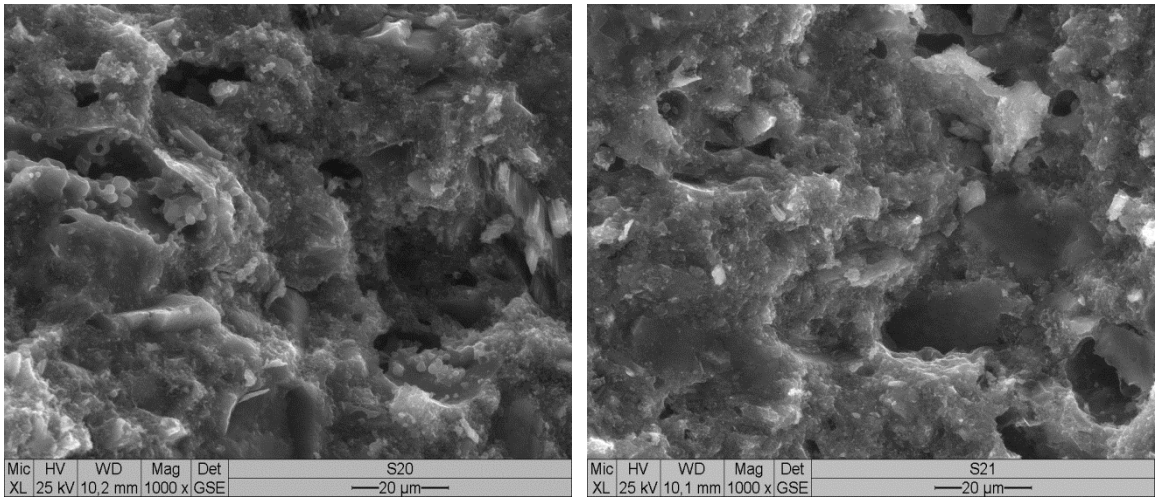

Fig. A.11 – ESEM pictures of the specimens with Z554 + KSE 100 and Z558 + KSE 100

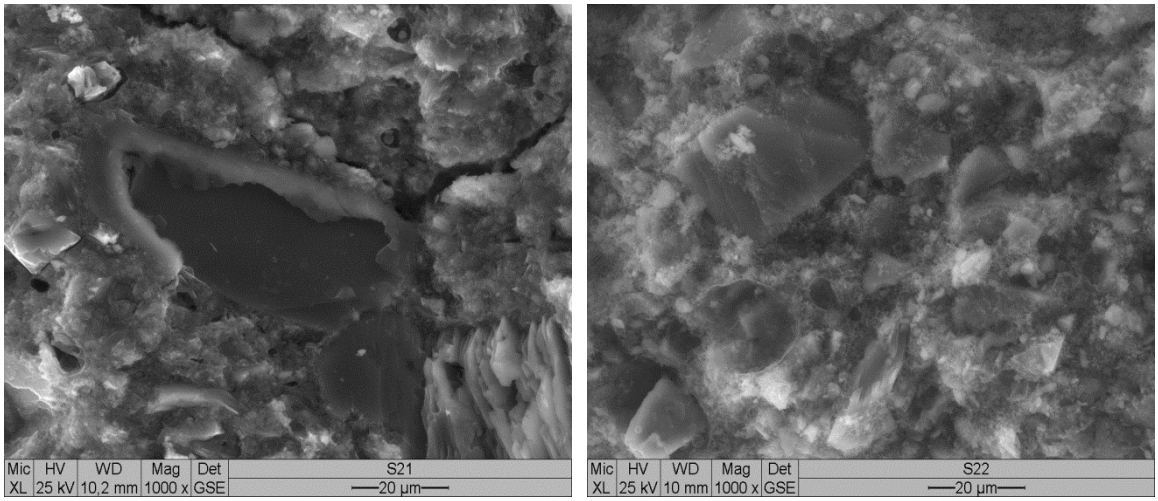

Fig. A.12 – ESEM pictures of the specimens with Z558 + KSE 100 and Z555 + KSE OH

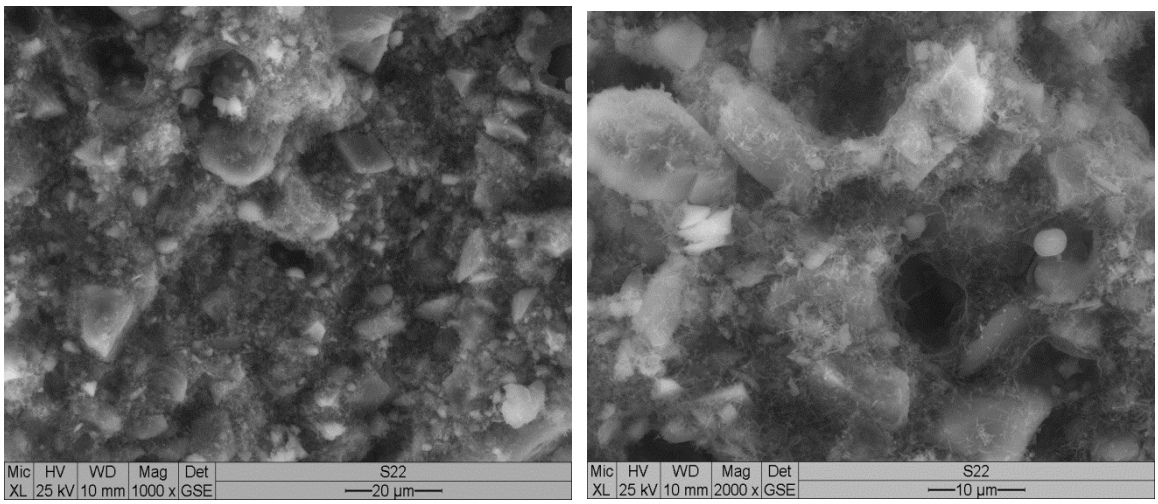

Fig. A.13 – ESEM pictures of the specimens with Z555 + KSE OH

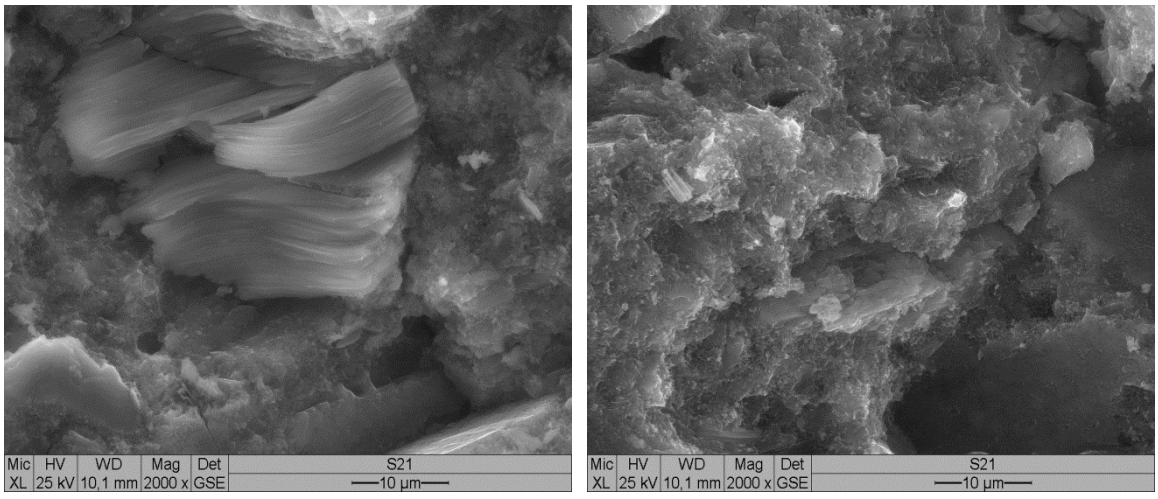

Fig. A.14 – ESEM pictures of the specimens with Z558 + KSE 100

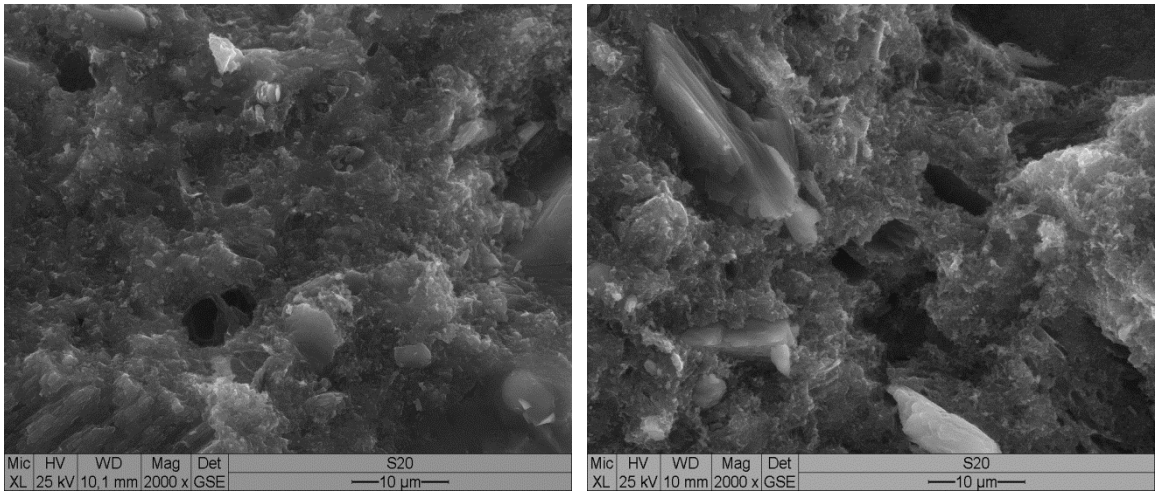

Fig. A.15 – ESEM pictures of the specimens with Z554 + KSE 100

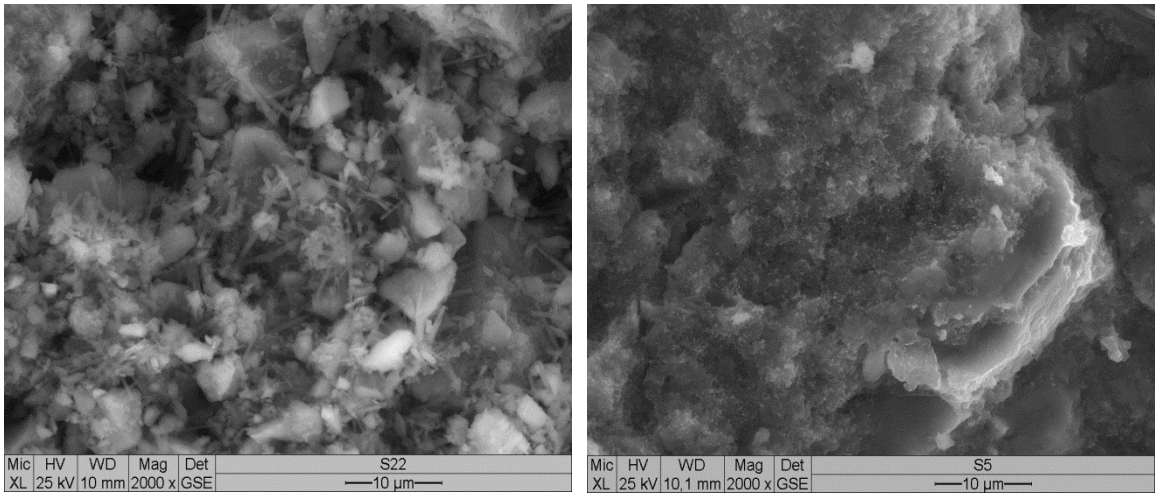

Fig. A.16 – ESEM pictures of the specimens with Z555 + KSE OH and Z559

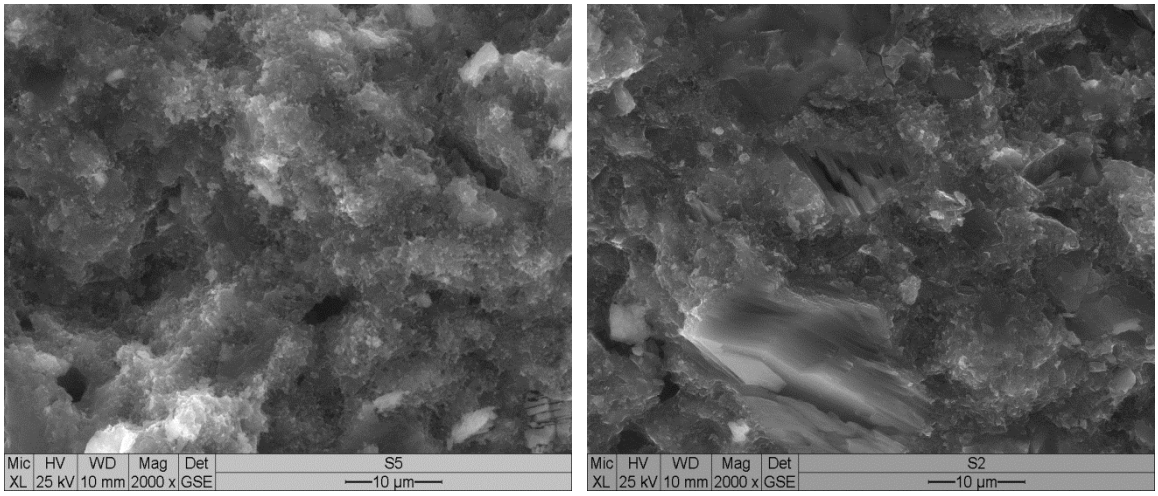

Fig. A.17 – ESEM pictures of the specimens with Z559 + KSE OH and Z556

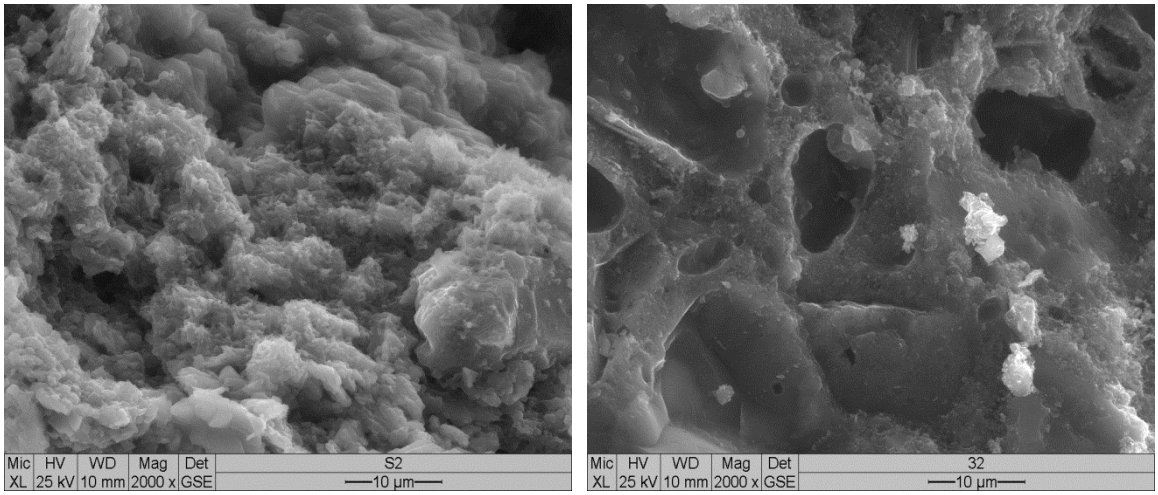

Fig. A.18 – ESEM pictures of the specimens with Z556 + KSE OH and Z556 + KSE 100

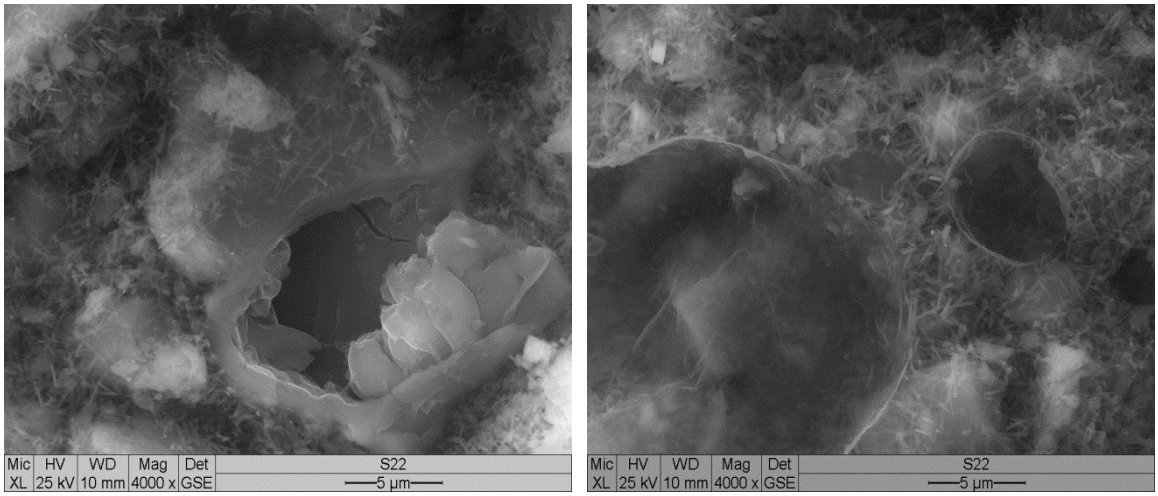

Fig. A.19 – ESEM pictures of the specimens with Z555 + KSE OH

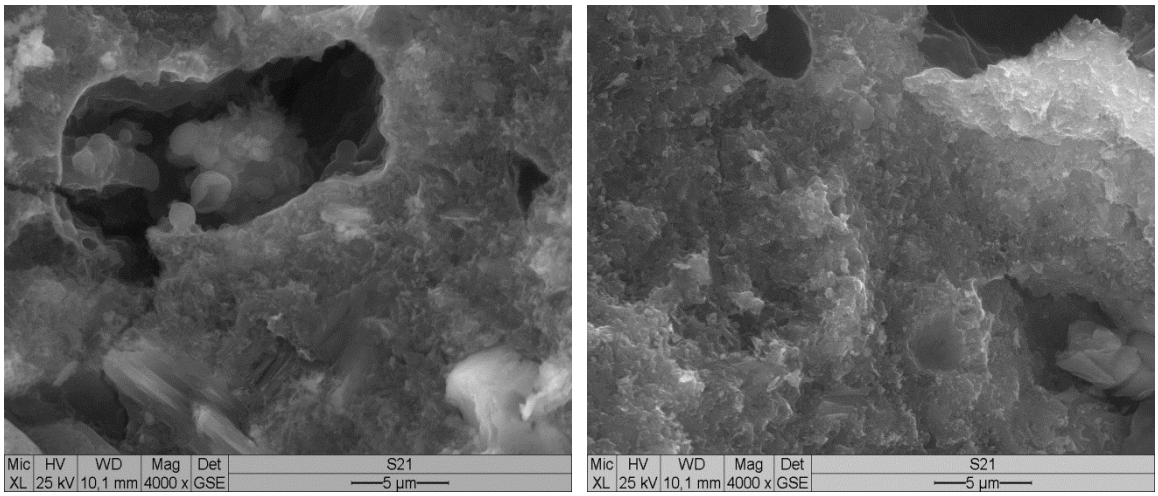

Fig. A.20 – ESEM pictures of the specimens with Z558 + KSE 100

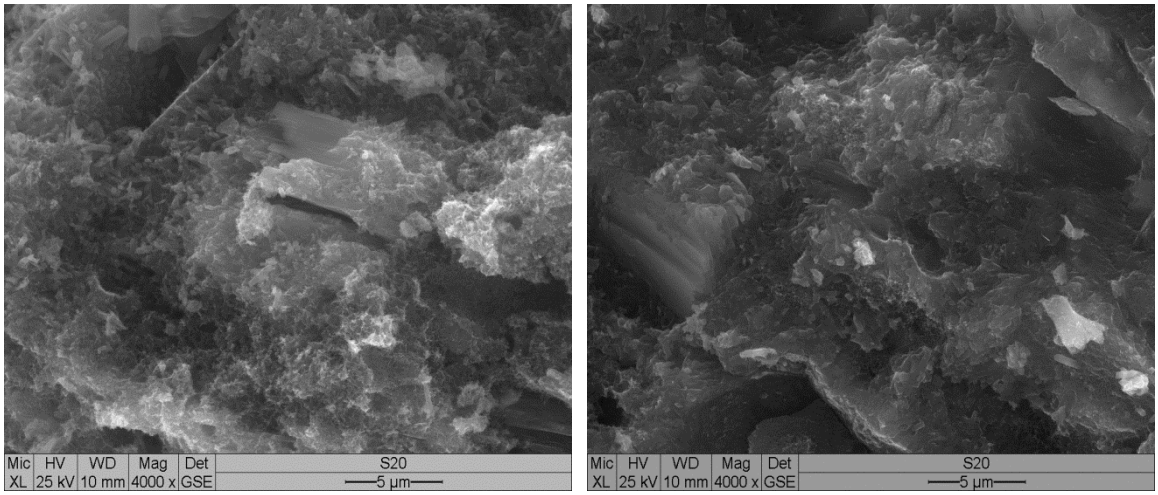

Fig. A.21 – ESEM pictures of the specimens with Z554 + KSE 100

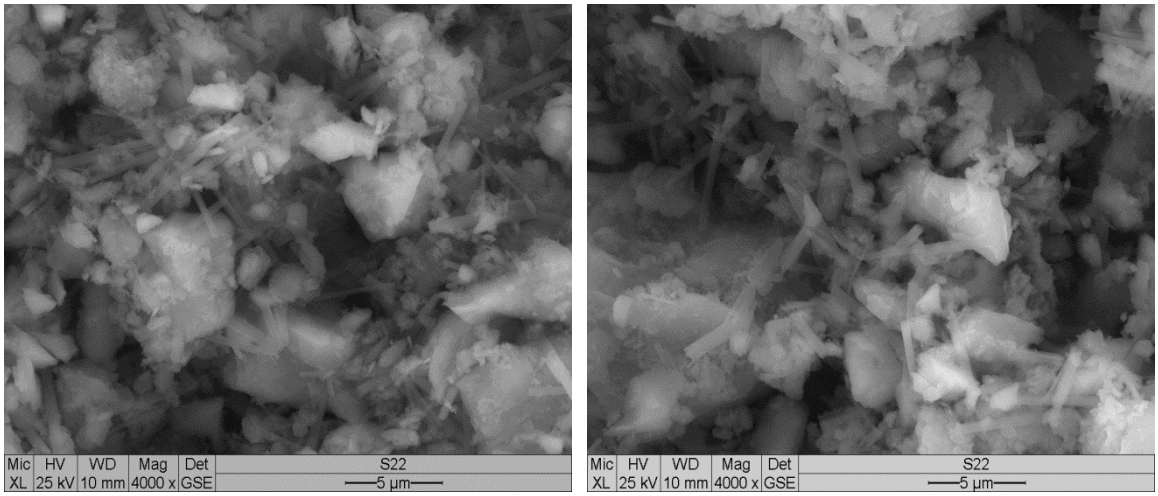

Fig. A.22 – ESEM pictures of the specimens with Z555 + KSE OH

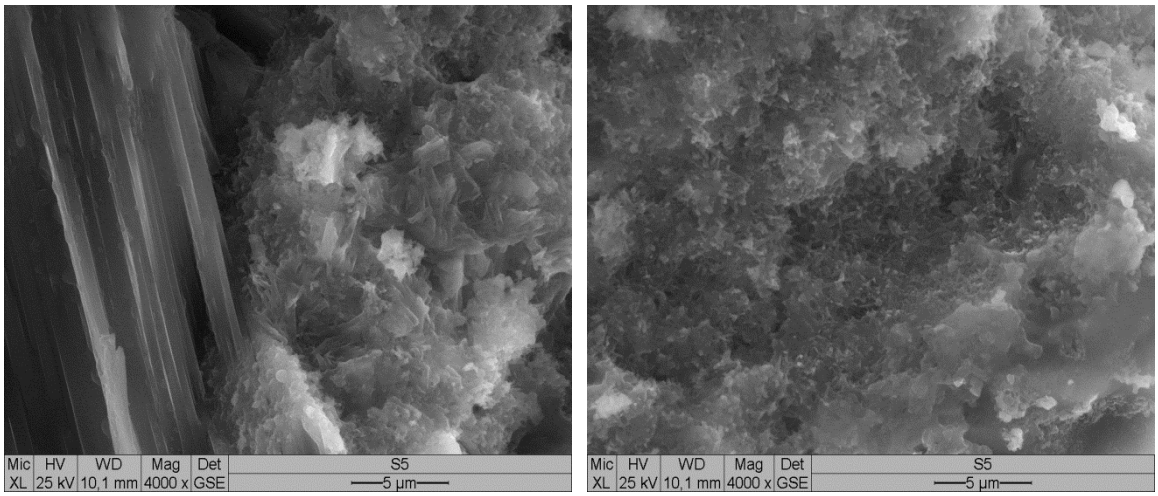

Fig. A.23 – ESEM pictures of the specimens with Z559

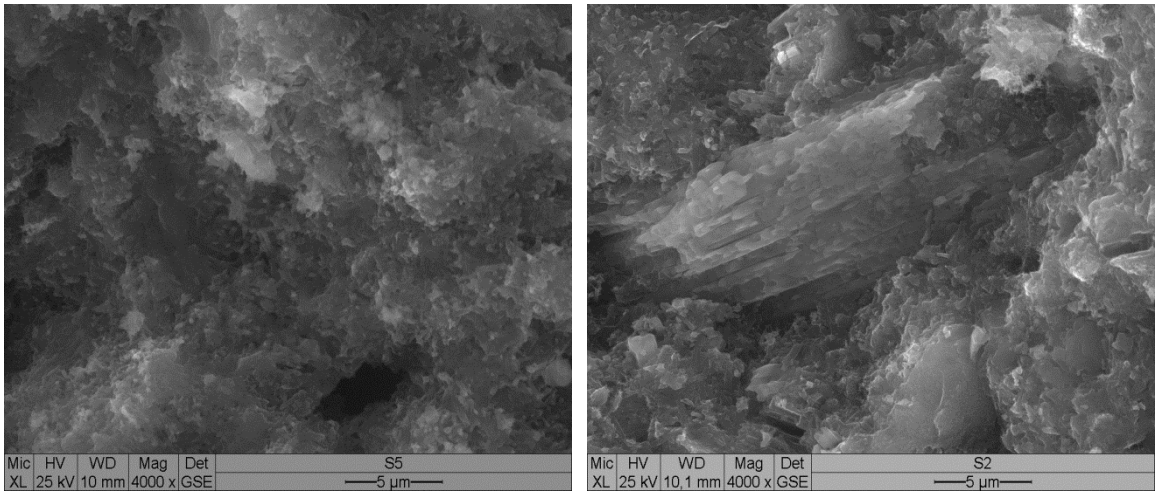

Fig. A.24 – ESEM pictures of the specimens with Z559 and Z556

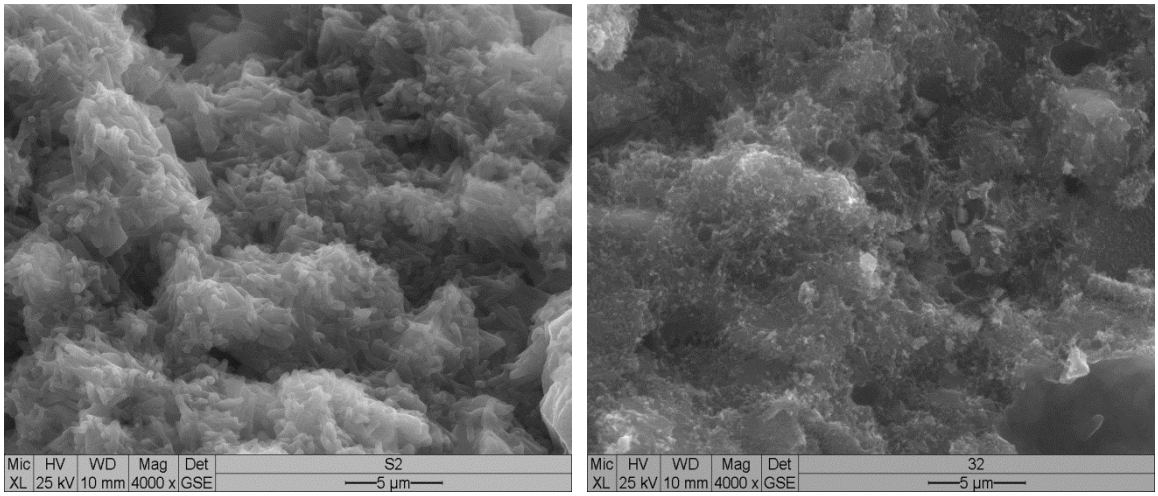

Fig. A.25 – ESEM pictures of the specimens with Z556 and Z556 + KSE 100

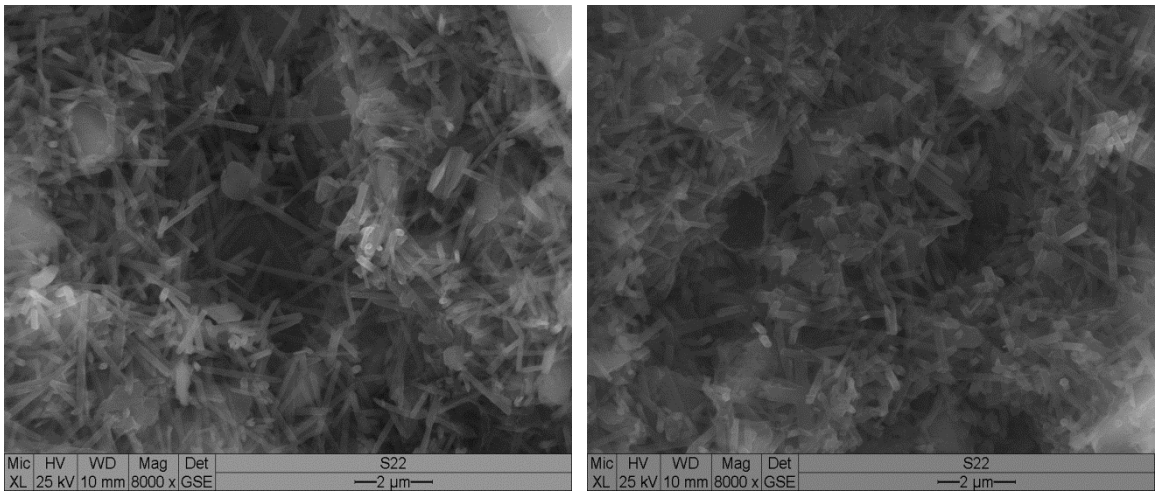

Fig. A.26 – ESEM pictures of the specimens with Z555 + KSE OH

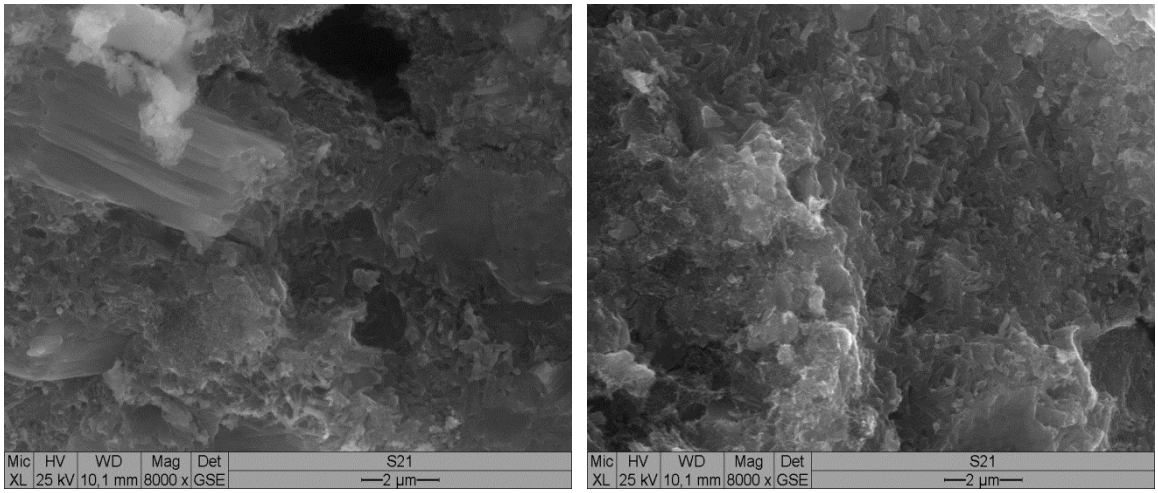

Fig. A.27 – ESEM pictures of the specimens with Z558 + KSE 100

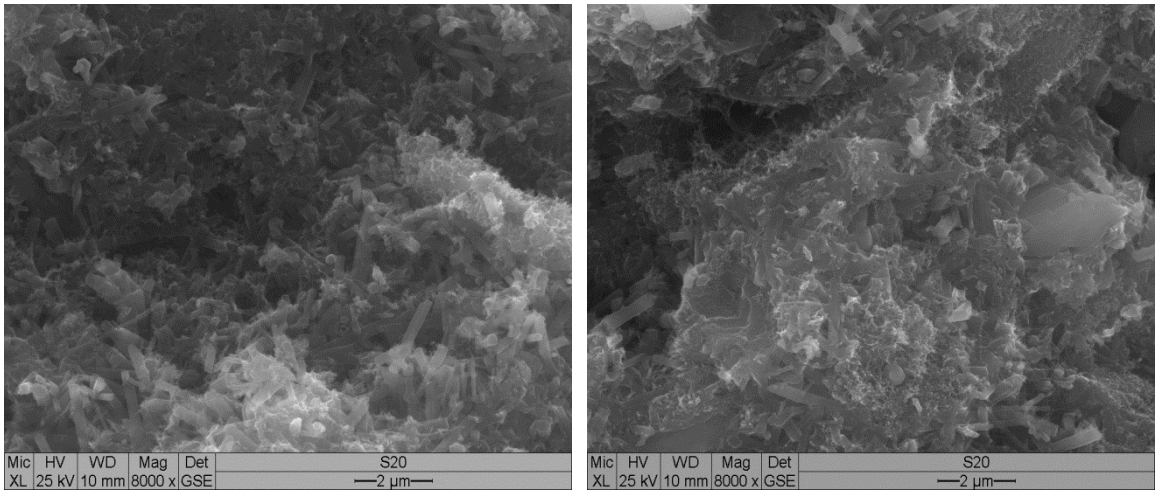

Fig. A.28 – ESEM pictures of the specimens with Z554 + KSE 100

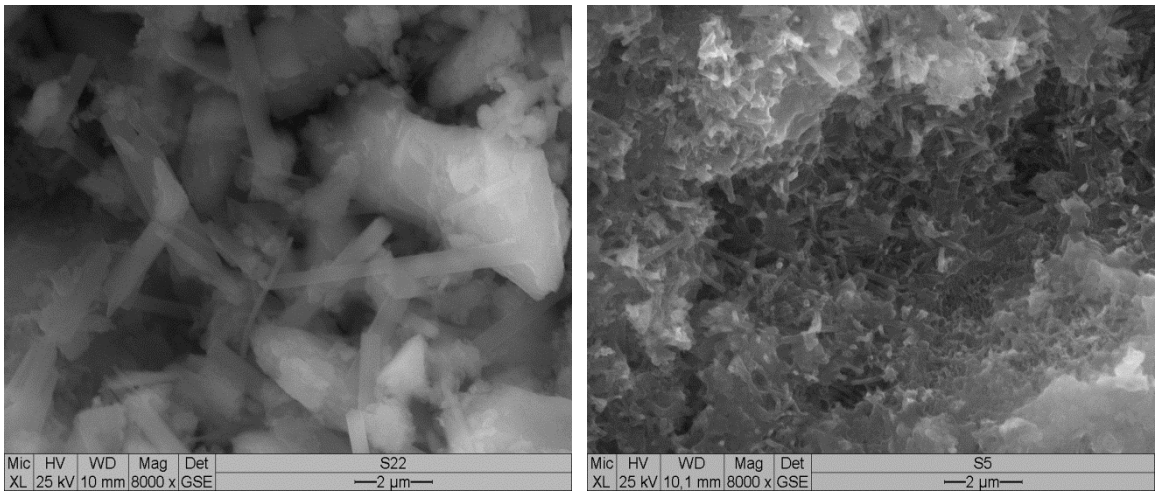

Fig. A.29 – ESEM pictures of the specimens with Z555 + KSE OH and Z559

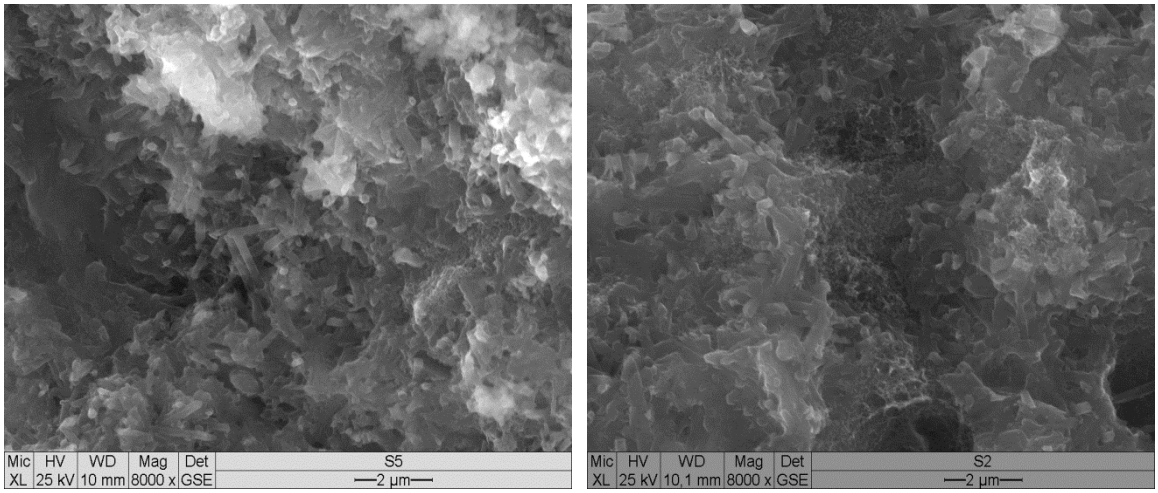

Fig. A.30 – ESEM pictures of the specimens with Z559 and KSE 556

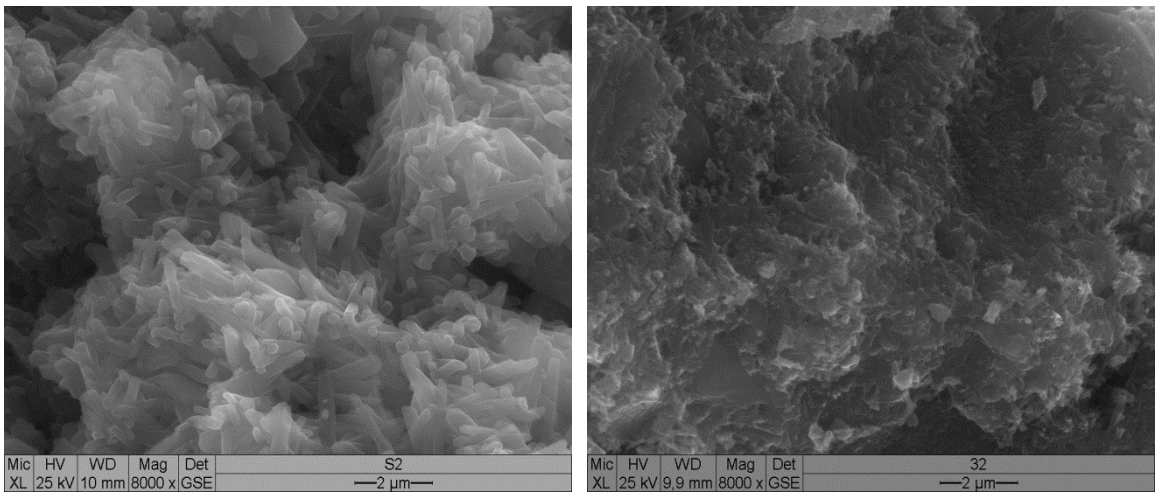

Fig. A.31 – ESEM pictures of the specimens with Z556 and Z556 + KSE 100

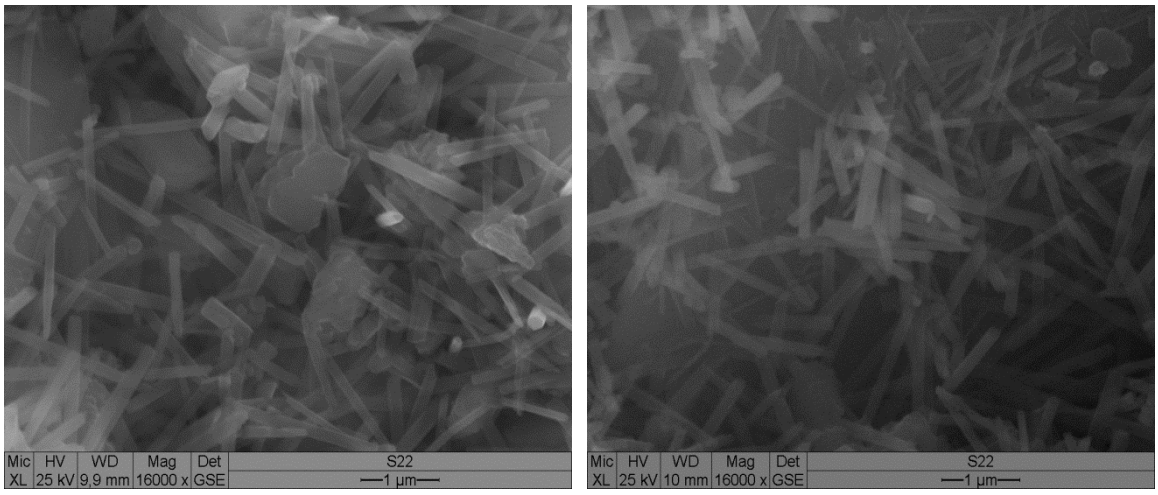

Fig. A.32 – ESEM pictures of the specimens with Z555 + KSE OH

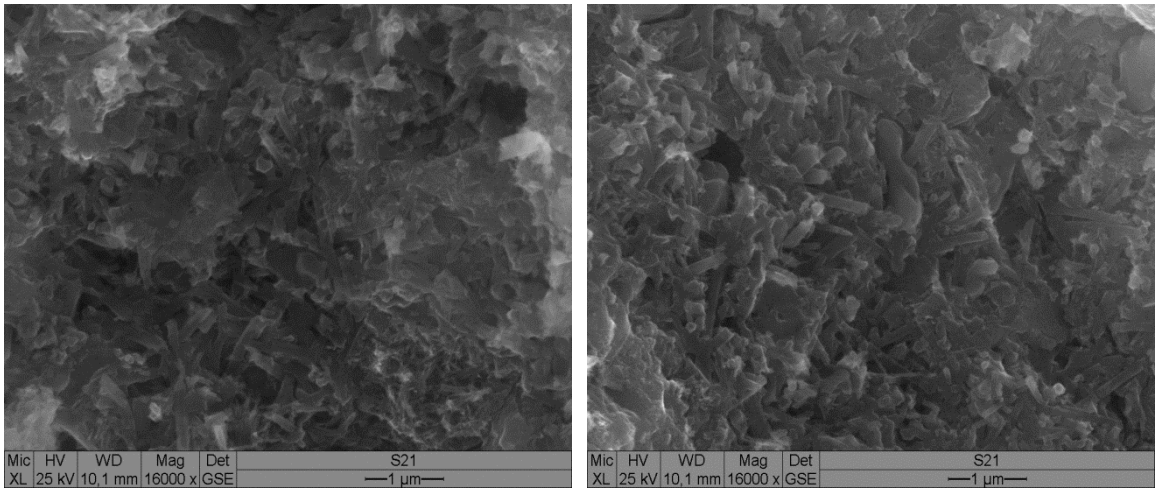

Fig. A.33 – ESEM pictures of the specimens with Z558 + KSE 100

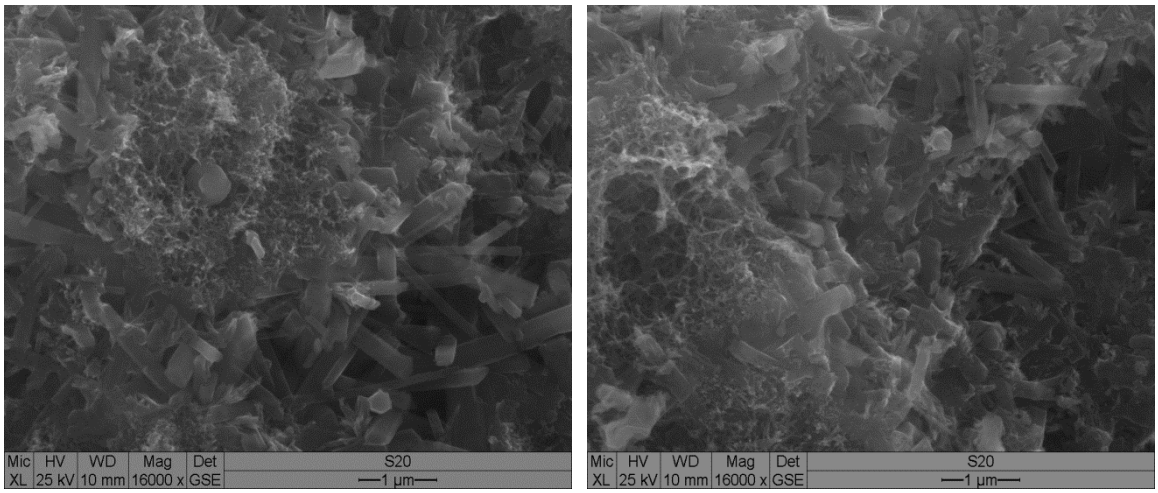

Fig. A.34 – ESEM pictures of the specimens with Z554 + KSE 100

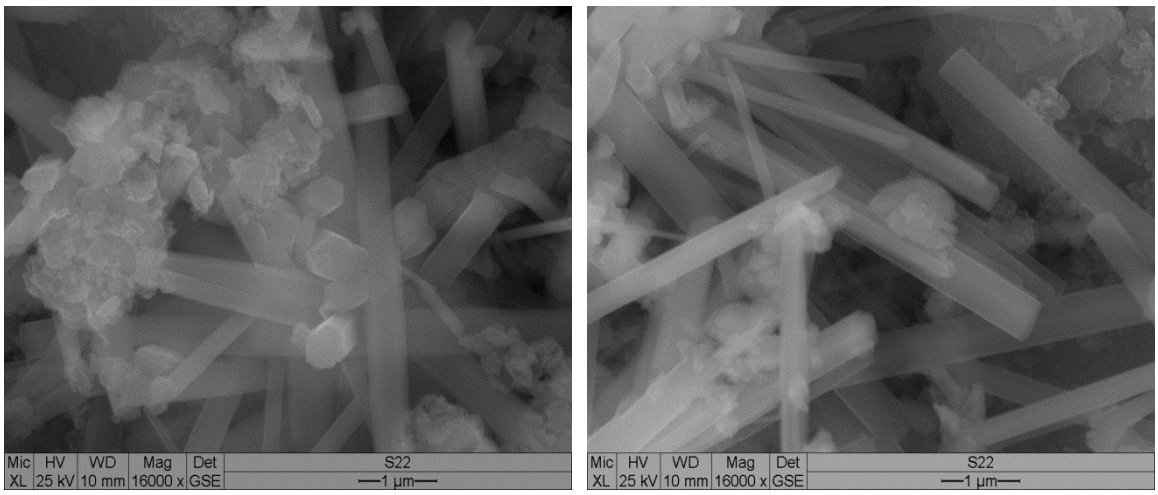

Fig. A.35 – ESEM pictures of the specimens with Z558 + KSE 100

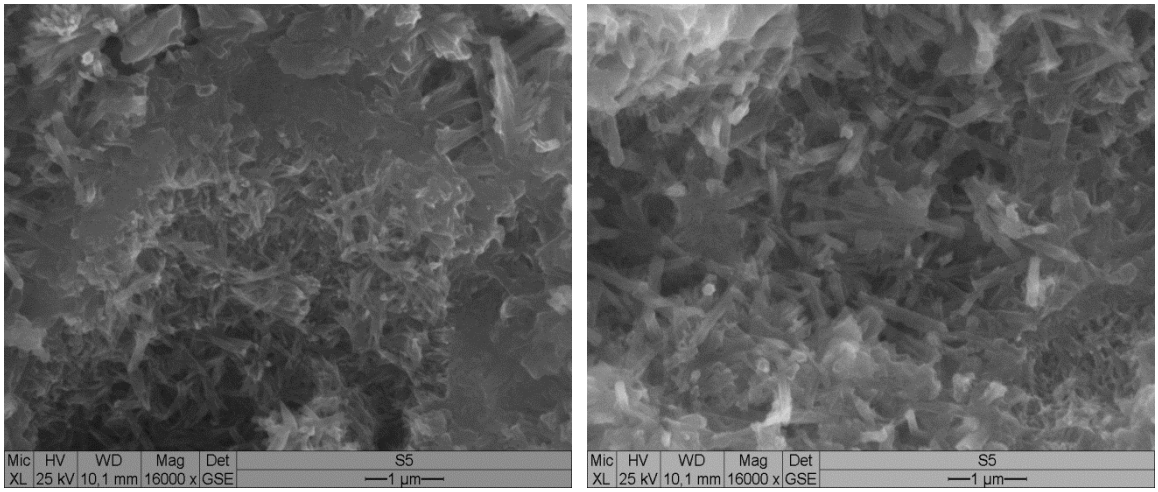

Fig. A.36 – ESEM pictures of the specimens with Z559

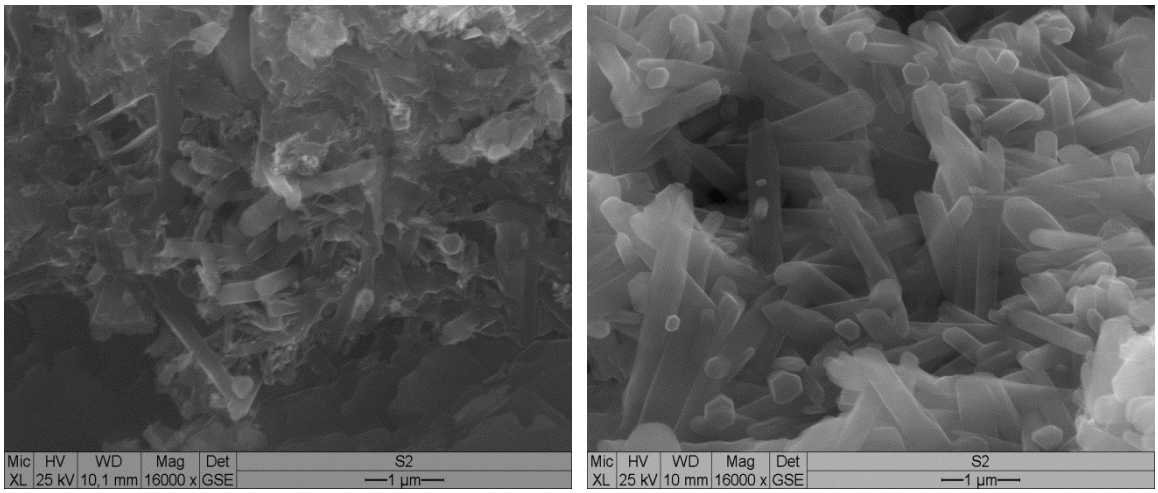

Fig. A.37 – ESEM pictures of the specimens with Z556

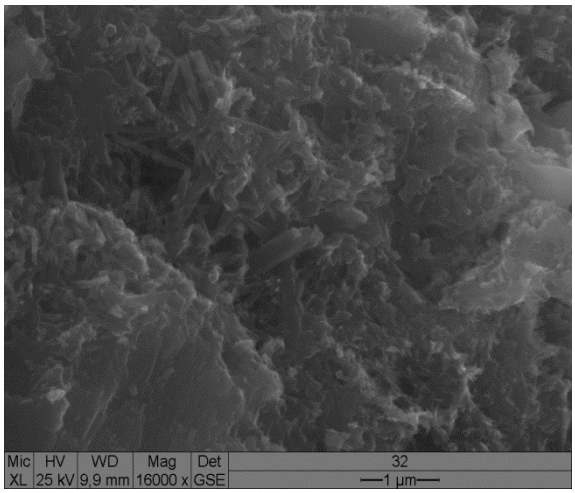

Fig. A.38 – ESEM pictures of the specimens with Z556 + KSE 100